

Cdc42 and β 1 integrin in cell migration

Dissertation der
Fakultät für Biologie der
Ludwig-Maximilians-Universität
München

vorgelegt von
Aleksandra Czuchra

München 2005

Hiermit erkläre ich, dass ich die vorliegende Dissertation selbständig und ohne unerlaubte Hilfe angefertigt habe. Ich habe weder anderweitig versucht, eine Dissertation einzureichen oder eine Doktorprüfung durchzuführen, noch habe ich diese Dissertation oder Teile derselben einer anderen Prüfungskommission vorgelegt.

Aleksandra Czuchra

München, den 19.09.2005

Die vorliegende Arbeit wurde zwischen August 2002 und August 2005 unter Anleitung von Dr. Cord Brakebusch am Max-Planck-Institut für Biochemie in Martinsried durchgeführt.

Wesentliche Teile dieser Arbeit sind in folgender Publikation veröffentlicht:

Czuchra, A., Wu, X., Meyer, H., van Hengel, J., Schroeder, T., Geffers, R., Rottner, K. and Brakebusch, C. (2005) Cdc42 is not essential for filopodium formation, directed migration, cell polarization and mitosis in fibroblastoid cells. *Mol Biol Cell* 16, 4473-4484.

Promotionsgesuch eingereicht am 19.09.2005

Tag der mündlichen Prüfung 12.12.2005

Erster Gutachter: Prof. Dr. Charles N. David

Zweiter Gutachter: Prof. Dr. Michael Schleicher

Sondergutachter: Dr. Cord Brakebusch

TABLE OF CONTENTS.....	4
ABBREVIATIONS.....	10
1 SUMMARY.....	13
2 INTRODUCTION.....	14
2.1 INTEGRINS.....	14
2.1.1 INTEGRIN CYTOPLASMIC DOMAINS.....	15
2.1.2 INTEGRIN ACTIVATION.....	16
2.1.3 INTEGRIN SIGNALLING.....	19
2.1.4 INTEGRINS IN SKIN.....	24
2.2 THE RHO GTPASES FAMILY.....	29
2.2.1 REGULATION OF THE RHO GTPASES FAMILY.....	31
2.2.2 THE CDC42 FAMILY.....	32
2.2.3 TOOLS OF TRADE: USE OF DOMINANT-NEGATIVE INHIBITORY MUTANTS OF THE RHO-FAMILY GTPASES.....	33
2.3 CELL MIGRATION.....	34
2.3.1 CDC42 IN CELL MIGRATION.....	35
2.3.1.1 Cdc42 as regulator of protrusion formation.....	36
2.3.1.2 Cdc42 as master regulator of cell polarity.....	38
2.3.2 INTEGRINS IN CELL MIGRATION.....	41
2.4 SIGNALLING NETWORKS LINKING INTEGRINS AND RHO GTPASES TO PROMOTE MIGRATION	43
2.5 AIM OF THIS STUDY.....	46
3 MATERIALS AND METHODS.....	48
3.1 MATERIALS.....	48
3.2 ANIMALS.....	48
3.3 GENERATION OF GENETICALLY MODIFIED MICE.....	48
3.3.1 PREPARATION OF FEEDER CELL LINES.....	48
3.3.2 PREPARATION OF DNA FOR ELECTROPORATION INTO EMBRYONIC STEM CELLS.....	49
3.3.3 ELECTROPORATION OF ES CELLS.....	49
3.3.4 SELECTION, PICKING AND FREEZING OF POSITIVE ES CELL CLONES.....	50
3.3.5 PREPARATION OF ES CELLS FOR BLASTOCYST INJECTION.....	50
3.3.6 PRODUCTION OF CHIMERIC ANIMALS.....	50
3.3.7 BREEDING SCHEMES.....	51

3.4	WOUNDING AND PREPARATION OF WOUND TISSUE.....	51
3.5	HISTOLOGICAL METHODS.....	52
3.5.1	ISOLATION AND EMBEDDING OF MOUSE SKIN	52
3.5.1.1	Embedding and cutting skin for cryosections	52
3.5.1.2	Embedding and cutting skin for paraffin sections.....	52
3.5.2	HAEMATOXYLIN AND EOSIN STAINING.....	53
3.5.3	LACZ STAINING.....	53
3.6	IMMUNOLOGICAL METHODS.....	54
3.6.1	IMMUNOFLUORESCENCE (IF)	54
3.6.1.1	Immunofluorescence on skin sections	54
3.6.1.2	Immunofluorescence on adherent cells.....	55
3.6.1.3	Immunofluorescence on suspension cells	55
3.6.1.4	Primary antibodies	55
3.6.1.5	Secondary antibodies	56
3.6.2	IMMUNOHISTOCHEMISTRY	56
3.6.2.1	BrdU staining.....	56
3.6.2.2	Terminal deoxynucleotidyltransferase-mediated dUTP nick end-labelling (TUNEL)	57
3.6.3	FLUORESCENCE ACTIVATED CELL SORTER (FACS)	57
3.7	CELLS AND CELL CULTURE METHODS	58
3.7.1	CELL LINES.....	58
3.7.2	CULTURE CONDITIONS AND MEDIA.....	58
3.7.2.1	Culturing of fibroblastoid cell lines and Phoenix cells	58
3.7.2.2	Culturing of ES cells and endodermal cells.....	59
3.7.2.3	Culturing of primary keratinocytes.....	59
3.7.2.4	Culturing of cells on coverslips	60
3.7.3	PASSAGING AND TRYPSINIZING OF CELLS.....	60
3.7.4	FREEZING OF CELLS.....	60
3.7.5	THAWING OF CELLS.....	61
3.8	BIOCHEMICAL METHODS	61
3.8.1	EXTRACTION OF PROTEINS FROM CELLS	61
3.8.1.1	Serum induced signalling.....	61
3.8.1.2	Wounding induced signalling	61
3.8.2	DETERMINATION OF PROTEIN CONCENTRATION	62
3.8.3	SDS-POLYACRYLAMIDE GEL ELECTROPHORESIS (SDS-PAGE).....	62
3.8.4	WESTERN BLOTTING (WB)	64
3.8.4.1	Immunostaining and chemoluminescence	64
3.8.5	PULL DOWN ASSAY	65

3.8.5.1	Rac1 pull down	66
3.8.5.2	RhoA pull down.....	67
3.9	CELL BIOLOGICAL METHODS	68
3.9.1	PRODUCTION OF RETROVIRUSES BY TRANSIENT TRANSFECTION	68
3.9.2	INFECTION OF FIBROBLASTOID CELL LINES BY RETROVIRUSES	70
3.9.3	GENERATION OF STABLE TRANSFECTED FIBROBLASTOID CELL LINES	70
3.9.4	ISOLATION OF PRIMARY KERATINOCYTES	70
3.9.4.1	Preparation of epidermal lysates for RNA preparation.....	71
3.9.5	CELL BIOLOGICAL ASSAYS.....	71
3.9.5.1	In vitro wound closure assay.....	71
3.9.5.2	Polarization assay.....	72
3.9.5.3	Adhesion assay.....	72
3.9.5.4	Spreading assay.....	72
3.10	BACTERIA CULTURE	72
3.10.1	BACTERIA STRAINS	72
3.10.2	BACTERIA CULTURE CONDITIONS AND MEDIA.....	73
3.10.2.1	Bacteria culture	73
3.10.2.2	Media	73
3.11	MOLECULAR BIOLOGY METHODS	73
3.11.1	OLIGONUCLEOTIDES	73
3.11.2	OLIGONUCLEOTIDES PHOSPHORYLATION AND ANNEALING	74
3.11.3	DIGESTION OF DNA WITH RESTRICTION ENZYMES.....	75
3.11.4	DEPHOSPHORYLATION OF 5`- ENDS	75
3.11.5	AGAROSE GEL ELECTROPHORESIS.....	75
3.11.6	EXTRACTION OF DNA FRAGMENTS FROM AGAROSE GEL.....	76
3.11.7	LIGATION OF DNA FRAGMENTS	76
3.11.8	PREPARATION OF COMPETENT BACTERIA	76
3.11.9	TRANSFORMATION OF BACTERIA.....	77
3.11.10	PREPARATION OF PLASMID DNA	78
3.11.10.1	Mini-preparation of plasmid DNA (miniprep).....	78
3.11.10.2	Maxi-preparation of plasmid DNA (maxiprep)	78
3.11.11	MUTAGENESIS.....	78
3.11.12	DNA SEQUENCING	79
3.11.13	GENOMIC DNA EXTRACTION.....	79
3.11.13.1	DNA isolation from tail snips	79
3.11.13.2	DNA isolation from cells	80
3.11.14	SOUTHERN BLOTTING.....	80

3.11.14.1	Digestion and transfer of the DNA	81
3.11.14.2	Radioactive probe labelling	82
3.11.14.3	Hybridisation, washing and signal detection	83
3.11.15	POLYMERASE CHAIN REACTION (PCR).....	83
3.11.16	RNA ISOLATION.....	84
3.11.17	REVERSE TRANSCRIPTASE POLYMERASE CHAIN REACTION (RT-PCR)	84
3.11.18	RNASE PROTECTION ASSAY	84
3.11.19	DNA MICROARRAY HYBRIDIZATION AND ANALYSIS	85
3.11.20	GENERATION OF THE TARGETING CONSTRUCTS FOR THE K1E15 AND K1E16 MOUSE STRAINS.	86
3.11.20.1	Generation of the cassette containing an artificial intron - exon border and neo resistance gene (pBluscript II KS / K1E15 and pBluscript II KS / K1E16)	86
3.11.20.2	Generation of constructs targeting exon 15 of the β 1 integrin gene	87
3.11.20.3	Generation of constructs targeting exon 16 of the β 1 integrin gene	88
3.12	MICROSCOPY	88
4	<u>RESULTS</u>	<u>90</u>
4.1	CDC42 IN CELL MIGRATION	90
4.1.1	GENERATION OF CDC42-DEFICIENT AND RECONSTITUTED FIBROBLASTOID CELL LINES	90
4.1.2	ALTERED MORPHOLOGY, BUT NORMAL ADHESION OF CDC42-NULL CELLS.....	92
4.1.3	CDC42 HAS ONLY LIMITED INFLUENCE ON SERUM INDUCED SIGNALLING PATHWAYS IN FIBROBLASTOID CELLS	96
4.1.4	DEFECTIVE RAC1 ACTIVATION IN THE ABSENCE OF CDC42	98
4.1.5	LOSS OF CDC42-NULL DOES NOT EFFECT RHOA ACTIVITY	99
4.1.6	NO COMPENSATORY EXPRESSION OF OTHER RHO GTPASES IN THE ABSENCE OF CDC42	99
4.1.7	CDC42-NULL CELLS HAVE NO MITOSIS DEFECT	100
4.1.8	LOSS OF CDC42 DOES NOT AFFECT THE FORMATION OF FILOPODIA AND LAMELLIPODIA	100
4.1.9	INCREASED BLEBBING AND TAIL RETRACTION DEFECTS IN CELLS EXPRESSING DNCD42	102
4.1.10	CDC42 IS NOT CRUCIAL FOR DIRECTED MIGRATION	104
4.1.11	CDC42 IS NOT ESSENTIAL FOR CELL POLARIZATION IN MIGRATING FIBROBLASTS, BUT CONTRIBUTES TO SINGLE CELL DIRECTIONALITY AND GOLGI RE-ORIENTATION	105
4.1.12	GOLGI RE-ORIENTATION IS NOT CORRELATING WITH INDUCED PHOSPHORYLATION OF GSK3 β	108
4.1.13	CDC42 IS NOT REQUIRED FOR EFFICIENT WOUND CLOSURE AND GOLGI RE-ORIENTATION DURING MIGRATION OF ENDODERMAL CELLS	111

4.2	STRUCTURE-FUNCTION RELATIONSHIP OF β1 INTEGRIN DURING MIGRATION IN VIVO AND IN VITRO	113
4.2.1	ANALYSIS OF β 1 INTEGRIN KNOCKIN MICE	114
4.2.1.1	Generation of the β 1 hypomorph mouse strain	114
4.2.1.2	Analysis of the wtKI mouse	116
4.2.1.3	Generation of the β 1 knockin mouse strains. Second approach	133
4.2.1.4	Analysis of the control knockin mice strains	140
4.2.1.5	Analysis of the mutant knockin mice strains	144
5	<u>DISCUSSION</u>	162
5.1	CDC42 CONTRIBUTES TO ACTIN CYTOSKELETON ORGANIZATION BUT IS NOT ESSENTIAL FOR INTEGRIN MEDIATED ADHESION, CELL SPREADING AND FILOPODIA FORMATION	162
5.1.1	CDC42 DOES NOT REGULATE INTEGRIN AVIDITY	162
5.1.2	FILOPODIA CAN FORM INDEPENDENTLY OF CDC42	163
5.1.3	REDUCED RAC1 ACTIVITY IN THE ABSENCE OF CDC42	164
5.1.4	CDC42 REGULATES CELL MORPHOLOGY	165
5.1.5	CDC42 AND CDC42 RELATED PROTEINS REGULATE TAIL RETRACTION IN MIGRATING CELLS	166
5.2	CDC42 IS NOT IMPORTANT FOR THE SPEED OF MIGRATION, BUT REGULATES TOGETHER WITH OTHER RHO GTPASES DIRECTIONALITY OF MIGRATION	166
5.2.1	CDC42 HAS NO MAJOR IMPACT ON WOUND CLOSURE SPEED	166
5.2.2	POLARIZED PROTRUSION FORMATION IN CDC42-NULL CELLS	167
5.2.3	CDC42 CONTRIBUTES TO GOLGI APPARATUS RE-ORIENTATION DURING WOUNDING INDUCED MIGRATION	168
5.2.4	GOLGI REORIENTATION IN FIBROBLASTOID CELLS DOES NOT CORRELATE WITH CHANGES IN GSK3 β PHOSPHORYLATION	169
5.3	REDUCED β1 INTEGRIN EXPRESSION IN RELATION TO KERATINOCYTE MIGRATION IN SKIN DEVELOPMENT AND MAINTENANCE IN VIVO AND IN KERATINOCYTES IN VITRO	170
5.3.1	REDUCTION OF β 1 INTEGRIN EXPRESSION RESULTS IN ABNORMAL SKIN DEVELOPMENT	170
5.3.2	β 1 INTEGRIN IS ESSENTIAL FOR THE FUNCTION OF STEM CELLS OF THE SKIN EPITHELIUM	172
5.3.3	REDUCED β 1 INTEGRIN EXPRESSION IS SUFFICIENT TO MEDIATE KERATINOCYTE MIGRATION IN VIVO	174
5.4	STRUCTURE-FUNCTION ANALYSIS OF THE β1 CYTOPLASMIC DOMAIN IN THE REGULATION OF KERATINOCYTE MIGRATION	175
5.4.1	β 1 INTEGRIN ACTIVATION AND INTEGRIN MEDIATED MIGRATION DOES NOT DEPEND ON INTEGRIN PHOSPHORYLATION IN KERATINOCYTES	175

5.4.2	LOSS OF SALT BRIDGE FORMATION BETWEEN $\beta 1$ INTEGRIN AND THE α SUBUNITS DOES NOT CASE $\beta 1$ INTEGRIN ACTIVATION IN KERATINOCYTES IN VIVO	179
5.4.3	DELETION OF THE PUTATIVE BINDING SITE FOR FAK ON THE $\beta 1$ INTEGRIN CYTOPLASMIC DOMAIN RESULTS IN A $\beta 1$ -NULL LIKE PHENOTYPE	180
6	<u>CONCLUSIONS</u>	182
7	<u>REFERENCES.....</u>	183
8	<u>SUPPLEMENTS</u>	198
8.1	SUPPLEMENTARY MATERIAL ON THE ATTACHED CD.....	198
9	<u>ACKNOWLEDGEMENTS.....</u>	199
10	<u>CURRICULUM VITAE.....</u>	200

A	Alanine	DMSO	Dimethylsulfoxide
AP-1	Activator Protein-1	DNA	Deoxyribonucleic Acid
APC	Adenomatous Polyposis Coli	DNase	deoxyribonuclease
APS	Ammonium Persulfate	dnCdc42	dominant negative Cdc42
AS/S	Antisense / Sense oligonucleotides	dNTP	Deoxynucleotide Triphosphate
ATP	Adenosine 5'-triphosphate	DOCK180	180-kDa protein downstream of Crk
BMP	Bone Morphogenetic Protein	DP	Dermal Papilla
bp	base pair	DTT	Dithiothreitol
BrdU	Bromodeoxyuridine	ECM	Extracellular Matrix
BSA	Bovine Serum Albumin	EDTA	Ethylenediamine Tetraacetic Acid
°C	degree Celsius	ELISA	Enzyme Linked Immunoabsorbent Assay
cAMP	cyclic Adenosine Monophosphate	Erk	Extracellular Regulated Kinase
cDNA	complementary DNA	ES cells	Embryonic Stem cells
CIB	Calcium and Integrin Binding Protein	FACS	Fluorescence Activated Cell Sorter
cm	centimetre	FAK	Focal Adhesion Kinase
CRIB	Cdc42/Rac Interactive Binding Motif	FCS	Foetal Calf Serum
Crk	Chicken Tumour Virus 10 Regulator of Kinase	FGF	Fibroblast Growth Factor
Δ	deletion	FIAU	1-2'-deoxy-2'-fluoro-b-D- arabinofuranosyl-5- iodouracil
D	Aspartic acid	fl	allele surrounded (floxed) by <i>loxP</i> sites
dd	double-distilled	FN	Fibronectin
DMBA	7,12-dimethylbenz [α] anthracene	g	gram
DMEM	Dulbecco's Modified Eagle's Medium	GAPs	GTPase-Activating Proteins
DAPI	4',6-Diamidino-2- phenylindole	GDI	Guanine Nucleotide- Dissociation Inhibitors
DEPEC	Diethylpyrocarbonate		

GEFs	Guanine Nucleotide– Exchange Factors	MAPK	Mitogen Activated Kinases
GFP	Green Fluorescent Protein	MCS	Multiple Cloning Site
GPCRs	G-protein coupled receptors	mDia	Mammalian Diaphanous
GST	Glutathion-S-Transferase	MEFs	Mouse Emryonic Fibroblasts
GTP	Guanosine Triphosphate	mg	milligram
h	hour	min	minutes
HEPES	N-(2-hydroxyethyl)-l- piperazineethanesulphonic acid	ml	millilitre
hpm	hypomorph	MLC	Myosin Light Chain
HRP	Horse Radish Peroxidase	MLCP	MLC Phosphatase
ICAP-1	Integrin Cytoplasmic Domain Associated Protein	MMP2	Matrix-Metalloproteinase-2
IF	Immunofluorescence	MRCK	Myotonic Dystrophy Kinase-Related Cdc42 Binding Kinase
ILK	Integrin Linked Kinase	mRNA	messenger RNA
IPTG	Isopropylthiogalactoside	MT	Microtubules
IRS	Inner Root Sheath	MTOC	Microtubule–Organising Centre
Irsp53	Insulin Receptor Substrate p53	n	number
JNK	c-JUN kinase	neo	neomycin resistance gene
K5	Keratin 5	ng	nanogram
K14	Keratin 14	nm	nanometre
kB	kilobase	NMR	Nuclear Magnetic Resonance
kDa	kilodalton	O/N	over night
KI	Knockin	OD	optical density
KO	Knockout	ORS	outer root sheath
l	litre	p	phospho-
LB	Luria – Bertani Medium	pA / polyA	polyadenylation signal
LN 5	Laminin 5	PAK	p21-Activated Ser/Thr Kinase Interacting Protein
loxP	locus of crossing-over of bacteriophage P1	PBS	Phosphate Buffered Saline
µl	microlitre	PCR	Polymerase Chain Reaction
µm	micrometer	PFA	Paraformaldehyd

PGK	murine Phosphoglycerate Kinase Promoter	SH	Src Homology Domain
PIP2	Phosphatidylinositol (4,5) Bisphosphate	SPF	Specified Pathogen Free
PIPKIγ-90	Phosphate Kinase Type I γ -90	SV	Simian Virus
PIX	PAK-Interactive Exchange Factor	T	Threonine
PKC	Protein Kinase C	TBS	Tris Buffered Saline
pmol	picomol	TEMED	N,N,N',N'-t etramethylethylenediamine
POD	Horseradish Peroxidase	tk	Herpes Simplex Virus thymidine kinase gene
PTB	Phosphotyrosine Binding Proteins	TPA	12- <i>O</i> - Tetradecanoylphorbol-13- Acetate
PtdIns4P	Phosphatidylinositol 4-phosphate 5-kinase	Tris	Tris- hydroxymethylamino- methane
PTP	Protein Tyrosine Phosphatase	TUNEL	terminal deoxynucleotidyl- transferase-mediated dUTP nick end-labelling
R	Arginine	U	Unit
RBD	Rho-GTP Binding Domain	uPA	Plasminogen Activator
RNA	Ribonucleic Acid	uPAR	Plasminogen Activator Receptor
RNAi	RNA interference	V	Volt
RNase	ribonuclease	W	Watt
ROCK	Rho Kinase	WASP	Wiskott–Aldrich-Syndrome Protein
RPA	RNase protection assay	wt	wilde type
RPM	Rotations per Minute	Y	Tyrosine
RT	Room Temperature		
RTKs	Receptor Tyrosine Kinases		
RT-PCR	Reverse Transcription PCR		
s or sec	second		
S	Serine		
SDS	Sodium Dodecyl Sulphate		
SDS-PAGE	SDS-Polyacrylamide Gel Electrophoresis		
SFKs	Src Family Kinases		

1 Summary

Cell migration plays a central role in the development and maintenance of multicellular organisms. It involves regulated cell adhesion, mediated by integrins, and polarized changes of the cytoskeleton, controlled by Rho GTPases such as Cdc42. Aim of this study was to investigate the role of integrins and Cdc42 in cell migration and in particular the cross-talk between these molecules. In addition, the structure–function relationship of $\beta 1$ integrin in mediating migration associated events was studied.

To test whether Cdc42 is essential for directed cell migration in mammalian cells and to investigate the cross-talks between integrin and Cdc42 mediated signalling, fibroblastoid cell lines lacking a functional Cdc42 gene were established and analyzed in wound closure assays. Contrary to the expectations, we could show that Cdc42 is neither required for integrin activation nor for integrin mediated protrusion formation. Moreover, Cdc42 has no significant influence on the speed of directed migration. However, it contributes to the directionality of migration and to the re-orientation of the Golgi apparatus into the direction of migration by a mechanism independent of Gsk3 β phosphorylation. Furthermore, we demonstrated that Cdc42 controls cell morphology, quite likely by regulating Rac1 activity.

Expression of dominant negative Cdc42 (dnCdc42) in Cdc42-null cells revealed that dnCdc42 non-specifically inhibits other Rho GTPases besides Cdc42, since it aggravates the impairments observed in Cdc42-null cells, resulting in strongly reduced directed migration, severely reduced single cell directionality, and complete loss of Golgi polarization and of directionality of protrusion formation towards the wound.

$\beta 1$ integrins were previously shown to activate Cdc42 in response to wounding and thus to regulate the directionality of migration. We demonstrated now, that fourfold reduction of $\beta 1$ integrin expression in keratinocytes *in vivo* did not impair wound healing. However, keratinocyte stem cells with normal levels of $\beta 1$ integrin had a competitive advantage over the hypomorphic cells and expanded steadily in the skin of mice harbouring both cell types in the epidermis.

Finally, we analysed the importance of specific amino acids of the intracellular domain of $\beta 1$ integrin in keratinocytes *in vivo* by generating 8 mice strains which in skin express only point or deletion mutants of $\beta 1$ integrin. Our data are for the most part strikingly different from previous results obtained *in vitro* and significantly revise proposed models for the role of serine and tyrosine phosphorylation and the function of a salt bridge between the integrin α subunits and the integrin β tails.

2 Introduction

2.1 Integrins

Integrins are heterodimeric adhesion receptors formed by non-covalent association of an α and a β subunit. Each subunit is a type I transmembrane glycoprotein with a large extracellular domain (700 – 900 amino acids) responsible for ligand binding, a single transmembrane domain and a cytoplasmic domain that consists of 20 – 60 amino acid residues, with the exception of the $\beta 4$ integrin which with ~ 1000 amino acids is much larger. Integrins are restricted to metazoans and the number of integrins in the genome increases with the complexity of the organism. Mammals contain 18 α and 8 β subunits that combine to 24 different heterodimers with different, sometimes overlapping specificities (Figure 2.1 B). Among the integrin ligands are extracellular matrix (ECM) molecules, cell-surface receptors and soluble protein ligands. Integrins mediate signal transduction through the cell membrane in both directions (Figure 2.1 A): binding of ligands to integrins transmits signals into the cell and results in cytoskeletal re-organization, gene expression and cellular differentiation (outside-in signalling); on the other side, integrins can also propagate signals from inside the cell, leading to a change in integrin ligand binding affinity and cell adhesion (inside-out signalling; Hynes, 2002; Travis et al., 2003; Calderwood, 2004).

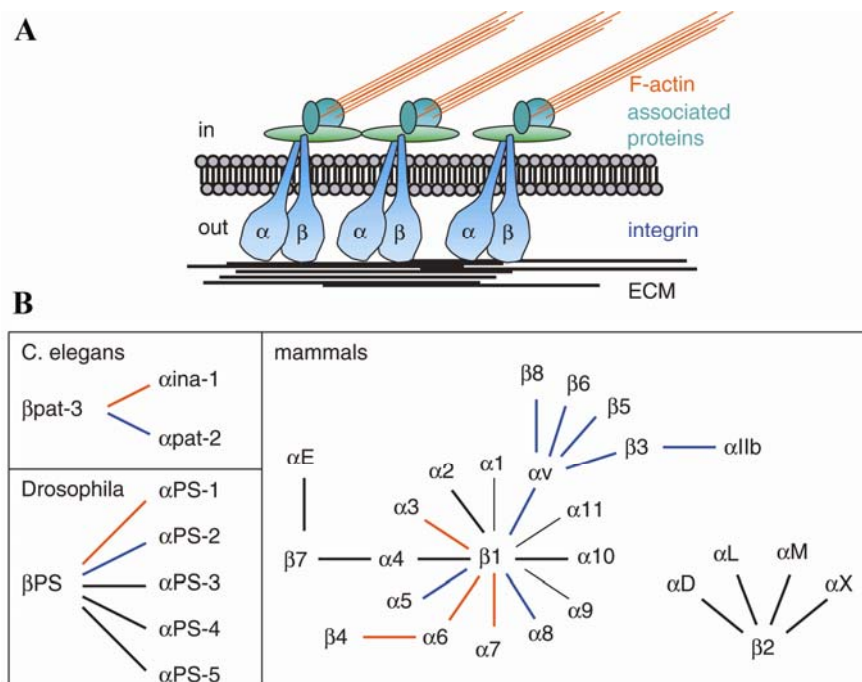


Figure 2.1 (A) Schematic representation of cell-matrix adhesion in which integrins connect the ECM with the actin cytoskeleton. (B) The integrin family. In blue, RGD-binding proteins; in red; laminin-binding integrins (modified from Danen and Sonnenberg, 2003).

2.1.1 Integrin cytoplasmic domains

Extensive mutational analysis has demonstrated that despite the fact that integrin cytoplasmic tails are much smaller than their extracellular domains they play a pivotal role in integrin functions. The absence of any detectable enzymatic activity in integrin cytoplasmic tails suggests that integrin mediated signalling requires direct binding of signalling proteins. Indeed, the cytoplasmic domains of integrins were found to bind to cytoskeletal and signalling molecules. To date at least 21 proteins are known to bind to one or more integrin tails, among them the actin-binding proteins α -actinin and filamin, adaptor proteins like ILK, FAK or talin, few enzymes and transcriptional co-activators (Table 1). Most of these proteins bind to β subunits. The cytoplasmic integrin tails are not only crucial for outside-in signalling, but also for inside-out signalling (Liu et al., 2000; Hynes, 2002).

Binding partner	Integrin tail	Detection	Reference
Actin-binding protein			
Talin	$\beta_{1A}, \beta_{1D}, \beta_2, \beta_3$	COIP, PEP, EQ, INT, SLS	Horwitz et al., 1986; Knezevic et al., 1996; Pfaff et al., 1998; Goldmann, 2000
Filamin	$\beta_{1A}, \beta_2, \beta_3, \beta_7$	COIP, PEP, 2HYB, SLS	Pavalko et al., 1989; Loo et al., 1998; Pfaff et al., 1998; Goldmann, 2000
α -actinin	β_{1A}, β_2	PEP, INT, COIP, SLS	Otey et al., 1990; Pavalko et al., 1991; Cattelino et al., 1999
F-actin	α_2	PEP	Kieffer et al., 1995
Myosin	β_3	PEP, COIP	Jenkins et al., 1998; Sajid et al., 2000
Skelemin	β_1, β_3	2HYB, PEP	Reddy et al., 1998
Signaling protein			
ILK	β_1, β_3	2HYB, COIP	Hannigan et al., 1996
FAK	$\beta_1, \beta_2, \beta_3$	PEP, COIP	Schaller et al., 1995; Chen et al., 2000
Cytohesin-1	β_2	2HYB, COIP, PEP	Kolanus et al., 1996
Cytohesin-3	β_2	2HYB	Hmama et al., 1999
Other protein			
Paxillin	$\beta_1, \beta_3, \alpha_4$	PEP, COIP	Schaller et al., 1995; Chen et al., 2000; Liu et al., 1999
Grb2	β_3	PEP	Law et al., 1996
Shc	β_3	PEP	Law et al., 1996
β_3 -endonexin	β_3	2HYB, INT, PEP	Shattil et al., 1995; Eigenthaler et al., 1997
TAP-20	β_5	PEP	Tang et al., 1999
CIB	α_{IIb}	2HYB, PEP, COIP	Naik et al., 1997; Shock et al., 1999; Valler et al., 199
Calreticulin	α	PEP, COIP	Rojiani et al., 1991; Leung-Hagesteijn et al., 1994; Coppolino et al., 1995
Caveolin-1	α	COIP	Wary et al., 1998
Rack1	$\beta_1, \beta_2, \beta_5$	2HYB, PEP, COIP	Liliental et al., 1998
WAIT-1	β_7	2HYB, PEP	Rietzler et al., 1998
JAB1	β_2	2HYB, PEP, COIP	Bianchi et al., 1998
Melusin	$\beta_{1A}, \beta_{1B}, \beta_{1D}$	2HYB, INT	Brancaccio et al., 1999
MIBP	β_{1A}, β_{1D}	2HYB, PEP, COIP	Li et al., 1999
ICAP-1	β_{1A}	2HYB, PEP, INT	Chang et al., 1997; Zhang and Hemler, 1999
CD98	β_{1A}, β_3	PEP	Zent et al., 2000
DRAL/FHL2	$\alpha_{3A}, \alpha_{3B}, \alpha_{7A}, \beta$	2HYB, PEP	Wixler et al., 2000

COIP--Coimmunoprecipitation; PEP--Synthetic/recombinant peptide studies; 2HYB--Yeast two-hybrid screen; INT--Binding to purified integrins; SLS--Static light scattering; EQ--Equilibrium gel filtration.

Table 1 List of proteins which bind to the integrin cytoplasmic domain (modified from Liu et al., 2000).

There is a great deal of sequence similarity between the β -subunit tails, whereas α -subunits share little sequence similarity, except for the membrane proximal $K\pi$ GFFKR sequence, in which π represents a conserved apolar residue (Figure 2.2; Humphries et al., 2003).

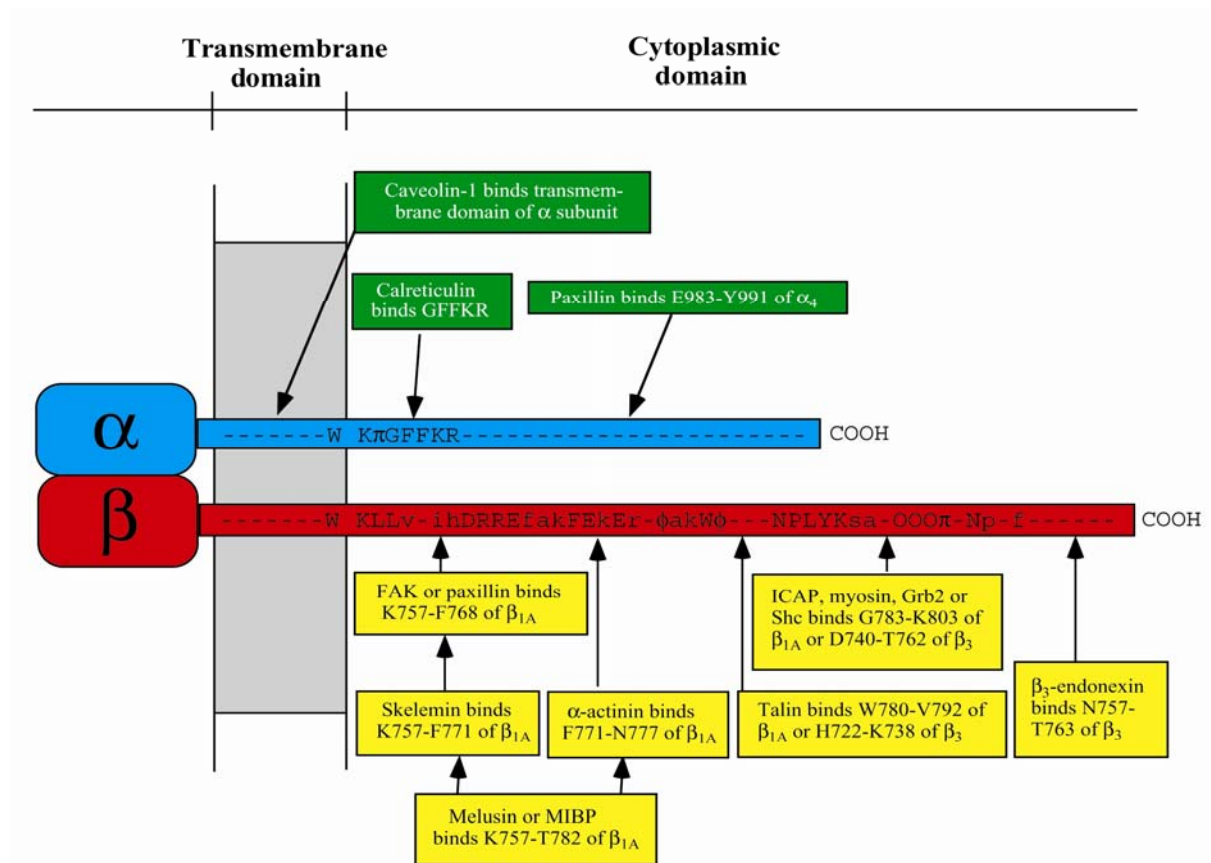


Figure 2.2 Binding sites on integrin α and β subunits for integrin cytoplasmic domain binding proteins. The reported interacting sites on integrin tails for integrin–tail–binding proteins are indicated by boxes and arrows: conserved amino acids sequences among integrin α and β cytoplasmic domains are indicated by uppercase letters (invariant residues) or lowercase letters (residues conserved in at least three subunits). O represents hydroxylated residues; π and Φ represent conserved apolar and polar residues, respectively. Dashes represent unconserved residues and / or gaps (modified from Liu et al., 2000).

2.1.2 Integrin activation

The integrin cytoplasmic domains control the transition of integrins from a resting to a ligand–binding competent state (Travis et al., 2003). Both biochemical and structural studies have shown that integrin cytoplasmic tails contact each other and that these interactions are abolished if the conserved GFFKR motif of the α -subunit is deleted (Vallar et al., 1999; Ginsberg et al., 2001). NMR studies revealed that the primary interactions are located at the α -helical membrane–proximal regions of the subunits which interact with each other via a combination of hydrophobic and electrostatic interactions, thus locking the integrins in a low–affinity state. The separation of the tails and / or transmembrane domains is suggested to cause integrin activation (Vinogradova et al. 2002; Gottschalk, 2005). Mutational analysis of the conserved R995 of the α IIB tail GFFKR motif and the D723 of the β_3 tail KLLITIH motif implicated the formation of a salt bridge between these two residues (Figure 2.3).

Charge reversals of either residue leads to activation of $\alpha\text{IIb}\beta_3$, whereas swapping the residues between tails does not result in activation (Hughes et al., 1996). Loss of the interaction between αIIb and β_3 tail upon introduction of the R995D mutation into the αIIb chain is also observed by NMR (Vinogradova et al. 2002). Similarly, mutation of the corresponding D753 on the β_1 chain results in an activated integrin (Sakai et al., 1998a and 1998b). However, the R to D mutation in the $\alpha_6\text{A}$ tail fails to activate $\alpha_6\text{A}\beta_1$ and mutation of the D residue in β_2 does not activate ligand binding in $\alpha\text{L}\beta_2$ or $\alpha\text{M}\beta_2$, suggesting different activation mechanisms in distinct integrin receptors (De Melker et al., 1997; Lu et al., 2001; Travis et al., 2003).

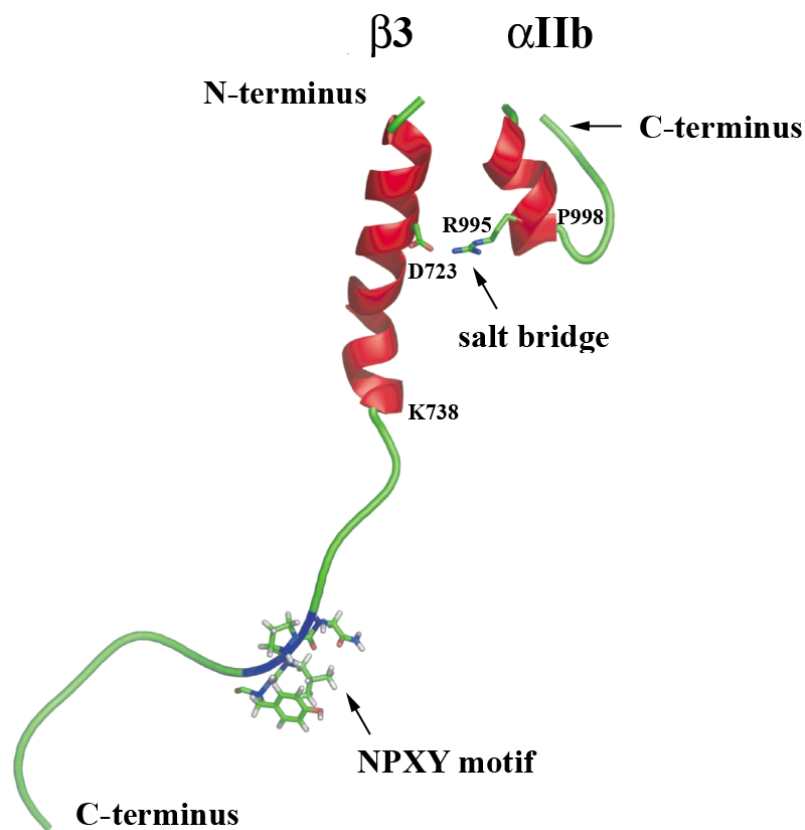


Figure 2.3 The structure and interactions of the integrin $\alpha\text{IIb}\beta_3$ cytoplasmic tail complex. The salt bridge between the D753 residue on the β_3 tail and the R995 residue on the αIIb chain that connects the two subunits as well as the NPXY motif are highlighted. Both tails possess N-terminal helical structures that terminate at P998 and K738 for the αIIb and β_3 subunits, respectively. This N-terminal helical structure of the αIIb cytoplasmic domain is followed by a turn that allows its acidic C-terminal portion to interact with its positively charged N-terminal region. By contrast NMR analysis of recombinant β_3 tails revealed that the N-terminal helical structure of the β_3 cytoplasmic domain is followed by a disordered C terminus, except for a turn that follows a conserved NPXY motif (modified from Travis et al., 2003 and Humphries et al., 2003).

Some of intracellular proteins that have been reported to bind to integrin cytoplasmic domains can influence integrin affinity by inside-out signalling. In particular, binding of the calcium

and integrin binding protein (CIB), $\beta 3$ endotoxin, cytohesin-1 and talin to integrin β -subunit cytoplasmic domains have been shown to result in activation of the integrin (Travis et al., 2003). A crucial role of talin was confirmed by RNAi knockdown of this protein, which in a variety of cell types results in inactive $\beta 1$ and $\beta 3$ integrins. Talin is an antiparallel homodimer of two ~ 270 kDa subunits with the major integrin-binding site within the talin head (Tadokoro et al., 2003; Calderwood, 2004). NMR studies revealed that binding of talin is able to efficiently compete with the α IIb tail for binding to the $\beta 3$ tail, thereby disrupting the interaction between the two tails resulting in integrin activation. Also the binding site on the $\beta 3$ tail was identified by structural analysis, encompassing a highly conserved NPXY motif of the tail (Figure 2.3; Vinogradova et al., 2002; Garcia-Alvarez et al., 2003). Tyrosine to alanine mutations in this motif strongly inhibit integrin activation and induce structural changes at the NPXY site and within the membrane-proximal region (Ulmer et al., 2001; Calderwood, 2004). Mutations in the NPXY motif perturb also the binding of several proteins to β integrin tails, among them talin (Liu et al., 2000). Several potential mechanisms are proposed to regulate talin-integrin interactions (Figure 2.4). One of them involves phosphorylation of integrins. Phosphorylation of the avian integrin tail NPXY motif inhibits talin binding (Tapley et al., 1989). V-Src infection of mammalian fibroblastoid cells results in tyrosine phosphorylation of $\beta 1$ integrin, reduced cell adhesion, displacement of integrins from focal adhesions and defective migration (Sakai et al., 2001). However, tails containing non-phosphorable NPXF motifs retain talin binding activity and can be activated by physiological stimuli (Calderwood, 2004). Since, v-Src was also shown to promote phosphorylation of the Ser/Thr cluster in-between the NPXY motifs (Sakai et al., 2001), integrin phosphorylation may be an important negative regulator of integrin activation (Calderwood, 2004). In addition to the phosphorylation mechanism, talin release from the β integrin tails is postulated to be regulated by competitive binding of other integrin NPXY motif binding proteins (PTB, phosphotyrosine binding proteins) like the integrin cytoplasmic domain associated protein (ICAP-1; Calderwood, 2004). ICAP-1 binding is proposed to inhibit $\beta 1$ integrin-talin association and since ICAP-1 is never found at adhesion sites it is suggested to dissolve these sites (Bouvard et al., 2003). These data indicate that ICAP-1 is a negative regulator of $\beta 1$ integrin avidity by preventing talin-mediated connection to the cytoskeleton and talin mediated signalling events. Another possible candidate for regulation of the integrin-talin interaction is the enzyme phosphatidylinositol phosphate kinase type I γ -90 (PIPKI γ -90), which was shown to compete with integrin β tails for overlapping binding sites in the talin

head domain. Thus, under some conditions PIPKI γ -90 might inhibit integrin activation by displacing talin from β tails (Barsukov et al., 2003).

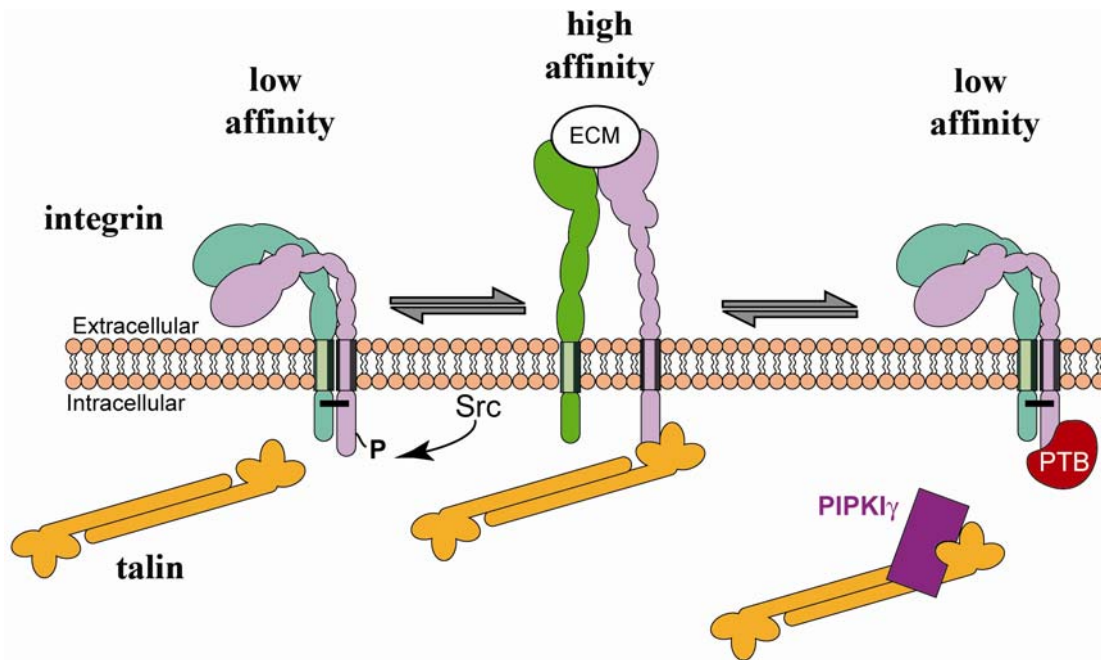


Figure 2.4 Possible mechanism of talin binding inhibition. C-src mediated phosphorylation (P) of integrin NPXY motifs, competition with other β tail binding proteins (PTB) or other talin binding proteins (PIPKI γ -90) may prevent integrin-talin interaction and inhibit integrin activation (modified from Calderwood, 2004).

2.1.3 Integrin signalling

Integrin interaction with ECM components at adhesion sites leads to the indirect attachment of integrins to the actin cytoskeleton, integrin clustering and to the recruitment of signalling molecules resulting in the activation of numerous signalling molecules including Rho GTPases, focal adhesion kinase (FAK), extracellular regulated-kinase (Erk), tyrosine phosphatases, cyclic AMP (cAMP)-dependent protein kinase, protein kinase C (PKC) as well as the production of phosphatidylinositol (4,5) bisphosphate (PIP₂). Through all these pathways integrin mediated adhesion to the ECM influences growth, differentiation, survival, cell shape and cell migration of diverse cell types including epithelial cells, endothelial cells, fibroblasts and other mesenchymal cell types (DeMali et al., 2003; Lee and Juliano, 2004). However, the signalling cascades initiated by integrins are often cell type specific and very complex. In addition, many aspects of integrin signalling are still only poorly understood, although data reported over the past years gave some interesting insight into the variety of possibilities how integrins provide signalling to promote cell migration and survival (Figure 2.5).

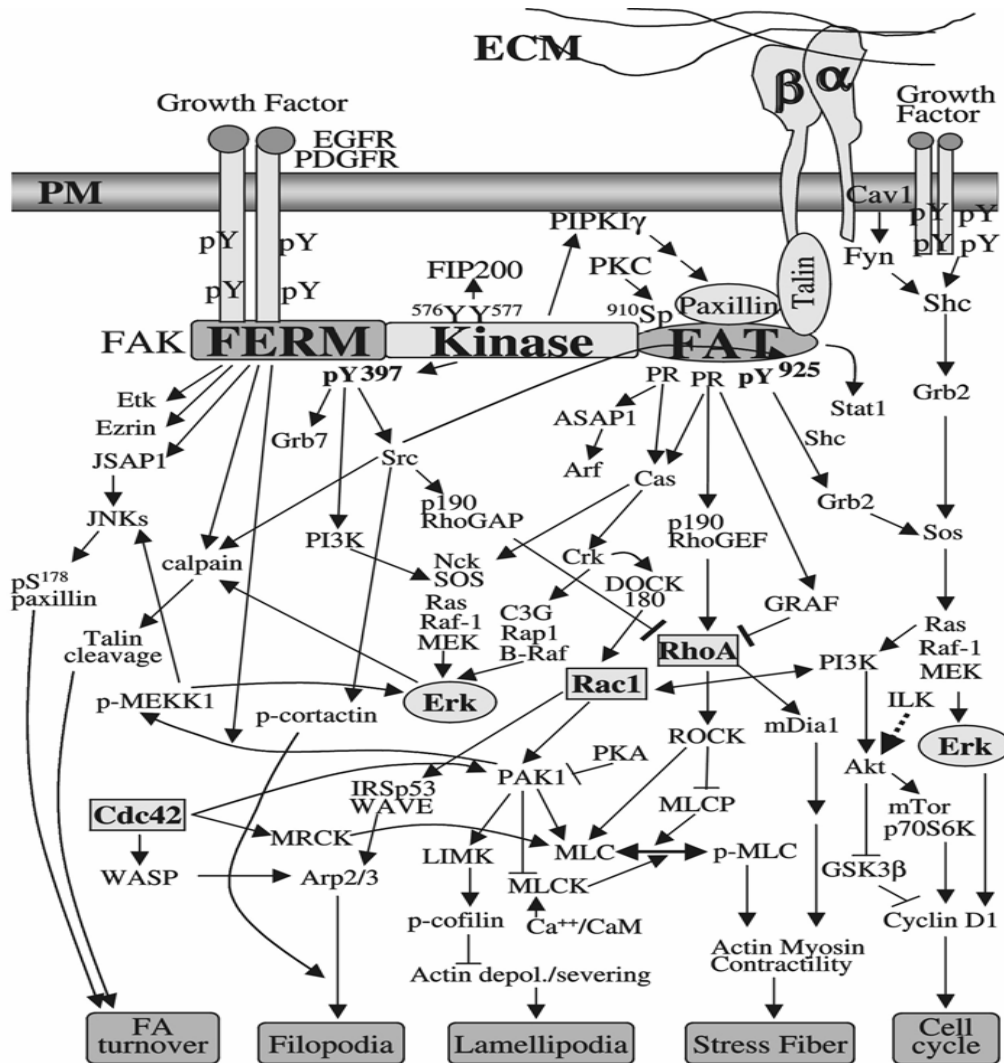


Figure 2.5 Intracellular signalling pathways regulated by either direct integrin mediated cell adhesion alone, or in collaboration with growth factor receptor mediated pathways (modified from Lee and Juliano, 2004).

Early events of the integrin signalling are mediated by Src kinases, tyrosine phosphatases and FAK. FAK is a non-receptor kinase that locates predominately in focal adhesions of adherent cells and is the major phospho-tyrosine protein activated by cell adhesion. FAK activation is characterised by autophosphorylation on position Y397 and is proposed to be regulated by integrins and the receptor tyrosine kinases (RTKs). The activation of FAK, therefore, integrates signals from integrins and RTKs (Brakebusch and Fässler, 2003; Guo and Giancotti, 2004). FAK is proposed to serve as an integrin-regulated scaffold that recruits Src family kinases (SFKs) to focal adhesions and positions them close to target-effectors that are crucial for cell migration and survival (Figure 2.5; Sieg et al., 2000).

Among other downstream targets FAK induces the phosphorylation of p130CAS which recruits Crk (chicken tumour virus 10 regulator of kinase) and leads to the activation of Rac, which is important for lamellipodial extension during migration (Cary et al., 1998; Klemke et al., 1998). In addition, the FAK-SFK signalling causes activation of the tyrosine kinase ETK.

Although the mechanism of action of this kinase is not known, ETK is expressed at high levels in metastatic carcinoma cells, and its suppression blocks the migration of carcinoma cells (Chen et al., 2001). Integrin dependent activity of Src-like kinases was also shown to induce the formation of a Cdc42, Par6 and PKC ζ complex, which through its action on Gsk3 β and adenomatous polyposis coli (APC) regulates the microtubular network and thereby directed movement of cells (Etienne-Manneville and Hall, 2003). Integrin mediated cell adhesion activates mitogen activated kinases (MAPK) including Erk1/2, c-JUN kinase (JNK) and p38 MAPK through the activity of FAK and Shc (Giancotti and Ruoslahti, 1999; Miranti and Brugge, 2002). Activation of MAPK leads to change in the expression of genes, which are critical for cell growth and differentiation. Moreover, MAPK have been shown to be involved in cell spreading and cell migration. Erk and JNK regulate cell migration by phosphorylating cytoskeletal components as well as by modifying gene expression. Erk is reported to induce contraction of actomyosin fibres through its activity on myosin light chain (MLC) kinase and JNK is implicated in the turnover of focal adhesions by phosphorylation of paxillin, which promotes this process (Klemke et al., 1997; Huang et al., 2003). In addition to their cytoplasmic functions, Erk and JNK also control cell migration through induction of activator protein-1 (AP-1) dependent gene expression (Li et al., 2003).

The connection of integrins to the actin cytoskeleton and the elicitation of signalling cascades are not separated events. In fact, recent research revealed that these processes are highly integrated and it is often not possible to distinguish “cytoskeletal” from “signalling” molecules. Actin binding proteins like talin or filamin link the integrins to the cytoskeleton. On the other hand, however, they bind to signalling molecules such as PIPKI γ -90 and are crucial for their activation. ILK-parvin, α -actinin, talin and filamin connect integrins to filamentous actin. Binding to vinculin, α -actinin and talin provides also a link to the Arp2/3 complex, which mediates actin nucleation. Furthermore, activation of Rho GTPases via ILK, filamin or downstream of talin, mediates changes in the organization of the cytoskeleton (Figure 2.6; Brakebusch and Fässler, 2003).

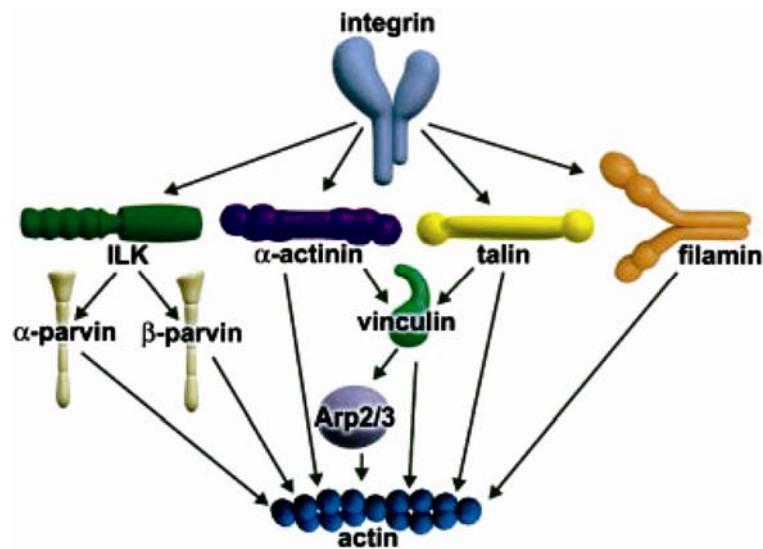


Figure 2.6 Overview of different pathways by which integrins can link to the actin cytoskeleton (modified from Brakebusch and Fässler, 2003).

ILK and talin are good examples for the complex relationship between integrins and their associated molecules. Upon integrin activation, which itself depends on talin binding to integrin, talin associates with PIPKI γ -90, which produces PIP₂. PIP₂ in turn strengthens the interaction between integrin and talin and recruits vinculin to talin. The interaction with talin facilitates vinculin binding to actin and recruits the Arp2/3 complex to sides of integrin clustering, which stimulates actin polymerization. This interaction is transient and requires both PIP₂ binding to vinculin and activation of the Arp2/3 complex by the small GTPase Rac1. In addition, talin binds also directly to filamentous actin via a distinct binding site in the tail region (Figure 2.7; DeMali et al., 2003; Brakebusch and Fässler, 2003).

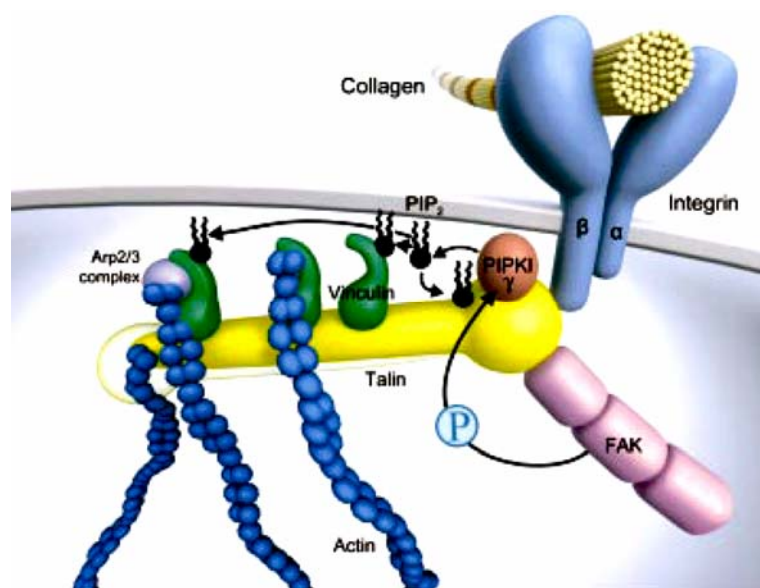


Figure 2.7 Talin and vinculin provide the link between actin polymerization machinery and integrins. Activated Arp2/3 complex binds directly to the hinge region of vinculin, an adhesion molecule that is recruited to integrins

via an interaction with talin. Binding of the Arp2/3 complex to vinculin does not stimulate the activity of the Arp2/3 complex, but rather localizes polymerization to new sites of integrin adhesion (modified from Brakebusch and Fässler, 2003)

ILK is known to be a crucial integrin-binding partner mediating integrin signalling (Grashoff et al., 2004). ILK is forming a ternary complex with PINCH and parvin, and it is this complex that mediates nearly all effects of ILK (Figure 2.8). ILK binding to PINCH and parvin stabilizes the complex and localizes it to the plasma membrane by ILK mediated binding to $\beta 1$ and $\beta 3$ integrins (Grashoff et al., 2004). PINCH in turn, binds with low affinity to the SH2/SH3 adaptor protein Nck2, which interacts with growth factor receptors and recruits a large number of modulators such as DOCK180 (180-kDa protein downstream for Crk), a protein activating Rho GTPases, and the p21-activated Ser/Thr kinase interacting protein PAK, an effector of Rho GTPases (Tu et al., 1998; Velyvis et al., 2003). However, whether Nck2 interacts with PINCH *in vivo* is not clear (Grashoff et al., 2004). Parvins on the other hand, bind to paxillin and F-actin. In addition, β -parvin was shown to interact with the guanine nucleotide-exchange factor α -PIX (PAK-interactive exchange factor α) and thereby activate Rac1 and Cdc42 to reorganise the actin cytoskeleton (Rosenberger et al., 2003). Furthermore, integrin binding to ILK induces the phosphorylation of Gsk3 β and Akt, maybe independent of the kinase function of ILK (Figure 2.8; Grashoff et al., 2004).

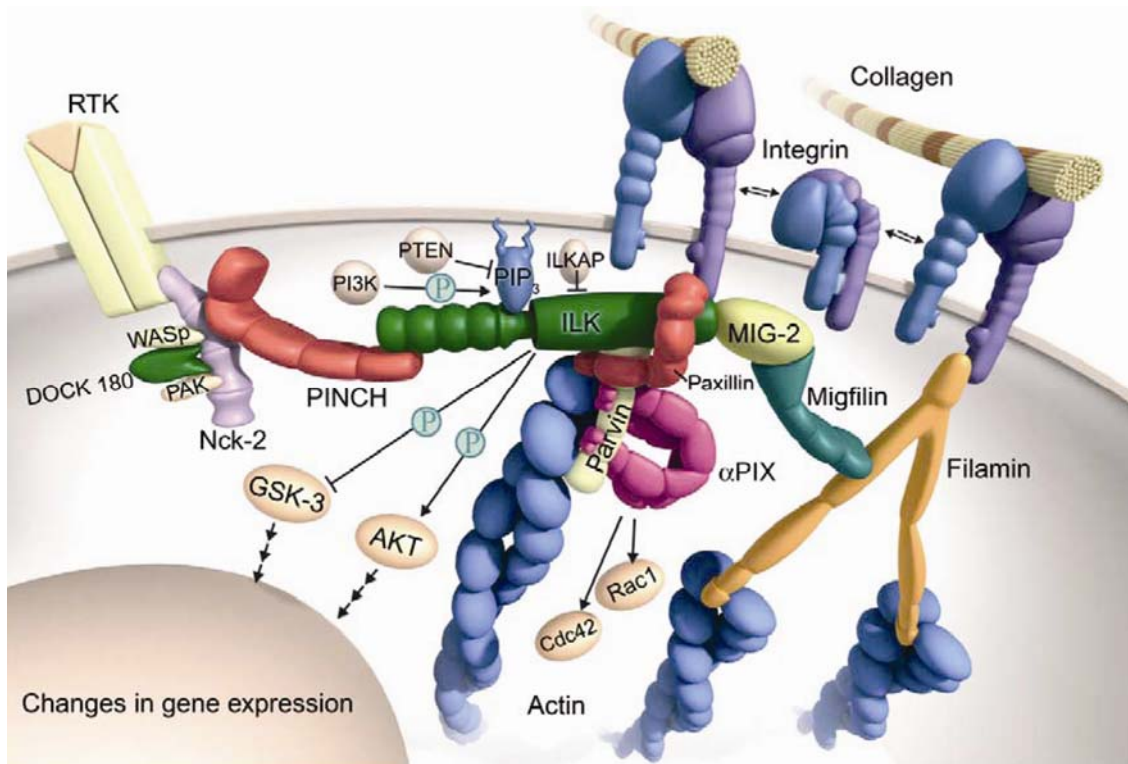


Figure 2.8 ILK binds Pinch and parvin and this ternary complex subsequently locates to the plasma membrane through the interaction with the cytoplasmic domain of activated $\beta 1$ and $\beta 3$ integrin subunits as well as unknown

FAs component(s). Binding to phospholipids results in the activation of the kinase function of ILK, which in turn leads to the phosphorylation of GSK3 β and PKB/Akt. Finally, ILK can recruit several adaptor proteins, which are able to regulate actin dynamics or actin attachment to FAs (modified from Grashoff et al., 2004).

The Rho GTPases represent an important group of downstream effectors of integrins. Integrin dependent activation of Cdc42 and Rac1 was shown to induce cell spreading through the formation of filopodia and lamellipodia protrusions, respectively (Price et al., 1998). Both Cdc42 and Rac1 promote actin polymerization through the actin-nucleating Arp2/3 complex at the leading edge of migrating cells and by coupling the actin cytoskeleton regulate integrin clustering and integrin mediated adhesion (Schwartz and Shattil, 2000). Integrin mediated activation of Rho, on the other hand induces the assembly and contraction of the actomyosin fibres, which pulls the trailing edge into the direction of migration. Two Rho effectors, Rho kinase (ROCK) and mammalian diaphanous (mDia), function cooperatively to induce the assembly of actomyosin fibres. The formin mDia stabilizes microtubules, whereas ROCK inhibits MLC phosphatase (MLCP) and promotes so the phosphorylation of MLC and contraction of actomyosin fibres. Phosphorylation of myosin promotes its interaction with actin filaments, which then leads to cell contraction (Figure 2.5; Raftopoulou and Hall, 2004). Moreover, integrin mediated activation of small GTPases has also been shown to be importantly involved in G1/S cell cycle transition (Figure 2.5; Juliano et al., 2004 and Lee and Juliano, 2004).

2.1.4 Integrins in skin

The skin covers the entire body and protects it from dehydration, injury and infection. Mammalian skin consists of two different components, the epidermis which is the outer part of the skin and the dermis which is the lower, thicker part of the skin. The epidermis is anchored to the basement membrane composed of extracellular matrix proteins, which separates the epidermis from the dermis. Below the dermis is the subcutis, which through its fat tissue connects the skin to the underlying muscles and tendons.

The epidermis consists of several layers of keratinocytes at various stages of differentiation. Melanocytes, Langerhans cells and Merkel cells account for only 5% of all cells found in the epidermis. The keratinocyte layer of cells directly contacting the basement membrane, the basal layer, contains stem cells and transiently amplifying cells (Figure 2.9). The stem cells ensure the self renewal of epidermis by giving rise to the proliferating keratinocytes, the transiently amplifying cells. As these cells cease proliferation they initiate terminal differentiation, upregulate the synthesis of certain keratins which assemble into intermediate filaments and migrate upwards into the suprabasal layers. These suprabasal keratinocytes are

connected by desmosomes. During terminal differentiation, an apoptosis related process, they deposit and enzymatically cross-link proteins beneath the plasma membrane to form a cornified envelope. In addition, they secrete granules filled with lipids which seal the cell-cell borders. Eventually these keratinocytes die and become cornified squames that constitute the cornified layer and are subsequently shed from the surface of skin. In mouse skin the entire differentiation process takes 10 – 14 days (Gandarillas et al., 2000; Alonso and Fuchs, 2003b).

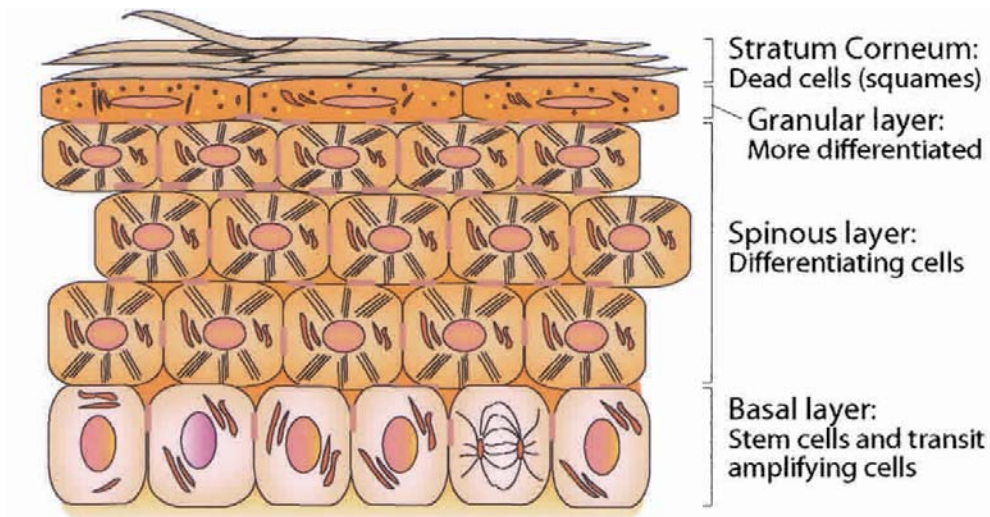


Figure 2.9 Schematic of the epidermal organization. Transit-amplifying cells in the basal layer of epidermis and the terminally differentiated cells are shown (modified from Alonso and Fuchs, 2003a).

An important appendage of the mammalian epidermis is the hair follicle that develops from the embryonic epidermis as an epithelial finger in response to signals arising in both the primitive epithelium and the underlying mesoderm. The anagen hair follicle consists of an upper permanent part above the muscle insertion and a lower, cycling portion that produces the hair (Figure 2.10 A). The outermost structure of the follicle is the outer root sheath (ORS), which is contiguous with and biochemically similar to the basal keratinocyte layer of the epidermis. The innermost layers of the hair follicle include three concentric layers of inner root sheath (IRS) and three concentric layers of hair-producing cells. Adjoining the ORS on the dermal side is a basket-like arrangement of two orthogonally arrayed layers of collagen fibres, the dermal sheath (Stenn and Paus, 2001; Alonso and Fuchs, 2003a; Rogers, 2004).

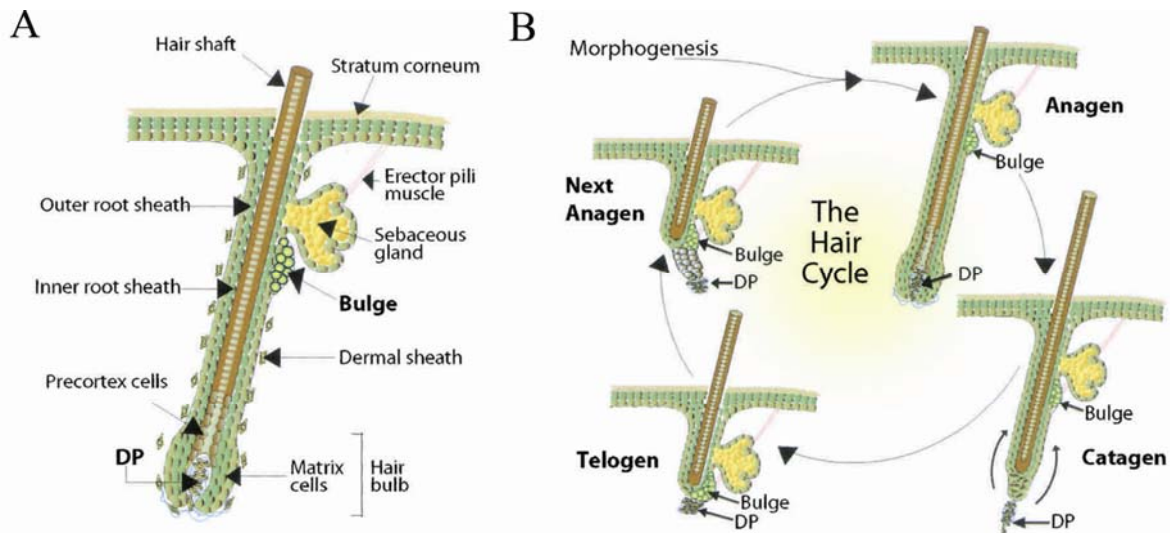


Figure 2.10 (A) Schematic of an anagen hair follicle. In the anagen hair follicle the dermal papilla (DP) is enclosed within the hair bulb, and the stem cell containing bulge is nested below the sebaceous gland. (B) Cycling hair follicle. During the hair cycle, the proximity of the DP and the bulge varies, with the closest contact occurring at telogen as the follicle prepares for a new anagen (modified from Alonso and Fuchs, 2003a).

All mature follicles undergo a growth cycle consisting of phases of growth (anagen), regression (catagen), rest (telogen), and shedding (exogen; Figure 2.10 B). During the growth phase of the hair cycle, keratinocyte progenitor cells proliferate rapidly in the hair matrix region of the hair bulb. After this expansion cells differentiate into cells of the 7 hair follicle lineages. The hair matrix surrounds a pocket of specialized mesenchymal cells, called the dermal papilla (DP), which provides essential stimuli for both follicle induction and hair growth. Prominent regulatory proteins involved in the cross-talk between the matrix cells and the dermal papilla in developing and anagen hair follicles include the BMPs, Sonic hedgehog FGFs and several WNT proteins as well as the corresponding receptors (Rogers, 2004).

In the mouse pelage, anagen lasts ~ 3 weeks and the first three hair cycles are fairly synchronous. Induction of new anagen occurs when the DP induces stem cells from the so called bulge region to proliferate and differentiate to regenerate the follicle. The hair follicle bulge resides within the ORS in a small niche just below the sebaceous gland, at or near the site of insertion of the arrector pili muscle (Figure 2.10). Stem cells from the bulge region are not only thought to move down to regenerate the hair follicle but are also believed to migrate upwards to the epidermis and the sebaceous glands. However, it is not clear, whether the stem cells found in the epidermis are progeny of the multipotent bulge cells, and if, whether they maintain their multipotency and molecular properties (Alonso and Fuchs, 2003b; So and Epstein, 2004).

Integrins are crucial for skin integrity and were reported to regulate the maintenance and differentiation of skin stem cells. In normal, undamaged skin, integrin expression is confined

to the basal layer of the epidermis and the outer root sheath of the hair follicles, with exception of $\alpha\nu\beta 8$ integrin which is exclusively found in the suprabasal cells. While some of the keratinocyte integrins such as $\alpha 3\beta 1$ and $\alpha 6\beta 4$ are expressed constitutively, others are induced by wounding or pathological changes as for example $\alpha\nu\beta 5$ (Table 2; Watt, 2002).

Integrin	Major ligand	Expression
$\alpha 2\beta 1$	Collagen	constitutive
$\alpha 3\beta 1$	Laminin	constitutive
$\alpha 6\beta 4$	Laminin	constitutive
$\alpha\nu\beta 5$	Vitronectin	weak, induced on wound healing
$\alpha 5\beta 1$	Fibronectin	induced in culture, on wounding and in pathological conditions
$\alpha\nu\beta 6$	Fibronectin and Tenascin	as $\alpha\nu\beta 5$
$\alpha 9\beta 1$	Tenascin	upregulated on wound healing
$\alpha\nu\beta 8$	Vitronectin	suprabasal

Table 2 Keratinocyte integrins (modified from Watt, 2002)

Whereas $\alpha 6\beta 4$ is primarily concentrated at the basement membrane zone as the major component of the hemidesmosomes, other integrins are distributed over the basal, lateral and apical surface of the basal cells. In pathological conditions integrins can also be found in the suprabasal layers of a hyperproliferative epidermis, for example during wound healing. Conversely, in some squamous cell carcinomas loss of integrins is observed (Watt, 2002). In the past years mutant mice with ubiquitous or keratinocyte specific deletion of integrin genes revealed the functions of specific integrin subunits in skin (Table 3). While $\alpha 6\beta 4$ and $\alpha 3\beta 1$ are crucial for the attachment of basal keratinocytes to the basement membrane, loss of $\alpha 2\beta 1$, $\alpha 9\beta 1$, $\alpha\nu\beta 5$ and $\alpha\nu\beta 6$ had no effect on skin development or maintenance (Watt, 2002).

Integrin subunit	Phenotype	Reference
$\alpha 3$	Disorganized basement membrane; occasional epidermal-dermal blistering, primarily on legs and footpads	DiPersio et al., 1997
$\beta 6$	Juvenile hair loss due to macrophage infiltration into skin; wound healing normal	Huang et al., 1996
$\alpha 9$	No defects observed	Huang et al., 2000b
$\beta 5$	Wound healing normal	Huang et al., 2000a
$\beta 1$	<p>$\beta 1$ floxed x K5Cre</p> <p>Abnormal hair follicles; hair loss with removal of follicles by infiltrating macrophages; epidermal-dermal blisters; reduced proliferation and abnormal differentiation of interfollicular epidermis; hyperthickened epidermis; disruption of basement membrane; reduced $\alpha 6\beta 4$ expression; reduced hemidesmosomes; dermal fibrosis; impaired wound healing</p> <p>$\beta 1$ floxed x K14Cre</p> <p>Epidermal-dermal blistering; basement membrane disruption; reduced hemidesmosomes; thin epidermis; reduced number of hair follicles; reduced $\alpha 6\beta 4$ expression</p>	<p>Brakebusch et al., 2000</p> <p>Grose et al., 2002</p> <p>Raghavan et al., 2000</p>
$\alpha 6$	Severe epidermal blistering	Georges-Labouesse et al., 1996
$\beta 4$	Severe epidermal blistering; absence of hemidesmosomes	Van der Neut et al., 1996; Dowling et al., 1996
$\alpha 3 + \alpha 6$	Epidermal blistering; proliferation, stratification and hair follicle morphogenesis normal in adherent epidermis	DiPersio et al., 2000
$\alpha 2$	No epidermal defects observed; wound healing normal	Chen et al., 2002 Holtkötter et al., 2002

Table 3 Epidermal phenotype of integrin knockout mice (modified from Watt, 2002). $\beta 1$ integrin skin phenotype is highlighted.

Mutant mice lacking $\beta 1$ integrin in skin showed in addition to blistering severe defects in the hair follicle morphology, progressive hair loss, disorganized and hyperthickened interfollicular epidermis, impaired proliferation in the interfollicular epidermis and the hair matrix cells, dermal fibrosis and defects in the interfollicular terminal differentiation (Brakebusch et al., 2000). However, despite these severe skin defects and loss of all hairs already at the age of 7 weeks, some of the $\beta 1$ skin specific conditional knockout mice survive up to the age of one year. These results were unexpected, since previous *in vitro* results had suggested an important role of $\beta 1$ integrin in the maintenance of skin stem cells (reviewed by Watt, 2002). Selection of keratinocytes for cells expressing high levels of $\beta 1$ integrin resulted in cells with high colony-forming efficiency, i.e. stem cell like properties. *In vivo* expression of $\beta 1$ integrin correlated with keratinocyte proliferation: $\beta 1$ integrin expressing basal keratinocytes proliferate, $\beta 1$ -deficient suprabasal keratinocytes do not proliferate. Moreover, ectopic expression of $\beta 1$ integrins in suprabasal cells lead to proliferation of these cells *in*

in vivo. In contrast, $\beta 1$ -deficient mice revealed, that also $\beta 1$ -null keratinocytes are able to proliferate *in vivo* (Brakebusch et al., 2000).

In vitro analysis of $\beta 1$ -null keratinocytes demonstrated an important role for $\beta 1$ integrin in adhesion, spreading and proliferation as well as cell migration. $\beta 1$ -deficient mice showed severely delayed wound healing, confirming the important role of $\beta 1$ integrin in keratinocyte migration (Grose et al., 2002).

2.2 The Rho GTPases family

The Rho family proteins belong to the Ras superfamily of small (~ 21 kDa) GTPases and are crucial integrin effectors and modulators. Currently 22 genes in humans have been identified, which encode at least 25 proteins. On the basis of the primary amino acid sequences, structural motifs and biological function, the Rho family can be subdivided into 10 groups that exhibit similar, but not identical properties. These are: Cdc42, Rac1, RhoA, RhoD, Rif/RhoF, Rnd3/RhoE, TTF/RhoH, Chp/RhoV, mitochondrial Rho (Miro1/RhoT1) and Rho-related BTB-domain containing protein (RhoBTB). The Rho-family proteins are defined by the presence of a Rho-type GTPase-like domain typically accompanied by short N-terminal and C-terminal extensions (Figure 2.11; Wennerberg and Der, 2004)

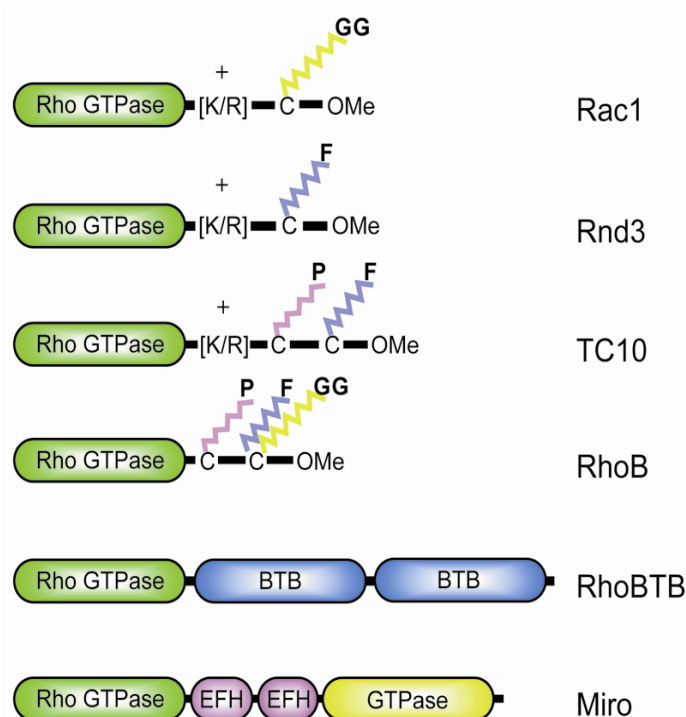


Figure 2.11 Post-translational modification of Rho proteins. Representation of the different C-termini, the posttranslational lipid modifications that occur at these sites in Rho proteins, and the additional membrane targeting signals are shown (F, farnesyl; GG, geranylgeranyl; OMe, carboxymethylation; [K/R] polybasic sequence; P, palmitoyl group). RhoBTB, which does not undergo any known post-translational modifications, contains two BTB domains C-terminal of the GTPase domain. Miro contains two EF-hand (EFH) motifs and one additional GTPase domain that are C-terminal of the Rho GTPase-like domain. Rac1 stands for Rac2, Rac3, Rho A, RhoC and Cdc42 (modified from Wennerberg and Der, 2004).

However, some of the more atypical family members can contain additional domains and can be more than 700 amino acids long. The GTPase domains share approximately 36% amino

acid identity with the Ras proteins and 40 - 95% identity within the family. In addition to the GTPase domain the majority of members undergo C-terminal post-translational modification by isoprenoid lipids, which together with other C-terminal modifications and sequences facilitate their subcellular localization and association with specific membranes, which is crucial for their function (Figure 2.11; Wennerberg and Der, 2004).

Like Ras, Rho proteins function as bi-molecular switches by adopting different conformational states in response to binding GDP or GTP. In contrast to Rho-GDP, Rho-GTP transduces signals by interacting with downstream effectors. The activation of Rho GTPases is mediated through various cell-surface receptors including integrins (discussed in paragraph 2.4), cytokine and tyrosine kinase receptors, as well as the G-protein coupled receptors (GPCRs). Bound to an effector they regulate the actin cytoskeleton, cell-cycle progression and gene transcription, contributing to cellular process like migration, adhesion, phagocytosis, cytokinesis, neurite extension, cellular morphogenesis, growth and survival (Figure 2.12). Furthermore, aberrant regulation of Rho-family proteins promotes malignant transformation and Rho GTPase activity is essential for the oncogenic properties of Ras and other oncogens (Wennerberg and Der, 2004; Rossman et al., 2005).

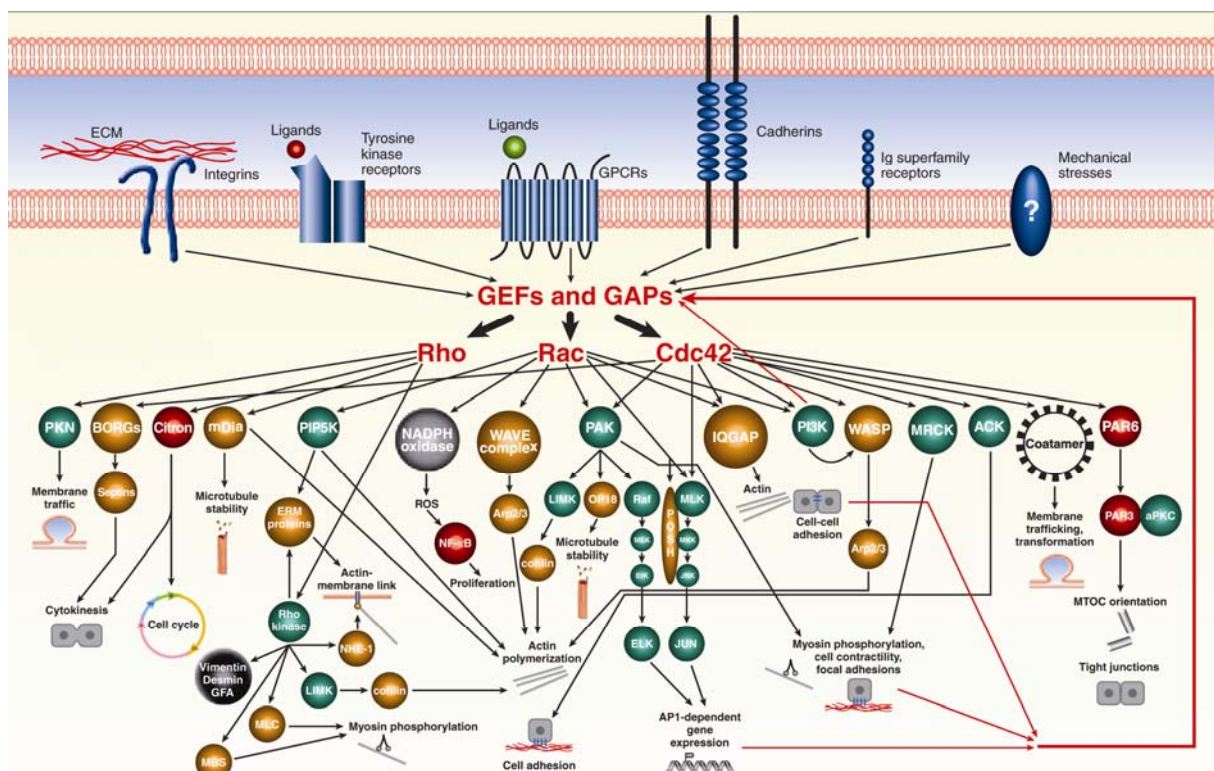


Figure 2.12 Schematic representation of the various activation and effector pathways of the small Rho GTPases family (modified from Schwartz, 2004).

2.2.1 Regulation of the Rho GTPases family

Rho proteins function as bi-molecular switches by adopting different conformational states in response to binding GDP or GTP. Cycling between GDP and GTP-bound states is required for effective signal flow through Rho GTPases to elicit downstream biological functions and is controlled primarily by two classes of regulatory molecules: GTPase-activating proteins (GAPs), which enhance the relatively low intrinsic GTPase activity of Rho proteins and guanine nucleotide-exchange factors (GEFs), which catalyse the exchange of GDP to GTP. GEFs stabilize nucleotide-depleted GTPases, however due to the relatively high concentration of intracellular GTP, these nucleotide depleted complexes rapidly dissociate into GTP-bound GTPases and free GEFs. GAPs suppress Rho activity whereas GEFs promote Rho activity. There is also a third set of regulatory proteins named the guanine nucleotide-dissociation inhibitors (GDIs), which sequester GTPases in the cytosol in a GDP-bound state and which might shuttle Rho GTPases between different membrane compartments. However, the mechanism by which Rho GTPases are released from GDIs is not completely understood (Figure 2.13).

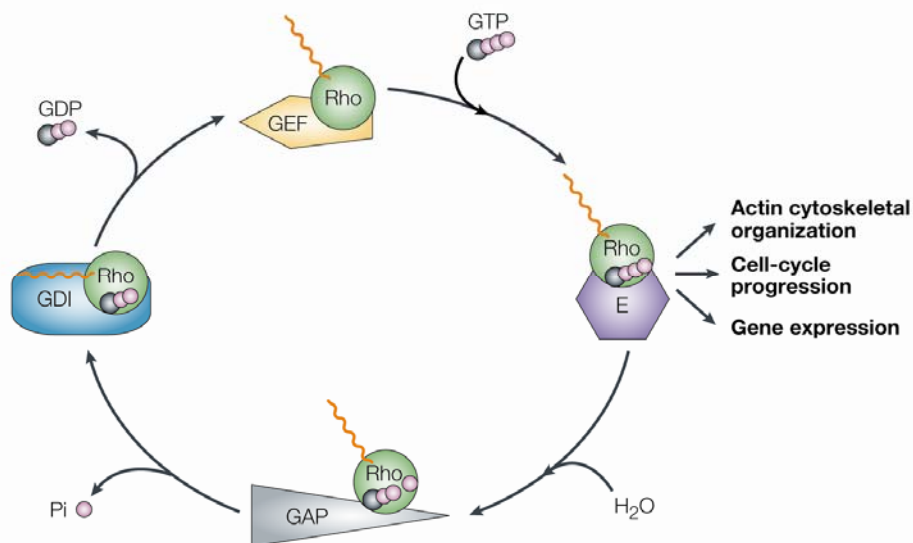


Figure 2.13 The Rho GTPase cycle. Isoprenyl moiety, orange wavy line; Pi, inorganic phosphate; E, effector protein (modified from Rossman et al., 2005).

Up to date 80 distinct GEFs (11 of the DOCK superfamily and 69 of the Dbl family), 80 GAPs and three GDIs have been identified. Importantly many of these regulators can interact with several distinct Rho GTPases and are not specific for only one GTPase. To illustrate this, the phylogenetic tree of the GEFs of the Dbl family together with their target Rho GTPases, known by now is shown (Figure 2.14; Cote and Vuori, 2002; Moon and Zheng, 2003; Rossman et al., 2005; DerMardirossian and Bokoch, 2005).

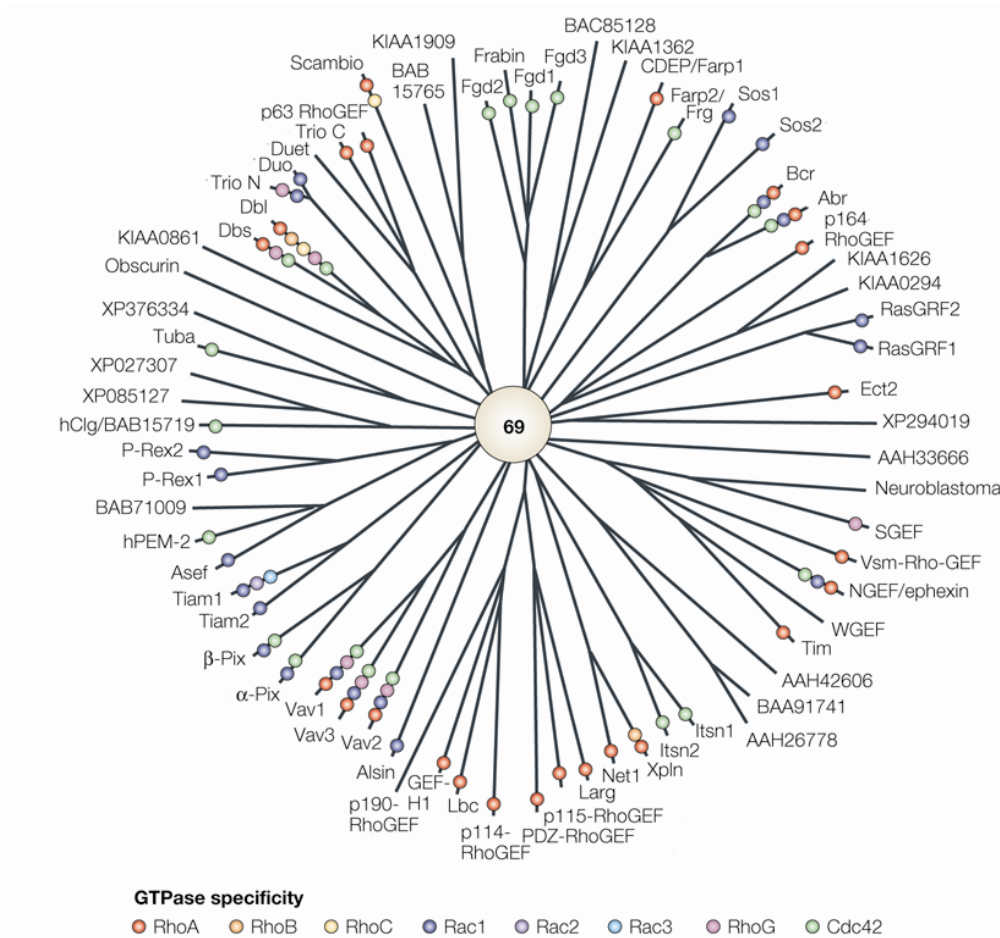


Figure 2.14 The Dbl family proteins and their target Rho GTPases. The specificity summary is not completed since the analysis of most of the GEFs was restricted primarily to RhoA, Rac1 and Cdc42 (modified from Rossman et al., 2005).

In addition to the regulation of Rho GTPases by GEFs, GDIs and GAPs, there is more and more evidence for a complex crosstalk between the distinct Rho GTPases, by which the amount of activated proteins is influenced (Evers et al., 2000). Moreover, a cross talk between these GTPases at the level of downstream pathways which regulate the cytoskeleton (some of them described in paragraph 2.3) has been uncovered (DerMardirossian et al., 2004; Nishimura et al., 2005).

2.2.2 The Cdc42 family

The Cdc42 subfamily of Rho GTPases consists of Cdc42, TCL, TC10, Wrch-1 and Wrch-2/Chp. The major function associated with all the Cdc42 related proteins is actin polymerization and filopodia formation (discussed in paragraph 2.3.1.1). With the exception of Wrch-1 all of them bind haematopoietic Wiskott–Aldrich-syndrome protein (WASP) and its ubiquitously expressed family member N-WASP, which by mediating the nucleation of actin polymerization provides the link to the cytoskeleton. There are two isoforms of human

and mouse Cdc42, which arise from alternative splicing of the same gene. Both are 191-residue proteins that differ at residue 163 and their C-terminal amino acids. The most studied isoform of Cdc42 (placental Cdc42p / Cdc42Hs / Cdc42a) is the ubiquitously expressed one, whereas the other is restricted to the brain (brain Cdc42b / G25K; Wennerberg and Der, 2004).

TC10 and TCL, for which two isoforms have been reported, are very closely related and have functions similar to Cdc42, since both have been shown to induce filopodia. TC10 and TCL interact with most known Cdc42 effectors although difference exists (Murphy et al., 1999; Neudauer et al., 1998). The activities of TC10 and TCL can at least sometimes be regulated independently of Cdc42 and by different stimuli (Chiang et al., 2001). In 3T3 cells, insulin stimulates TC10 via the RAP GEF C3G without any change in Cdc42 activity (Chiang et al., 2001). RhoGDI-1, on the other hand, binds to Cdc42, but not to TC10, since it possess a palmitate modification preventing its binding (Michaelson et al., 2001).

The rat protein Chp and its human version Wrch-2 have also been identified to belong to the Cdc42 family since they interact with the Cdc42 effectors PAK and N-WASP, and were shown to stimulate filopodia formation (Aronheim et al., 1998). Wrch-1 does not bind to N-WASP and was implicated in Wnt-dependent signalling and APC inactivation (Aspenström et al., 2004). There are no GAPs, GEFs or GDIs known to interact with Chp and Wrch-1. Interestingly, both Rho GTPases possess a proline-rich sequence that might serve as Src-homology (SH3) domain and additional C-terminal modifications which distinguish them from those of the more classical Cdc42-related proteins (Wennerberg and Der, 2004).

2.2.3 Tools of trade: use of dominant-negative inhibitory mutants of the Rho-family GTPases

Over the last years the most popular tool to study the function of Rho GTPases, and thus also Cdc42, was the use of dominant-inhibitory proteins. These molecules carry a mutation of the serine residue at position 17 (threonine in Cdc42) to an asparagine, and bind to the corresponding activating GEFs with higher affinity than wild type Rho GTPases. Yet, they cannot interact with effector molecules and therefore are “dead-end” complexes. This prevents the activation of endogenous Rho GTPases (Feig, 1999). The use of dominant negative mutants, however, may have disadvantages. Since many GEFs are not specific for a single Rho GTPase, dominant negative forms of distinct Rho GTPases may also inhibit the activation of other Rho GTPases (Figure 2.14; Schmidt and Hall, 2002). In addition, the degree of inhibition is dependent on the expression level of the dominant negative mutant

(Braga et al., 2000). Thus, although very powerful, the use of dominant-negative mutants has clear drawbacks.

2.3 Cell migration

Cell migration is a highly integrated multistep process which plays a central role in the development and maintenance of multicellular organisms. It is involved in embryonic morphogenesis, tissue repair and regeneration, as well as immune surveillance. Cell migration also occurs in many diseases; in cancer, for instance, it leads to invasion and metastasis, but also mental retardation, atherosclerosis and arthritis are migration dependent events (Ridley, 2001). Cell migration is usually initiated in response to extracellular cues, which can be diffusible factors, signals on neighbouring cells or from the extracellular matrix. These cues then stimulate transmembrane receptors to initiate intracellular signalling. Independently of the cell type the actin cytoskeleton is generally regarded as providing the major driving forces required for cell migration (Ridley, 2001).

Cell migration can be divided into mechanistically separate steps: cell polarization, protrusion and extension formation, establishment of new adhesions, cell body contraction and rear detachment (Figure 2.15). The initial response of a cell to a migratory stimulus is to polarize and extend protrusions in the direction of migration. These protrusions are structures formed by polymerised actin which can be organized into a cross-linked meshwork and form large sheath like structures called lamellipodia or organize into thin parallel bundles described as filopodia (Wood and Martin, 2002; Small et al., 2002). Immediately behind the leading edge new adhesions are formed by integrin mediated adhesion to the ECM or via transmembrane receptors of adjacent cells linked to the actin cytoskeleton. These adhesions serve as traction sites for migration as the cell moves forward over them and they are disassembled at the cell rear, allowing it to detach.

Many different signalling molecules have been implicated in the regulation of these distinct steps including integrins, Rho GTPases, calcium regulated proteins, mitogen activated protein kinase cascades, protein kinase C (PKC), phosphatidylinositide kinases, phospholipases C and D and tyrosine kinases. Here we focus on the function of integrins and Cdc42 which have been both shown to be the key players in regulating cell migration associated events.

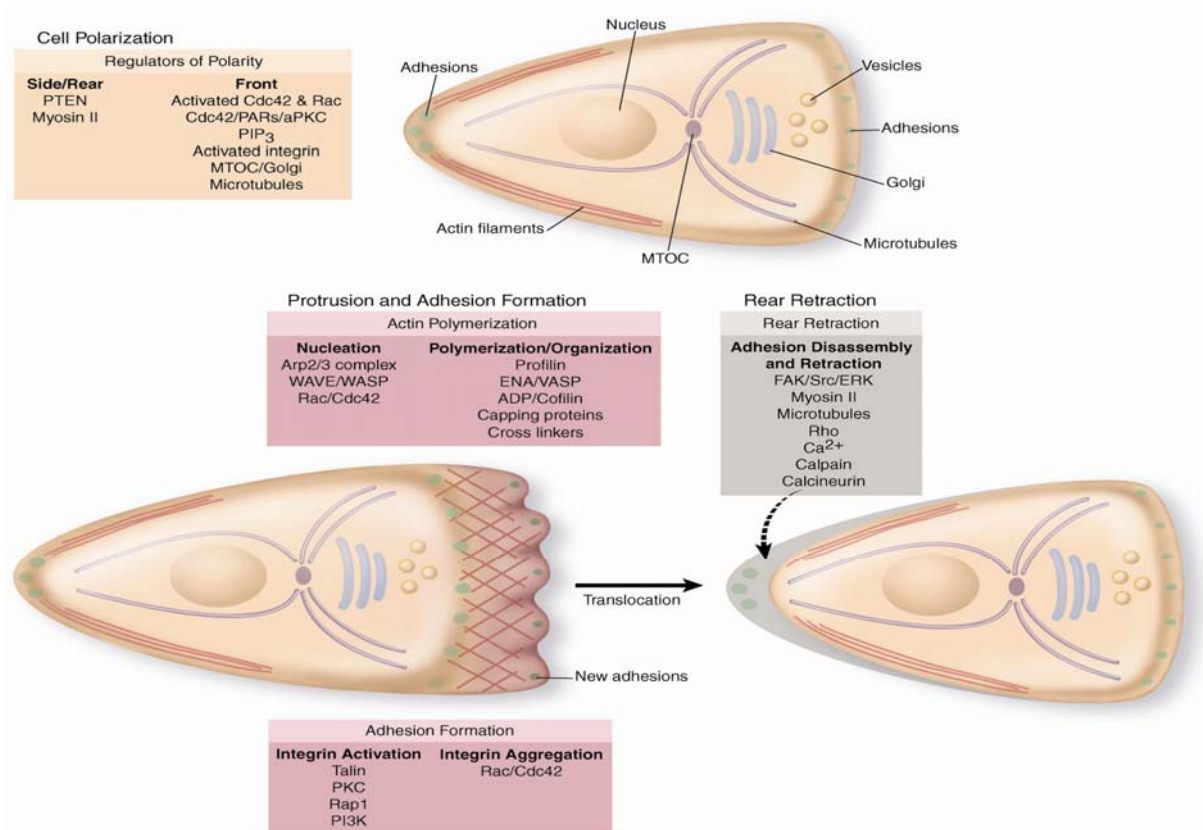


Figure 2.15 Crucial steps in cell migration. A migrating cell polarizes and extends a protrusion at the front. This extension is stabilized through the formation of new adhesions to the extracellular matrix. The cell body is moved forward by actomyosin-mediated contraction. Finally the tail of the cell detaches from the substratum and retracts. Proteins regulating cell polarization, protrusion and adhesion formation as well as rear retraction are indicated (modified from Ridley et al., 2003).

2.3.1 *Cdc42* in cell migration

A significant body of evidence has indicated a crucial role for *Cdc42* in cell migration (Fukata et al., 2003). Dominant negative inhibition of *Cdc42* in primary rat fibroblasts and astrocytes results in impaired directed migration (Nobes and Hall, 1999; Etienne-Manneville and Hall, 2001). In *Drosophila* *Cdc42*-deficient hemocytes and hemocytes expressing dn*Cdc42* showed a two-fold increased migration speed in response to wound-induced cues (Stramer et al., 2005). In contrast, however, dominant negative inhibition of *Cdc42* restricted to macrophages of *Drosophila* embryos did not reveal any difference in migration speed or distribution of these cells, suggesting that *Cdc42* is not required for macrophages migration (Paladi and Tepass, 2004).

Cdc42 has been reported to control cell migration by regulating the polarization of lamellipodial activity and Golgi re-orientation in fibroblasts and astrocytes (Nobes and Hall, 1999, Cau and Hall, 2005). Also in *Drosophila*, *Cdc42* is crucial for the maintenance of polarized lamellipodia formation (Stramer et al., 2005). In addition, *Cdc42* through its effect

on filopodia formation was described to be required for direction sensing during chemotaxis (Allen et al., 1998; Nobes and Hall; 1999, Ridley, 2001), although the mechanism of that action is not known.

2.3.1.1 Cdc42 as regulator of protrusion formation

The assembly of actin-based membrane projections at the leading edge of migrating cells is promoted by two members of the Rho GTPases family, Rac and Cdc42. Activation of Rac1 induces the formation of lamellipodia, while Cdc42 activation elicits filopodia. Lamellipodia are brush-like actin filament structures that are able to push along a broad length of plasma membrane. Polarized lamellipodia formation provides the basis for directional migration. Filopodia are fingerlike protrusions containing parallel bundled actin filaments, which seem to be particularly well designed to explore the local environment (Ridley et al., 2003; Raftopoulou and Hall, 2004).

In confluent serum-starved Swiss 3T3 cells, expression of constitutively active Rac1 was shown to rapidly stimulate actin filament accumulation at the plasma membrane and lamellipodia formation. Also several growth factors and activated H-ras were capable of inducing lamellipodia, whereas this response was prevented by a dominant inhibitory mutant of Rac1 (Ridley et al., 1992, Nobes and Hall, 1999). Cdc42 induces the formation of actively protruding filopodia with or without concomitant lamellipodium formation depending on the cell type. Conversely, expression of dominant negative Cdc42 (dnCdc42) was described to prevent filopodium formation in Swiss 3T3 cells and primary fibroblasts (Nobes and Hall, 1995; Kozma et al., 1995; Nobes and Hall, 1999). Moreover, Cdc42-deficient embryonic stem (ES) cells were reported to lack spike-like protrusions which were readily observed in wild type ES cells (Chen et al., 2000). Recently, other Rho GTPases have also been reported to induce filopodia (Neudauer et al, 1998; Murphy et al., 1999; Ellis and Mellor, 2000; Tao et al., 2001; Vignal et al. 2000; Abe et al., 2003; Aspenström et al., 2004). A constitutively active form of Rif was suggested to induce filopodia in a Cdc42-independent manner, since expression of dnCdc42 did not interfere with these protrusions (Ellis and Mellor, 2000). In contrast, RhoG-induced filopodium formation was shown to be dependent on Cdc42 (Gauthier-Rouviere et al., 1998). Whether Cdc42 is required for filopodium formation induced by TC10, TCL, RhoD, or Wrch-1 is currently unknown.

In the past years potential pathways for the transduction of signals from active Cdc42 to actin polymerization have been uncovered (Figure 2.16). Of the many effector proteins that interact specifically with GTP-Cdc42 only WASP and its ubiquitously expressed family member N-

WASP provide a direct link to actin assembly through activation of the nucleating activity of the Arp2/3 complex. The Arp2/3 complex binds to the sides or tips of pre-existing actin filaments and induces the formation of daughter filament that branches off the mother filaments (Pollard et al., 2000). However, N-WASP knockout models demonstrated that N-WASP is not essential for Cdc42 based filopodium formation, thus these interaction may not account for Cdc42's ability to induce filopodia (Lommel et al., 2001; Snapper et al., 2001). An alternative Arp2/3-independent pathway was proposed, which involved the insulin receptor substrate Irs53, shown to be recruited to the tips of both filopodia and lamellipodia and induce filopodia in a Cdc42 dependent manner (Miki et al., 2000; Govind et al., 2001). Irs53 has a partial Cdc42/Rac interacting motif (CRIB) and binds to the Ena/Vasp family member Mena. The Ena/VASP proteins are enriched at the filopodia tips and bind the barbed ends of actin filaments and antagonize both actin capping and branching, thereby allowing continuous elongation of filaments (Krugmann et al., 2001). In addition Irs53 was shown to interact through its SH3 domain with WAVE, another scaffold protein regulating the Arp2/3 complex, thus providing the link to Cdc42 and Rac induced lamellipodia (Miki et al., 2000). Another signalling pathway implicated in lamellipodium formation involves the family of PAK proteins, which have been identified as direct downstream effectors of Rac and Cdc42. Pak interaction with Cdc42/Rac was shown to increase the levels of phosphorylation of myosin light chain (MLC), which is believed to be required for anchoring of lamellipodia and focal adhesion turnover. PAK was also reported to activate LIM kinase, which in turn blocks the severing / depolymerising activity of cofilin, which is essential for promoting filament treadmilling at the front of migrating cells (Daniels and Bokoch, 1999; Bagrodia and Cerione, 1999).

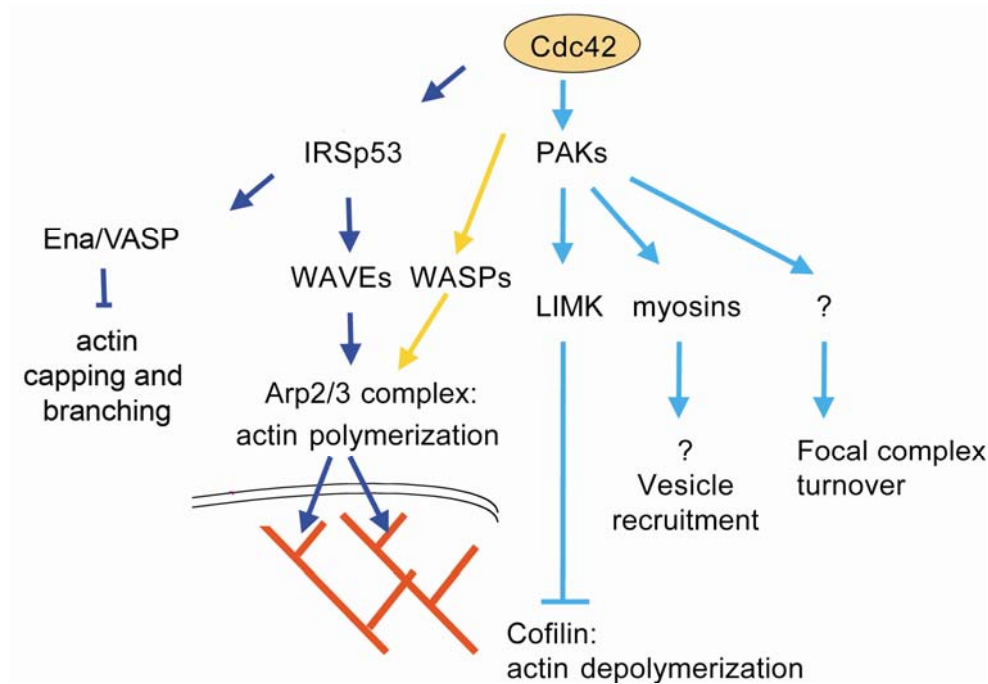


Figure 2.16 Cdc42 regulated pathways affecting actin filament organization. Cdc42 acts through several downstream targets to regulate F-actin accumulation at the leading edge of cells. It stimulates Arp2/3-complex-induced actin polymerization by interacting with WASP and Irs53 proteins. In addition the interaction with Irs53 provides the link to the Ena/VASP family and promotes filopodia extension. Finally, Cdc42 acts via PAK to stimulate LIMK, which binds and inhibits cofilin-induced actin depolymerization, allowing increased accumulation of polymerized actin at the leading edge of cells (modified from Ridley, 2001).

2.3.1.2 *Cdc42 as master regulator of cell polarity*

Cells are dynamically polarised in response to the extracellular gradients of signals for example during directed cell migration or during the formation of an immunological synapse between T cells and dendritic cells. Cellular polarization is also observed in the establishment of apico-basolateral cell polarity in epithelial cells and in the process of axon specification from neurites in neuronal cells. These processes are accompanied by asymmetric distribution of signalling and adhesion molecules, directed membrane trafficking and cytoskeleton reorganization (Fukata et al., 2003).

For a cell to migrate, it must be polarized, since the molecular processes at the front and the back of a moving cell are different. In migrating fibroblasts during wound healing, a polarised shape develops 1 – 6h after the injury and is characterized by protrusion formation at the leading edge, reorientation of the microtubule-organising centre (MTOC) and the Golgi apparatus towards the direction of migrating and temporal capture and stabilization of microtubule (MT) plus ends near the leading front. The stabilization of the MT plus ends facilitates cargo transport to the leading edge via motor proteins like dynein and kinesin (Fukata et al., 2003; Raftopoulou and Hall, 2004). Interestingly, in fast migrating cells such as

neutrophils and T cells, the MTOC is polarized opposite to the direction of migration (Serrador et al., 1999).

Cdc42 was shown to be a master regulator of cell polarity in eukaryotic organisms ranging from yeast to humans (Fukata et al., 2003). Cdc42 is active at the front of migrating cells (Itoh et al., 2002) and has been proposed to restrict the site of lamellipodia formation and to localize MTOC and Golgi apparatus in front of the nucleus. In migrating astrocytes, Cdc42 activation is dependent on $\beta 1$ integrins. How Cdc42 is regulated in other cells during migration is not known. Re-orientation of MTOC might facilitate microtubule growth into the lamella and microtubule-mediated delivery of Golgi-derived vesicles to the leading edge, providing membrane and associated proteins needed for forward protrusion (Etienne-Manneville and Hall, 2002; Rodriguez, 2003; Etienne-Manneville and Hall, 2003, Cau and Hall, 2005). In fibroblasts and astrocytes, Cdc42 activation induces MTOC re-orientation by recruiting and activating a cytoplasmic Par6/PKC ζ complex. Upon activation of PKC ζ , Gsk3 β is inactivated by phosphorylation. Inactivation of Gsk3 β was proposed to allow APC to bind to tubulin and stabilize the growing end of microtubules at the leading edge. Through a dynein or dynactin-dependent mechanism, this then results in microtubule re-organization and centrosome reorientation (Figure 2.17; Etienne-Manneville and Hall, 2003; Cau and Hall, 2005). In addition, APC was shown to recruit the Rac GEF Asef to the leading edge, thereby stimulating lamellipodia formation (Kawasaki et al., 2003).

The polarized protrusion formation is controlled by a different Cdc42 pathway. Upon wounding induced cues Cdc42 activates PAK1/2 at the leading edge of migrating cells. This localized PAK activation is essential for recruitment of the Rac GEF Pak interacting exchange factor (β PIX) and Rac activation at the front of the cell, thus, restricting the actin polymerization and lamellipodium formation to the leading edge of migrating cells (Figure 2.17; Cau and Hall, 2005). Interestingly, PAK1 is not only an effector of Cdc42, but can also contribute to Cdc42 activation, since it binds to G protein-coupled receptors, which are activated by many chemoattractants and link them to α -PIX, which activates Cdc42. In leukocytes this pathway results in a high Cdc42 activity at the leading edge and is essential for the persistent direction during chemotactic migration (Li et al., 2003).

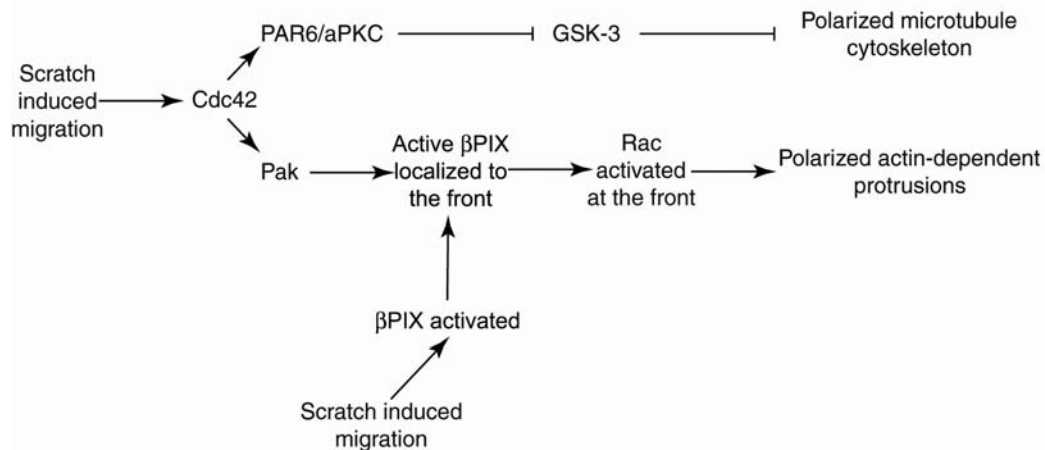


Figure 2.17 Cdc42 controls two distinct polarity pathways in migrating cells. Microtubule cytoskeleton polarization occurs through activation of Par6/aPKC and subsequent inhibition of GSK-3, whereas Pak controls the localization, though not the activity, of the Rac-GEF β PIX, allowing the polarization of actin-rich, Rac-dependent protrusions (modified from Cau and Hall, 2005).

A different mechanism for MTOC reorientation was proposed by Gregg Gundersen and his group (Gomes et al., 2005). They show that MTOC reorientation is established by active movement of the nucleus rather than the MTOC and suggest that nuclear positioning is an initial event in migrating cells. In this model Cdc42 is necessary and sufficient to activate the myotonic dystrophy kinase-related Cdc42 binding kinase (MRCK) that stimulates myosin phosphorylation. Thus, the nuclear movement is myosin dependent and driven by actin retrograde flow. Factors previously implicated in MTOC reorientation, dynein, Par6 and PKC ζ do not participate in nuclear movement but instead contribute to MTOC reorientation by maintaining the MTOC at the cell centroid (Figure 2.18).

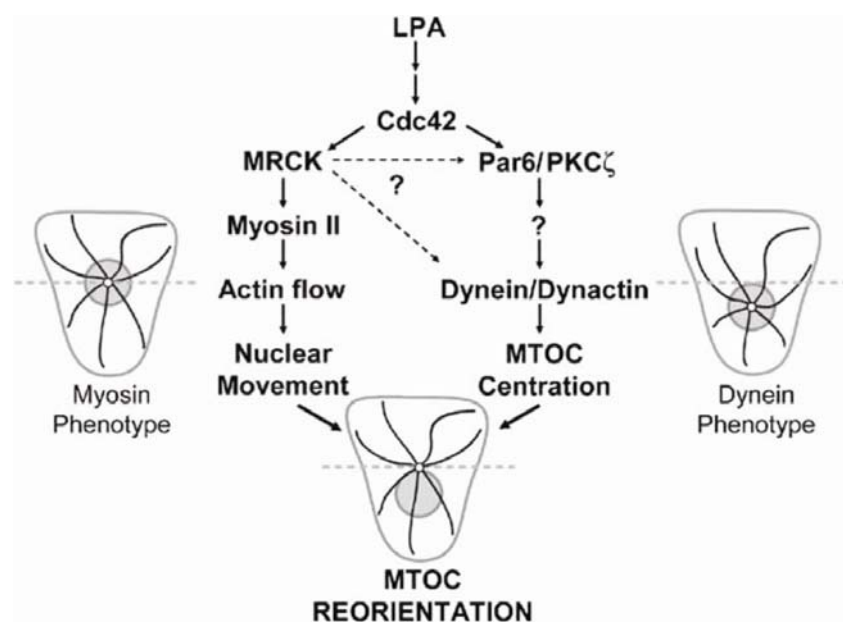


Figure 2.18 The two Cdc42-regulated pathways lead to MTOC reorientation. LPA activates Cdc42 to regulate

separate actin- and MT-dependent pathways that result in MTOC reorientation. Cell diagrams (nucleus, grey circle; MTOC, small white circle; MT, black lines) show phenotypes resulting from inhibition of each pathway. Horizontal dashed line represents a lone through the cell centre. MRCK is sufficient to stimulate MTOC reorientation and so may also regulate the Par6-PKC ζ -dynein-dynactin pathway (dotted arrows; modified from Gomes et al., 2005).

A third mechanism for Cdc42 mediated polarization involves a microtubule plus-end-capturing protein CLIP-170, which was shown to interact with the Cdc42/Rac1 effector protein IQGAP1, which in turn binds to actin filaments and APC. The two Rho GTPases were proposed to mark the cortical spots at the leading edge to which the IQGAP1-CLIP-170-APC complex is targeted. This in turn leads to the formation of polarized microtubule arrays and cell polarization (Figure 2.19; Noritake et al., 2005).

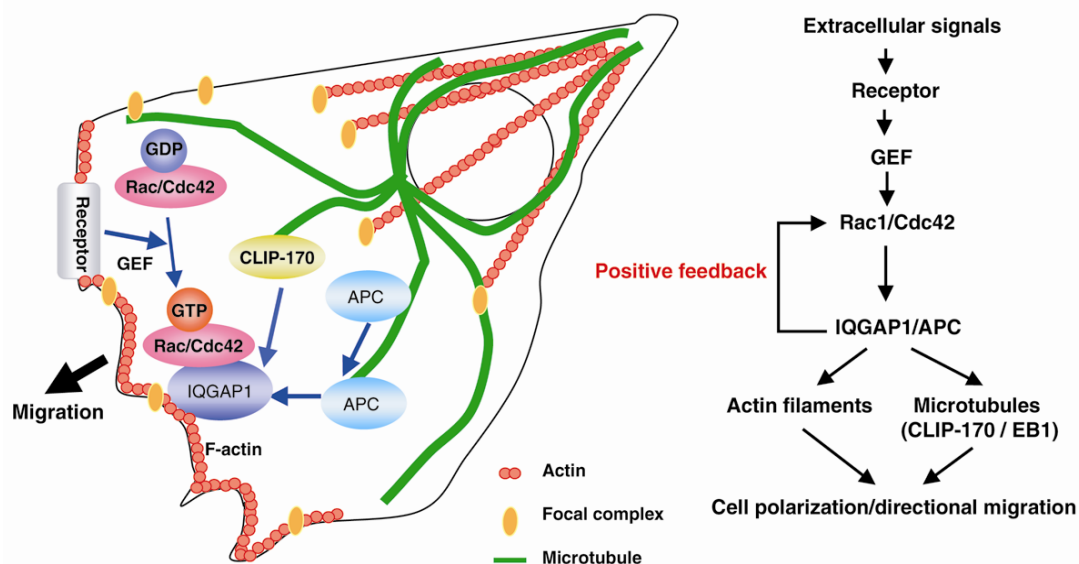


Figure 2.19 The IQGAP1-CLIP-170-APC complex in regulation of protrusion formation and cell polarization (modified from Noritake et al., 2005).

Taken together, most reports indicate a crucial role of Cdc42 for the directionality of cells during migration, although quite diverse mechanistical explanations have been proposed.

2.3.2 Integrins in cell migration

For migration to occur the newly formed protrusion must be stabilized by attaching to the surroundings. Integrins are the major family of adhesion mediating receptors and studies over the past years provided clear evidence for the essential role of integrins in migration, both *in vitro* and *in vivo* (Ridley et al., 2003; Danen and Sonnenberg, 2003). By connecting the ECM to the intracellular cytoskeleton integrins serve as traction sites over which the cell moves as well as sensors which transmit information about the physical state of the ECM into the cell to alter cytoskeletal dynamics. In addition, integrins not only provide the anchorage that is

necessary for migration, but they also activate pro-migratory signals that regulate the cytoskeleton as well as gene expression. The mechanisms by which integrin signals orchestrate cell migration are incompletely understood, but some pathways are quite well established (Ridley et al., 2003; Guo and Giancotti, 2004).

Integrins have been shown to be activated at the leading edge of migrating cells where a cascade of events is initiated. Upon activation integrins bind through their cytoplasmic domains to several adaptor proteins, among them actin binding proteins which functions as platforms, bringing kinases and substrates together and which strengthen the actin integrin connection (Brakebusch and Fässler, 2003; Lee and Juliano, 2004). One of the most important scaffold proteins providing integrin signalling promoting cell migration is FAK (Figure 2.20). FAK recruits SFKs to focal adhesions and positions them close to target-effectors. These target effectors are then phosphorylated and mediate migration associated events (Sieg et al, 2000). FAK and Shc have been shown to activate Erk and JNK and thereby promote actomyosin fibre contraction and focal adhesions turnover, respectively. FAK and SFK signalling were also shown to activate Rac1 to induce lamellipodial extension (Cary et al., 1998; Klemke et al., 1998), whereas integrin mediated adhesion stimulates filopodia formation possibly through a Cdc42-PAK pathway (Price et al., 1998). Integrin dependent activation of Cdc42 was also shown to regulate the microtubular network and cell polarization during directed movement of cells (Etienne-Manneville and Hall, 2003). Moreover, integrins activate RhoA to promote actomyosin fibre contraction and tail retraction (Ridley et al., 2003). Finally integrins have been shown to recruit matrix-metalloproteinase-2 (MMP2) to the cell surface to allow the local degradation of extracellular matrix and the generation of new integrin-binding sites for migration. Several integrins have also been associated with the uPA receptor, uPAR. On binding uPAR, uPA is converted to an active form, which processes plasminogen to plasmin. Plasmin induces ECM degradation directly, but also indirectly by activating various MMPs (Guo and Giancotti, 2004).

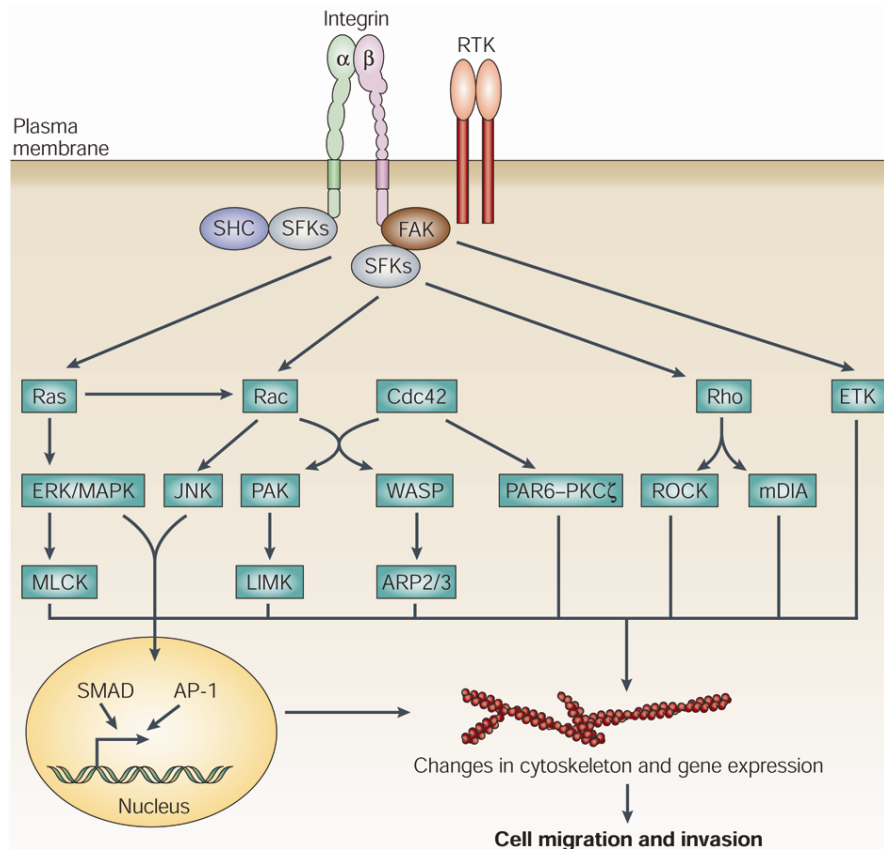


Figure 2.20 Integrin dependent tyrosine kinase signalling promotes cell migration and invasion. FAK and Src-family kinases (SFKs) integrate pro-migratory signals from integrins and receptor tyrosine kinases (RTKs) by orchestrating changes in the cytoskeleton and inducing gene expression. Both Rac and Cdc42 activate WASP and PAK, which then activate the Arp2/3 complex and LIM kinase (LIMK), respectively, to induce actin polymerization. Myosin light chain kinase (MLCK), and the Rho effectors Rho kinase (ROCK) and mammalian diaphanous (mDIA), regulate bundling and contraction of actomyosin fibres. PAR6 and protein kinase C (PKC ζ) function downstream of Cdc42 to control cell polarity during migration. JNK and ERK, which can be activated by Shc or FAK, promote cell migration by activating activator protein-1 (AP-1)-dependent gene expression. Finally, the activation by FAK of ETK tyrosine kinase is also important for cell migration (modified from Guo and Giancotti, 2004).

2.4 Signalling networks linking integrins and Rho GTPases to promote migration

Rho GTPases and integrins have a complex relationship (Schwartz and Shattil, 2000). Early studies reported that cells plated on ECM proteins rapidly developed extended filopodia and lamellipodia indicating the activation of Cdc42 and Rac1; and indeed both Rho GTPases are activated upon integrin mediated adhesion as proved in pull down analysis for the active form of these proteins (Price et al., 1998, DelPozo et al., 2000). It has also been reported that integrin mediated activation of Cdc42 is necessary to promote Golgi reorientation in astrocytes, thus polarization of the cells (Etienne-Manneville and Hall, 2002). Interestingly,

RhoA activity has been shown to initially decrease and finally increase when cells accomplished spreading (Ren et al., 1999). This is consistent with the function of these Rho GTPases, since Cdc42 and Rac1 are both involved in actin polymerization and polarized protrusion formation as well as stabilization of new adhesion sites necessary in the initial phase of cell migration, whereas RhoA activity increases cell contractility and transmits the tension to the sites of integrin ligation required at the later stages.

There have been numerous of studies that showed that the Rho GTPases play a role in specific integrin pathways. Cdc42 has been shown to contribute to integrin mediated activation of the lipid kinase PI 3-kinase, the protein kinases Akt and Cdc42 associated tyrosine kinase-2 (ACK-2) and MAPK. Rac1 has been implicated in MAPK and JNK activation and Rho in the activation of MAPK, FAK and phosphatidylinositol 4-phosphate (PtdIns4P) 5-kinase (Schwartz and Shattil, 2000). So how do integrins activate Rho GTPases? As already indicated upon integrin interaction with ECM, several non-receptor tyrosine kinases including FAK and c-Src are activated. These tyrosine kinases in turn can phosphorylate other downstream molecules including GEFs (e.g. Vav) and adaptor proteins such as paxillin and PKL or p130CAS, Crk and ELMO that binds GEFs like PIX or DOCK180 (Figure 2.21 A; DeMali et al., 2003; Lee and Juliano, 2004). Also the adaptor protein β -parvin, which interacts with integrins through the ILK-PINCH complex provides a link to the GEF β -PIX, since it was shown to interact directly with β -PIX in a two hybrid screen (Rosenberger et al., 2000). Interestingly β 1 integrin was also shown to specifically bind to ICAP-1, which was reported to function as a Rho-GDI by binding Rac1 and Cdc42 and sequestering them in the cytosol (Degani et al., 2002). Thus, ICAP-1 binding to β 1 integrin would release the inhibition of the Rho GTPases (Brakebusch and Fässler, 2003). All these phosphorylations and formation of protein complexes lead to activation of Cdc42 and Rac1. Integrins also regulate RhoA activity, but in a complex manner. Initially stimulation of c-Src leads to activation of the p190RhoGAP, which triggers the inactivation of Rho (Figure 2.21 B). Later integrins contribute to Rho activation. One possible mechanism involves the protein tyrosine phosphatase α (PTP α), which activates Fyn, which presumably phosphorylates and activates a Rho GEF leading to Rho activation (Figure 2.21 B; DeMali et al., 2003). In addition, integrin dependent activation of FAK promotes the coupling of Rho to its effector protein mDia in lipid rafts at the leading edge of migrating fibroblasts (Figure 2.21 C; Palazzo et al., 2004). Lipid rafts are cholesterol- and sphingolipid rich plasma membrane domains that are enriched for a variety of proteins, thus, facilitating their interaction (Guan, 2004). Similarly to Rho, also Rac1 was shown to be specifically targeted to lipid rafts where it can interact with its

downstream effector PAK (Figure 2.21 C). Integrins have been proposed to modulate lipid rafts, since markers for these membrane structures were rapidly internalized upon cell detachment and reappeared on the cell surface when cells become attached to fibronectin (DelPozo et al., 2004).

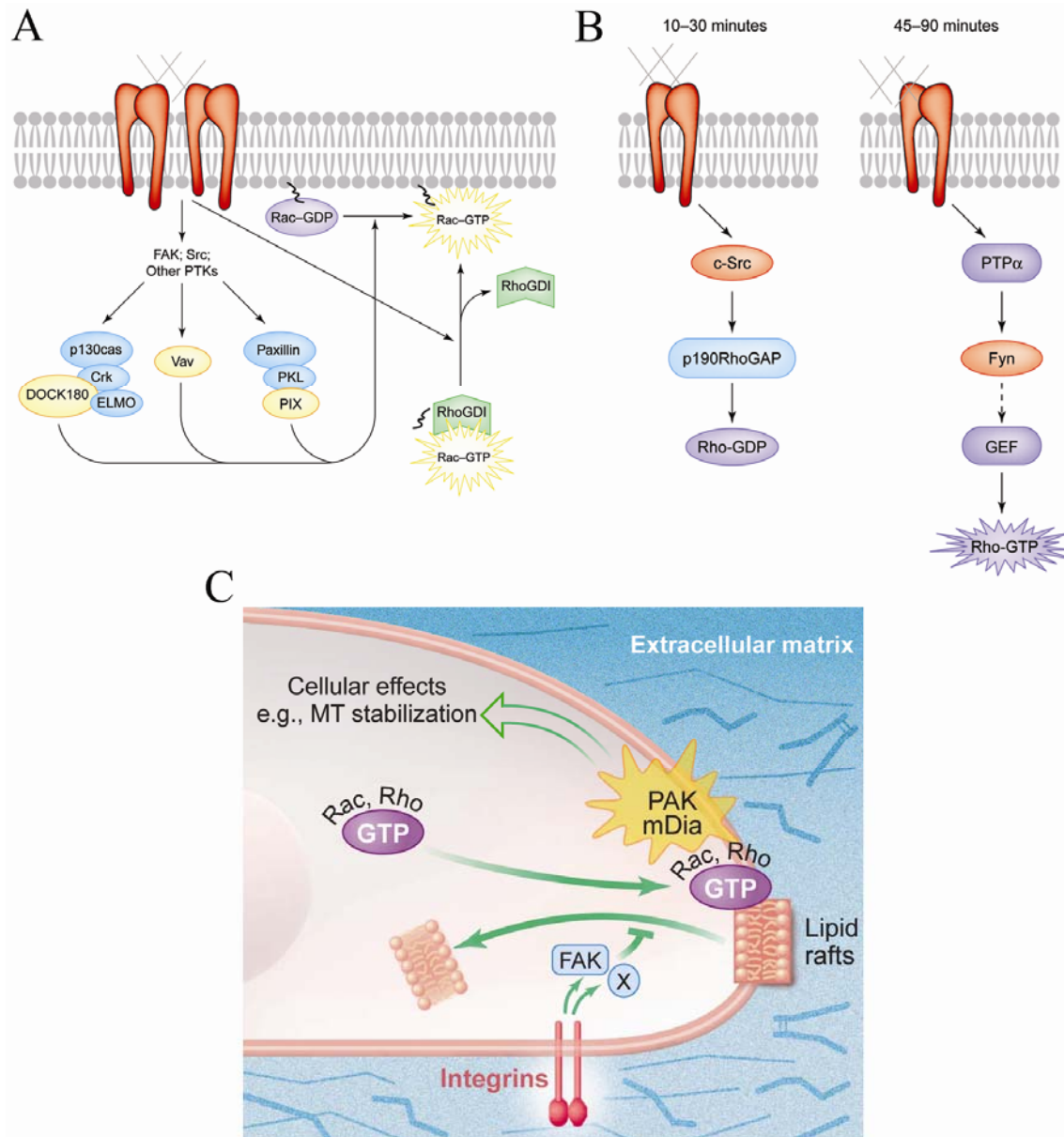


Figure 2.21 Integrin mediated activation of Rho GTPases. (A) Integrin mediated activation of Rac1 and Cdc42 (only Rac1 is indicated). Yellow circle, GEFs; blue circles, adaptor protein complexes. (B) Integrins in Rho activation (modified from DeMali et al., 2003). (C) Lipid rafts and integrin signalling coupling Rho GTPases and their effector proteins at the plasma membrane (modified from Guan, 2004).

Rho GTPases are not only effectors of integrins, they also modulate integrin mediated adhesion and signalling by regulating integrin clustering. Activation of Cdc42 and Rac1 is required for clustering of ligand-bound integrins to focal complexes, which then further mature into focal adhesions by RhoA mediated aggregation. Such receptor oligomerization

promotes ECM ligand binding through chelate and rebinding effects, strengthening adhesive contacts and the quality and quantity of signalling events downstream of integrins (Figure 2.22; Schwartz and Shattil, 2000).

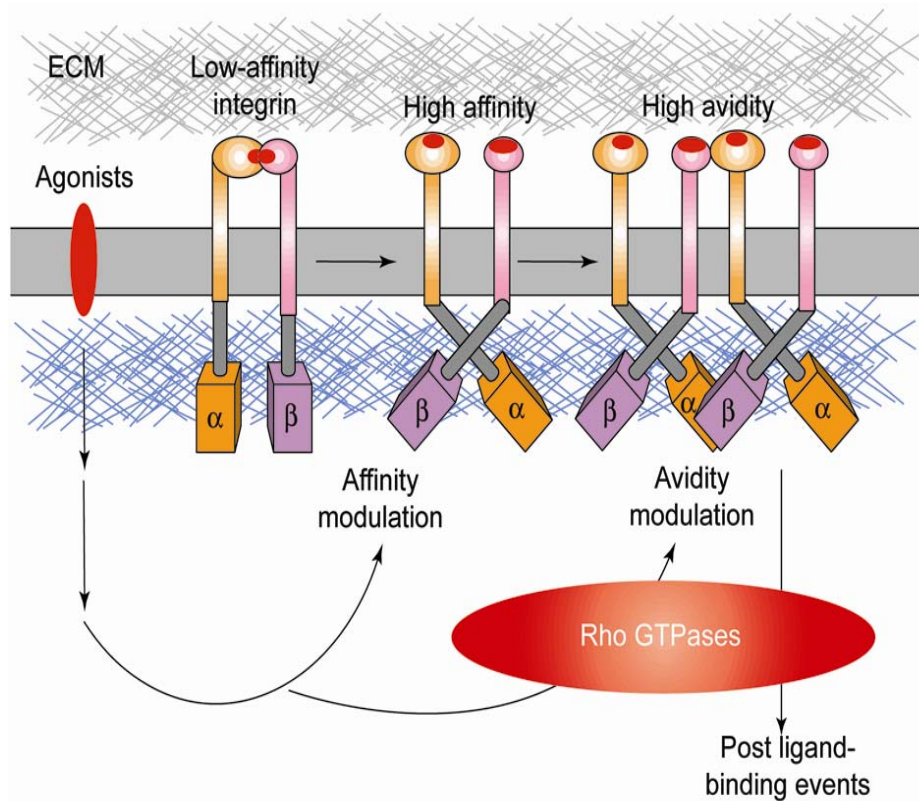


Figure 2.22 Regulation of integrins by Rho family GTPases. In resting cells integrins are often found in their low-affinity and low-avidity state with respect to ECM ligands. Upon activation by agonists, like growth factors and cytokines the integrin activity and avidity increases, triggered by the interaction of adaptor proteins with the β cytoplasmic tails of integrins (described in paragraph 2.1.2). Further avidity modulation could be triggered by Rho GTPases by regulating the interaction of integrin tails with the actin cytoskeleton. These in turn would induce post ligand-binding events, such as cell spreading which is clearly under the control of Rho GTPases (modified from, Schwartz and Shattil, 2000).

2.5 Aim of this study

Integrins and among them $\beta 1$ integrins, as well as Cdc42 are the key players in mediating migration associated events and there is a number of processes in which both of these proteins interact. In order to mediate signalling, integrins have to be activated but the mechanisms required for the activation are not fully understood, moreover, all we know about the possible activation mechanisms was so far only demonstrated *in vitro* and mainly for the $\beta 3$ integrins. Here we investigated the relevance of some of the postulated models *in vivo* and found that neither integrin phosphorylation of the NPXY motifs on the $\beta 1$ integrin tails nor disruption of

the salt bridge connecting the α and β subunits plays a significant role in integrin activation in keratinocytes *in vivo*. Cdc42 was shown to be the effector protein of integrins, mediating protrusion formation and cell polarization. Furthermore, Cdc42 was suggested to regulate integrins avidity. Nearly the entire knowledge about the role of Cdc42 in cell migration arises from studies with dominant negative inhibitory mutants, which may have unspecific effects. To exclude these unspecific effects we generated cells lacking a functional Cdc42 gene. Furthermore, these cells were transfected with a dominant negative mutant of Cdc42 to experimentally assess the specificity of dominant negative inhibition. We could show that Cdc42 does not influence integrin binding to ligands and migration speed, but regulates cell morphology and controls some aspects of cell polarity. However, we show that also other Rho GTPases contribute to these processes.

3 Materials and methods

3.1 Materials

The common chemicals used in this study were purchased from the following companies: Riedel-de Haen, Serva, Merck, Sigma and Roth. All substances were diluted in double-distilled water (ddH₂O), purified using the Milli-Q-System (Millipore). Cell culture media were purchased from Gibco and Sigma, cell culture media supplements were bought from Gibco and Sigma and cell culture plastic was purchased from Falcon, Nunclon and Corning.

3.2 Animals

All mice were maintained and bred under SPF (Specified Pathogen Free) conditions in the barrier animal facility of the Max-Planck-Institute for Biochemistry in Martinsried. The light cycle was set for 12 hours and mice had free access to standard rodent diets and water.

Mice used for phenotypic analysis were weaned at the age of three weeks, marked by ear tags (Hauptner) and housed in cages separated by sex. At the time of weaning, tail tips were clipped and stored at -20°C for genotypic analysis. Alternatively mice were toe-clipped at the age of 4 to 5 days. For breeding males at the age of at least 8 weeks and females at the age of at least 6 weeks were used.

All experiments were carried out according to the German Animal Protection Law.

3.3 Generation of genetically modified mice

3.3.1 Preparation of feeder cell lines

Co-culture of ES cells with feeder cells, which produce the differentiation inhibiting factor LIF, is helpful for maintaining the totipotency of ES cells. Feeder cells are isolated from 14.5 day embryos expressing the neomycin resistance gene.

Preparation of feeder cells was started with cervical dislocation of a pregnant mouse, which was then washed with 70% ethanol and placed in a sterile hood. Next, the peritoneal cavity of the mouse was surgically opened. The uteri containing embryos were removed and placed on a Petri dish filled with 20 ml of phosphate buffered saline (PBS). Subsequently, the embryos were dissected out of the uterus and the amnion. After cutting at the umbilical cord of the foetus, the head was removed. The remnants were transferred to a new Petri dish, filled with 20 ml PBS where the intestine, liver, kidneys and spleen were removed. The remaining

embryos were cut in small pieces and incubated in 1x trypsin / EDTA (Gibco), (1 ml / embryo) for 10 min at 37°C, pipetted up and down with a 5 ml pipette to break the tissue and incubated again for 10 min. Then the tissue was broken again by pipetting up and down with a 2 ml pipette and the resulting cell suspension was mixed with EF medium (see 3.7.2.1) and seeded into tissue culture flasks (two 175 cm² flasks per embryo). Cells were incubated at 37°C, 5% CO₂ without medium change, until they reached confluence, plus 3 days. Then the cells were trypsinised (see 3.7.3) and 1:10 of the cells were further subcultivated. The remaining cells were pelleted and γ -irradiated with 60 Gray, in order to mitotically inactivate the feeder cells, and frozen (see 3.7.4). The same procedure was repeated with the subcultivated cells, 3 days after they reached confluence.

3.3.2 Preparation of DNA for electroporation into embryonic stem cells

For efficient electroporation of the targeting vector into ES cells, the constructs had to be pure and 100% linearized.

First, the targeting construct DNA was linearized in the multiple cloning site of the vector by cutting 100 μ g of DNA with 100 U of the appropriate restriction enzyme (here, XhoI), for 6 to 8 hours in 37°C (see also 3.11.3). 2 μ l of the reaction were checked on agarose gel (see 3.11.5) to test for complete linearization of the targeting construct. Then the DNA was extracted with 1 volume of phenol / chloroform and the upper aqueous phase was transferred to a new tube, and extracted with chloroform. The upper aqueous phase was transferred to a new tube with 0.1 volume of 3M Na-acetate (pH 5.2) and mixed. Next, 2.5 volume of absolute ethanol was added. After vigorous mixing, white, coiled DNA precipitated. This DNA was transferred with a metal rod to a sterile 1.5 ml screw tube filled with 1 ml 70% ethanol and inverted several times. Finally, the supernatant was removed with a blue tip and the DNA was air dried in a sterile hood at RT for 5 – 10 min. Then, the pellet was re-suspended in 700 μ l of 1x PBS and was incubated at 37°C until the pellet was completely dissolved. DNA prepared according to this protocol was electroporated into ES cells.

3.3.3 Electroporation of ES cells

Prior to the electroporation ES cells were detached from cell culture plastic (see 3.7.3), re-suspend in 10 ml ES medium, transferred into a 15 ml tube and spun down (1500 RPM, 5 min). The cells were washed twice with 1x PBS and finally a cell pellet of 4×10^7 cells was re-suspended in the 700 μ l PBS / DNA solution by flicking the tube with a finger. Next, the ES cell / DNA solution was transferred with a Pasteur pipette to a sterile electrocuvette (BioRad)

and the electroporation at 0.8 kV and 3 μ F was performed with a Gene Pulser (BioRad) at RT. The electroporation was successful if the time constant for the decay of the electric field was 0.04 ms. The electroporated cells were split into 8, 10 cm cell culture dishes containing subconfluent layers of feeder cells.

3.3.4 Selection, picking and freezing of positive ES cell clones

Stably transfected ES cells were selected by addition of antibiotic to the growth medium. Thus, 24 hours after electroporation selection of stably transfected ES cell clones was started with ES medium containing 500 μ g / ml G418 (Geneticin, Gibco or Sigma). The medium was changed every 24 hours and clones were picked under a stereomicroscope (Zeiss, Stemi SV6), when becoming clearly visible by eye, 6 days after beginning of the selection. The clones were scratched from the feeder cell layer by a sterile tip and transferred to a pre-warmed (37°C), sterile 96-well plate filled with 150 μ l 1x trypsin / EDTA. The presence of colonies in the wells was checked under microscope and cells were dispersed after about 20 min incubation at 37°C in 150 μ l of ES medium with G418. The cell suspensions were transferred to wells of a 24-well plate containing feeder cells and cultured under standard conditions. The medium was changed the next day. 3 to 5 days later, when the medium started to turn yellow, the clones were frozen according to standard protocol (1 ml ice cold freezing medium per well, see also 3.7.4). About 40% of the cell suspension in freezing medium was left in the well and cultured further after addition of 1.5 ml of non selective ES medium. The medium was changed the next day to 1 ml ES medium / well. When the medium was bright yellow, genomic DNA was isolated from the cells (3.11.13.2) and tested by Southern blot (3.11.14) for homologous recombination.

3.3.5 Preparation of ES cells for blastocyst injection

$2\text{-}5 \times 10^6$ ES cells (1 vial, see 3.3.4) were seeded together with feeder cells on a 6-well plate and incubated for 1 to 2 days. On the day of injection ES medium was changed 1 to 2 hours prior to trypsinisation (see 3.7.3), after which the cells were re-suspended in 3 ml 1:1 solution of ES medium and flush medium (high glucose DMEM without NaHCO_3 , buffered with 20 mM HEPES at pH 7.4, supplemented with 10% FCS). Cells were kept on ice before being injected into blastocysts (see 3.3.6)

3.3.6 Production of chimeric animals

In order to generate chimeric animals, ES cells (see 3.3.5) were injected into the cavity of blastocysts, in which the ES cells intermingle with the inner cell mass cells (carried out by Dr.

Michael Bösel, Transgenic facility, MPI for Biochemistry). The injected blastocysts were then transferred into the uterus of pseudopregnant foster mice (E 2.5), where they developed to chimeric mice containing blastocyst and ES-cell-derived cells. The contribution of ES cells to the chimeric mice was assessed based on the difference in coat colour genes of the blastocysts and ES cell used for injection. Blastocysts were derived from black C57Bl/6J mice and ES cells were derived from aguti 129/Sv mice, so that the percentage of aguti coat colour of the chimera roughly indicated the contribution of ES cells. For further breeding male chimeras with highest ES cells contributions were used.

3.3.7 Breeding schemes

To test for the germ-line contribution of the ES cells male chimeras were mated to female C57Bl/6J mice. Because the aguti coat colour is dominant over black coat colour, mice which developed from ES cell-derived germ cells were easily distinguished by their aguti fur. Heterozygous aguti offspring were further mated with mice carrying heterozygously the floxed $\beta 1$ integrin (Brakebusch et al., 2000) and a Cre recombinase under the control of keratin-5 (K5) promoter (Ramirez et al., 2004), to achieve skin specific expression of the knockin allele.

3.4 Wounding and preparation of wound tissue

In order to study keratinocyte migration *in vivo*, wound healing studies have been performed in collaboration with Prof. Sabine Werner, ETH, Zürich, Switzerland.

Briefly, prior to wounding mice were anaesthetised by intraperitoneal injection of 100 μ l ketamine (10 g / l) / xylazine (8 g / l) solution. Two full-thickness excisional wounds, 3 mm in diameter, were made on either side of the dorsal midline by excising skin and panniculus carnosus. Wounds were left uncovered and harvested at indicated time points after injury. For expression analysis (see 3.11.18), the complete wounds including 2 mm of the epithelial margins were excised and immediately frozen in liquid nitrogen. Non-wounded back skin served as control. For histological analysis, the complete excisional wounds were isolated, bisected and fixed (see 3.5.1 and 3.5.2).

3.5 *Histological methods*

3.5.1 *Isolation and embedding of mouse skin*

For the back skin isolation, mice were sacrificed at selected time points by cervical dislocation and subsequently shaved using an electric shaver (Thrive ®) in order to remove the fur. The back skin was dissected at subcutis level, placed on a Hybond-XL membrane (Amersham Biosciences) and smoothened. The tissue was then either directly embedded in O.C.T.TM compound (Thermo Shandon) for cryosections or fixed O/N at 4°C in 4% paraformaldehyd (PFA) / 1x PBS for paraffin sections.

10x PBS

NaCl	40g
KCl	1 g
Na ₂ HPO ₄ x 2H ₂ O	7.2g
KH ₂ PO ₄	1 g
filled up to 500 ml with ddH ₂ O	

3.5.1.1 *Embedding and cutting skin for cryosections*

In order to embed skin pieces in O.C.T.TM compound, small plastic containers (tissue teks, Sakura) were placed on a cooper plate situated on dry ice. Small amounts of O.C.T.TM compound were added to the tissue teks and the skin piece was placed into the slowly freezing embedding medium. Subsequently the tissue was fully covered with the O.C.T.TM compound and after freezing stored at -80°C. Skin samples embedded in the O.C.T.TM compound were cut into 10 µm slices at -20°C using a cryostate (Microm). Frozen sections were transferred to positively charged glass microscope slides (SuperFrost®Plus, Menzel–Gläser), air-drayed for 30 min at room temperature (RT) and stored at -80°C.

3.5.1.2 *Embedding and cutting skin for paraffin sections*

Skin pieces fixed O/N at 4°C in 4% PFA / 1x PBS were subsequently dehydrated at RT in a row of ethanol dilutions: 50%, 70%, 80%, 90% and 3 times 100%, 60 min each. After two incubations in xylol for 30 min, the tissue was placed in a paraffin solution, for three, 90 min long, consecutive incubations at 56°C. Embedding in paraffin was done at -7°C by means of an embedding machine (Shandon). Paraffin blocks were stored at 4°C and cut using a microtome (Microm) into 8µm slices. These slides were than smoothen in the 40°C water bath of the microtome, laid flat on the surface of positively charged glass microscope slides and drayed at 37°C. Paraffin sections were stored at 4°C.

3.5.2 *Haematoxylin and Eosin staining*

In order to investigate the morphology of the skin, paraffin sections were stained using a Haematoxylin and Eosin staining, a commonly used technique in the histology. Haematoxylin has an affinity for negatively charged (basophilic) molecules and therefore reveals with a purple staining the distribution of DNA, RNA and acidic proteins; eosin stains eosinophilic structures of the cell, like the cytoplasm, muscles and collagen in pink.

To perform the staining, paraffin sections were deparaffinised at RT in xylol, two times, 5 min, and then by an ethanol row of 2 min incubations: 100%, 100%, 95%, 90%, 80% and 70%. In the next step, slides were stained for 1 min in Haematoxylin (Meyer's hemalaum solution, MERCK) / ddH₂O (0.1%) and the reaction was stopped by a washing step in tap water. The subsequent staining with Eosin (Eosin gelblich, Merck) / ddH₂O (1:2) for 1 min was also terminated by a washing step in tap water. The staining was continued with a dehydration row of the following ethanol / water dilutions: 70%, 90%, 95%, 100%, 2 min each. After washing twice with xylol, sections were mounted with Entellan (Entellan new, Merck) and stored at 4°C.

3.5.3 *LacZ staining*

The *E. coli* lacZ gene is the most commonly used reporter gene system in histochemistry. The expression of lacZ results in the production of β -galactosidase (β -gal) which can be readily detected by a number of chromogenic or fluorogenic β -gal substrates. Here the β -gal substrate 5-Bromo-4-chloroindoxyl-beta-D-galactopyranoside (X-gal) that produces blue, insoluble precipitates was used to detect production of β -gal.

In order to detect the β -galactosidase in skin samples, cryosections (see 3.5.1.2) were warmed up for 1 hour at RT, encircled with a Pap-Pen (G. Kisker-Produkte für die Biotechnologie) to create a water repellent area and fixed with solution B for 5 min. Next, the sections were washed 3 times, 5 min with solution C and subsequently stained O/N at RT, dark, in X-gal containing solution D. Slides were stored at 4°C. Eventually, sections were counterstained like described in 3.6.2.1 and mounted with Elvanol.

SOLUTIONS FOR LACZ ASSAY

10x Sol. A

1 M KPP, pH 7.4

(228.23 g K₂HPO₄ x 3 H₂O, adjust pH with HCl)

4x Sol. A2

10 x Sol A	400 ml
1M MgCl ₂	128 ml
EDTA	7.6g

filled up to 1 l with ddH₂O, pH adjusted to 7.4

Sol. B (always fresh)

1x Sol. A2	250 ml
25% glutaraldehyde	2 ml

2x Sol. C

4x Sol. A2	500 ml
Na deoxycholate (Sigma D-6750)	0.2 g
NP-40 (Sigma N-6507)	0.4 ml

filled up to 1 l with ddH₂O

K3 (100 mM K₃Fe(CN)₆)

3.3 g mM K₃Fe(CN)₆ in 100 ml ddH₂O (stored in the dark)

K4 (100 mM K₄Fe(CN)₆)

34.2 g mM K₄Fe(CN)₆ x 3 H₂O in 100 ml ddH₂O (stored in the dark)

50 mg/ml X-gal

1 g X-gal in 20 ml DMSO or DMF (aliquots stored at -20°C)

Sol. D (sterile filtrate before use, stored in the dark, reuse possible)

2x Sol. C	250 ml
K3	50 ml
K4	50 ml
X-gal	5 ml
ddH ₂ O	145 ml

3.6 Immunological methods

3.6.1 Immunofluorescence (IF)

3.6.1.1 Immunofluorescence on skin sections

To visualize certain proteins in skin samples, immunofluorescence staining was performed on skin cryosections (see 3.5.1.2). Prior to staining, sections were warmed up for 1 hour at RT, encircled with a Pap-Pen to minimize staining solution and fixed 20 min, RT with 4% PFA / 1x PBS. After 3 washing steps with 1x PBS, 5 min each, the sections were permeabilized on ice using a 0.1% TritonX100 / 1x PBS solution and shortly rinsed with 1x PBS. Subsequently sections were blocked in 3% BSA / 1x PBS, either 30 min RT or O/N at 4°C. After blocking a 90 min incubation with 80 µl of the primary antibody, diluted in 1% BSA / 1x PBS, in a humidized chamber in the dark, followed (for dilutions see 3.6.1.4). In the next step sections

were again washed 3 times, 5 min, with 1x PBS and incubated for 60 min with 80 μ l of the secondary antibody diluted in 1% BSA / 1x PBS (for dilutions see 3.6.1.5). In double stainings the respective primary antibody and secondary reagents were combined, if cross-detection could be excluded. Eventually, a 5 min incubation with 100 μ l of the 4',6-Diamidino-2-phenylindole (DAPI, Sigma; 1:10.000) / 1x PBS was performed, in order to visualize the nuclei. Sections were washed 3 times with 1x PBS, 5 min each, mounted with Elvanol and air-dried for 15 min. Immunostained sections were stored at -20°C in a dark box.

3.6.1.2 Immunofluorescence on adherent cells

In order to visualize proteins in a cell monolayer, immunofluorescence staining was performed. Cells were washed 3 times with 1x PBS and fixed 20 min, RT with 4% PFA / 1x PBS. For following steps see 3.6.1.1.

3.6.1.3 Immunofluorescence on suspension cells

Prior to the normal staining procedure, suspension cells (e.g. freshly isolated keratinocytes) had to be attached to the glass microscope slides. In order to do so, 10.000 cells were dissolved in 1x PBS / 1% BSA and spun down using a cyto-spin centrifuge (Hetten). Cells were air-dried for 5 min and fixed 20 min, RT with 4% PFA / 1x PBS. For following steps see 3.6.1.1.

3.6.1.4 Primary antibodies

ANTIBODY	COMPANY	DILUTION FOR IHC	DILUTION FOR IF	DILUTION FOR WB	SPECIAL BLOCKING / ANTIBODY SOLUTION FOR WB
β 1 integrin	Chemicon	1:400	1:400		
β -catenin	BD Biosciences			1:500	
Akt	Cell Signalling			1:1000	5%BSA antibody solution
BrdU-POD	Roche	1:40			
Cdc42	BD Biosciences			1:333	
FAK	Upstate			1:1000	
GM-130	BD Biosciences		1:250		
Gsk3 β	Cell Signalling			1:1000	
ILK	Cell signalling		1:100		
Integrin α 6 FITC	PharMingen		1:600		
JNK1&2	Biosource			1:1000	Blocking 4% BSA , 4°C, O/N; 1%BSA antibody solution
Keratin 10	Covance		1:600		
LN5 1097+E(2) anti γ α 2LE4-LE6	Brakebush et al., 2000		1:200		
p44/42 MAPK	Cell Signalling			1:1000	
Paxillin	BD Biosciences		1:300		
Paxillin pY118	BD Biosciences			1:250	
Phalloidin FITC	MolecularProbes		1:600		
pTpY180/182 p38	Biosource			1:1000	Blocking 5% BSA , 4°C, O/N; 3%BSA antibody solution
pTpY183/185 JNK1&2	Biosource			1:1000	Blocking 4.5% BSA , 4°C, O/N; 1%BSA antibody solution
pY397FAK	Biosource		1:100	1:1000	
Rac1	BD Biosciences			1:2000	
RhoA	Santa Cruz			1:5000	
SAPK2a/p38	Biosource			1:1000	Blocking 4.5% BSA , 4°C, O/N; 1%BSA antibody solution

ANTIBODY	COMPANY	DILUTION FOR IHC	DILUTION FOR IF	DILUTION FOR WB	SPECIAL BLOCKING / ANTIBODY SOLUTION FOR WB
Ser437Akt	Cell Signalling			1:1000	5%BSA antibody solution
Ser9Gsk3 β	Cell Signalling			1:1000	
Thr202/Tyr204 p44/42 MAPK	Cell Signalling			1:1000	
Tubulin	obtained from Jürgen Wehland, Braunschweig, Germany		1:600	1:10000	

3.6.1.5 Secondary antibodies

ANTIBODY	COMPANY	DILUTION FOR IF	DILUTION FOR WB
Goat anti mouse HRP	Jascon Immunoresearch		1:10000
Goat anti rabbit HRP	Jascon Immunoresearch		1:10000
Donkey anti rat HRP	Jascon Immunoresearch		1:10000
Goat anti mouse Cy3	Jascon Immunoresearch	1:800	
Donkey anti rabbit Cy3	Jascon Immunoresearch	1:600	
Goat anti rat Cy3	Jascon Immunoresearch	1:600	
Goat anti mouse FITC	Jascon Immunoresearch	1:600	
Goat anti rabbit FITC	Jascon Immunoresearch	1:600	

3.6.2 Immunohistochemistry

3.6.2.1 BrdU staining

Bromodeoxyuridine (BrdU) is an analogue of thymidine, which can be incorporated into DNA. Proliferating cells can be pulse-labelled with BrdU, since cells that are synthesizing DNA (in S-phase of the cell cycle) will incorporate BrdU into the DNA. Anti-BrdU antibody can then be used to identify cells that undergo DNA synthesis during exposure to BrdU.

In order to identify proliferating cells in skin samples, mice were injected with 5 mg / ml BrdU / 1x PBS solution, per 10 g of body weight and sacrificed 2 hours later. Paraffin sections (see 3.5.1.2) from injected mice were deparaffinised at RT in xylol, two times 5 min, followed by an ethanol / water row of 3 min incubations: 100%, 100%, 95%, 90%, 80%, 70% and water. Next, the slides were transferred for 5 min into 1x PBS, and then subsequently for 20 min in 4N HCl and 5 min in ddH₂O. Then sections were incubated in a water bath at 37°C, for 20 min, in a jar with pre-warmed 0.1% trypsin (Gibco) / 0.1% CaCl₂ solution and washed 5 min in ddH₂O. After blocking of the endogenous peroxidase in 75 ml methanol / 2.5 ml 30% peroxidase solution for 10 min at RT, the tissue was washed 3 times, 5 min, in x1 PBS. Finally the sections were blocked at RT, 3 times, 5 min with 0.5% BSA / 0.1% TweenX20 / 1x PBS solution and the tissue pieces were encircled with a Pap-Pen to minimize the use of staining solution. An O/N incubation with 50 μ l BrdU-POD antibody / blocking solution at 4°C followed. After the incubation with the antibody, slides were washed 3 times with 1x PBS. The horseradish peroxidase (POD) which is conjugated to the antibody catalyzes in the

presence of hydrogen peroxide the oxidation of Diaminobenzidine (DAB, Sigma) producing a coloured reaction product. To perform this reaction, washed slides were incubated in the substrate solution and the ongoing reaction was controlled at different time points by microscopic examination. The reaction was stopped latest after 10 min, with 10 min incubation in ddH₂O. Afterwards, the tissue was counterstained in Mayer's hemalaum solution (Merck, 1:5 in tap water), 5 times, 10 sec, and washed 10 min in tap water. A dehydration row of ethanol / water dilutions followed: 70%, 90%, 95%, 2 times 100%, 3 min each. After washing twice with xylol, sections were mounted with Entellan and stored at 4°C.

SUBSTRATE (DAB) - SOLUTION

ddH ₂ O	45ml
1M Tris-HCl, pH 7.6	50ml
stock I:	0.027g DAB in 5ml ddH ₂ O (freshly prepared, added just before use)
stock II:	100 µl ddH ₂ O + 20 µl 30% H ₂ O ₂ (added just before use)

3.6.2.2 Terminal deoxynucleotidyltransferase-mediated dUTP nick end-labelling (TUNEL)

The TUNEL assay is based on the observation that late stages of apoptosis are associated with extensive DNA degradation. The cleavage of the DNA yields double-stranded as well as single strand breaks ("nicks"). Those DNA strand breaks can be detected by enzymatic labelling of the free 3'-OH termini with modified nucleotides (e.g. fluorescein-dUTP).

To detect apoptotic cells by TUNEL, the *in Situ* Cell Death Detection Kit from Roche was applied according to the protocol of the manufacturer. As counterstaining the DAPI labelling was performed.

3.6.3 Fluorescence Activated Cell Sorter (FACS)

To assess the surface expression levels of integrins, FACS analysis was performed. In this technique cells in a cell suspension are first directly or indirectly labelled with antibodies conjugated to different fluorochromes (like FITC, PE and Cy5) and then are introduced into a flow system, in which they individually pass through a cuvette where fluorescence and light scattering is measured. The forward scatter (FSC) is roughly proportional to the cellular size, while side scatter (SSC) is proportional to the cellular granularity.

To assess the expression level of integrins, 7×10^5 to 1×10^6 cells were pelleted and re-suspended in 200 µl 1% BSA / 1x PBS, transferred to a U-bottom well of a 96-well plate and centrifuged 5 min, 1500 RPM at 4°C. Subsequently cells were re-suspended in 50µl of the

primary antibody solution. Both unconjugated and conjugated antibodies (all PharMingen) were diluted 1:200 and incubated 30 min on ice, in the dark. After a washing step with 200 μ l 1% BSA / 1x PBS, cells were centrifuged again for 5 min, 1500 RPM at 4°C. If non-conjugated primary antibodies were applied in the first incubation step, cells were re-suspended in 50 μ l of secondary antibody solution (all 1:250 or 1:500, all Jackson Immunoresearch) and left for further 15 min on ice, in dark. In a following step, cells were washed again with 200 μ l 1% BSA / 1x PBS and centrifuged. Finally cells were resuspended in 200 μ l 1% BSA / 1x PBS, transferred into FACS tubes (Alpha Laboratories Ltd.) and kept covered on ice until the analysis was performed. Immediately before the measurement in a flow cytometer (FACSCalibur, Becton Dickinson) dead cells were stained with propidium iodide (stock: 1 mg / ml, diluted 1:400) and vortexed, in order to distinguish between dead and living cells. The analysis was done with the CellQuest™ software.

3.7 Cells and cell culture methods

3.7.1 Cell lines

- Cdc42 fl/- and -/- ES cells, clone #81 and #66, respectively.
- Cdc42 fl/- ES cells derived fibroblastoid cell lines: parental clone: 3.9 and 3.5 (Cdc42fl/-) and from the 3.9 clone descending clones 3.9.7 (Cdc42-/-) and 3.9.9 (Cdc42-/-).
- 3.9.7 (Cdc42-/-) derived fibroblastoid cell lines: #35 (Cdc42fl/- + wtCdc42); #40 and #42 (Cdc42-/- + dnCdc42).
- GATA4 Cdc42 fl/- and -/- endodermal cells, clones #1, #4 and #1, #2; respectively.
- Phoenix cells (kindly provided by Dr. Gary Nolan, Stanford University, USA)

3.7.2 Culture conditions and media

3.7.2.1 Culturing of fibroblastoid cell lines and Phoenix cells

Cells were cultured in EF medium containing Dulbecco's modified Eagle's medium (DMEM with GlutaMAX™ I, 4500 mg/L D-Glucose, Sodium Pyruvate; Gibco) and 10% heat inactivated (56°C, 30 min) foetal calf serum (FCS, Gibco); at 37°C, 5% CO₂ and 100% humidity. For stable transfected cell lines: #35, #40 and #42 medium was additionally supplemented with 100 μ g / ml Hygromycin B (Calbiochem). All cells lines were cultured in sterile cell culture dishes (Falcon). Cells were subcultivated (1:3 or 1:4) twice to three times a week.

3.7.2.2 *Culturing of ES cells and endodermal cells*

To assure totipotency and germ-line transmission of ES cells, ES cells were kept at low passage number and low density, and were cultured in sterile cell culture dishes (Falcon) on feeder cells, in special ES medium supplemented with LIF to prevent differentiation. ES medium contained: Dulbecco's modified Eagle's medium (DMEM with GlutaMAX™ I, 4500 mg/L D-Glucose, Sodium Pyruvate; Gibco) with 20% heat inactivated (56°C, 30 min) foetal calf serum (FCS, Gibco), 0.1mM 2-mercaptoethanol, 1x nonessential amino acids (100x stock, Gibco) and 1000 U / ml leukaemia inhibitory factor (LIF, ESGRO from Gibco). ES cells were cultured at 37°C, 5% CO₂ and 100% humidity. ES medium was changed every day and cells were subcultivated (1:3 or 1:4) three times a week. Endodermal cells were cultured under the same conditions as ES cells, only the medium was changed every second day. Endodermal cells were grown without the feeder cell layer.

3.7.2.3 *Culturing of primary keratinocytes*

Primary keratinocytes were cultured in special keratinocytes medium, in cell culture dishes (Falcon) coated for 1 to 4 hours, at 37°C with 1x collagen I (Cohesion) and 0.01 mg / ml fibronectin (Invitrogen; coated dishes can be stored at 4°C). Keratinocytes were kept at 34°C, 5% CO₂, 100% humidity and could be subcultivated twice (1:1.5 or 1:2). Keratinocyte medium was changed every second day.

KERATINOCYTE MEDIUM

	MEDIUM / SUPPLEMENT	COMPANY	FINAL CONCENTRATION
500 ml	MEM	(Sigma #M8167)	
500 µl	Insulin (5 mg / ml in 4 mM HCl)	(Sigma #I5500)	5 µg / ml
25 µl	EGF (200 µg / ml in PBS)	(Sigma #E9644)	10 ng / ml
1000µl	Transferin (5 mg / ml in PBS)	(Sigma #T8158)	10 µg / ml
500 µl	Phosphoethanolamine (10 mM in PBS)	(Sigma #P0503)	10 mM
500 µl	Ethanolamine (10 mM in PBS)	(Sigma #E0135)	10 µM
36 µl	Hydrocortisone (5 mg / ml in Ethanol)	(Calbiochem #386698)	0.36 µg / ml
5 ml	Glutamine (100x)	(Invitrogen)	1x
5 ml	Pen / Strep (100x)	(Invitrogen)	1x
40 ml	Chelex treated foetal calf serum (FCS)		8%

To remove calcium from the FCS the serum was treated with chelex beads, which chelate Ca²⁺ ions. The chelex resin was filtered through a folded filter (Schleicher&Schuell) and the chelex beads were placed in 100 ml heat inactivated FCS (Gibco), and stirred O/N at 4°C. To remove the chelex, the solution was filtered again through a folded filter and the filtrate was spun down, 8000 RPM, 5 min. FCS was sterilized by passing it through a 0.2 µm filter.

CHELATED FCS

Chelex (BioRad) 40 g
 filled up to 1000 ml with ddH₂O
 pH 7.4 adjusted with HCl

KERATINOCYTE COATING MEDIUM

25 ml	MEM	(Sigma #M8167)	
2.5 ml	BSA Fraction V (1 mg / ml)	(PAA Laboratories)	filter to sterilize
500 µl	Hepes pH 7.3 (1M)	(Sigma #H0887)	
250 µl	Vitrogen 100x collagen	(Cohesion FXP-019)	
250 µl	Fibronectin (1 mg / ml)	(Invitrogen #33016-015)	filter to sterilize
290 µl	CaCl ₂ (100 mM)		filter to sterilize

3.7.2.4 Culturing of cells on coverslips

24 mm x 24 mm glass cover slides (Menzel-Gläser) were treated for 30 min with a solution containing 60% ethanol and 40% HCl and then washed several times with ddH₂O. Treated coverslips were then added to wells of a 6 well plate and sterilized for 15 min, 800 W in a microwave. Before plating the cells, the 6-well plates were preincubated for 1 hour with growth medium (fibroblastoid cell lines) or coated with 1x collagen I and 10 µg / ml fibronectin (keratinocytes) or fibronectin (5 µg / ml in FCS containing growth medium, endodermal cells).

3.7.3 Passaging and trypsinizing of cells

Adherent cells were washed once (twice for ES cells) with 1xPBS and detached from the cell culture dish by incubating them for 1–2 min (6–10 min for keratinocytes) at 37°C in a 1x trypsin – EDTA solution (Gibco, stock x10). The trypsin treatment was stopped by adding fresh, pre-warmed growth medium and cells were transferred at the desired density to a new culture dish. In case of ES cells, the cells were not directly plated but first pelleted 5 min at 1500 RPM, resuspended and then seeded together with feeder cells.

3.7.4 Freezing of cells

In order to freeze cells, cells were detached from cell culture dishes (see 3.7.3) re-suspended in pre-warmed growth medium, and spun down at 1500 RPM, 5 min. The cell pellet was re-suspended in pre-cooled freezing medium (growth medium + 10% dimethylsulfoxide (DMSO; Sigma). Cells were immediately frozen in 1.5 ml cryo-vials (Corning) on dry ice, transferred to -80°C and then for longer storage into liquid nitrogen.

3.7.5 Thawing of cells

Cryo-vials were removed from -80°C or liquid nitrogen and placed into a 37°C water bath, until the frozen medium had melted. The thawed cells were transferred into 5 ml of warm growth medium, centrifuged for 5 min at 1500 RPM, re-suspended in growth medium and plated on culture dishes.

3.8 Biochemical methods

3.8.1 Extraction of proteins from cells

In order to extract proteins from cells, cells were grown on 10 cm plastic culture dishes (Falcon) and prior to lysis, washed once with ice cold 1x PBS. Cells were lysed on ice, for 30 min, in 700 μl of modified RIPA lysis buffer. Finally cells were scraped from the plastic dish with a cell scraper (costar) and stored at -20°C until they were further analysed by SDS-PAGE (see 3.8.3).

LYSIS BUFFER (modified RIPA buffer)

CHEMICAL	STOCK CONCENTRATION	FINAL CONCENTRATION	FOR 10 ml of LYSIS BUFFER
TritonX-100	10 %, 1 ml / 10 ml	1 %	1000 μl
Na-deoxycholate	10 %, 1 g / 10 ml	1 %	1000 μl
SDS	20 %, 200 g / 1 l	0,1 %	100 μl
HEPES pH 7.4	1 M, 23.83 g / 100 ml	50 mM	500 μl
NaCl	5 M, 146.1g /500 ml	150 mM	300 μl
glycerol	96 %	10 %	1150 μl
NaF	1 M, 0.42 g / 10 ml	100 mM	1000 μl
$\text{Na}_4\text{P}_2\text{O}_7$	100 mM, 0.45 g / 10 ml	10 mM	1000 μl
MgCl_2	1 M, 10.2 g / 50 ml	1.5 mM	15 μl
EGTA	50 mM, 1.2 g / 50 ml	1mM	200 μl
Na_3VO_4	100 mM, 0.092 g / 5 ml	1mM	100 μl
EDTA-free proteinase inhibitors (Roche)	-	-	1 tablet (according to the protocol of the manufacturer)

3.8.1.1 Serum induced signalling

To check for serum induced activation of signalling pathways, cells were grown to confluence and subsequently starved for 12h in 0.5% FCS containing medium. Next, cells were induced for indicated times with complete growth medium and lysed.

3.8.1.2 Wounding induced signalling

To investigate wound-induced signalling fibroblastoid cells were grown to confluence and scraped several times with 0.7 mm needles in order to remove approximately 50% of the cells

(Etienne-Manneville and Hall, 2003). Cells were allowed to migrate for indicated time. To investigate wound-induced signalling in keratinocytes, cells were starved for 24h in medium deprived of FCS, before migration was induced.

3.8.2 Determination of protein concentration

The protein concentration in cell extracts (see 3.8.1) was measured by means of a MicroBC Assay (Uptima). The MicroBC Assay is a colorimetric assay which involves the reduction of Cu^{2+} to Cu^{+} by peptide bonds of proteins. The Bicinchoninic acid (BC) chelates Cu^{+} ions with very high specificity to form a water soluble purple coloured complex. This reaction is measured by the high optical absorbance of the final Cu^{+} complex at 562 nm. Absorbance is directly proportional to the protein concentration, with a broad linear range between 1 $\mu\text{g} / \text{ml}$ to 100 mg / ml .

To measure the protein concentration in a given sample, a set of protein standards of known concentration was prepared, by serially diluting bovine serum albumin (BSA; Interchim), stock solution (2 mg / ml), in the lysis buffer (see 3.8.1). 5 μl of the samples, a blank control (lysis buffer alone) and the standards were pipetted on a 96-well plate. Then 200 μl of the solution B diluted 1:50 in solution A were added to each sample according to protocol of the manufacturer. After 35 min incubation at 37°C, the absorbance was measured at 562 nm with an ELISA reader (Dynatech). The protein concentration was calculated from the reference curve obtained for the standard protein.

3.8.3 SDS-Polyacrylamide gel electrophoresis (SDS-PAGE)

The proteins were separated by means of the Mini Protean II System (BioRad). The polyacrylamide gels were constructed of two different acrylamide gels, one on top of the other. The upper or stacking gel contained 5% acrylamide, the lower resolving gel contained a higher acrylamide concentration of 10% or 12%. These gels were differentially buffered to create an ionic strength discontinuity between the stacking gel and the running gel. As current was applied the difference in ionic strength resulted in a voltage discontinuity and concentration of the sample to a thin zone at the stacking gel-resolving gel boundary. This stacking effect results in superior resolution within the running gel, where polypeptides enter and migrate much more slowly, according to their size and shape. The gels were poured between two glass plates, between which 1.5 mm thick spacers were applied.

Prior to separation 15 – 20 mg of proteins from the cell extract were diluted in 3x sample buffer and denatured 5 min at 95°C. If a 10-well comb was used, the final volume of the sample loaded on the gel was 50 μl , if a 15-well comb was applied, the total volume was 30

μ l. The proteins were separated in the presence of a protein standard (Broad Range, BioRad) to estimate the protein size. Electrophoresis was performed at 40 mA until the proteins reached the border of the separating gel. Then the current was increased to 100 mA and the separation was stopped when the bromphenol blue reached the bottom of separating gel. Finally the gel was removed from the electrophoresis chamber and the separated proteins were transferred to a PVDF membrane (see 3.8.4).

Eventually the gel was stained for 30 min in a Coomassie brilliant blue solution, which binds non-specifically to virtually all proteins. To remove the non-bound dye, the gels were destained for 24h in 10% acetic acid and photographed.

STACKING GEL (2 gel size) 5%

ddH ₂ O	5.5 ml
0.5M Tris-HCl, pH6.8	1 ml
30% acrylamide (ProtoGel, National diagnostics)	1.3 ml
10% SDS	800 μ l
10% ammonium persulfate (APS)	800 μ l
TEMED (Sigma)	8 μ l

RESOLVING GEL (2 gel size)

	10%	12%
ddH ₂ O	7.9 ml	6.6 ml
0.5M Tris-HCl, pH8.8	5 ml	5 ml
30% acrylamide (ProtoGel, National diagnostics)	6.7 ml	8 ml
10% SDS	200 μ l	200 μ l
10% ammonium persulfate (APS)	200 μ l	200 μ l
TEMED (Sigma)	8 μ l	8 μ l

10x SDS-PAGE RUNNING BUFFER

Tris-Base	30.3 g
Glycine	144 g
SDS	10 g
filled up to 1 l with ddH ₂ O	

3x SAMPLE BUFFER

SDS	3 g
87% Glycerol	7.3 ml
1M Tris-HCl pH 6.8	3 ml
2-Mercaptoethanol	2 ml
bromphenol blue	10 mg
filled up to 20 with ddH ₂ O	
dissolved at 60°C, stored in aliquots at -20°C	

COOMASIE BRILIANT BLUE SOLUTION

0.1% Coomassie brilliant blue
 10% acetic acid
 40% methanol
 in ddH₂O

DESTAINING SOLUTION

10% acetic acid in ddH₂O

3.8.4 Western blotting (WB)

Western blotting is a technique which enables specific detection of proteins separated by size by means of the SDS-PAGE technique (see 3.8.3). Here the separated proteins were transferred onto a PVDF membrane (Immobilon-P, Millipore) by electrophoretic transfer (Mini Trans-Blot cell, BioRad) to be further detected by specific antibodies.

First a protein-containing polyacrylamide gel was placed in direct contact with a piece of methanol activated PVDF membrane (10 sec in 100% methanol) and "sandwiched" between two electrodes submerged in a conducting blotting buffer (Figure 3.1). By application of an electric field (usually 100 V, 100 min or 30 V O/N at 4°C), the proteins moved out of the polyacrylamide gel and became tightly attached onto the surface of the membrane. These proteins were then detected using specific antibodies.

10x BLOTTING BUFFER

Tris-Base	15.1 g
Glycine	72 g
filled up to 500 ml with ddH ₂ O	
The buffer was stored at 4°C, before use 20% methanol was added.	

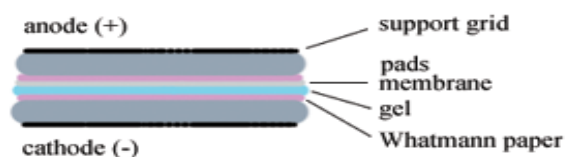


Figure 3.1 Schematic representation of a transfer "sandwich".

3.8.4.1 Immunostaining and chemoluminescence

After blotting the membrane was disassembled from the blotting sandwich, incubated for 5 min in Ponceau S solution (Sigma) to visualize the blotted protein bands and to mark the size of the protein standard (Broad Range, BioRad) on the membrane. Subsequently, the membrane was washed 3 times, 5 min in 1x TBS-T and blocked for 90 min at RT or O/N at 4°C in 5% skim milk powder (Fluka) / TBS-T (for special conditions see 3.6.1.4). An O/N

incubation step at 4°C with primary antibody followed (for dilutions and special conditions see 3.6.1.4). If the blocking solution was different from the solution in which the antibody was diluted, these two steps were separated by 3 washing steps with TBS-T, 5 min each. After the incubation with the primary antibody the membrane was washed again with TBS-T, 3 times, 5 min, and incubated for 90 min with an appropriate peroxidase - conjugated (HRP, horse radish peroxidase) secondary antibody, diluted in 5% skim milk powder / TBS-T (for dilutions see 3.6.1.5). Prior to the detection of the immobilized antigen the membrane was washed again and then the detection solution (ECL™ Western blotting detection reagent, Amersham Biosciences) was applied according to the protocol of the manufacture. The detection was based on a chemoluminescence reaction in which Luminol is oxidised in the presence of H₂O₂ by the peroxidase conjugated to the secondary antibody. Hereby light is emitted which can be detected by exposing the membrane, sealed under plastic, to an ECL film (Amersham Biosciences). The exposed film was developed in a developing machine and / or the quantification of chemiluminescence signals was performed by using a CCD camera (LAS 1000, Fujifilm) and the software programs Image Reader LAS 1000 V1.1 and Image Gauge V3.01 (Fujifilm).

10x TBS

Tris-Base	24.2 g
NaCl	80 g
filled up to 1000 ml with ddH ₂ O	
The pH value was adjusted to pH 7.6 with acetic acid	

1x TBS-T

10x TBS	100 ml
Tween X20	1 ml
filled up to 1000 ml with ddH ₂ O	

3.8.5 Pull Down assay

In order to determine the amount of active, GTP-bound Rho-GTPases pull down assays were performed, which detect only the activated form. This is accomplished by precipitating GTP-bound Rho GTPases from cell lysates with the GTPase binding domain (GBD) of a specific effector molecule, which recognizes the active, but not the inactive form of the Rho GTPase, followed by SDS-PAGE and Western blot for the respective Rho GTPase.

To detect active RhoA, the GTPase binding domain of rho-kinase (amino acids 7-89; 358 bp) fused to the C-terminus of GST (Glutathion-S-Transferase) was used (Reid et al., 1996; Zondag et al., 2000). The GBD-GST was expressed from the glutathione S-transferase fusion vector, pGEX-2T (Figure 3.2; obtained from Dr. Erik Danen, Netherlands Cancer Institute),

in *E. coli* BL21 strain and immobilized on Glutathion coated Sepharose beads (Glutathion Sepharose 4 Fast Flow, Amersham Pharmacia Biotech). The ‘loaded’ beads were subsequently incubated with the cell extracts of interest, washed and eluted with sample buffer. Precipitated RhoA-GTP was detected by SDS-PAGE and Western blot (see 3.8.3 and 3.8.4) for RhoA.

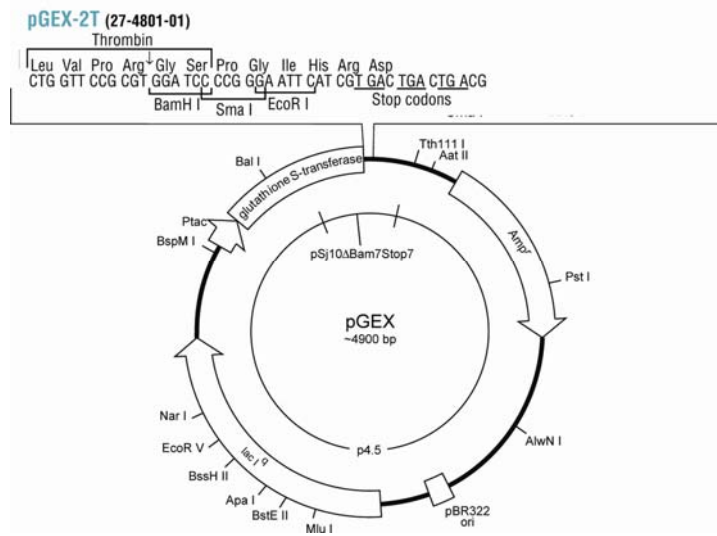


Figure 3.2 Schematic representation of the glutathione S-transferase fusion pGEX-2T vector. The rhotekin aa 7-89 fragment was cloned into the MCS using the BamHI and EcoRI sites.

Active Rac1 was bound to Biotin-PAK-CRIB peptide (kindly provided by Dr. Erik Danen), immobilized on streptavidin coated beads (Sigma) and detected by Western blot (see 3.8.4) for Rac1.

3.8.5.1 Rac1 pull down

In order to determine the level of active Rac1, cells were grown on 10 cm plastic culture dishes, washed once with ice cold 1x PBS and lysed on ice, for 10 min in 700 μ l of the GST-fish lysis buffer containing 1.3 μ l of the PAK-CRIB peptide (2 mg / ml). Subsequently cells were scraped from the plastic dish with a cell scraper and spun down 15 min, 10.000 RPM at 4°C. Supernatant was transferred to a new tube. To determine the total levels of Rac1 20 μ l, from the total cell extract was collected and stored at -20°C until they were further analysed. The remaining lysate was tumbled 45 min at 4°C, and after adding 30 μ l streptavidin-coated beads, rotated for further 30 min. Finally, the biotin-PAK-CRIB beads were spun down 30 sec, 6000 RPM, washed 3 times in 1 ml GST-fish lysis buffer, resuspended in 1x sample buffer and analysed together with the total extract by SDS-PAGE and Western Blotting. The amount of active Rac1 was normalized for the total amount of Rac1 in the cell extract. The

total amount of Rac1 was normalized for the amount of tubulin as determined by Western blot.

GST-FISH LYSIS BUFFER

1M Tris-Base pH 7.4	5 ml
5M NaCl	2 ml
NP-40	1 ml
87% glycerol	10 ml
2M MgCl ₂	100 µl
filled up to 100 ml with dd ddH ₂ O	

Prior to use 1 tablet of protease inhibitor cocktail (Roche) and 100µl of 1M Na₃VO₄ were added for each 10ml of the lysis buffer.

3.8.5.2 RhoA pull down

3.8.5.2.1 Preparation of GBP-GTP fusion proteins

In order to pull down the active form of RhoA, the rhotekin-GST fusion protein was expressed in *E. coli* BL21 bacteria.

First the pGEX-2T vector, containing the GTPase binding domain of rhotekin was transformed (Figure 3.2) into competent BL21 bacteria. Subsequently 3 ml of ampicillin containing LB medium (see 3.10.2.2) were inoculated with a single clone and incubated O/N. 2 ml of this pre-culture were then used to inoculate 100 ml of ampicillin containing LB medium. Bacteria were grown at 37°C until OD₆₀₀ was 0.5 – 0.6 and then induced with 100 µl sterile filtered 1M IPTG. After 6 hours of incubation at 26°C bacteria were spun down for 10 min, 4000 RPM at 4°C and washed in ice cold buffer A. The pellets were either stored at -80°C or directly resuspended in ice cold buffer A+. After sonicating 4 times, 15 sec (Gerhard Heinemann, Laboratoriums-Ausrüstungen; small tip, output control 5), 50 µl Triton-X100 (1% final concentration) were added and the samples were tumbled 20 min at 4°C. Then 550 µl of glycerol (10% final concentration) was added, the supernatant was distributed to 1.5 ml tubes and spun down, 15 min, 13000 RPM, 4°C. The supernatants were aliquoted and stored at -80°C. 20 µl of the bacterial extracts were separated together with the pellet on 12% SDS-PAGE and stained by Coomassie to confirm induction of the fusion protein.

Finally, the fusion protein was immobilized on glutathione beads. For this 40 µl of GS-Sepharose slurry (Gluthation Sepharose 4 Fast Flow, Amersham Pharmacia Biotech) per sample, were spun down 30 sec, 13000 RPM, washed 4 times in 1 ml of ice cold CLB+ and incubated with 100 µl of the bacterial extract, 40 min, 4°C, tumbling. Finally the beads were washed 3 times in 1 ml CLB+, and stored on ice until being incubated with the cell extracts.

3.8.5.2.2 Pull down

In order to determine the level of active RhoA, cells were grown on 10 cm plastic culture dishes, washed twice with ice cold 1x PBS and lysed on ice, for 5 min in 700 μ l of CLB+. Subsequently cells were scraped from the plastic dish with a cell scraper, spun down 10 min, 13.000 RPM. The supernatant was added to loaded GS-Sepharose beads (see 3.8.5.2.1) and tumbled 60 min at 4°C. 20 μ l of the total lysate was stored at -20°C to later determine the total amount of the protein. Beads were washed 4 times in 1 ml of ice cold CLB+, resuspended in 20 μ l x2 sample buffer and analysed together with the total extract by SDS-PAGE and Western Blotting. The amount of active RhoA was normalized for the total amount of RhoA in the cell extract. The total amount of Rho was normalized for the amount of tubulin as determined by Western blot.

BUFFER A

1M Tris, pH 7.4	25 ml
2M MgCl ₂	1.25 ml
5M NaCl	5 ml

filled up to 500 ml with ddH₂O and autoclaved

BUFFER A+

Add freshly to 10 ml Buffer A

0.1M PMSF	100 μ l
1M DTT	10 μ l

1 tablet of protease inhibitor cocktail (Roche)

CLB+

1M Tris, pH 7.4	1 ml
2M MgCl ₂	50 μ l
5M NaCl	800 μ l
1M Na ₃ VO ₄	100 μ l
NP-40	200 μ l
87% glycerol	2 ml
0.1M PMSF	200 μ l

1 tablet of protease inhibitor cocktail (Roche)
filled up to 10 ml with dd ddH₂O

3.9 Cell biological methods

3.9.1 Production of retroviruses by transient transfection

Retroviral infection is an efficient way to introduce genes in the genome of the replicating cells. Retroviral vectors lack the retroviral genes gag, pol and env necessary for reverse transcription and packaging of the retroviral DNA. In order to produce retroviruses from

retroviral vectors, these vectors have to be transfected into so called packaging cell lines which provide the missing proteins, allowing the secretion of infectious, though replication deficient retrovirus into the cell supernatant.

To produce retroviruses, 18-24 hours prior to transfection, $1.5 - 2 \times 10^6$ Phoenix packaging cells for ecotropic retroviruses were plated in EF medium on 6 cm plates. The best transfection efficiencies were achieved with cells being 70 - 80% confluent at time of transfection. Shortly before the transfection, 8 μg DNA (pM hyg wtCdc42 and pM hyg dnCdc42 constructs containing the ψ^+ signal, Figure 3.3) was placed in a 1.5 ml snap cap tube and filled up to 387.5 μl with ddH₂O (sterile). Then, 112.5 μl 1M CaCl₂ (sterile) was added. Finally, 500 μl 2x HBS (50mM Hepes, 1.5mM Na₂HPO₄ and 150mM NaCl, pH 7.1) was added drop wise to the tube, which was gently vortexed during this procedure. About 5 minutes prior to transfection, 2 μl chloroquine (100 mM) was added to the cells in order to inhibit lysosomal DNAses, by neutralizing vesicle pH (DNA delivered by Ca₃(PO₄)₂ transfection is thought to transit through lysosomes). Then the DNA / Ca₃(PO₄)₂ solution was applied to the cells, resulting in a fine, black precipitate visible under the microscope. The cells were then cultured under standard conditions and the chloroquine containing medium was changed for EF medium 12 hours later. Virus containing supernatant was collected after 24, 48 and 72 hours, frozen at -20°C and replaced by fresh medium. After thawing virus suspension was centrifuged for 5 min at 1000 RPM and only the supernatant was used for infection of target cells.

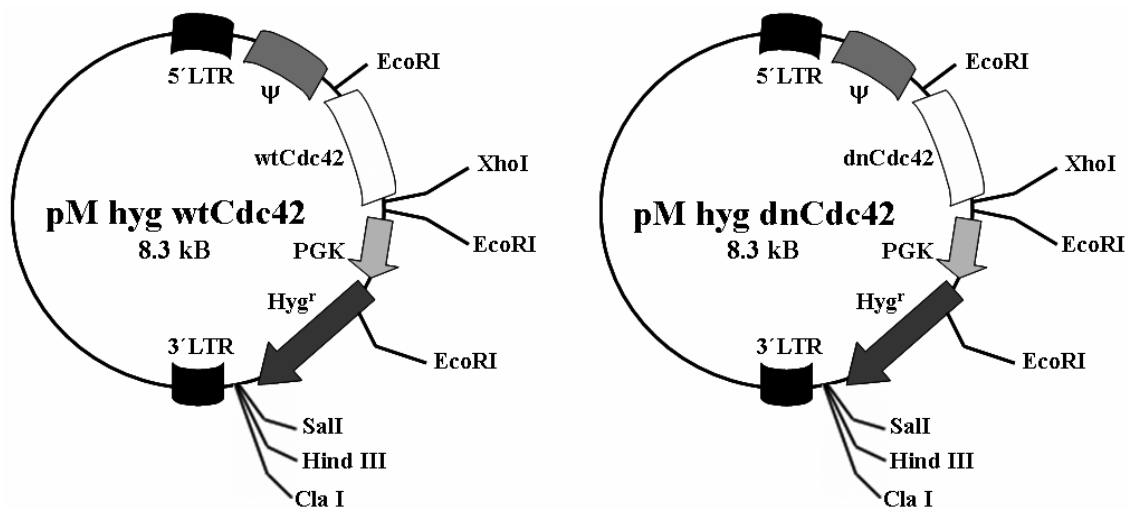


Figure 3.3 Schematic representation of the modified Murine Stem Cell Virus (MSCV) hyg^r vectors pM hyg wtCdc42 and pM hyg dnCdc42 vectors used for transfection of the Phoenix packaging cell line. Upon transfection, the pM hyg vectors integrate and stably expresses, a transcript containing the extended viral packaging signal Ψ^+ , the hygromycin resistance gene, and wtCdc42 or dnCdc42, respectively. The 5' long

terminal repeat (LTR) of these vectors achieves stable, high-level gene expression in stem cells and other mammalian cell lines. The murine phosphoglycerate kinase (PKG) promoter controls expression of the hygromycin resistance gene (Hyg^r) for antibiotic selection in eukaryotic cells. These vectors were generated by Ursula Kuhn, MPI of Biochemistry, Martinsried, Germany.

3.9.2 Infection of fibroblastoid cell lines by retroviruses

In order to stably express wild type Cdc42 or dominant negative mutant of Cdc42 in Cdc42(-/-) cells (clone 3.9.7), the fibroblastoid cell line was infected by the retrovirus carrying the wt Cdc42 or the dnCdc42 DNA, respectively.

Prior to infection fibroblastoid cells were seeded 30 - 40% confluent on a 6-well plate. 12 hours later the medium was replaced by 1.5 to 3 ml of the harvested retrovirus containing supernatant, mixed with 1 µl 4 mg / ml polybrene solution. 2 to 3 days later the cells were transferred to a 10 cm culture dish and selected in EF medium containing 100 µg / ml hygromycin B. The medium was changed every second day. When reaching confluency, the cells were frozen (see 3.7.4). Part of the cells was diluted to established clonal cell lines.

3.9.3 Generation of stable transfected fibroblastoid cell lines

Clones which successfully grew under the selection conditions (see 3.9.2) were picked sterile under a stereomicroscope (Zeiss, Stemi SV6) with a tip and were subsequently re-suspended in 200 µl EF medium (+ 100 µg / ml Hygromycin B) on a 96-well plate. When grown to confluence, cells were transferred onto 24-well plate, than on a 12-well plate, 6-well plate, 25 ml flask up to a 75 ml flask, from which they were finally frozen (see 3.7.4). The presence of the transfected cDNA was verified on protein level by SDS-PAGE and Western blotting (see 3.8.3 and 3.8.4).

3.9.4 Isolation of primary keratinocytes

Primary keratinocytes were established from adult knockin mice in order to analyze them by FACS and in cell biological assays.

Adult mice were sacrificed by cervical dislocation, shaved with an electrical shaver, placed under a sterile hood and sterilized by treatment for 60 sec with iodine, for 10 sec with ddH₂O and for 60 sec with 70% ethanol. Subsequently, the entire skin was peeled off from the trunk and placed in a sterile bacteriological Petri dish. The fat was completely removed by a scalpel and the skin was cut in several pieces and placed, dermis up, in an antibiotic solution (2x Penicillin / Streptomycin (PAA Laboratories GmbH), 2x Nystatin (Gibco), 2x Fungizone (Gibco; in 1x PBS) for 5 to 10 min. Next, the skin pieces were transferred, epidermis up, into

a new Petri dish with 20 ml 0.8% trypsin solution in 1x PBS (Trypsin 1.250, Invitrogen) and incubated at 37°C for 50 min. After this incubation the skin pieces were transferred onto a new bacteriological dish, and the epidermis was separated from the dermis. The separated epidermis was placed in 25 ml DNase medium (MEM with 8% chelated FCS; see 3.7.2.3) and 0.25 mg / ml DNase (Sigma) and shaken for 30 min in a 37°C water bath. Next, the cell suspension was filtered through a 70 µm cell strainer (Becton Dickinson) and pelleted for 5 min at 1000 RPM. Cells were washed with DNase medium, centrifuged and plated on a fibronectin / collagen I coated dishes (6×10^6 cells / 10 cm culture dish; 2 - $2,5 \times 10^6$ cells / well of a 6-well plate). Cells were incubated under standard conditions (see 3.7.2.3). Medium was changed the next day.

3.9.4.1 Preparation of epidermal lysates for RNA preparation

In order to isolate RNA from keratinocytes, epidermis was separated from the dermis (see 3.9.4) and washed at 37°C, 5 min in normal EF medium. Subsequently, the keratinocyte suspension was spun down at 1000 RPM for 5 min and the keratinocyte pellet was washed with 1x PBS. The suspension was spun down again, frozen on dry ice in 30 – 50 µl aliquots and stored at -80°C.

3.9.5 Cell biological assays

3.9.5.1 In vitro wound closure assay

To determine directed migration in a wound closure assay, cells were seeded confluent on 6-well plates in growth medium (see 3.7.2) and wounded 1 day later by scraping across the monolayers. Two wounds were applied per well using a Pasteur pipette with a rounded end. The wound width varied between 300 to 400 µm for fibroblastoid cells and 150 to 250 µm for endodermal cells or keratinocytes and was closed depending of the cell line within 6 to 8 hours for fibroblastoid cells, 3 to 4 hours for endodermal cells and after 6 hours for keratinocytes. In each experiment 10 to 15 randomly chosen regions of the wound (each 660µm long) were photographed using a microscope (Leica, Zeiss, Axiovert 135) with a digital camera (Canon EOS 300D) starting from time point 0 every 120 min (fibroblastoid cells and keratinocytes) or 30 min (endodermal cells). Wound closure was estimated by measuring the width of the wound.

3.9.5.2 Polarization assay

To test the ability of cells to polarize their Golgi apparatus during an *in vitro* scratch assay cells were seeded confluent on cover slips in 6-well plates (see 3.7.2.4) and wounded (see 3.9.5.1) one day later. 1, 2 and 5 hours (fibroblastoid cells) or 0.5, 2.5 and 5 hours after wounding (endodermal cells), cells were fixed and immunostained (see 3.6.1.2) for the Golgi marker GM130 (see 3.6.1.4). Nuclei were fluorescently labelled with DAPI. Cells in which Golgi localized to a 120° sector facing the wound were scored as being polarized (Nobes and Hall, 1999). If there is no preferred location of the Golgi with respect to the nucleus, 33.3% of cells should have the Golgi localized in this 120° sector towards the wound (“random polarization”). In each experiment 100 - 500 cells of the first migrating row were examined.

3.9.5.3 Adhesion assay

Cell adhesion assays were performed using vitronectin (from human placenta, Yatohgo et al., 1988), fibronectin (Behringwerke, Marburg), laminin-1 (Paulsson et al., 1987) and collagen I (Cohesion) coated 96-wells. The wells were coated at 4°C, O/N, at a concentration of 0.05-50 µg/ml per well. Next, all wells were blocked with 2% BSA / in 1x PBS, containing 1 mM Ca²⁺ and 1 mM Mg²⁺. Cells in a cell suspension were allowed to attach to the wells for 60 min at 37°C, and subsequently non-adherent cells were washed away with 1x PBS. Remaining cells were fixed for 20 min at RT with 150 µl 70 % ethanol. Thereafter, cells were stained for 30 min at RT, with 50 µl 5 mg / ml crystal violet in 20 % methanol, washed 4 times with 1x PBS, and extracted for 30 min with 50 ml 0.1 mol / l sodium citrate pH 4.2. Finally, the microplates were colorimetrically evaluated in an ELISA reader at 562 nm.

3.9.5.4 Spreading assay

In order to assess the spreading kinetic of cells, cells were plated on plastic and photographed at selected time points using a microscope (Leica, Zeiss, Axiovert 135) and a digital camera (Canon EOS 300D).

3.10 Bacteria culture

3.10.1 Bacteria strains

- *Escherichia coli*: DH5α, BL21 and ES 1301 *mutS* (Promega)

3.10.2 Bacteria culture conditions and media

3.10.2.1 Bacteria culture

Bacteria were cultured in a bacteria shaker (Buchner Laboratories) at 37°C, at 200 RPM.

Long term storage of bacteria was performed in glycerol stocks at -80°C. For this 600 µl of a fresh bacteria culture (minipreps, see 3.11.10.1) were mixed with 400 µl sterile glycerol (87%).

3.10.2.2 Media

All bacteria media were autoclaved for 30 min at 120°C. Heat sensible components were sterile filtered and added to the autoclaved media. All media were stored at 4°C.

LURIA – BERTANI (LB) MEDIUM

Bacto-tryptone	10 g
Bacto-yeast extract	5 g
NaCl	10 g
filled up to 1000 ml with ddH ₂ O	

AGAR-LB PLATES

LB medium	1000 ml
Agar	10 g

The solution was autoclaved, swirled and cooled down to 50°C. After addition of a desired antibiotic solution (ampicillin, final concentration 100 µg / ml, stock 100 mg / ml) the plates were directly poured from the flask into 90 mm Petri dishes. Hardened plates were inverted and stored at 4°C.

3.11 Molecular biology methods

3.11.1 Oligonucleotides

NAME	SEQUENCE (5' → 3')	APPLICATION
T56	AGG TGC CCT TCC CTC TAG A	Genotyping (β1 floxed allele)
L1	GTG AAG TAG GTG AAA GGT AAC	Genotyping (β1 floxed allele)
CRE 3'	TTC GGA TCA TCA GCT ACA CC	Genotyping (Cre transgene)
CRE 5'	AAC ATG CTT CAT CGT CGG	Genotyping (Cre transgene)
T59 short	GTC CTA CTG GTC CCG AC	Genotyping (β1 K1wt allele)
L31	TGC TCT CAG TAA TGT TTC ATA AC	Genotyping (β1 K1wt allele)
Sall[mLoxP]-S	TCG AGA TAA CTT CGT ATA ATG TAT ACT ATA CGA AGT TAT G	Genotyping (β1 K1e16 & 15 allele) & Generation of β1 integrin knockin targeting constructs
ME16-AS	CCA AAA CTA CCC TAC TGT GAC	Genotyping (β1 K1e16 allele) and RT-PCR
Pst-Seq +	AGC TGT AAA GGT TCT GTG TGG	Genotyping (β1 K1e16 allele) and RT-PCR
ME15-S	ACA TGT GGT CAG TCT TGT TAG C	Genotyping (β1 K1e15 allele)
INT14-AS	GTA GTA AAG ATG ATT GGC AGC C	Genotyping (β1 K1e15 allele)
Y783F_AS	GTG AAA ATC CTA TTT TTA AGA GTG CCG TG	Mutagenesis
D759A_AS	TTA ATG ATA ATT CAT GCT AGA AGG GAA TTT GC	Mutagenesis

NAME	SEQUENCE (5' → 3')	APPLICATION
AmpRep_AS	CAC CAC GAT GCC TGC AGC AAT GGC AAC	Mutagenesis
Y795F_AS	AAT CCG AAG TTT GAG GGA AAA	Mutagenesis
Y783/789F_AS	GTG AAA ATC CTA TTT TTA AGA GTG CCG TGA CAA CTG TGG TCA ATC CGA AGT TTG AGG GAA AAT GAA	Mutagenesis
S785A_AS	AAT CCT ATT TAC AAG GCG GCC GTG ACA ACT	Mutagenesis
795_771_AS	TTT TAA TGA TAA TTC ATA ATG CCA AGT GGG	Mutagenesis
S 785D_AS	AAT CCT ATT TAC AAG GAC GCC GTG ACA ACT	Mutagenesis
TT778/789AA_AS	AGA GTG CCG TGG CAG CTG TGG TCA ATC	Mutagenesis
exo16_AS2	GCG GGA TCC TGA AAA AGG TAA ATG TAC AGC C	Southern blotting (Exon16 internal probe)
exo16_S	GCG TCT AGA CAG AAG ACT TGA GAA AGG ATC	Southern blotting (Exon16 internal probe)
T43	CCA GGA CTG CCA GCA TTT C	Southern blotting (3' probe internal probe)
T36	GAT TAG ATT TAG TAT AAT CAC AC	Southern blotting (3' probe internal probe)
L10	TGC TCT GCA CAG ACG CCA AG	Southern blotting (5' probe internal probe)
T19	GCG AAT TCG TGC AAT GAG GGG CGT GTT G	Southern blotting (5' probe internal probe)
T3	AAT TAA CCC TCA CTA AAG GG	Sequencing
T7	GTA ATA CGA CTC ACT ATA GGG C	Sequencing
SP6	TAT TTA GGT GAC ACT ATA G	Sequencing
seqAS1	CGA AGT AGC CTA ATG TAG G	Sequencing
seqAS2	TTG ACC ACA GTT GTC ACG	Sequencing
M13	GTA AAA CGA CGG CCA GT	Sequencing
15E_AS	GCA ACT TCT TTG GAT TTT GAA	Sequencing
16E_AS	AAC CCT GGC CAC AGA GCC	Sequencing
NcoI-sequ	GAG ACT TTG ATT GAC ATG GC	Sequencing
PstI-sequ	CTG TAA AGG TTC TGT GTG G	Sequencing
Bam_Xho-S	GAT CCG CGC CGC TCG AGG AAT TCC GAC GCG TCG ACG	Generation of $\beta 1$ integrin knockin targeting constructs
Bam_Xho-AS	TCG ACG TCG ACG CGT CGG AAT TCC TCG AGC GGC GCG	Generation of $\beta 1$ integrin knockin targeting constructs
NcoI[Not_Sall]-S	CAT GGG CGG CCG CTA AAC TAT ACG CGT CGA CG	Generation of $\beta 1$ integrin knockin targeting constructs
NcoI[Not_Sall]-AS	CAT GCG TCG ACG CGT ATA GTT TAG CGG CCG GC	Generation of $\beta 1$ integrin knockin targeting constructs
PstI[Not_Sall]-S	CGC GGC CGC TAA ACT ATA CGC GTC GAC GTG CA	Generation of $\beta 1$ integrin knockin targeting constructs
PstI[Not_Sall]-AS2	CGT CGA CGC GTA TAG TTT AGC GGC CGC GTG CA	Generation of $\beta 1$ integrin knockin targeting constructs
Sall[mLoxP]-AS	TCG ACA TAA CTT CGT ATA GTA TAC ATT ATA CGA AGT TAT C	Generation of $\beta 1$ integrin knockin targeting constructs
KpnI[Xho]NheI-S	CTA C TAT AAC TAT ACT CGA GTA AAC TAT AG	Generation of $\beta 1$ integrin knockin targeting constructs
KpnI[Xho]NheI-AS	CTA GCT ATA GTT TAC TCG AGT ATA GTT TAG GTA C	Generation of $\beta 1$ integrin knockin targeting constructs
NotI[mloxP_int14/exo15] BamHI-S	GGC CGC ATA ACT TCG TAT AAT GTA TAC TAT ACG AAG TTA TTT CAT TTG TAG ACT GTC CTA CTG GTC CCG ACT AGG	Generation of $\beta 1$ integrin knockin targeting constructs
NotI[mloxP_int14/exo15] BamHI-AS	GAT CCC TAG TCG GGA CCA GTA GGA CAG TCT ACA AAT GAA ATA ACT TCG TAT AGT ATA CAT TAT ACG AAG TTA TGC	Generation of $\beta 1$ integrin knockin targeting constructs
NotI[mloxP_int15/exo16] BamHI-S	GGC CGC ATA ACT TCG TAT AAT GTA TAC TAT ACG AAG TTA TGT TTT TTT TAG GGT TAG G	Generation of $\beta 1$ integrin knockin targeting constructs
NotI[mloxP_int15/exo16] BamHI-AS	GAT CCC TAA CCC TAA AAA AAA CAT AAC TTC GTA TAG TAT ACA TTA TAC GAA GTT ATG C	Generation of $\beta 1$ integrin knockin targeting constructs
E13-P0	GCT TGT AAG TGC ACA GAT	RT-PCR
E14-P1	AGG ACA TTG ATG ACT GCT GG	RT-PCR
D-P3	AAA CTC AGA GAC CAG CTT TAC	RT-PCR
KI-P4	TTT CTG CAG ACT TAC AGC GG	RT-PCR
E15-P5	CGT GTC CCA CTT GGC ATT C	RT-PCR

3.11.2 Oligonucleotides phosphorylation and annealing

Prior to ligation with a desired vector (see 3.11.7), oligonucleotides had to be phosphorylated and annealed in the following reaction:

100 pmol / μ l oligo S	1 μ l
100 pmol / μ l oligo AS	1 μ l
x10 T4 oligonucleotide kinase buffer	1 μ l
10mM ATP	1 μ l
ddH ₂ O	5 μ l
T4 DNA polynucleotide kinase (PNK)	1 μ

The reaction was mixed and incubated 1 hour at 37°C. Then 17 μ l ddH₂O and 3 μ l 0.5 M NaCl were added and the reaction was incubated for 10 min at 90°C in a heating block

(Eppendorf). Finally, the block was switched off and the samples were taken out when the block temperature decreased below 30°C.

3.11.3 Digestion of DNA with restriction enzymes

Restriction enzymes bind specifically to mainly palindromic recognition sites within a DNA molecule and cut it by hydrolyzing two phosphodiester bounds. Depending on the restriction enzyme “blunt” (no 5’ or 3’ overhang) or “sticky” (5’ and 3’ overhangs) ends will be generated. The restriction enzymes were purchased together with their corresponding x10 buffers from BioLabs. Restriction enzyme digests were performed at temperatures recommended by the manufacturer (mostly 37°C) in a thermo block for 90 to 120 min, depending on the enzyme. Usually 10 units of enzyme were used to cut each microgram of DNA. The digestion was performed in the presence of an appropriate 10x buffer, BSA (10 mg / ml) and ddH₂O.

3.11.4 Dephosphorylation of 5` - ends

To prevent re-ligation of a cut vector (see 3.11.3) the phosphate groups from the 5’ - ends of the DNA were removed by a treatment with Calf Intestinal Phosphatase (CIP, Roche). The following components were directly added to the restriction enzyme reaction after complete digest:

CIP	x / 10 µl
Plasmid DNA	x µl

The mixture was incubated for 30 min at 37°C and than subsequently 30 min in 56°C. Next, half of the initially used amount of CIP was added to the reaction. The reaction was first incubated 20 min at 37°C, and than 20 min at 56°C. Finally, the DNA was purified from an agarose gel by QIAquick Gal Extraction Kit (Qiagen) according to manufactures protocol (see 3.11.6).

3.11.5 Agarose gel electrophoresis

In order to separate DNA fragments according to their size in an applied electric field agarose gel electrophoresis was performed.

An agarose (Invitrogen) solution of 1 or 2% in TAE buffer agarose was heated in a microwave until the agarose was dissolved. To visualize the DNA bands, the DNA intercalating agent ethidium bromide (5 µl per 100 ml agarose solution) was added. The agarose solution was poured into a gel chamber into which a comb was assembled and allowed to cool down and harden. Finally, DNA or standard size marker (1kB ladder, Invitrogen) were dissolved in a 6x loading buffer and were loaded into the slots of the gels.

The DNA was separated in 1x TAE buffer at 4-6 V / m of the gel chamber. The gel was photographed under UV light at 366 nm to visualize the ethidium bromide stained DNA fragments.

50x TAE BUFFER (Tris-Acetate-EDTA)

Tris-Base	242 g
Glacial acetic acid	57.1 ml
0.5M EDTA (pH 8)	100 ml
filled up to 1000ml with ddH ₂ O	

3.11.6 Extraction of DNA fragments from agarose gel

To isolate DNA fragments from agarose gels, the desired DNA fragments were excised from the gel, weighted and extracted using the QIAquick Gel Extraction Kit (Qiagen) according to protocol of the manufacturer. To verify successful purification, the DNA was rechecked on an agarose gel and the amount was estimated using the standard size marker as a reference.

3.11.7 Ligation of DNA fragments

In order to ligate a vector DNA with the desired insert DNA, both cut with the same or compatible set of restriction enzymes, a T4-DNA-ligase was applied which catalyses the formation of a phosphodiester bond between the 3'-OH and 5'-phosphate ends.

Ligation reaction:

Vector DNA	10 - 100 ng
Insert DNA	3 - 4x the amount of vector DNA
5x ligase buffer (Invitrogen)	4 µl
T4-DNA-ligase (Invitrogen)	1 µl
Filled up with ddH ₂ O to a volume of 20 µl	

The ligation reaction was prepared in 1.5 ml tubes and incubated O/N in cold room, in a 16°C water bath.

3.11.8 Preparation of competent bacteria

Special pre-treatment of bacteria facilitates their uptake of DNA and makes them “competent” for transformation of foreign DNA.

To prepare competent bacteria 5 ml of LB medium supplemented with 0.02M MgSO₄ and 0.01M KCl was inoculated with starter culture of bacteria (DH5α or B21 cells) and incubated O/N at 37°C. Subsequently, 1 ml of the overnight culture was subcultured in 150 ml LB medium supplemented with 0.02M MgSO₄ and 0.01M KCl until the OD₆₀₀ reached 0.3 – 0.4. At this OD, bacteria were transferred to an ice bath, divided into 50 ml tubes incubated for 10 min, and spun down for 10 min at 6000 RPM, at 4°C. The pellets were gently resuspended in

an equal volume of ice-cold TFB1. After 10 min incubation on ice, cells were again pelleted for 10 min at 6000 RPM, 4°C and re-suspended in 1/10 volume of TFB2. Finally, the cell suspension was divided into 50 µl aliquots, which were quickly frozen in dry ice / isopropanol bath and stored at -80°C.

E. coli ES1301 *mutS* bacteria used to introduce mutations into target DNA were prepared by a slightly modified protocol according to the recommendation of the manufacturer (Promega, Altered Sites® II *in vitro* Mutagenesis System).

TFB1

5M KAc	1 ml
1M MnCl ₂	10 ml
1M RbCl	20 ml
1M CaCl ₂	2 ml
ddH ₂ O	132 ml

The solution was sterile filtered and 34.5 ml of autoclaved 87% glycerol was added.

TFB2

1M MOPS (pH 7)	500 µl
1M CaCl ₂	3.75 ml
1M RbCl	500 µl
87% glycerol	8.75 ml
ddH ₂ O	36.5 ml

The solution was autoclaved.

3.11.9 Transformation of bacteria

In order to transform the competent DH5α or B21 bacteria with the desired DNA, a tube with competent bacteria (see 3.11.8) was thawed on ice and mixed with 10 µl ligation reaction (see 3.11.7). After 30 min incubation on ice, cells were heat shocked for 60 to 90 sec, at 42°C in order to promote uptake of DNA. Next 1 ml LB medium was added and the transformation solution was transferred to a 15 ml round bottomed tube and incubated for 1 h at 37°C, shaking at 200 RPM. Finally, cells were spun down, 800 µl of the supernatant was discarded, the pellet was re-suspended in the remaining 200 µl and spread with a sterile Drigalsky spatula over the surface of the agar plate. These plates were subsequently inverted and incubated at 37°C. Colonies appeared within 12-16 hours.

E. coli ES1301 *mutS* bacteria used to introduce mutations into target DNA were transformed by a slightly modified protocol according to the recommendations of the manufacturer (Promega, Altered Sites® II *in vitro* Mutagenesis System).

3.11.10 Preparation of plasmid DNA

3.11.10.1 Mini-preparation of plasmid DNA (miniprep)

In order to isolate analytical amounts of plasmid DNA, 2ml LB medium (with antibiotics) was inoculated with a bacterial colony, picked with a yellow tip and incubated overnight at 37°C, shaking. Next, 1.5 ml bacterial suspension was transferred to a 1.5 ml tube and spun at maximum speed for 25 sec. After removing the supernatant, the pellet was re-suspend in 200 µl of P1 and then 200 µl of P2 were added. The solution was thoroughly mixed and incubated for 5 min at RT. Then 200µl of cold P3 were added, thoroughly mixed and incubated for 5 min incubation on ice. After 5 min centrifugation at maximum speed at RT, the supernatants were transferred to a new tube, mixed with 500 µl isopropanol and centrifuged for 5 min at maximum speed. The pellet was washed with 70% ethanol, spun shortly again to remove remaining traces of the wash solution and re-suspended in 50 µl of water. The DNA concentration was calculated from OD₂₆₀ nm measurement (Gene Quant II, Amersham Pharmacia Biotech). The DNA was stored at -20°C.

P1: 50 mM Tris-HCl, 10 mM EDTA, 100 µg / ml RNase A, pH 8.0

P2: 200 mM NaOH, 1% SDS

P3: 3 M Kac, pH 5.5

3.11.10.2 Maxi-preparation of plasmid DNA (maxiprep)

Maxi-preparation was performed to obtain preparative amounts of plasmid DNA. The maxiprep was done according to the QIAGEN Plasmid Maxi Protocol (Qiagen) with QIAgentip 500. The DNA concentration was calculated from OD₂₆₀ nm measurement (Gene Quant II, Amersham Pharmacia Biotech). The DNA was stored at -20°C.

3.11.11 Mutagenesis

All mutations in the knockin targeting constructs (see 3.11.20.2 and 3.11.20.3) were introduced by means of the Altered Sites® II *in vitro* Mutagenesis System (Promega) according to the protocol of the manufacturer. In order to introduce mutations in exon 15 of the β1 integrin gene a Sall/SacI fragment of the wt targeting construct (wtK1e15) was cloned into the pALTER®-1 Vector (Figure 3.4). The first step in exon 16 mutagenesis was cloning of the KpnI/Sall fragment of the wt targeting construct (wtK1e16) into the pALTER®-1 Vector. For the oligonucleotides used see 3.11.1.

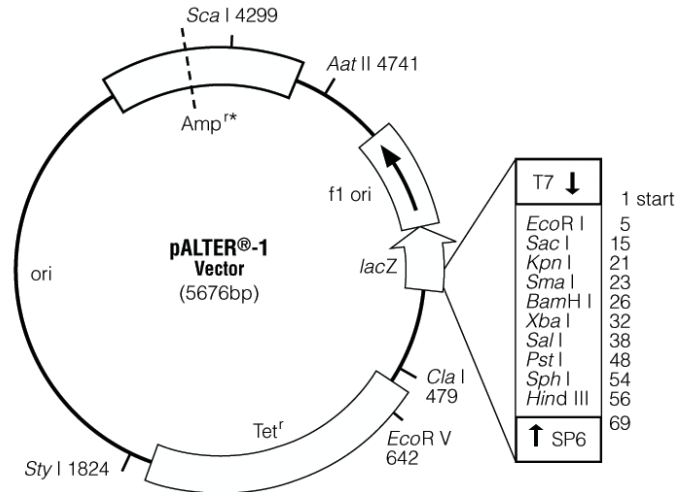


Figure 3.4 Schematic representation of the pALTER®-1 vector.

3.11.12 DNA sequencing

In order to verify the correct sequence of a given DNA, 1 - 2 µg of air dried plasmid DNA (see 3.11.10.1) or 20 ng per 100 bases of amplified PCR fragment, also air dried (see 3.11.15), was send for sequencing, together with 10 µl (10 pmol / µl) of an adequate primer per reaction, to MWG Biotech AG (<http://www.mwg-biotech.com/html/all/index.php>).

3.11.13 Genomic DNA extraction

3.11.13.1 DNA isolation from tail snips

For genotyping of mice tail tips or toe pieces were clipped and stored at -20°C (see 3.2). The 3 - 5 mm tail fragments or 1 mm toe pieces were then incubated O/N at 55°C in 1.5 ml tubes in 500 µl lysis buffer with freshly added 100 µg / ml proteinase K.

LYSIS BUFFER

1M Tris pH 8.5 (final 100mM)	100 ml
0,5M EDTA (final 5mM)	10 ml
20% SDS (final 0.2%)	10 ml
5M NaCl (final 200mM)	40 ml
filled up to 1000 ml with ddH ₂ O	

After the O/N digestion, the solution was either stored at -20°C or directly processed further. Non-digested debris was spun down 10 min at maximum speed and the supernatant was transferred into tubes with 500 µl isopropanol. After mixing, the DNA was spun down for 5 min at maximum speed and washed once with 70% ethanol. Dried DNA was re-suspended in

300 µl ddH₂O and stored at 4°C. If toe clipping was applied, the resulting DNA was re-suspended in 100 µl ddH₂O.

3.11.13.2 DNA isolation from cells

In order to identify positive, recombined ES clones by Southern blotting (see 3.11.14), cells were incubated with lysis buffer (see 3.11.13.1), 500 µl per well of a 24-well plate, O/N in a 37°C incubator. Next, 0.5 ml of isopropanol was added and plates were shaken for 8 – 24 hours at 300 RPM at RT. During this time, DNA became visible as white web-like structure, which could be picked by a metal rod and re-suspended in 100 µl ddH₂O in 1.5 ml tubes. The DNA was incubated O/N in a 55°C oven and stored at -20°C.

3.11.14 Southern blotting

The genomic DNA isolated from ES cell clones (see 3.11.13.2) was further analyzed by restriction digest (see 3.11.3) and Southern blotting. Southern blotting is a commonly used technique for the identification of DNA fragments that are complementary to a known DNA sequence (probe).

It is necessary to check both sides of the electroporated constructs for homologous recombination by hybridizing the blot with an external probe, which is not contained in the targeting construct. Such a probe will detect homologous recombination, but not random integration into the genome. In addition also an internal probe was used for hybridisation, in order to check for heterologous integrations. This probe will detect all integrations of the targeting construct into the genome. Probes used for Southern blotting:

External probes

Probe 5' (pβ1int3'A4 plasmid fragment amplified using L10 and T19 primers, see Figure 3.10 and paragraph 3.11.1)

Probe 3' (pβ1int3'A4 plasmid fragment amplified using T43 and T36 primers, see Figure 3.10 and paragraph 3.11.1)

Internal probes

Neo probe (for exon 15; BamHI / BamHI fragment of the pLoxPHSVtkneotkLoxP plasmid, see Figure 3.5)

Exo16 (for exon 16; pβ1int3'A4 plasmid fragment amplified using exo16_AS2 and exo16_S primers, see 3.11.1)

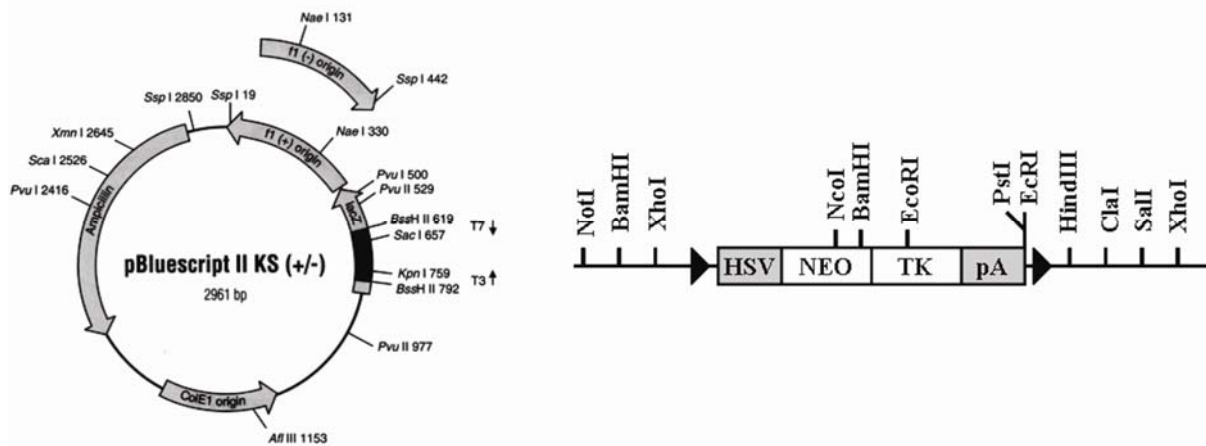


Figure 3.5 Schematic representation of the pBluescript II KS (+/-) and the modified multiple cloning site (pLoxPHSVtkneotkLoxP). HSV, HSV tk promoter; \blacktriangleright , *loxP*; pA, polyadenylation signal, NEO, neomycin resistance gene; tk, thymidine kinase gene.

3.11.14.1 Digestion and transfer of the DNA

Prior to transfer to the membrane, ES DNA was digested with an appropriate enzyme in a following digestion solution:

ES DNA	20 μ l
10 mg / ml BSA	0.3 μ l
10x buffer	3 μ l
40U / μ l enzyme	1 μ l
ddH ₂ O	5.7 μ l

The reaction was stopped after 8 hours incubation at 37°C and the DNA was separated on an 1x TAE buffered 0.7% agarose gel (see 3.11.5). The gel was run until the bromphenol blue reached the end of the gel; at 120 V (6 to 8 hours) or at 40 V O/N (electrode distance 35 cm). Thereafter, the gel was photographed with a ruler and shaken 45 min in denaturation solution. After being rinsed several times with water, the gel was incubated 45 min in neutralization solution. Next, the denatured gel was placed onto 2 sheaths of wet filter paper (Whatmann 3MM), which bend down to a buffer reservoir filled with 10 x SSC. A positively charged membrane (HybondN+ membrane; Amersham Biosciences) was laid over the gel on which again 2 sheaths of Whatmann paper were placed. Bubbles between filter paper, gel and blotting membrane were removed by gently rolling with a 10 ml pipette across the stack. On top, 10 cm layer of paper towels was assembled together with a 0.5 kg weight. This ensures that the buffer from the reservoir will move up by capillary action through the gel together with single stranded DNA, which will finally bind to the positively charged membrane. The assembly of an air bubble free transfer track is shown in Figure 3.6. The transfer was performed O/N at RT.

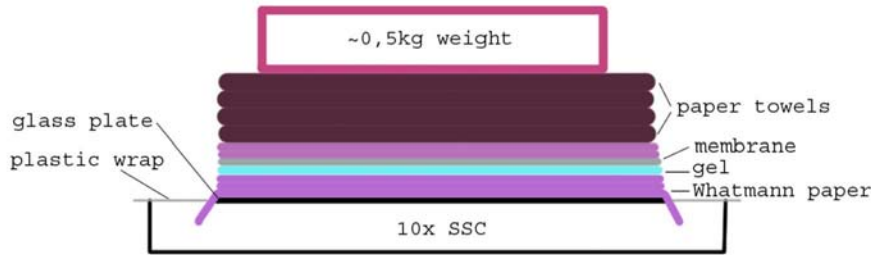


Figure 3.6 Schematic representation of a transfer track

Next day the transfer was stopped, slots were marked on the membrane with a pencil and the nucleic acids were cross-linked to the membrane by exposition to UV light ($120 \text{ J} / \text{cm}^2$) using a crosslinker (Stratagene) and by baking at 80°C for two hours. The cross-linked membrane was stored at RT or directly hybridised.

DENATURATION SOLUTION

NaCl	438.8 g
NaOH	100 g
filled up with ddH ₂ O to 5 l	

NEUTRALIZATION SOLUTION

NaCl	438.8 g
Tris-base	302.85 g
filled up with ddH ₂ O to 5 l	
pH adjusted to 8	

20x SSC

NaCl	175.2 g (3M)
Sodium citrate	88.2 g (0.3M)

3.11.14.2 *Radioactive probe labelling*

In the next step, the DNA probe was radioactively labelled with ^{32}P (high energy β -particle emitter). In order to do so, first mini - columns were prepared. 1 ml fine dosage syringes (Braun) were filled with Sepharose G-50 in TE (Tris-base pH 8, 1mM EDTA) and spun down 3 min, 2000 RPM. Then the DNA probe, diluted to a concentration of 2.5 – 25 ng in 45 μl TE buffer, was denatured 6 min at 99°C and snap cooled on ice for 5 min. Finally, this DNA was added to a Rediprime II reaction mix (Amersham Biosciences), which contains an improved exonuclease free Klenow fragment and 5 μl of Redivue [^{32}P dCTP] (Amersham Biosciences). The reaction was incubated 10 min in 37°C . Then, 50 μl ddH₂O were added and the reaction was transferred to the Sepharose column. The column was placed in a 1.5 ml tube and spun 3 min, 2000 RPM. 1.5 μl of the probe was checked using a scintillator counter.

3.11.14.3 *Hybridisation, washing and signal detection*

The cross-linked membrane was placed into a glass tube and pre-hybridised in 15 ml Church buffer, 1 hour, at 65°C in a hybridization oven. 50 – 100 µl of the radioactively labelled probe (see 3.11.14.2) was denatured 5 min at 95°C, mixed with the prehybridisation solution and hybridised O/N at 65°C. After hybridisation the membranes were washed twice for 30 min with 0.4x SSC, 1% SDS and exposed to an autoradiography film for 12 to 36 hours at -80°C. Finally, the film was developed in the developing machine. At positions where the probe bound, β-emissions from the probe will cause the X-ray film to blacken.

CHURCH BUFFER

Na ₂ HPO ₄ dihydrate	89 g
85% H ₃ PO ₄	4 ml
filled up with ddH ₂ O to 1 l	
Sodium phosphate buffer	500 ml
BSA	10 g
20% SDS	350 ml
0.5M EDTA	2 ml
filled up with ddH ₂ O to 1 l	

3.11.15 *Polymerase chain reaction (PCR)*

Polymerase chain reaction is an easy and quick method to specifically amplify DNA from smallest amounts of DNA. This technique was routinely used to genotype mice and to amplify fragments of a desired genomic or vector DNA.

All PCR reactions were prepared in 0.2 ml tubes (TreffLab), on ice, in a volume of 20 µl or 100 µl for preparative PCR. A typical reaction was set up as follows:

Genomic DNA (see 3.11.13) or 1 µg vector DNA	2 µl
10x PCR buffer	2 µl
50mM MgCl ₂	0.6 µl
10mM dNTPs	0.4 µl
100 pmol / µl sense primer (S)	0.2 µl
100 pmol / µl anti-sense primer (AS)	0.2 µl
<i>Taq</i> DNA polymerase	0.2 µl
ddH ₂ O	14.4 µl

After mixing of these components the tubes were placed in the PCR machine (Biometra) at 95°C and run with the following touchdown protocol. The annealing temperature was chosen dependent of the primer pair (see 3.11.1).

Denaturation 30 sec, 95°C

Annealing 30sec, 65°C

Elongation 30 sec, 72°C

These 3 steps were repeated 10 times. The annealing temperature was decreased each time by 1°C.

Denaturation 30 sec, 95°C

Annealing 30sec, 55°C

Elongation 30 sec, 72°C

These 3 steps were repeated 35 times.

Pause at 4°C

The PCR products were analysed by agarose gel electrophoresis (see 3.11.5).

10x Taq Polymerase buffer

Tris-HCl (pH 9) 100 mM

KCl 500 mM

MgCl₂ 20 mM

3.11.16 RNA isolation

Epidermal lysates (see 3.9.4.1) and liver or muscle samples dissected from mice, were resuspended in 0.5 ml Trizol (Gibco) and homogenized (Polytron). After centrifugation for 10 min, 12000 RPM at 4°C, the supernatants were kept for 5 min at RT and then mixed for 3 min with 200 µl of CHCl₃. Spun down again, the supernatants were transferred to a tube with 500 µl isopropanol and incubated 10 min at RT. RNA was pelleted by 10 min centrifugation at 12000 RPM, 4°C and the pellet was washed with 1 ml of 75% ethanol / DEPC, air dried and dissolved in 30 µl DEPC water. The concentration of RNA was measured (Gene Quant II, Amersham Pharmacia Biotech) and checked on an agarose gel for degradation (see 3.11.5).

3.11.17 Reverse transcriptase polymerase chain reaction (RT-PCR)

RT-PCR (reverse transcription-polymerase chain reaction) is a sensitive technique for mRNA detection. In order to analyse the RNA from a cellular lysate (see 3.9.4.1 and 3.11.16) the SuperScript™ III Reverse Transcriptase from Invitrogen was used, which synthesises the first-strand cDNA. The synthesis was done according to manufactures protocol. The resulting cDNA was then applied as a template in a standard PCR reaction (see 3.11.15).

3.11.18 RNase protection assay

In order to investigate the inflammatory response in wounded mouse skin, the amount of interleukin 1β mRNA in harvested wounds was determined by RNase protection assay (RPA). This assay is a highly sensitive and specific method for the detection of mRNA species. First, specific, radioactively labelled RNA probe is hybridized in excess to target RNA. These double-stranded RNA regions are resistant to RNase digestion. Next, the free probe and other

single-stranded RNA are digested with RNases. The remaining "RNase-protected" probes are purified, resolved on polyacrylamide gels, and quantified. The quantity of each mRNA species in the original RNA sample can then be determined based on the intensity of the appropriately-sized, protected probe fragment.

As a loading control, 1 µg of each RNA sample was resolved through a 1% agarose gel and stained with ethidium bromide. Alternatively, the RNAs were hybridised with an antisense RNA probe to the housekeeping gene glyceraldehyde-3-phosphate dehydrogenase. As template for the interleukin 1β probe, the published cDNA sequence was used (Hübner et al., 1996). RNase protection assays, on RNA isolated from harvested wounds (see 3.4), were performed in the laboratory of Prof. Sabine Werner, ETH, Zürich, Switzerland.

3.11.19 DNA Microarray Hybridization and Analysis

Array analysis was performed in collaboration with Robert Geffers, GBF, Braunschweig, Germany. In brief, quality and integrity of the total RNA isolated from 2×10^6 fibroblastoid cells for each cell line, were controlled by running all samples on an Agilent Technologies 2100 Bioanalyzer (Agilent Technologies; Waldbronn, Germany). For biotin-labelled target synthesis starting from 3 µg of total RNA, reactions were performed using standard protocols supplied by the manufacturer (Affymetrix, Santa Clara, CA). Briefly, 5 µg total RNA was converted to dsDNA using 100 pmol of a T7T23V primer (Eurogentec; Seraing, Belgium) containing a T7 promotor. The cDNA was then used directly in an *in vitro* transcription reaction in the presence of biotinylated nucleotides.

The concentration of biotin-labelled cRNA was determined by UV absorbance. In all cases, 12.5 µg of each biotinylated cRNA preparation were fragmented and placed in a hybridization cocktail containing four biotinylated hybridization controls (BioB, BioC, BioD, and Cre) as recommended by the manufacturer. Samples were hybridized to an identical lot of Affymetrix MOE430A for 16 hours. After hybridization, the GeneChips were washed, stained with SA-PE and read using an Affymetrix GeneChip fluidic station and scanner. Gene expression levels were determined by means of Affymetrix's Microarray Suite 5.0 (MAS 5.0).

3.11.20 Generation of the targeting constructs for the *KIe15* and *KIe16* mouse strains

3.11.20.1 Generation of the cassette containing an artificial intron - exon border and neo resistance gene (*pBluscript II KS / KIe15* and *pBluscript II KS / KIe16*)

In order to generate the targeting vectors the floxed cassette containing the artificial exon and the neo resistance gene had to be constructed. First the multiple cloning site (MCS) of the *pBluscript II KS (+/-)* (Figure 3.7) was modified.

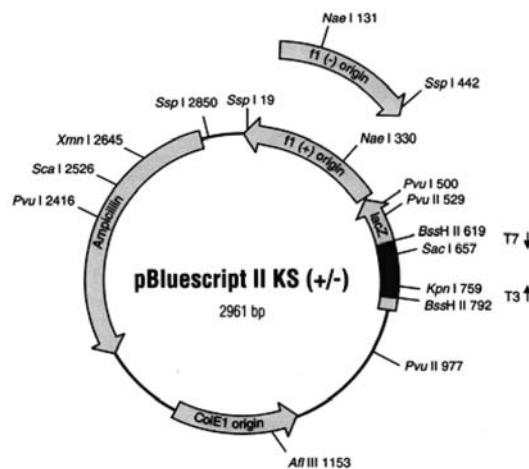


Figure 3.7 Schematic representation of the *pBluscript II KS (+/-)* vector.

The BamHI - XhoI fragment of the vector was deleted and the double stranded oligonucleotides BamHI_Xho-sense and BamHI_Xho-anti-sense (S/AS oligonucleotides) were introduced, which contained the following restriction sites: BamHI, XhoI, EcoRI, Sall and an XhoI overhang. Introduction of that oligo destroyed the XhoI in the original MCS. Next the BamHI-Sall fragment of the *pGEM7(KJ1)Sall* vector (Figure 3.8), containing the polyA sequence was subcloned into the modified MCS.

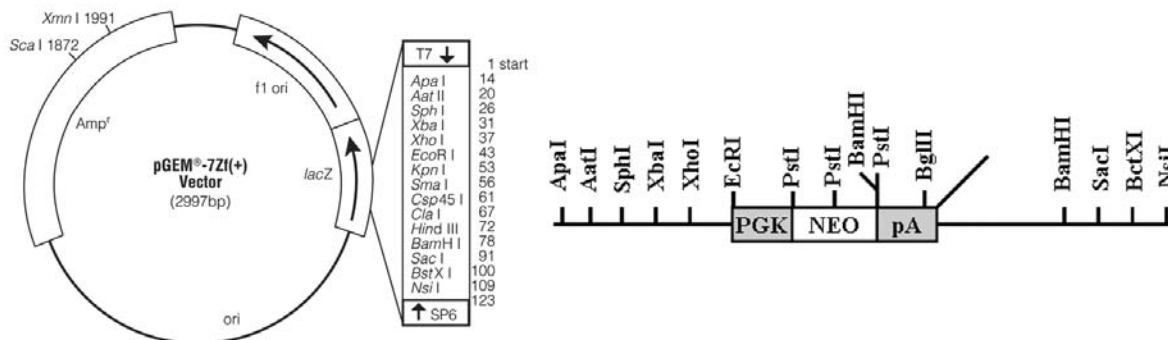


Figure 3.8 Schematic representation of the *pGEM[®]-7Zf(+)* vector and the modified MCS (*pGEM7 (KJ1) Sall*). PGK, PGK promoter; NEO, neomycin resistance gene; pA, polyadenylation signal.

Downstream of the polyA site the artificial exon was inserted by the introduction of the NotI[mloxP_int14/exo15]BamHI-S/AS oligo for the exon 15 targeting vector and NotI[mloxP_int15/exo16]BamHI-S/AS oligo for the exon 16 targeting vector. Both oligonucleotides contained the NotI restriction site followed by the *mloxP* site and twelve 3' nucleotides of the respective intron, twenty 5' nucleotides of exon 15 and three of exon 16, respectively. In both cases the exon sequence was terminated by a stop codon and a BamHI site. Next the modified pBluscript II KS (+/-) vectors were opened again using an EcoRI and SalI digestion, and the EcoRI - SalI fragment of the pGEM7(KJ1)SalI-*mloxP* vector was inserted. This fragment contained the PGK promoter, the neo resistance gene, a polyA signal and the *mloxP* site. The size of the entire cassette inserted in the pBluscript II KS (+/-) was 2.4 kB (Figure 3.9 A and B).

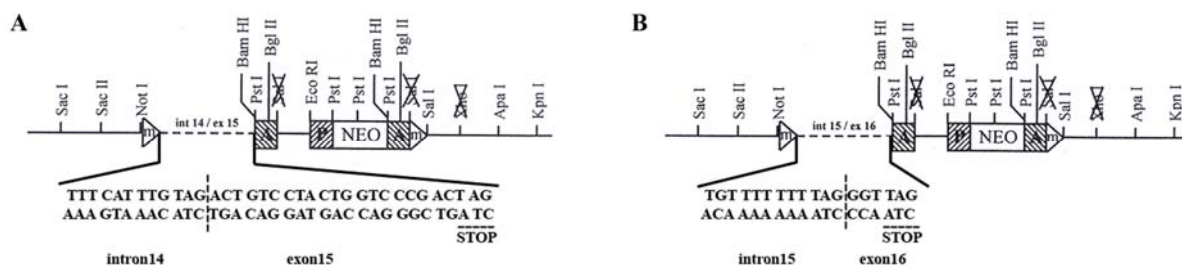


Figure 3.9 Schematic representation of the vectors containing an artificial intron - exon border and the neo resistance gene. (A) pBluscript II KS / KIe15 and (B) pBluscript II KS / KIe16. (A, polyA signal; P, PGK promoter; neo, neomycin resistance gene; \blacktriangle , *mloxP* site; important and removed restriction sites are shown).

3.11.20.2 Generation of constructs targeting exon 15 of the $\beta 1$ integrin gene

In the following steps the exon 15 and 16 DNA containing pBluscript II KS (+/-) vector (p $\beta 1$ int3'A4, Figure 3.10) was modified in order to enable the insertion of the floxed cassette described in paragraph 3.11.20.1., upstream of exon 15.

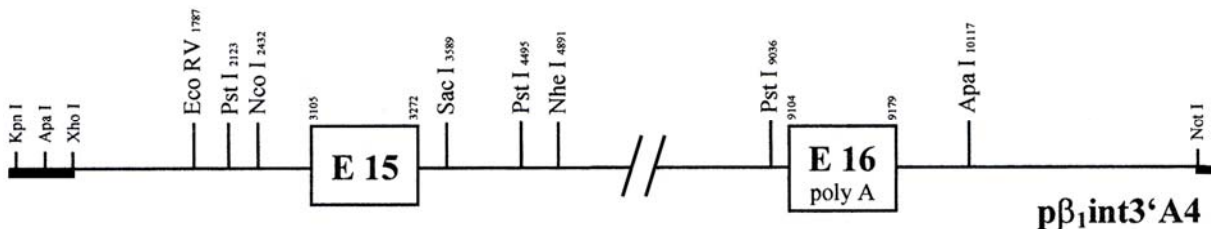


Figure 3.10 Schematic representation of the p $\beta 1$ int3'A4 vector. The $\beta 1$ integrin DNA fragment containing exon 15 and 16 was cloned into pBluscript II KS (+/-) vector. The vector backbone is indicated by a thick line. (polyA, polyadenylation signal; E, exon).

First the MCS of the pBluscript II KS (+/-) (Figure 3.7) was cut with NotI, filled in and religated with blunt ends destroying the NotI restriction site. Next the NcoI site (2423) (Figure 3.10) within the DNA sequence was opened and the NcoI(NotI_SalI)-S/AS oligo was

inserted in order to create two new restriction sites: NotI and Sall upstream of the NcoI site. Digestion of these newly generated sites enabled the insertion of the NotI-Sall fragment of the pBluscript II / K1e15 vector (Figure 3.9 A). The correct sequence and orientation of the targeting vector was confirmed by sequencing. In order to introduce the D759A and Δ D759-M771 mutations a Sall-SacI fragment of the wild type targeting construct was subcloned into the pALTER-1 vector and mutagenesis was performed (see 3.11.11). After confirmation of the presence of the mutated residues (3.11.12) the Sall-SacI fragment was cloned back into the backbone of the targeting construct and sequenced again (3.11.12).

3.11.20.3 Generation of constructs targeting exon 16 of the β 1 integrin gene

The p β 1int3'A4 vector with the destroyed NotI site (compare paragraph 3.11.20.2) was further modified in order to enable the insertion of the floxed cassette described in paragraph 3.11.20.1., upstream of exon 16. First the KpnI-NheI fragment of the vector was deleted and the KpnI[XhoI]NheI-S/AS oligonucleotides were introduced, which in the final step of construct generation served as the site of the reintroduction of the exon 15 fragment. Next the PstI site (9036) in the DNA fragment (Figure 3.10) was opened and the PstI[NotI_Sall]-S/AS oligo was inserted. The newly created sites NotI and Sall were the insertion sites for the NotI-Sall fragment of the pBluscript II / K1e16 vector (Figure 3.9 B). In the last step, the XhoI-NheI fragment of p β 1int3'A4 vector was reintroduced into the targeting vector. The correct sequence and orientation of the targeting construct was confirmed by sequencing (3.11.12). In order to introduce the Y783F, Y795F, YY783/795FF, S785A, S785D and the TT788/789AA mutations a KpnI-Sall fragment of the wild type targeting construct was subcloned into the pALTER-1 vector and mutagenesis was performed (see 3.11.11). After confirmation of the presence of the mutated residues (3.11.12) the KpnI-Sall fragment was cloned back into the backbone of the targeting construct and sequenced again (3.11.12).

3.12 Microscopy

In order to investigate the morphology of tissues and cells as well as the distribution of certain structures within a cell, following microscope-camera systems were used: Zeiss, Axiovert 135 (phase contrast microscopy); Zeiss, Axioskop + Leica DC500 camera (phase contrast microscopy); Leica, Leica DMRA2 + Hamamatsu ORCA-ER camera (fluorescence microscopy); Leica, Leica DMIRE2 + Leica TSC SP2 (confocal microscopy). Images were processed with Photoshop (Adobe).

Phase-contrast and fluorescence video microscopy were performed in an closed chamber supplied with 5% CO₂, at 37°C and 40% humidity using Zeiss, Axivert 200M microscope and a camera system from Visitron Systems.

To perform single cell analysis of migrating cells, prior to fluorescence video microscopy, nuclei were stained for 30 min with 1 µg / ml Hoechst 33342 (Sigma), washed 3 times with growth medium and tracked using MetaMorph 6.0 software.

For some experiments, performed in collaboration with Klemens Rottner, GBF, Braunschweig, Germany, cells were transiently transfected with constructs driving the expression of EGFP-VASP (Carl et al., 1999) or EGFP-β-actin (BD Biosciences) using FuGENE6 (Roche Molecular Biochemicals) and plated on fibronectin-coated (50µg / ml, Roche) or collagen I-coated (50µg / ml, CellSystems) glass coverslips for high magnification video microscopy.

4 Results

4.1 *Cdc42* in cell migration

A significant body of evidence has indicated a crucial role for Cdc42 in cell migration and cross-talk between this Rho GTPase and integrins in mediating migration associated events. Loss of Cdc42 was shown to impair directed migration of fibroblasts and astrocytes by reducing the wound closure speed and directionality of migration, as determined by polarized protrusion formation and reorientation of the Golgi apparatus (Nobes and Hall, 1999; Cau and Hall, 2005). Furthermore, it was shown that Cdc42 mediates filopodia formation upon integrin mediated adhesion (Nobes and Hall, 1999, Kozma et al., 1995) and that Cdc42 regulates integrin clustering, thus focal adhesion formation, essential for proper cell migration (Nobes and Hall, 1995). However, in all these studies Cdc42 function was only inhibited by various means, which might have non-specific side effects. Recently, investigation of *Drosophila* embryos lacking a functional Cdc42 gene showed that loss of Cdc42 results in impaired cell polarity and increased migration speed of hemocytes upon wound-induced cues (Stramer et al., 2005). In this study, however, the involvement of integrins was not studied.

To test whether Cdc42 is essential for directed cell migration in mammalian cells and to investigate the cross-talks between integrin and Cdc42 mediated signalling, fibroblastoid cell lines lacking the functional Cdc42 gene were established and analyzed in wound closure assays. In addition, these cells were used to experimentally assess the specificity of dominant negative inhibition of Cdc42 by transducing Cdc42-deficient cells with dominant negative Cdc42 (dnCdc42). This inhibition should not result in any phenotype if inhibition by dnCdc42 is specific for Cdc42.

4.1.1 *Generation of Cdc42-deficient and reconstituted fibroblastoid cell lines*

Fibroblastoid cells were generated by differentiation and immortalization of embryonic stem (ES) cells carrying a conditional and a null allele (fl/-). First, wild type ES cells were modified by two rounds of homologous recombination to obtain (fl/-) and (-/-) ES cells using a targeting construct for a conditional inactivation of the Cdc42 gene (Figure 4.1 A). The gene deletion and the absence of Cdc42 protein were confirmed by Southern and Western blotting, respectively (Figure 4.1 B and C). ES cells carrying a conditional and a null allele were differentiated *in vitro* in the presence of 0.5% DMSO, immortalised by retroviral transduction of the SV40 large T antigen and cloned (Cdc42(fl/-)). By adenoviral transduction of the

fibroblastoid cells with the Cre recombinase, which is a Type I topoisomerase from bacteriophage P1 catalyzing the site-specific recombination of DNA between *loxP* sites, *Cdc42*-null cells were obtained and cloned (*Cdc42*^{-/-}). Analysis of isolated clones by Western blotting confirmed the absence of *Cdc42* protein (Figure 4.2). The (*fl*^{-/-}) and (*-/-*) ES cells and the (*fl*^{-/-}) and (*-/-*) fibroblastoid cell line were established by Xunwei Wu, MPI for Biochemistry, Martinsried, Germany.

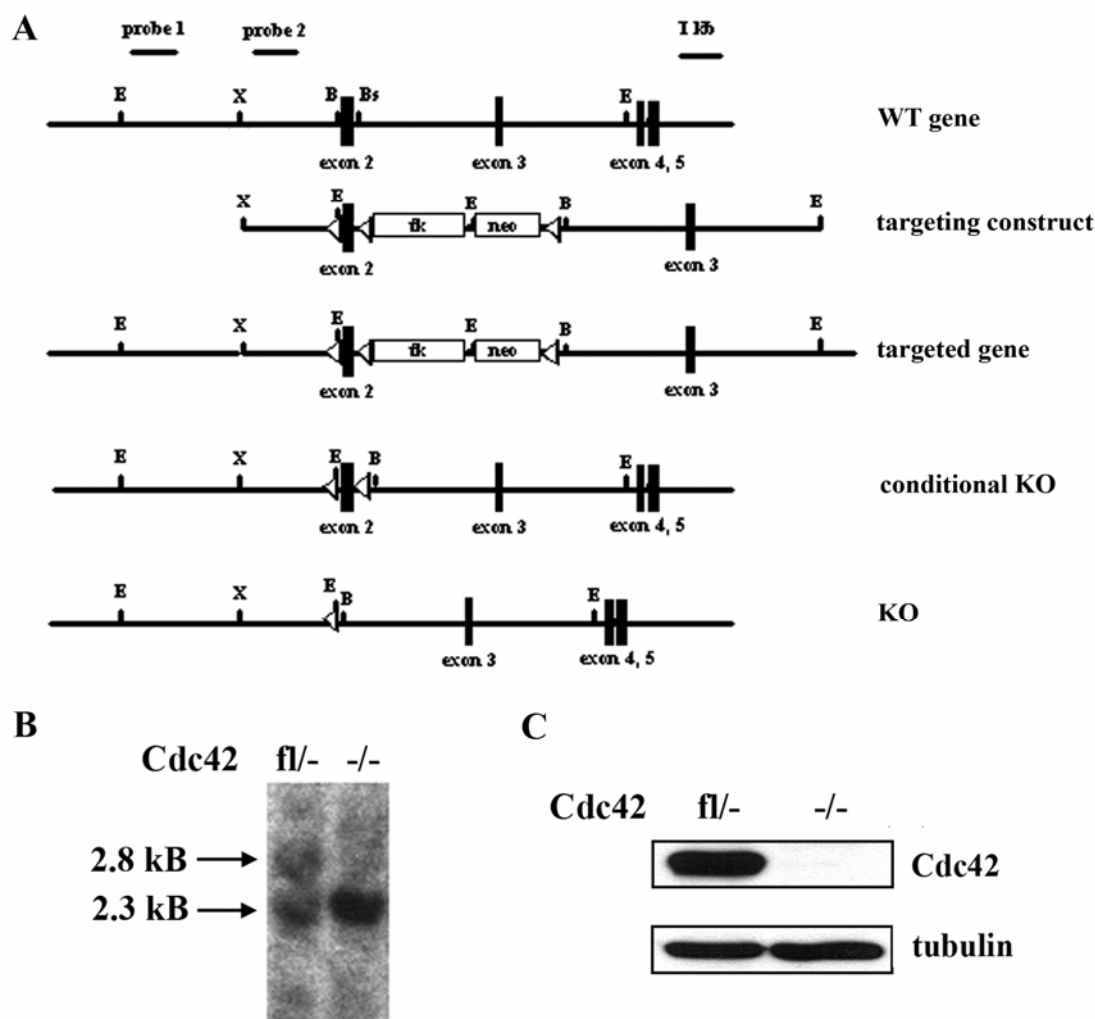


Figure 4.1 Targeting strategy and the generation of the *Cdc42*(*fl*^{-/-}) and *Cdc42*(*-/-*) ES cells. (A) In order to inactivate the *Cdc42* gene the ATG containing exon 2 was flanked by two *loxP*-sites, followed by a neo-tk selection cassette. After two rounds of recombination *Cdc42*(*fl*^{-/-}) and *Cdc42*(*-/-*) cells were obtained. (B) Southern blot analysis with external probe (probe 2) shows efficient *Cdc42* gene deletion. (C) Western blotting using the anti-*Cdc42* antibody confirmed the absence of the *Cdc42* protein in *Cdc42*(*-/-*) ES cells.

To assess the specificity of dominant negative inhibition and to prove that reintroduction of wt *Cdc42* into null cells rescues the mutant phenotype, the *Cdc42*-deficient cells were infected with a retrovirus expressing dn*Cdc42* (*Cdc42*(*-/-*) + N17) or wild type *Cdc42* (*Cdc42*(*-/-*) + wt) together with a hygromycin resistance gene. After selection of stably

transduced cells in Hygromycin B supplemented medium, single clones were picked and analysed for Cdc42 expression by Western blotting. Those with highest Cdc42 and dnCdc42 expression were selected (Figure 4.2). The expression level of wt Cdc42 transduced into null cells was comparable to endogenous Cdc42 in Cdc42 (fl/-) cells, while that of dnCdc42 was slightly lower (Figure 4.2). For all further experiments 2 independent clones of each mutant cell line were analyzed which behaved virtually the same.

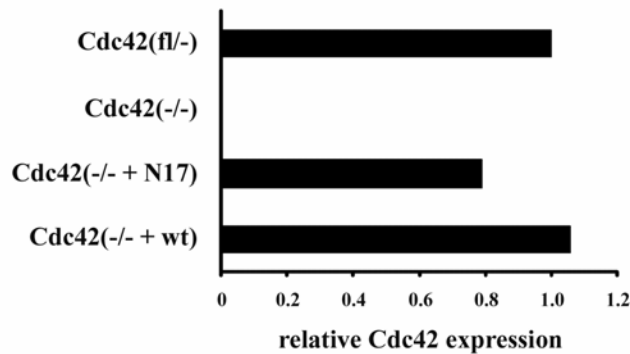
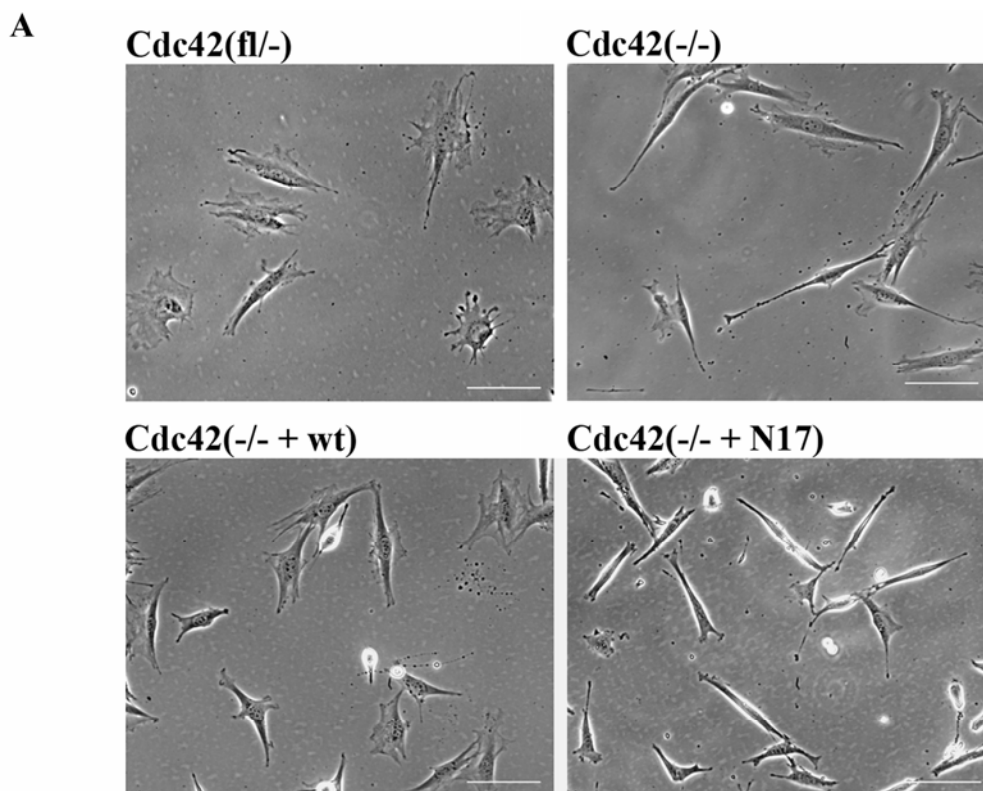


Figure 4.2 Quantification of Western blot analyses showing relative Cdc42 expression in the fibroblastoid cell lines studied. Western blot analysis confirmed loss of Cdc42 expression in Cdc42(-/-) cells and re-expression of Cdc42 or dnCdc42 in Cdc42(-/- + wt) and Cdc42(-/- + N17) cell lines. Cdc42 expression levels were normalized to tubulin, which served as a loading control.

4.1.2 Altered morphology, but normal adhesion of Cdc42-null cells

Cell morphology is known to be regulated by members of the Rho family of GTPases, including Cdc42. Furthermore, Rho GTPases control clustering of integrin receptors and thus integrin mediated cell adhesion (Nobes and Hall, 1995; Ridley, 2000).

Investigation of the cell morphology of our fibroblastoid cells seeded on plastic showed that in comparison to the well-spread polygonal morphology of the parental Cdc42(fl/-) cells, Cdc42-null clones and Cdc42-null clones expressing dnCdc42 (Cdc42(-/- + N17)) were less spread and more spindle-shaped. However, expression of wild type Cdc42 in Cdc42-deficient cells (Cdc42(-/- + wt)) restored the parental phenotype (Figure 4.3 A). In order to quantify the differences between the cell lines, we seeded the cells on plastic and determined the cell area and cell elongation ratio, described as the ratio of long to short axis of the cell. Compared to Cdc42(fl/-) control cells ($5641 \pm 1423 \mu\text{m}^2$), cell area was significantly reduced in Cdc42(-/-) cells ($3184 \pm 1024 \mu\text{m}^2$) and even further in Cdc42(-/- + N17) cells ($1544 \pm 449 \mu\text{m}^2$). Cell elongation increased from control (2.7 ± 1.1) to Cdc42-null (5.7 ± 1.1) and Cdc42(-/- + N17) cells (6.1 ± 3.6 ; Figure 4.3 B).



B

Cell line	Cell area [μm^2]		Elongation ratio	
Cdc42(fl/-)	5641 (± 1423)	n=18	2.7 (± 1.1)	n=20
Cdc42(-/-)	3184 (± 1024)*	n=23	5.7 (± 2.8)*	n=22
Cdc42(-/- + N17)	1544 (± 449)* **	n=28	6.1 (± 3.6)*	n=31

* $p < 0.05$ Cdc42(fl/-) versus Cdc42(-/-) or Cdc42(-/- + N17)

** $p < 0.05$ Cdc42(-/-) versus Cdc42(-/- + N17)

Figure 4.3 Cdc42 mutant cells have spindle-shape morphology. (A) Phase-contrast images of fibroblastoid cell lines studied. Cdc42(-/-) and Cdc42(-/- + N17) mutants display spindle-shape morphology, while the mutant morphology is rescued in Cdc42(-/- + wt) cells (scale bar = 100 μm). (B) Quantification of cell area and elongation ratio in Cdc42(fl/-) cells and both mutant fibroblastoid cell lines reveals reduced cell area and increased elongation ratio in mutant cells. Quantification was performed using MetaMorph 6.0 software.

We then analyzed the actin cytoskeleton of the cells. Immunostaining with FITC-conjugated phalloidin, which directly binds to filamentous actin, revealed that stress fibres are formed in Cdc42(fl/-), Cdc42(-/-), Cdc42(-/- + N17) and Cdc42(-/- + wt) cells. In Cdc42-mutant cells, however, nearly all stress fibres appeared to be parallel to each other and to the long axis of the cell, while in control and wt reconstituted cells, differentially oriented groups of stress fibres could be identified. The formation of focal contacts was not altered in the mutant cell lines, as assessed by paxillin staining (Figure 4.4).

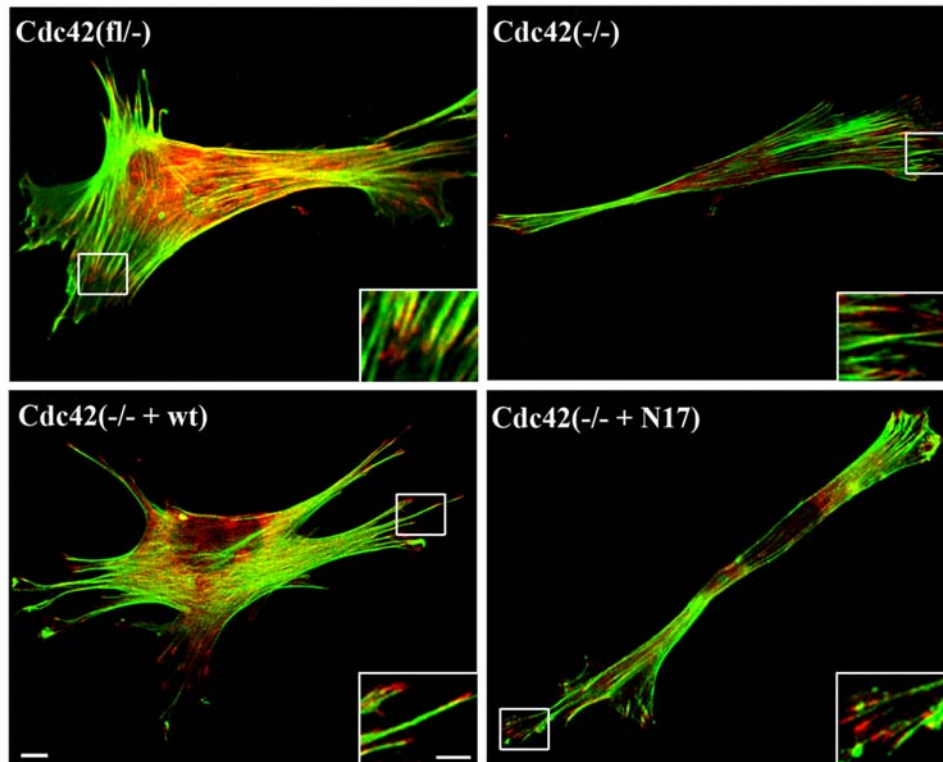


Figure 4.4 Cc42 is important for the actin cytoskeleton organization in fibroblastoid cells. *Cdc42(-/-)* and *Cdc42(-/- + N17)* mutants form focal contacts but display actin organization rather different from the control (*fl/-*) and reconstituted (*-/- + wt*) cell lines as determined by paxillin (red) and phalloidin (green) staining (scale bar = 10 μ m). Insets show enlargements of the focal contacts at the tips of actin filaments (scale bar = 5 μ m).

Cdc42 was shown to increase integrin clustering and thus integrin avidity (Nobes and Hall, 1995). Therefore, it was expected that lack of *Cdc42* would reduce integrin mediated adhesion to ECM components. Furthermore, Chen et al. (2000), mentioned in their paper preliminary data suggesting that fibroblast-like cells differentiated from *Cdc42(-/-)* ES cells have defective adhesion. However, adhesion of our *Cdc42*-deficient fibroblastoid cells on laminin, fibronectin and vitronectin was similar to the parental cells and was not significantly altered (Figure 4.5 A). Adhesion to collagen was poor in both *Cdc42*-null and parental cells, presumably due to the absence of the collagen binding integrin receptors $\alpha 1\beta 1$ and $\alpha 2\beta 1$ on both cell types as determined by FACS analysis. Expression of $\alpha 5$, αv , $\beta 1$ and $\beta 3$ integrins were similar in *Cdc42*-deficient and control cells (Figure 4.5 B) suggesting that there is no link between *Cdc42* expression and the availability of integrin receptors on the cell surface.

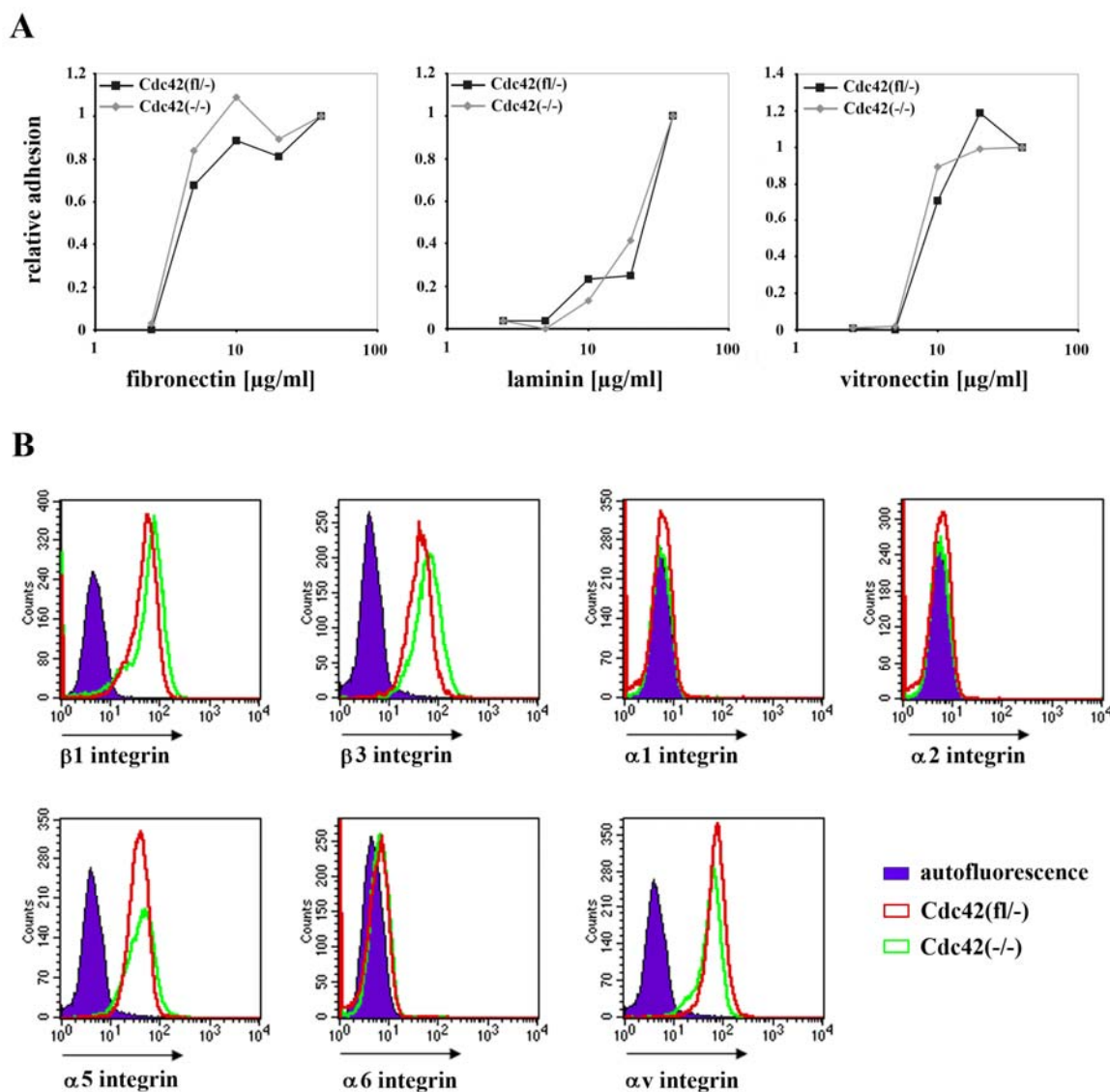


Figure 4.5 Cell adhesion is not changed in Cdc42-null cells. (A) Cell adhesion to different ECM components normalized to the adhesion of the Cdc42(fl/-) cells is shown (n=2). (B) Integrin expression was not changed in the absence of Cdc42 as assessed by FACS analysis; the background staining was identical for both cell lines.

Integrin-dependent activation of Cdc42 and Rac1 was reported to be crucial in mediating cell spreading (Price et al., 1998). In order to investigate the time course of spreading in our Cdc42-null fibroblastoid cells, we compared Cdc42(fl/-) and Cdc42(-/-) cells 5, 15, 30, 60, 120, 240 min and 24 h after seeding on a plastic culture dish. After 15 min, the majority of cells of both lines were adherent (Figure 4.6). No obvious difference in the kinetics of spreading was observed in Cdc42-deficient fibroblastoid cells compared to controls (Figure 4.6).

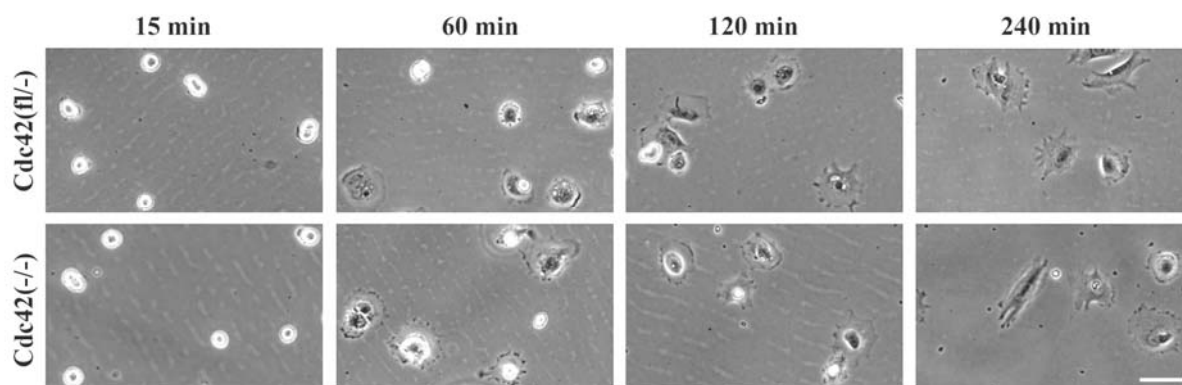


Figure 4.6 Normal spreading in the absence of Cdc42. Spreading kinetics of Cdc42-null cells on plastic is similar to control cells (scale bar = 100 μ m).

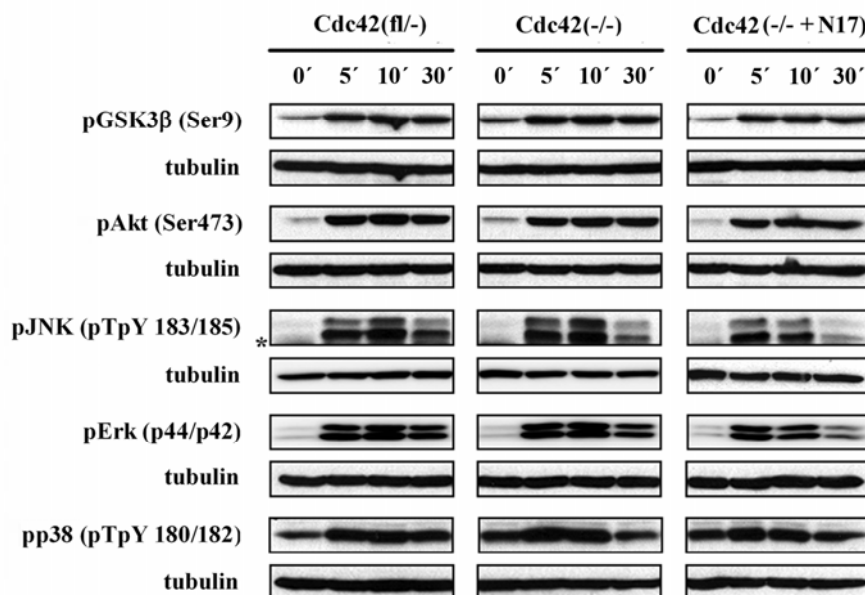
These data show that Cdc42 regulates the actin cytoskeleton organization but has no influence on focal contact formation, cell adhesion, integrin expression and spreading kinetics contrary to previous suggestions (Price et al., 1998; Chen et al., 2000).

4.1.3 Cdc42 has only limited influence on serum induced signalling pathways in fibroblastoid cells

Cdc42 was previously demonstrated to activate Erk, JNK, p38, Akt and GSK3 β , although cell type specific differences were reported (Frost et al., 1997; Chen et al., 2000; Zugasti et al., 2001). We therefore tested the basal and serum stimulated levels of Erk, JNK, p38, Akt and GSK3 β in the fibroblastoid Cdc42 (fl/-), Cdc42 (-/-) and Cdc42 (-/- + N17) cell lines.

Confluent monolayers of cells were starved for 12h in 0.5% FCS and induced with full growth medium for 0, 5, 10 and 30 min. We could not observe significant differences in basal activation levels of Erk, JNK, Akt, Gsk3 β and p38. Furthermore, all cell lines showed significantly induced phosphorylation of these proteins after serum treatment (Figure 4.7 A and B). In Cdc42(-/- + N17) cells, however, the activation of Erk decayed significantly faster than in control and null cells and the stimulation of JNK tended to decrease more quickly in both mutant cell lines (Figure 4.7 A and B). These data indicate that loss or dominant negative inhibition of Cdc42 does not have major influence on serum induced signalling pathways in fibroblastoid cells.

A



B

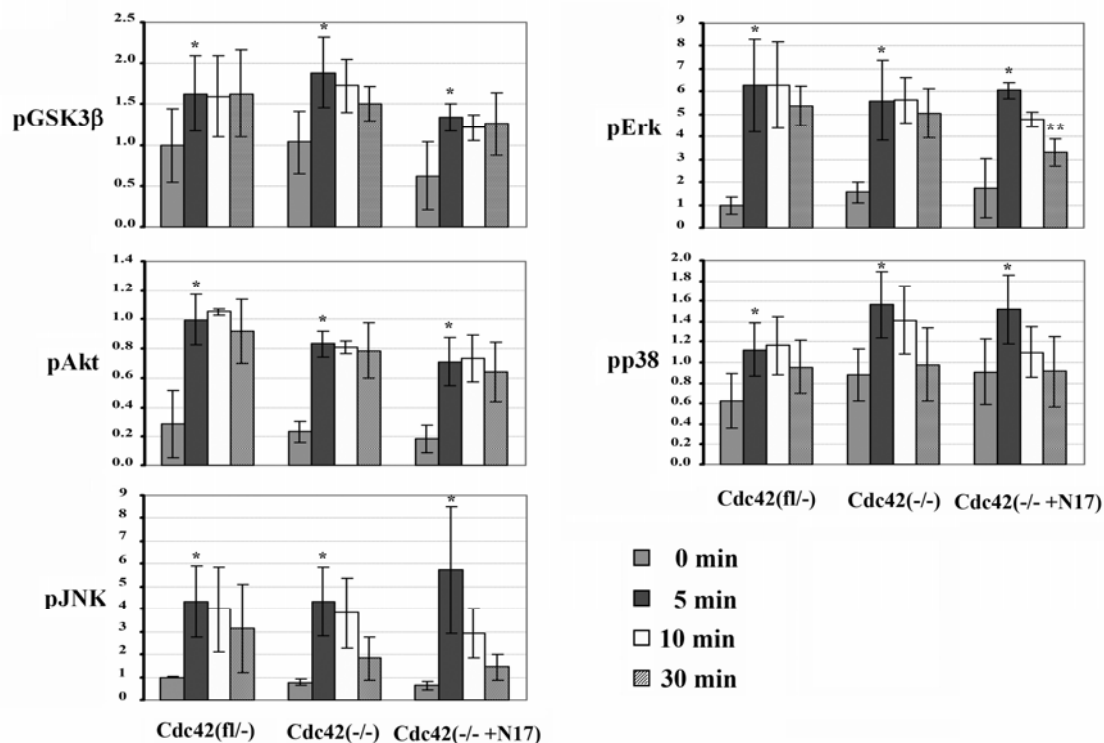


Figure 4.7 Serum induced activation of possible Cdc42 effectors. (A) Western blots of starved confluent Cdc42(fl/-), Cdc42(-/-), and Cdc42(-/- + N17) cells stimulated with serum for the indicated times. Representative results of three independent experiments are shown. Asterisk denotes an unspecific band. (B) Quantification of chemiluminescence signals using a CCD camera revealed that serum induced activation of all molecules tested is similar in all the cell lines investigated. Asterisks indicate significant increase of the signal ($p < 0.05$) between time point 0 min and 5 min within a given cell line. Activation of Erk was decaying significantly faster in Cdc42(-/- + N17) than in control and null cells, whereas the stimulation of JNK tended to decrease more quickly in both mutant cell lines. Two asterisks indicate significant difference ($p < 0.05$) between the induction after 5 min and 30 min.

4.1.4 Defective Rac1 activation in the absence of Cdc42

Cdc42 was shown to induce lamellipodia that are inhibited by dnRac1, suggesting that Cdc42 can activate Rac1 (Nobes and Hall, 1995). More recently, possible mechanisms of Rac1 activation by Cdc42 have been described. The first one proposed that Cdc42, through its action on PAK1, mediates RhoGDI phosphorylation and subsequent Rac1 activation (DerMardirossian et al., 2004). Another one suggested that Cdc42 induces Rac1 activation through the Par6-Par3 complex and the Rac-GEFs, STEF and Tiam1 (Nishimura et al., 2005). However, it remained unknown to what extent Rac1 activity is dependent on Cdc42.

In our fibroblastoid cell lines, loss of Cdc42 reduced the relative level of activated Rac1 to 52% (Cdc42(-/-); Figure 4.8 B) as determined by pull down assay with the Rac1-GTP binding domain CRIB of PAK1. This shows that in fibroblasts a substantial part of Rac1 activity is dependent on Cdc42. Re-expression of wt Cdc42 restored Rac1-GTP levels (Cdc42(-/- + wt), but expression of dnCdc42 further decreased Rac1 activity to 36% (Cdc42(-/- + N17; Figure 4.8 B). Rac1 expression was not altered in the absence of Cdc42 or in the presence of dnCdc42 (Figure 4.8 A). These data suggest that dnCdc42 decreases Rac1 activation not only by blocking Cdc42-dependent activation of Rac1, but also by other pathways, most likely by the inhibition of GEFs which can activate both Cdc42 and Rac1.

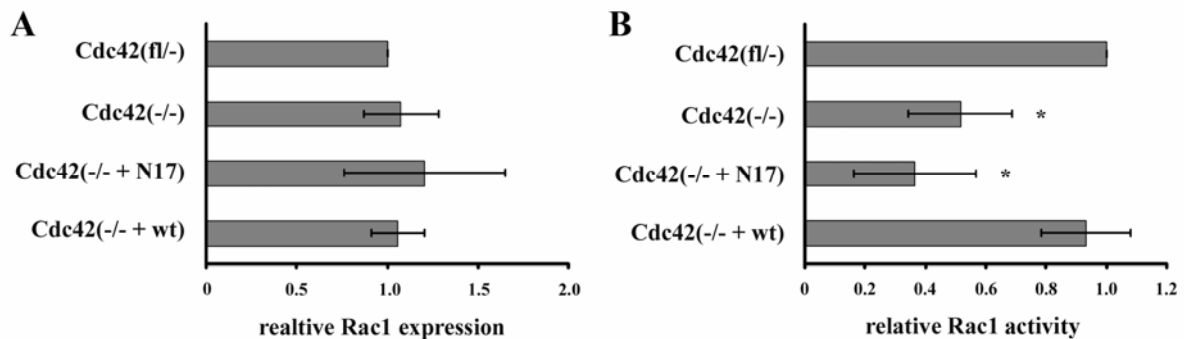


Figure 4.8 Reduced levels of GTP-Rac1 in Cdc42 mutant cells. (A) Expression levels of total Rac1 were similar in all these cell lines (n=3). Western blots for tubulin were used for correction of different loading. (B) Rac1 activity relative to total Rac1 as determined by pull down experiments demonstrating decreased Rac1 activity in Cdc42(-/-) cells (n=5), a further reduction in Cdc42(-/- + N17) cells (n=3), and normal levels in Cdc42(-/- + wt) cells (n=2), relative to Cdc42(f1/-) cells (n=5). Asterisk denotes p<0.05 when compared to control cells.

To test whether reduced levels of active Rac1 are responsible for morphological alterations of Cdc42 deficient fibroblastoid cells (see 4.1.2) we transiently overexpressed constitutively active Rac1 in Cdc42-null cells. Increased cell spreading and a highly migratory phenotype with strong lamellipodium formation was observed, thus no simple rescue of the null-phenotype (data not shown).

4.1.5 Loss of *Cdc42*-null does not effect *RhoA* activity

In addition to the reported influence of *Cdc42* on *Rac1* activity, there is also evidence for both direct and indirect control of *Cdc42* over *RhoA* activity (Evers et al., 2000). Since *RhoA* was shown to induce the assembly of contractile actin and myosin filaments (Ridley and Hall, 1992), we wondered whether the changes in the organization of the actin cytoskeleton (see 4.1.2) observed in the *Cdc42* null cells could be due to a change in *RhoA* activity.

To determine the levels of active *RhoA* we performed pull down analysis using the *Rho*-GTP binding domain (RBD) of the mouse rhotekin protein, expressed as a GST-tagged recombinant protein in *E. coli*. The Rhotekin-RBD protein specifically recognizes and binds to the active, GTP-bound, form of *RhoA*, *RhoB* or *RhoC* protein. *RhoA* activity and expression as determined by western blotting using an *RhoA* specific antibody was not altered in *Cdc42*(*-/-*) and *Cdc42*(*-/-* + N17) compared to control cells (Figure 4.9 A and B), suggesting negligible activation of GEFs which can activate both *Cdc42* and *RhoA* and also negligible crosstalk between *Cdc42* and *Rac1* under normal growth conditions.

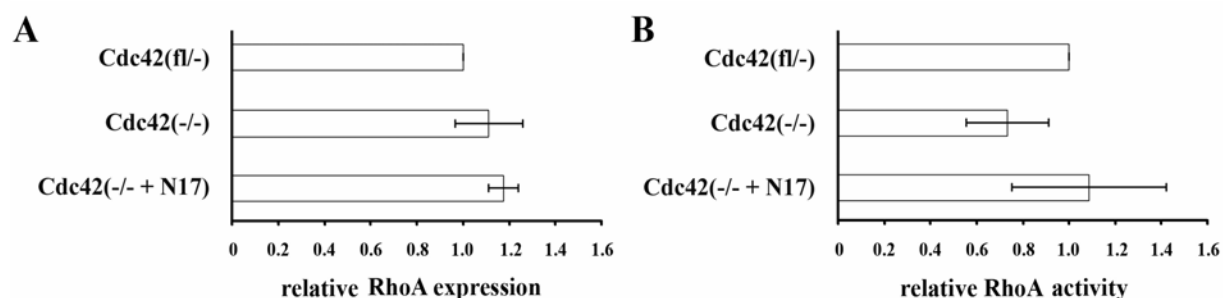


Figure 4.9 RhoA activity is not changed in *Cdc42* mutant cells. (A) Total *RhoA* levels are not significantly different (n=3). Western blots for tubulin were used for correction of different loading. (B) *RhoA* activity as assessed by pull down assay is similar in control and mutant cell lines, thus does not correlate with observed morphological alterations described in paragraph 4.1.2 (n=3).

4.1.6 No compensatory expression of other *Rho* GTPases in the absence of *Cdc42*

Lack of a functional *Cdc42* gene could induce a compensatory expression of other members of the *Rho* GTPases family. To test this possibility we performed an array expression analysis of 2 *Cdc42*(fl/-) and 2 *Cdc42*(-/-) clones (Affymetrix). All cell lines tested expressed high amounts of *RhoA*, *RhoB*, *RhoC*, *Rac1*, and *Cdc42* (in case of *Cdc42*(-/-) cells the mRNA will not result in the expression of functional protein), medium levels of *TC10*, *Wrch-2*, *Rnd3*, *RhoG*, and *Miro-1* and low or no detectable levels of *Rac2*, *Rac3*, *TCL*, *Wrch-1*, *RhoH*, *Miro-*

2 and RhoD. No significant change in Rho GTPase expression was found between control and mutant cell lines. Rif, Rnd1, and Rnd2 were not present on the array.

The array analysis was performed in collaboration with Robert Geffers, GBF, Braunschweig, Germany.

4.1.7 Cdc42-null cells have no mitosis defect

Dominant negative inhibition of Cdc42 in HeLa cells was demonstrated to result in a high amount of multinucleated cells indicating a crucial role of Cdc42 in chromosome segregation (Yasuda et al., 2004). To test whether Cdc42-null cells displayed any mitosis defect, we seeded our cells at low density, fixed and stained the DNA with DAPI and counted the percentage of cells with aberrant or multiple nuclei. Of 1300 cells of each cell line counted 24 h after plating, Cdc42(fl/-) and Cdc42(-/-) cells displayed similar percentages of cells with aberrant or multiple nuclei, with $4.2\% \pm 1.5$ and $3.5\% \pm 1.6$, respectively. In Cdc42(-/- + N17) the frequency of cells with aberrant nuclei increased to $6.9\% \pm 2.9$. This difference, however, was not significant ($p > 0.05$) when compared to control cells. Clearly, Cdc42 is not required for normal chromosome segregation as suggested previously, whereas dominant negative inhibition might lead to mitosis defects.

4.1.8 Loss of Cdc42 does not affect the formation of filopodia and lamellipodia

Expression of dnCdc42 in primary rat embryonic fibroblasts and Swiss 3T3 cells was shown to block the formation of filopodia (Nobes and Hall, 1995; Kozma et al., 1995) and Cdc42-null ES-cells generated by Chen et al. (2000) were reported to be incapable of formation of any peripheral protrusion including filopodia. To test whether the inactivation of the Cdc42 gene in our fibroblastoid cells prevents the formation of filopodia or lamellipodia we performed phase contrast time lapse microscopy, which most directly allows distinction between actively protruding filopodia and other non-protrusive peripheral structures such as retraction fibers. In addition we transfected our cells with GFP-actin or GFP-VASP, which is present at the tips of these protrusive structures (Rottner et al., 1999). Examination of the dynamics of these protrusions by phase contrast and fluorescence video microscopy, revealed normal lamellipodia and filopodia formation in Cdc42(-/-) cells (Figure 4.10; Supplementary Movie 1). In addition, these data indicated recruitment of prominent components of the actin polymerization machinery such as Ena/VASP proteins to the tips of these protrusions as in control cells.

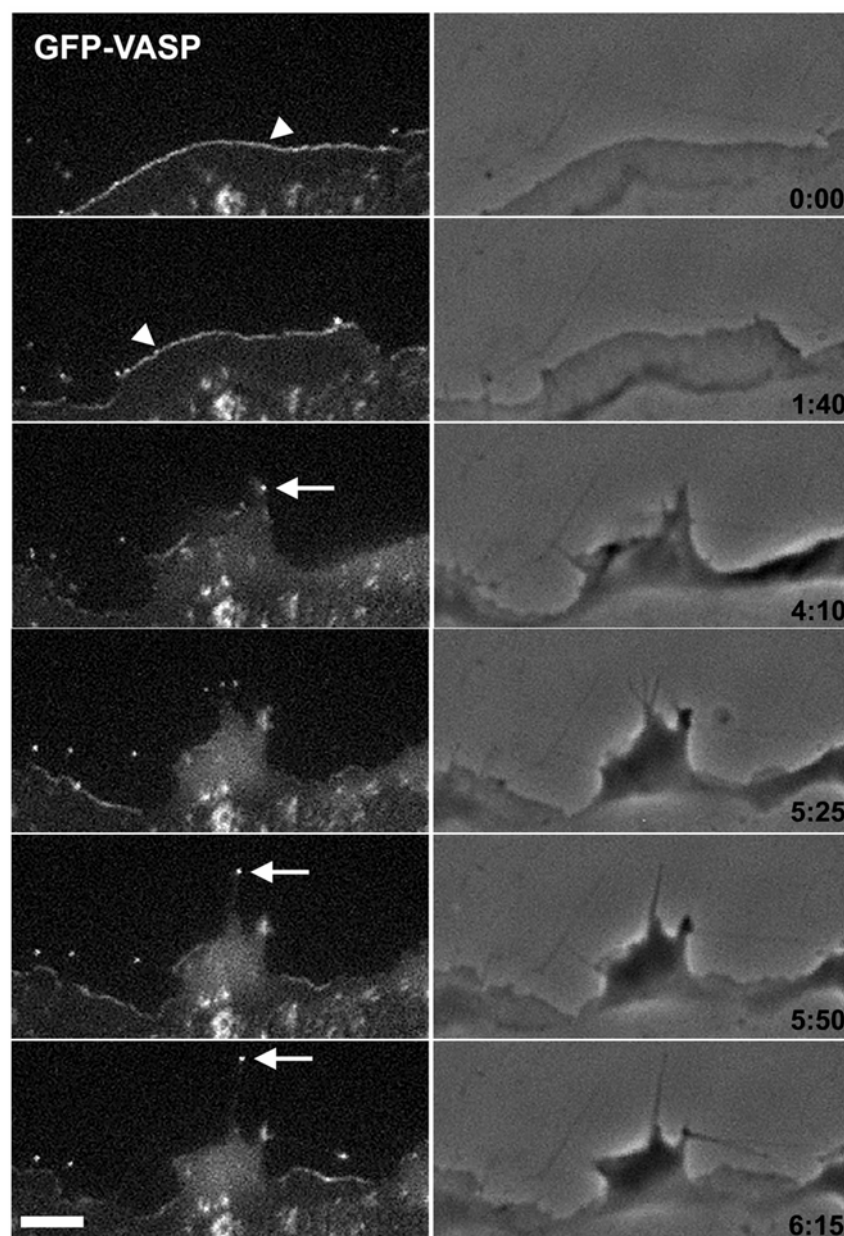


Figure 4.10 Loss of Cdc42 does not abrogate lamellipodia and filopodia protrusions. Fluorescence and phase contrast video microscopy (min:sec) taken from a EGFP-VASP expressing Cdc42-null cell revealing normal filopodia and lamellipodia formation, as well as recruitment of the VASP protein to the tips of lamellipodia (arrowheads) and filopodia (arrows; scale bar = 5 μ m).

Interestingly, in dnCdc42 expressing cells, filopodium formation was still observed and lamellipodia were still present. This does not exclude that at higher amounts of dnCdc42, filopodium or lamellipodium formation might be completely abrogated as described previously (Nobes and Hall, 1995; Kozma et al., 1995).

To confirm that filopodium formation observed in the absence of Cdc42 is not restricted to fibroblastoid cells, we analysed protrusion formation of Cdc42(-/-) ES cells by phase contrast time lapse video microscopy. After panning of feeder cells, control and null ES cells were seeded on collagen I coated glass and allowed to attach for 6h. Individual Cdc42-null ES cells

attached to the substratum had a round, smooth surface similar to control ES cells and showed frequent formation of lamellipodia and filopodia (Figure 4.11 and Supplementary Movies 6 and 7). These data suggest that Cdc42 is not essential for filopodium formation irrespective of cell type or transformation.

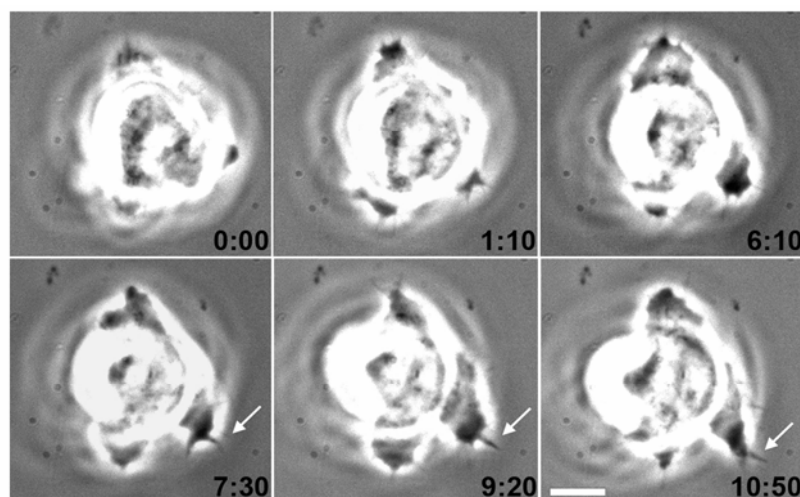


Figure 4.11 Filopodia formation in Cdc42(-/-) ES cells. Phase contrast video microscopy (min:sec) demonstrating formation of a filopodium (arrows) in Cdc42 null ES cells (scale bar = 10 μ m).

4.1.9 Increased blebbing and tail retraction defects in cells expressing dnCdc42

High frequency blebbing – the protrusion and subsequent retraction of plasma membrane - is a phenomenon that has been associated with both physiological and pathological situations. However, it is not clear, how these membrane protrusions form and what their function is. Blebs have been described to occur during mitosis, to precede cell spreading, and to be present at the leading edge of moving cells (Hagmann et al., 1999, and reference therein). Blebs also form when cells undergo apoptosis. However, these blebs have been proposed to be structurally different (Laster and Mackenzie, 1996). Some studies suggested that increase of the intracellular pressure upon cell contraction can lead to bleb formation, depending on the state of the actin cytoskeleton (Cunningham, 1995). Recent studies demonstrated that blebbing can be associated with increased Rho kinase (ROCK) activity (Saras et al., 2004).

When our fibroblastoid cell lines were analysed by phase contrast video microscopy, we observed that 7% of the parental cells analysed (n=16) formed blebs during the 6h of observation and that this frequency was increased to 18% in Cdc42-deficient cells (n=22). Expression of dnCdc42 in Cdc42-null cells further increased the incidence of blebbing, with 47% of cells showing bleb formation within the same time interval (n=28; Figure 4.12 A, small arrows; Supplementary Movie 2 and data not shown). To assess, whether the observed blebbing is a result of increased apoptosis in the Cdc42(-/- + N17) cells, we seeded the Cdc42(fl/-), Cdc42(-/-) and Cdc42(-/- + N17) cells sparsely and performed TUNEL staining

48h later. We could not find any detectable TUNEL positive, apoptotic cells (Figure 4.12 B). These data suggest that the blebbing observed in *Cdc42*-deficient cells is not related to programmed cell death. Since Rho activity was not increased in *Cdc42*(*-/-*) and *Cdc42*(*-/-* + N17) cells compared to controls (see 4.1.5), blebbing also seems not to be related to the Rho–ROCK pathway.

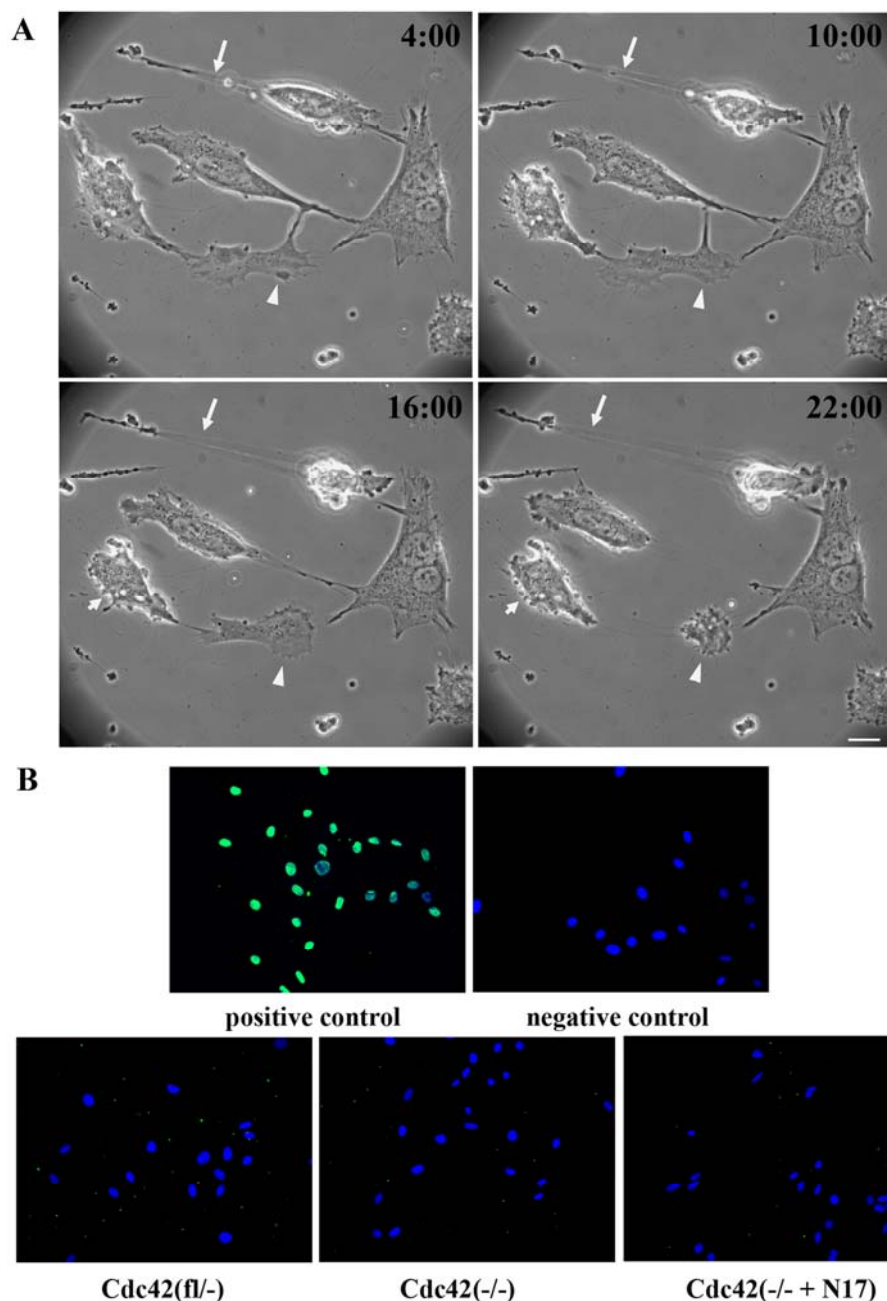


Figure 4.12 Increased blebbing and tail retraction defects in *Cdc42*(*-/-* + N17) cells. (A) Phase contrast video microscopy of cells expressing dnCdc42 displaying prominent membrane blebbing (small arrows). These cells often also lack proper retraction of the trailing edge, which is commonly left behind (arrows), causing the frequent formation of a-nucleated cytoplasts (arrowheads; scale bar = 10 μ m). (B) TUNEL staining on sparsely seeded, fixed cells, revealed the absence of apoptotic cells (TUNEL in green; nuclei counterstained with DAPI, blue).

Careful investigation of the phase contrast videos revealed that Cdc42 null cells and particularly the dnCdc42 expressing cells, frequently lost their trailing edge (Figure 4.12 A). To quantify these observations we defined the tail as a thin, trailing end opposite to the leading edge, and found that the tail length increased from Cdc42(fl/-) to Cdc42(-/-) to Cdc42(-/- + N17) cells (Table 4). Due to high cell-to-cell variations the difference was not significant between control and null cells. Yet, the tail length was significantly increased when Cdc42(fl/-) and Cdc42(-/- + N17) cells were compared. The observed defect could be a result of either defective rear detachment or reduced rigidity of the cell body, both phenomena associated with the action of RhoA, which was shown to control cell contractility and the tail retraction of migrating cells (Ridley et al., 2003). Although in Cdc42(-/-) and Cdc42(-/- + N17) cells RhoA activity was not detectably altered, it could still be that there are local changes in RhoA activity (e.g. only at the rear of the cell) not detectable in total lysates. These data indicate that loss of Cdc42 or expression of dnCdc42 may interfere with proper tail retraction.

Cell line	Tail length [μm]	
Cdc42(fl/-)	52.9 (± 25.5)	n=17
Cdc42(-/-)	65.0 (± 43.0)	n=20
Cdc42(-/- + N17)	72.2 (± 28.5)*	n=23

* $p < 0.05$ Cdc42(fl/-) versus Cdc42(-/-) or Cdc42(-/- + N17)

Table 4 Members of the Cdc42 family interfere with proper tail retraction. Quantification of the tail length in Cdc42(fl/-) cells and both mutant fibroblastoid cell lines shows increased tail length in Cdc42(-/- + N17) cells. Quantification was performed using MetaMorph 6.0 software.

4.1.10 Cdc42 is not crucial for directed migration

In previous studies, primary fibroblasts expressing dnCdc42 or WASp (201-321), which binds and inhibits Cdc42, showed a 50% reduction of wound closure in an *in vitro* wound closure assay, whereas in *Drosophila* Cdc42-deficient hemocytes showed a two-fold increased migration speed in response to wound-induced cues (Nobes and Hall, 1999 and Stramer et al., 2005). Both studies, therefore, suggested an important function of Cdc42 in directed migration. To analyse the directed migration of Cdc42-null mammalian cells we performed *in vitro* scratch assay with our cells and monitored the cells by phase contrast video microscopy. Quantification of these assays showed that fibroblastoid Cdc42(-/-) cells displayed a wound

closure speed highly comparable to Cdc42(fl/-) and Cdc42(-/- + wt) cells demonstrating that Cdc42 is not crucial for directed migration (Figure 4.13). In contrast, expression of dnCdc42 in Cdc42(-/-) cells resulted, similarly to the previous report by Nobes and Hall (1999), in a 45% decrease of wound closure speed revealing that Rho GTPases other than Cdc42 contribute to directed migration (Figure 4.13).

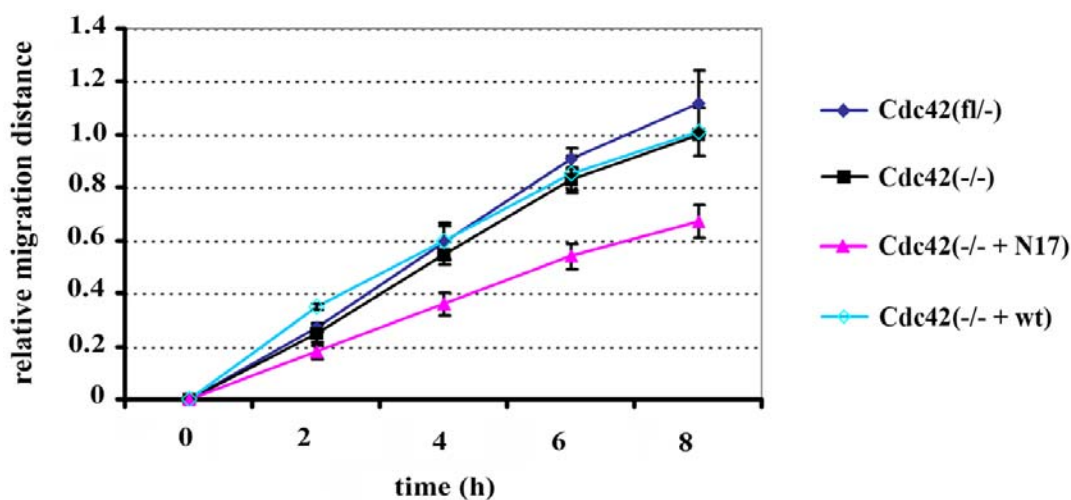


Figure 4.13 Cdc42 is not essential for directed cell migration. Relative migration of Cdc42(fl/-), Cdc42(-/-), Cdc42(-/- + wt) and Cdc42(-/- + N17) cells in a wounding assay (n=5). Only Cdc42(-/- + N17) cells show a significantly reduced directed migration.

To investigate the migration speed of individual cells during directed migration we performed single cell tracking analysis of wound closure experiments. To facilitate the tracking of migrating cells the nuclei of living cells were pre-stained with Hoechst 33342 (Haraguchi et al., 1999), and paths of individual cells were tracked and analyzed statistically using the MetaMorph 6.0 software. While Cdc42(fl/-) and Cdc42(-/-) cells showed similar average velocities (Cdc42(fl/-): $1.0 \pm 0.28 \mu\text{m}/\text{min}$; Cdc42(-/-): $1.0 \pm 0.17 \mu\text{m}/\text{min}$; n=60), Cdc42(-/- + N17) cells had a strongly reduced migration speed ($0.7 \pm 0.12 \mu\text{m}/\text{min}$; n=60, $p < 0.05$ versus control and null cells). This finding strengthens the observation that Cdc42 does not influence the speed of cell migration.

4.1.11 Cdc42 is not essential for cell polarization in migrating fibroblasts, but contributes to single cell directionality and Golgi re-orientation

In primary rat fibroblasts, expression of dnCdc42 was found to result in a complete loss of cell polarization with lamellipodial activity seen all around the cell periphery (Nobes and Hall, 1999; Cau and Hall, 2005) and in *Drosophila* Cdc42-deficient hemocytes showed inability to maintain persistent polarity in response to wound-induced cues (Stramer et al., 2005).

We analysed our fibroblastoid Cdc42(fl/-) cells by time lapse microscopy in an *in vitro* wounding assay and observed cell polarization characterized by lamellipodium formation stably oriented towards the wound during 6h of observation (Figure 4.14 A; Supplementary Movie 3). Unexpectedly, however, also in the absence of Cdc42, protrusion formation was polarized with rather stable directionality (Figure 4.14 A; Supplementary Movie 4). To further explore these phenomena we overlaid the migration paths of different migrating cells stained with Hoechst 33342 (compare paragraph 4.1.10) and found out that the directionality of Cdc42(-/-) cells is slightly lower than of control cells (Figure 4.14 B). Mutant cells seem to sense the direction towards the wound, but are less able to maintain it. A sensitive parameter for directionality is the mean angle vector, which obtains the value of 1 for a straight line and the value of 0 for random walk. Cdc42(-/-) cells had a significantly decreased mean angle vector compared to control cells (Cdc42(fl/-): 0.82 ± 0.1 ; n=60; Cdc42(-/-): 0.55 ± 0.11 ; n=60, $p < 0.05$ versus control cells). Expression of wild type Cdc42 in Cdc42-null cells restored the single-cell directionality to levels close to control cells (mean angle vector: 0.71 ± 0.07 ; n=60; Figure 4.15 B).

Video microscopy revealed that Cdc42(-/- + N17) cells could polarize, but that the protrusion formation was not stably oriented towards the wound (Figure 4.14 A, arrows; Supplementary Movie 5). As demonstrated by overlays of the migration paths of different dnCdc42 expressing cells, these mutant cells often stopped and migrated backwards or sideways (Figure 4.14 B). This resulted in a significantly reduced mean angle vector (0.38 ± 0.14 ; n=60, $p < 0.05$ versus control and null cells) of Cdc42(-/- + N17) cells compared to Cdc42-deficient cells (Figure 4.14 B) and together with the reduced single-cell velocity explains the reduced wound closure speed.

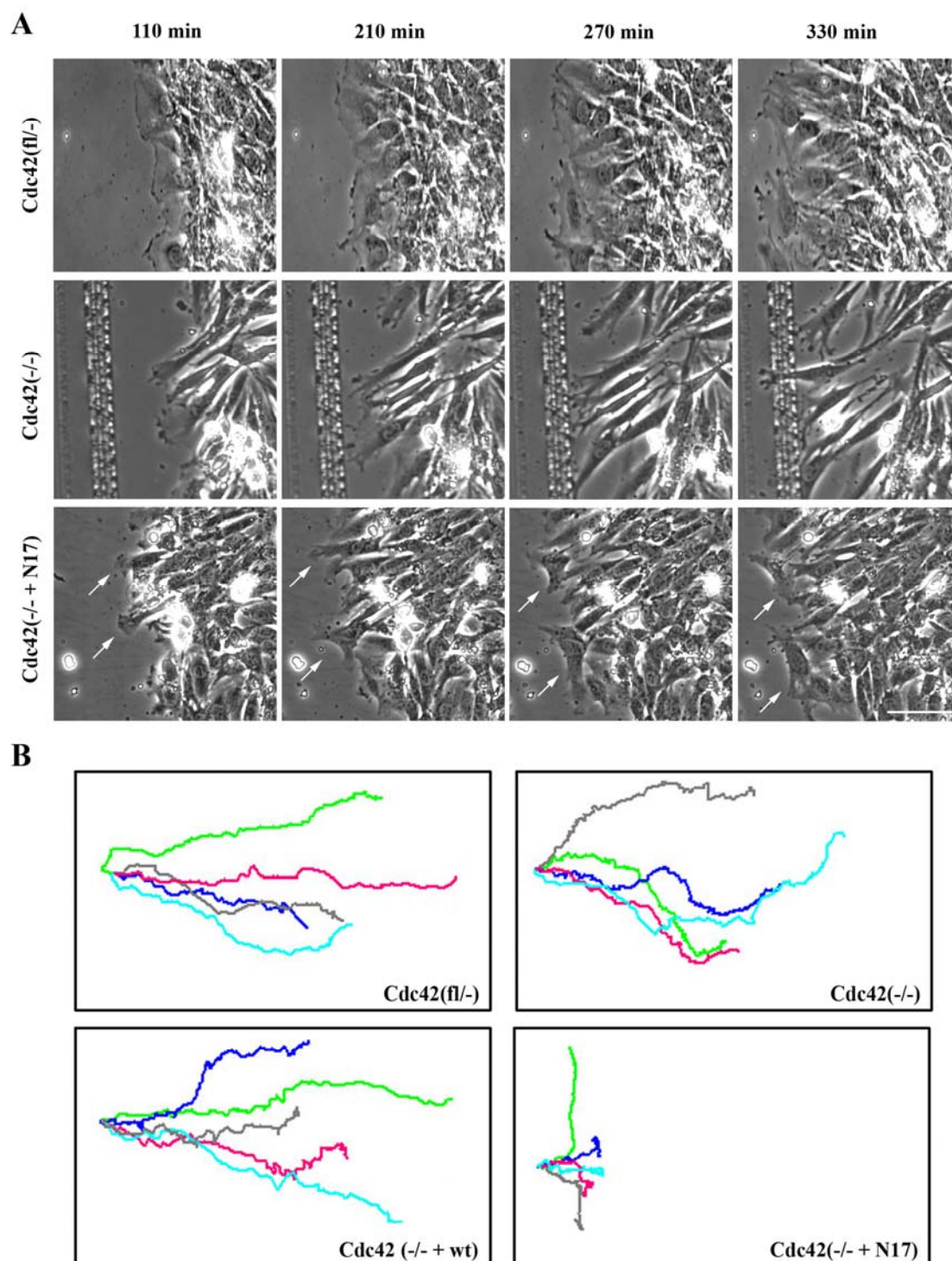


Figure 4.14 Cdc42 contributes to several aspects of single cell directionality during directed cell migration.

(A) Phase contrast time-lapse microscopy of Cdc42(fl/-), Cdc42(-/-) and Cdc42(-/- + N17) cells during a scratch assay, demonstrating stable polarization of lamellipodial activity oriented towards the scratch in Cdc42(fl/-) and Cdc42(-/-) cells and instable polarization in the Cdc42(-/- + N17) cells with lamellipodial protrusions also pointing into other directions than the scratch (arrows; scale bar = 100µm). (B) Single cell tracking of migrating cells revealed stable directionality of Cdc42(fl/-) and Cdc42(-/- + wt) rescued cells, reduced directionality of Cdc42(-/-) cells and further reduction in Cdc42(-/- + N17) cells. Lines represent individual cell tracks; 5 representative tracks per cell line are shown (n=60).

Expression of dnCdc42 in rat fibroblasts completely blocked the re-orientation of the Golgi apparatus into the direction of migration (Nobes and Hall, 1999). Since the Golgi apparatus is always positioned around the MTOC, these data suggested an essential role of Cdc42 in the polarization of the microtubule system (Rios and Bornens, 2003).

To test this hypothesis, we investigated whether the Cdc42 null fibroblastoid cells are able to polarize the Golgi apparatus during directed migration. In Cdc42(fl/-) control cells the Golgi apparatus slowly oriented into the direction of migration, whereas non-random polarization of the Golgi apparatus was reduced by 50% in Cdc42-deficient cells 5h after wounding (Figure 4.15). The expression of dnCdc42 in Cdc42-deficient cells completely abrogated polarization of the Golgi apparatus similar to the data reported by Nobes and Hall (1999) for primary fibroblasts (Figure 4.15). Expression of wild type Cdc42 in Cdc42-null cells restored the re-orientation of the Golgi to levels close to control cells (Figure 4.15). These data indicate a partial role of Cdc42 in Golgi re-orientation during migration and suggest that other Rho GTPases regulate this aspect of cell polarization together with Cdc42.

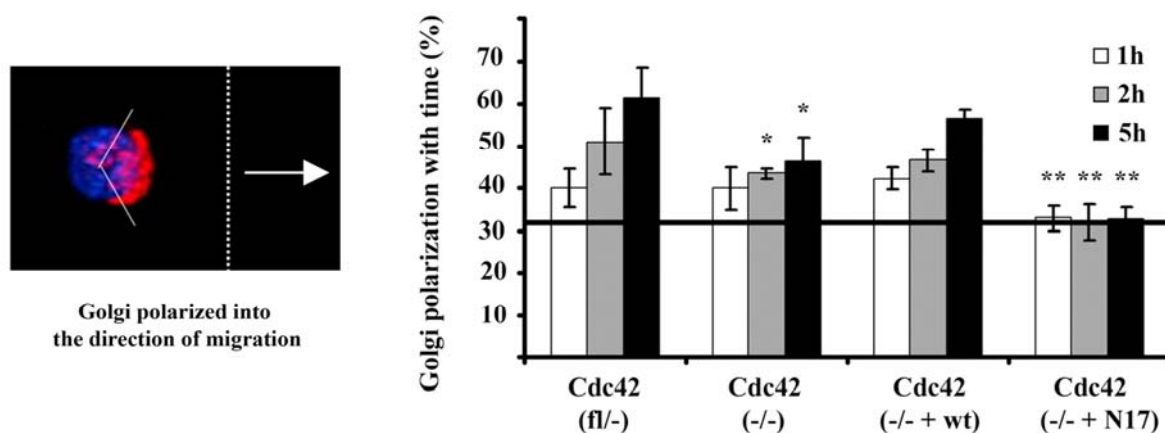


Figure 4.15 Cdc42 is not essential for Golgi polarization during directed cell migration. Percentage of cells with their Golgi apparatus oriented to the direction of migration (random polarization of 33.3% is indicated by solid line). Cdc42(-/-) cells showed a 50% reduction of non-randomly polarized cells at 5h of migration, while Cdc42(-/- + N17) cells showed no non-random polarization at all (n=5). Results significantly different from control cells are indicated by an asterisk (p<0.05), results significantly different from control and null cells are indicated by 2 asterisks (p<0.05). Blue, nucleus stained with DAPI; red, Golgi apparatus.

4.1.12 Golgi re-orientation is not correlated with induced phosphorylation of GSK3 β

In astrocytes and in primary rat fibroblasts, the polarization of the Golgi was suggested to be controlled via Cdc42-mediated phosphorylation of GSK3 β (Etienne-Manneville and Hall, 2003; Cau and Hall, 2005). Phosphorylation of GSK3 β was also required for the stabilization

of β -catenin and its translocation to the leading edge. However, $Cdc42(f1/-)$ cells did not display a detectable change in GSK3 β phosphorylation after wounding (Figure 4.17 A and B), suggesting that in the fibroblastoid cells Golgi re-orientation does not require the induction of GSK3 β phosphorylation. Furthermore, there was no obvious stabilization of β -catenin (Figure 4.17 A and B). Targeting of β -catenin to the leading edge occurred in all cell types tested (Figure 4.16), indicating that subcellular positioning of this protein neither requires stabilization of β -catenin nor GSK3 β phosphorylation. Apparently, different pathways are used to regulate the re-orientation of the Golgi apparatus during directed migration of our fibroblastoid cells *versus* astrocytes and primary rat fibroblasts.

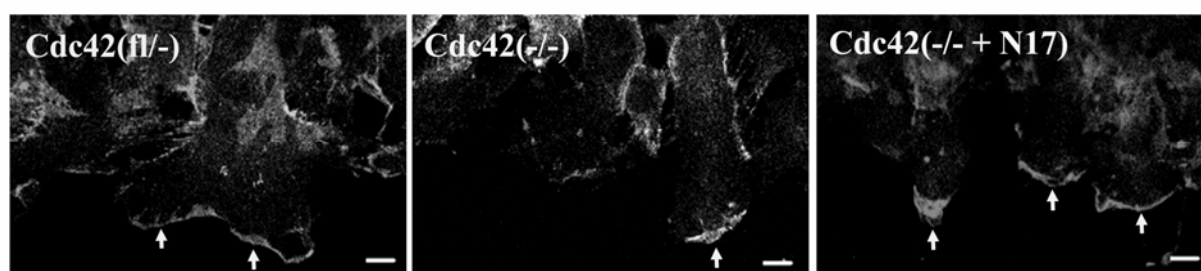


Figure 4.16 β -catenin localizes to the leading edge of migrating fibroblast irrespective of $Cdc42$. Polarized β -catenin localization was visualized in cells fixed 2 h after wounding at the leading edge in migrating $Cdc42(f1/-)$, $Cdc42(-/-)$ and $Cdc42(-/- + N17)$ cells (scale bar = 10 μ m).

To assess how the activation of known downstream effectors of $Cdc42$ during wounding correlates with the observed phenotypes, we determined the relative activation of Erk, p38, JNK and Akt, at different time points after wounding. In three independent experiments, wounding of the monolayer induced phosphorylation of Erk and JNK in control and mutant cells, although the changes were not significant. Phosphorylation of Akt and p38 were not changed (Figure 4.17 A and B). Activation of JNK tended to be reduced and to decrease more quickly in $Cdc42(-/-)$ and $Cdc42(-/- + N17)$ cells, although the relevance of these observations remains to be determined. These data do not reveal a striking correlation of the strong defects in polarization and migration observed in $Cdc42(-/- + N17)$ cells with changes in the activation of Erk, JNK, p38 or Akt.

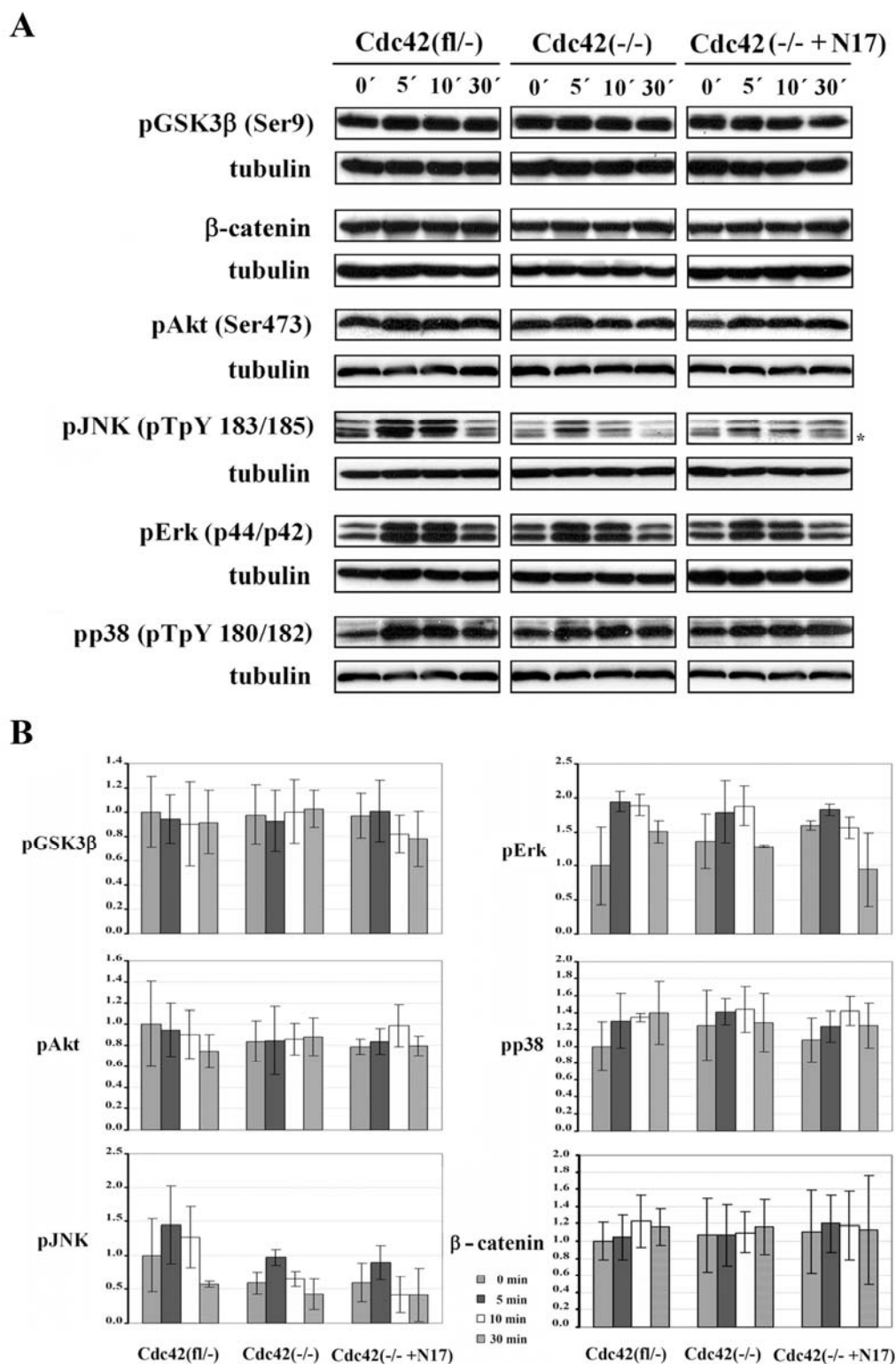


Figure 4.17 Wounding induced activation of Cdc42 effectors. (A) Confluent monolayers of cells were wounded and the activation of pGSK3 β , β -catenin, pAkt, pJNK, pErk and pp38 was determined by Western blotting. No induction of Gsk3 β , pAkt, pp38 or β -catenin stabilization was observed and this was consistent in all the cell lines studied. pErk and pJNK were induced, whereas pJNK activation was reduced and tended to decrease more quickly in mutant cells. Representative results of three independent experiments are shown. Asterisk denotes an unspecific band. (B) Quantification of chemiluminescence signals by using a CCD camera.

Rac1 has been reported to be important for cell migration (Nobes and Hall, 1999; Wells et al., 2004, Stramer et al., 2005). However, although Cdc42 null cells have only 50% of Rac1 activity when compared to controls (Figure 4.8 B) they have a rather normal wound closure speed. Only cells expressing dominant negative Cdc42, in which Rac1 activity was reduced further to 36%, display a migration defect. To investigate whether during migration Rac1 activity is different from the activity in cell monolayers, we wounded control Cdc42(fl/-) cells and performed pull down assays after 5 and 30 min. We could not observe a significant change in Rac1 activity at any of the time points tested (Figure 4.18) indicating that either Rac1 activity is not changed during migration or, more likely, that the changes are locally restricted and not detectable in the total lysates.

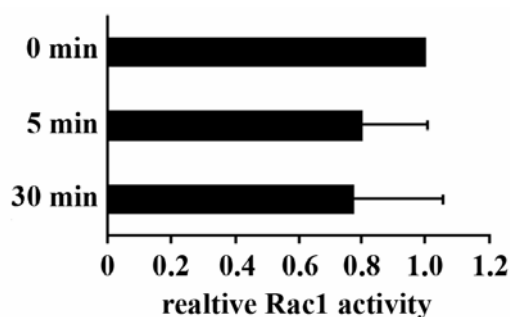


Figure 4.18 Rac1 activity is not changed upon wounding. Confluent monolayers of Cdc42(fl/-) control cells were wounded and the amount of active Rac1 relative to total Rac1 levels was assessed by pull down assay (n=4). No induction of Rac1 activity was observed.

4.1.13 Cdc42 is not required for efficient wound closure and Golgi re-orientation during migration of endodermal cells

Due to the unexpected ability of Cdc42-deficient fibroblastoid cell lines to polarize, we wondered whether this observation is restricted to transformed fibroblastoid cells or could also be made with other, preferentially untransformed cell types. ES cells are not transformed, but migrate only poorly. To obtain highly migratory cells, we forced the Cdc42(fl/-) and Cdc42(-/-) ES cells to differentiate into the endodermal lineage by transfecting them with a Gata-4 transcription factor encoding expression vector (this work was done by Xunwei Wu, MPI for Biochemistry, Martinsried, Germany). Gata-4 is a 46 kDa member of the GATA family of zinc finger-containing transcription factors that has been shown to be sufficient to induce differentiation of ES cells towards the extraembryonic endoderm (Fujikura et al., 2002). Western blot analysis confirmed the presence of Cdc42 in control and its absence in mutant endodermal cells (Figure 4.19).

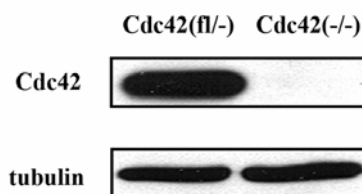


Figure 4.19 Cdc42 is efficiently deleted in Cdc42-null endodermal cells. Western blot analysis confirmed the absence of the Cdc42 protein. Tubulin served as loading control.

Such untransformed endodermal cells are highly migratory, but have significantly less cell-cell contacts than fibroblasts. Cdc42-null endodermal cells had a similar morphology to Cdc42(fl/-) control cells, although in highly dense monolayers mutant cells were less attached to each other than control cells. Following wounding, control and mutant cells closed the gap with similar speed (Figure 4.20 A and B). Measuring the average velocity of individually migrating cells, no significant difference was found between Cdc42(fl/-) and Cdc42(-/-) endodermal cells (Cdc42(fl/-): 1.61 ± 0.44 $\mu\text{m}/\text{min}$; Cdc42(-/-): 1.55 ± 0.46 $\mu\text{m}/\text{min}$; $n=40$). Compared to the fibroblastoid cell lines, endodermal cell lines migrated about 1.5 times as fast. Quite likely due to the reduced cell-cell contacts of endodermal cells compared to fibroblasts, the directionality of migrating control endodermal cells was lower than that of control fibroblastoid cells. Taking the average mean angle vector of individually migrating cells as a very sensitive indicator for directionality, the directionality of endodermal cells lacking Cdc42 was reduced compared to Cdc42(fl/-) control cells (Cdc42(fl/-): 0.45 ± 0.14 ; Cdc42(-/-): 0.38 ± 0.13 ; $n=40$, $p<0.05$), similar to fibroblastoid cells. Both control and mutant endodermal cells were able to slowly re-orient the Golgi into the direction of migration (Figure 4.20 C).

These data prove that the non-essential role of Cdc42 with respect to cell polarization during migration is not restricted to fibroblastoid cells and not related to cell transformation.

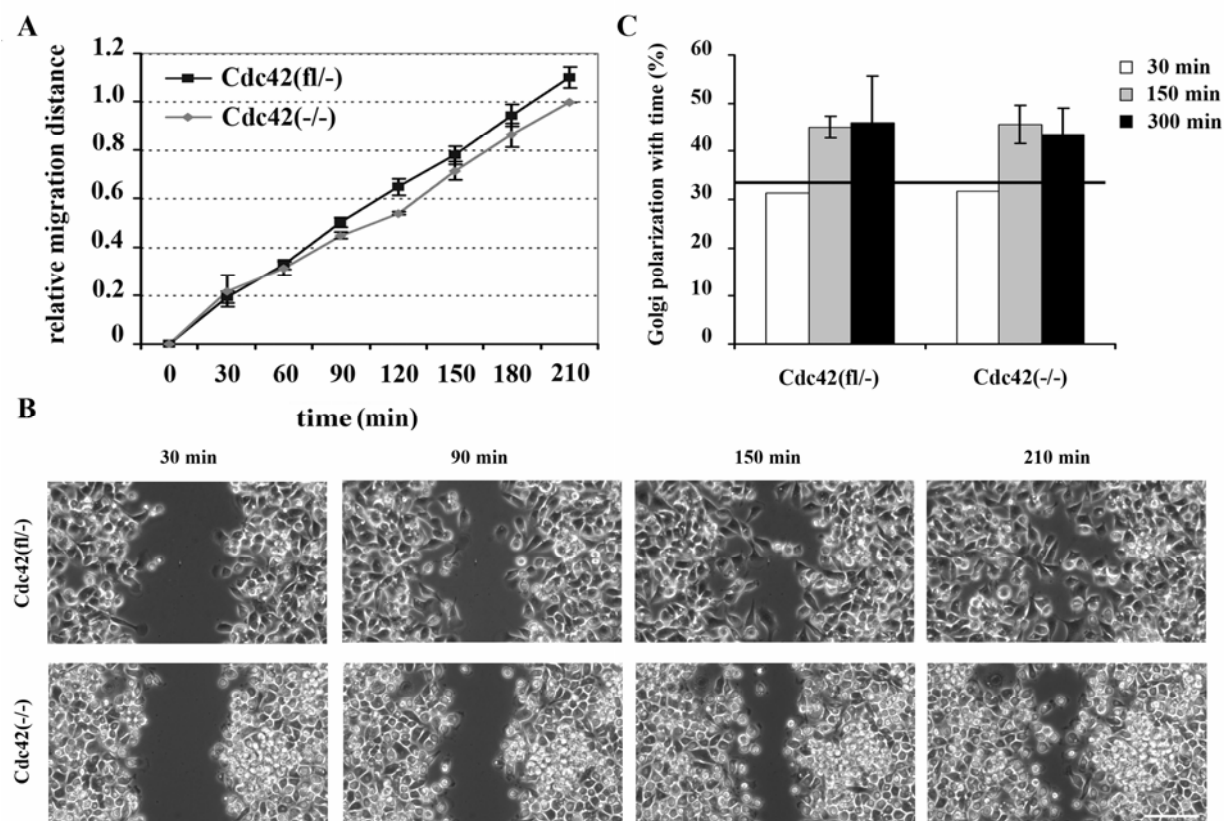


Figure 4.20 Cdc42 endodermal cells display migration and polarization capacity similar to control cells. (A) Similar relative migration of Cdc42(fl/-) and Cdc42(-/-) endodermal cells in a wounding assay. (n=3). (B) Phase contrast pictures of migrating endodermal cells. Endodermal cells have reduced cell–cell contacts in the migrating front of both cell lines (scale bar = 100 μ m). (C) Percentage of cells with their Golgi apparatus oriented in the direction of migration. Cdc42 null cells show polarization ability not significantly different from control cells at 150 and 300 min of migration. Initial polarization was assessed 30 min after wounding (n=1) and was close to random polarization of 33.3%, indicated by solid line.

4.2 Structure-function relationship of β 1 integrin during migration *in vivo* and *in vitro*

Integrins have been implicated in the regulation of various aspects of tissue development and function, many of them requiring efficient cell migration (Danen and Sonnenberg, 2003).

β 1 integrin was shown to be crucial for cell migration, both in keratinocytes *in vitro* and in skin development and regeneration *in vivo*, as these processes were strongly inhibited when β 1 integrin was absent (Brakebusch et al. 2000; Grose et al., 2002). Similarly, data reported for other non-keratinocyte cell lines pointed to a crucial role of this integrin in cell migration (Gimond et al., 1999; Sakai et al., 1999; Danen et al., 2005). In astrocytes it was shown that blocking of β 1 integrin function with RGD peptides results in loss of Cdc42 mediated migration (Etienne-Manneville and Hall, 2001). Yet, the signalling pathways crucial for the

$\beta 1$ integrin mediated signalling are not completely understood. To understand the function of $\beta 1$ integrin in skin development and wound healing, we generated mice with reduced expression of $\beta 1$ in keratinocytes. In addition, mice were made, which express in keratinocytes only mutated forms of $\beta 1$ integrin, in order to study the structure-function relationship of $\beta 1$ integrin *in vivo*. The developed knockin (KI) mouse strains carried mutations in the cytoplasmic domain of the $\beta 1$ integrin, which is the binding domain for integrin-associated proteins, essential for providing integrin mediated signalling. The introduced mutations were selected based on *in vitro* data, showing crucial function of the mutated residues for migration, focal contact formation, spreading, actin cytoskeleton organization and fibronectin (FN) assembly (Lin et al., 1997; Sakai et al., 1998a and 1998b; Wennerberg et al., 1998 and 2000; Stroeken et al., 2000; Moolroney et al., 2001). As mice with a constitutive knockout (KO) of the $\beta 1$ integrin die during the embryonic development around implantation (Fässler and Meyer, 1995) we aimed to express our mutations in a skin specific manner using the Cre-*loxP* system to avoid a lethal phenotype due to impaired $\beta 1$ function in non-skin tissues.

4.2.1 Analysis of $\beta 1$ integrin knockin mice

4.2.1.1 Generation of the $\beta 1$ hypomorph mouse strain

In order to establish KI mice carrying mutations in the cytoplasmic tail of the $\beta 1$ integrin chain, a strategy was developed, in which a mutated cDNA encoding the cytoplasmic domain of $\beta 1$ integrin was introduced into the $\beta 1$ integrin gene. In order to assure that this modification of the targeted $\beta 1$ integrin locus does not lead to a phenotype *per se*, first a non-mutated cDNA was introduced and the wild type KI (wtKI) mouse strain was developed.

The cytoplasmic domain of $\beta 1$ integrin is encoded by part of exon 15 and exon 16, which contains the polyadenylation signal. We introduced a wt 160 bp cDNA fragment coding for the complete cytoplasmic domain, including the stop codon, into exon 15, just behind and in frame with the sequence coding for the transmembrane region of the $\beta 1$ integrin chain. This cDNA fragment was followed by a floxed neo tk selection cassette, which enabled us to select for stably transfected ES cells (Figure 4.21 A). Homologously recombined ES cells were identified by Southern blot analysis (Figure 4.21 B') and electroporated with a Cre recombinase expressing vector, to remove the floxed selection cassette. ES cells were selected with FIAU for the absence of the tk gene and tested by Southern blot for the correct deletion of the floxed neo tk cassette (Figure 4.21 B''), leaving just a single *loxP* site behind in the non

coding region. One of the positive clones was injected into blastocysts and gave rise to high percentage chimeras. The wtKI mouse strain was established by Cord Brakebusch, MPI for Biochemistry, Martinsried, Germany.

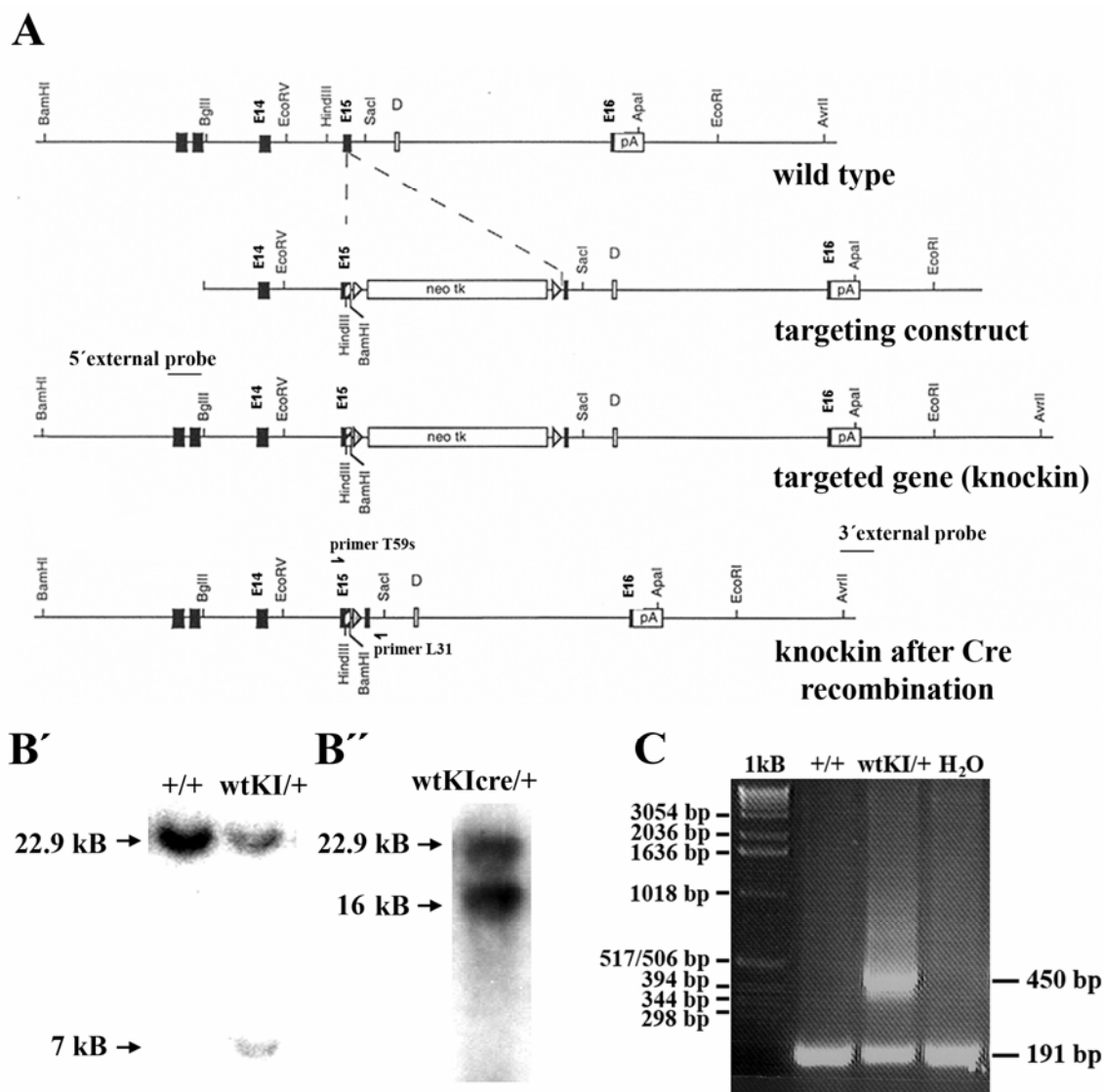


Figure 4.21 Schematic representation of the targeting strategy for the wtKI mouse. (A) Cre-mediated deletion the neo tk cassette leads to the expression of wild type $\beta 1$ integrin chain. (B') Southern blot analysis with 5' external probe shows recombination of the targeting construct into the wt $\beta 1$ integrin locus. Expected sizes were for the wt allele: 22.9 kB and for the knockin allele: 7 kB. (B'') Southern blot analysis with 3' external probe shows efficient deletion of the neo tk selection cassette in the knockin allele. Expected sizes were for the wt allele: 22.9 kB and 16 kB for the wtKI allele after Cre recombination of the selection cassette (wtKI Cre). (C) Genomic PCR on DNA from the offspring of the wtKI chimeric mice. The 0.45 kB DNA fragment present only in the targeted wtKI allele was amplified using primers T59s and L31, which bind to the coding region of wt exon 15 and in the non-coding region downstream of exon 15, respectively. The 191 bp band corresponds to the expected size of the wt allele. Southern probe, primers T59s and L31, and important digestion sites are indicated. (E, exons; D, splice variant; pA, polyadenylation sequence; \blacktriangleright , *loxP* sites).

After germ line transmission heterozygous mice were identified by genomic PCR (Figure 4.21 C) and bred into mice containing the keratin-5 (K5) promoter driven Cre recombinase transgene and the floxed $\beta 1$ ($\beta 1^{fl}$) integrin gene (described by Brakebusch et al. 2000). This strategy led to an epidermis expressing only the KI allele, since the deletion of the $\beta 1$ integrin gene is occurring in epithelial skin stem cells from which all cells in epidermis, hair follicles and sebaceous glands are derived.

4.2.1.2 Analysis of the wtKI mouse

4.2.1.2.1 Insertion of the wt 160 bp cDNA fragment into the $\beta 1$ integrin locus, results in decreased $\beta 1$ integrin expression levels and a hypomorph phenotype

Mice carrying the wtKI allele and the $\beta 1$ integrin conditional allele together with the keratin-5 Cre transgene were born without an obvious phenotype. Two days after birth a reduced pigmentation of the back skin became visible in the midline and in several lines parallel to the ribs. Unexpectedly, these mice developed a phenotype similar to mice expressing no $\beta 1$ integrin in keratinocytes (Brakebusch et al., 2000), although the kinetic of phenotype development was much slower than in $\beta 1$ null mice. During the next months, the hair coat decreased and the mutant mice were almost completely bald by the age of one year (Figure 4.22). In the $\beta 1$ -null mice this stage is reached already after 5 weeks of age (Figure 4.22). In contrast to the $\beta 1$ skin specific knockout mice the wtKI mice displayed no wounds or walking abnormalities, characteristic for the conditional knockout. Knockin mice were fertile and had a normal life expectancy.

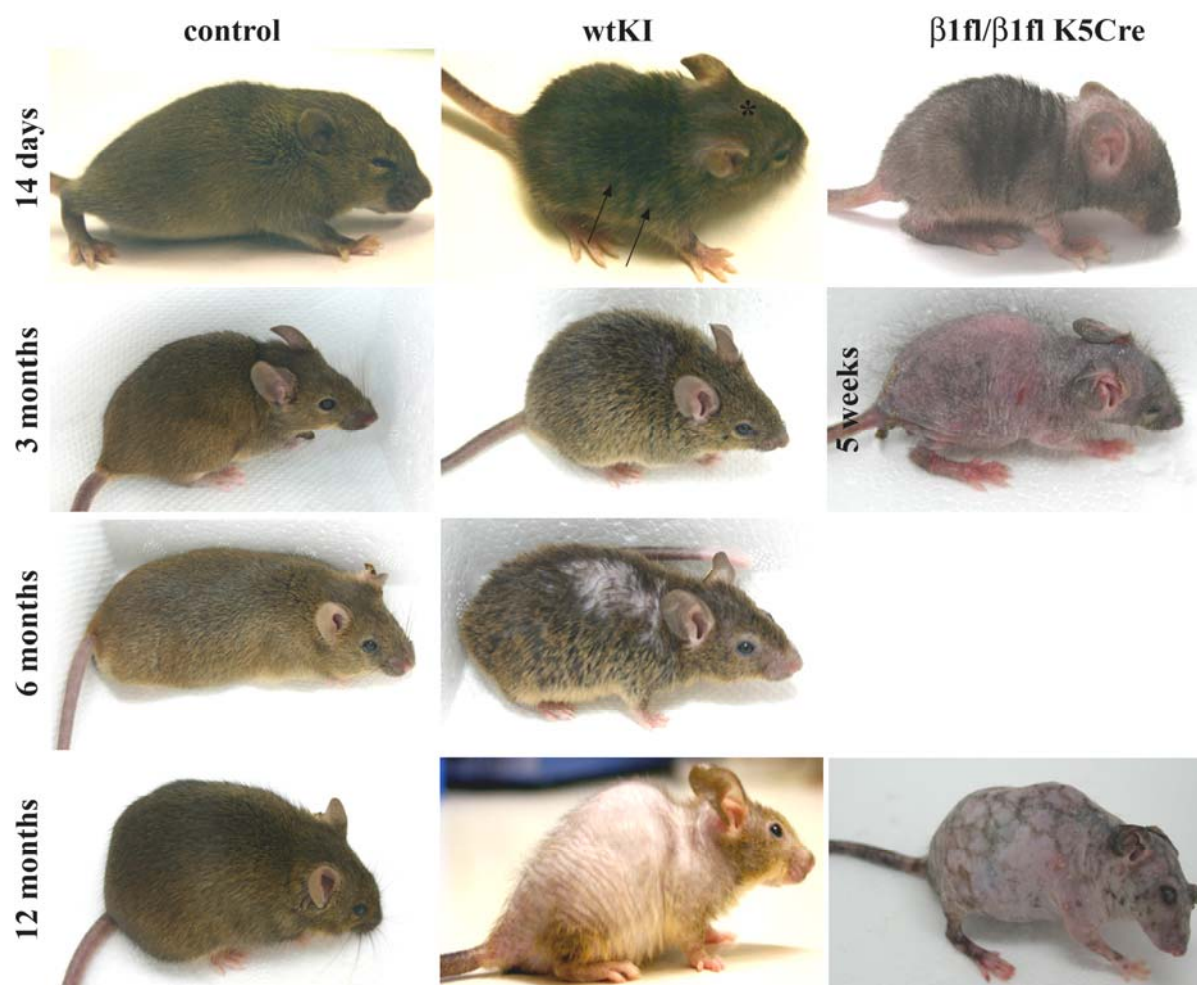


Figure 4.22 Progressive hair loss in the wtKI mice. At the age of 14 days wtKI mutant mice showed reduced number of hairs (arrows and asterisk) compared to control animals. With age continued loss of hairs is observed. Mutant mice at the age of 3 months and 6 months are shown. By the age of 12 months almost all hairs are lost in the wtKI mice. As comparison $\beta 1$ skin specific knockout mice at the age of 14 days, 5 weeks and 1 year is shown.

The $\beta 1$ floxed allele contains a promoterless lacZ reporter gene that was introduced after the downstream *loxP* site. After Cre mediated ablation of the $\beta 1$ integrin gene, the lacZ reporter is expressed under the control of the $\beta 1$ integrin promoter, allowing to monitor gene deletion and $\beta 1$ integrin promoter activity in $\beta 1$ -deficient cells (Brakebusch et al., 2000). LacZ staining on cryosections from the mutant mice showed clear staining in the basal keratinocytes and hair follicles confirming the deletion of the $\beta 1$ integrin gene (Figure 4.23 A-D). Therefore, the only allele which can lead to $\beta 1$ integrin expression in our mutant mice is the wild type knockin allele.

One explanation for the similar, although milder phenotype of the wtKI mice, compared to the $\beta 1$ -null mice, is a reduced expression of the $\beta 1$ integrin in the wtKI animals. To check this hypothesis we performed immunostainings for $\beta 1$ integrin on cryosections from 14 days old

mice. Indeed, we found no detectable $\beta 1$ integrin staining in the basal keratinocytes and the outer root sheath (ORS) of the hair follicles (Figure 4.23 E-H). The mutant hair follicles were surrounded by $\beta 1$ integrin expressing cells, which are most likely dermal fibroblast and Schwann cells of nerves innervating the hair follicle. In contrast to the $\beta 1$ integrin null-mice, $\alpha 6$ integrin expression was not changed in the basal keratinocytes and the hair follicles (Figure 4.23 E-H).

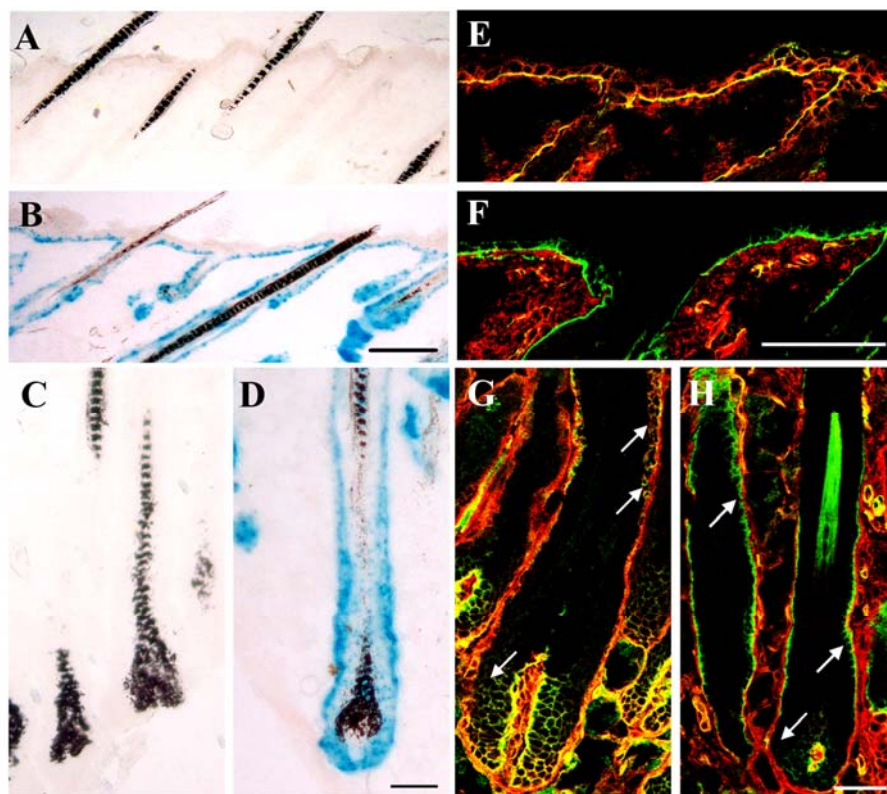


Figure 4.23 The $\beta 1$ conditional allele is efficiently deleted in the skin of wtKI mice. (B) and (D) shows LacZ staining on sections from the wtKI mouse confirming the deletion of the $\beta 1$ integrin gene from the $\beta 1$ floxed allele. LacZ staining is missing in the epidermis and the hair follicles of a control mouse (A) and (C), respectively. Normal $\beta 1$ (red) and $\alpha 6$ integrin (green) staining in the epidermis (E) and hair follicles (G, arrows) of a control mouse is shown, which is not detectable in the mutant mouse (F) and (H). Scale bar in B and F = 50 μ m; in D and H = 25 μ m.

Lack of any detectable $\beta 1$ integrin staining in the ORS and interfollicular epidermis of the wtKI does not exclude any $\beta 1$ integrin expression. It could be that the expression levels of $\beta 1$ integrin are so low, that they are not detectable by immunofluorescence. To test this, we performed FACS analysis on freshly isolated keratinocytes from 3 months old control (wtKI/ $\beta 1$ fl) and mutant (wtKI/ $\beta 1$ fl K5Cre) mice. We first analyzed the keratinocytes subpopulations present in such a mixture of cells by staining with keratin 10 antibody, which is a specific marker for suprabasal keratinocytes. We found that they account for

approximately 25% of the entire wt keratinocyte population (data not shown). This matched well the size of keratinocyte population weakly expressing $\beta 1$ integrin in FACS analysis, which accounted for 20% of the entire population. All other keratinocytes expressed high levels of $\beta 1$ integrin (Figure 4.24 A). These data suggests that suprabasal keratinocytes express low levels of $\beta 1$ integrin, which is in contrast to current belief, that expression of $\beta 1$ integrin is restricted to basal keratinocytes and is absent in the suprabasal ones (Watt, 2002). In contrast, analysis of the $\alpha 2$ integrin expression (Figure 4.24 B) revealed the presence of only one cell population expressing this integrin, suggesting that either suprabasal cells do not express this integrin, or that the suprabasal and basal cells express similar or only slightly different levels, that are not resolved in the analysis. Keratinocytes expressing low levels of $\beta 1$ integrin expressed also low levels of $\alpha 6$ and $\beta 4$ integrin (Figure 4.24 C and D), indicating that also these integrins are expressed suprabasally.

$\beta 1$ integrin expression levels on the wtKI keratinocytes were reduced by 80% and only one population of cells was distinguishable (Figure 4.24 A). This suggests, that expression levels of this integrin are similar in basal and suprabasal keratinocytes. Expression of the $\beta 1$ integrin binding partner $\alpha 2$ in the mutant mice was reduced by 85% when compared to the control animal (Figure 4.24 B). $\alpha 6$ and $\beta 4$ integrin expression, which were reduced in the conditional $\beta 1$ integrin knockout mice ($\beta 1^{fl/fl}$ K5Cre), were not affected in the wtKI mice (Figure 4.24 C and D), confirming the immunostaining data (Figure 4.23 F and H). $\alpha 4$ and αv expression was not changed as well, whereas $\beta 2$, $\beta 3$, $\beta 7$, $\alpha 1$ and $\alpha 5$ were not expressed at all (data not shown). These integrins are reported not be expressed on keratinocytes, or only under particular stress conditions (Watt, 2002). $\alpha 3$ integrin was not included in the analysis.

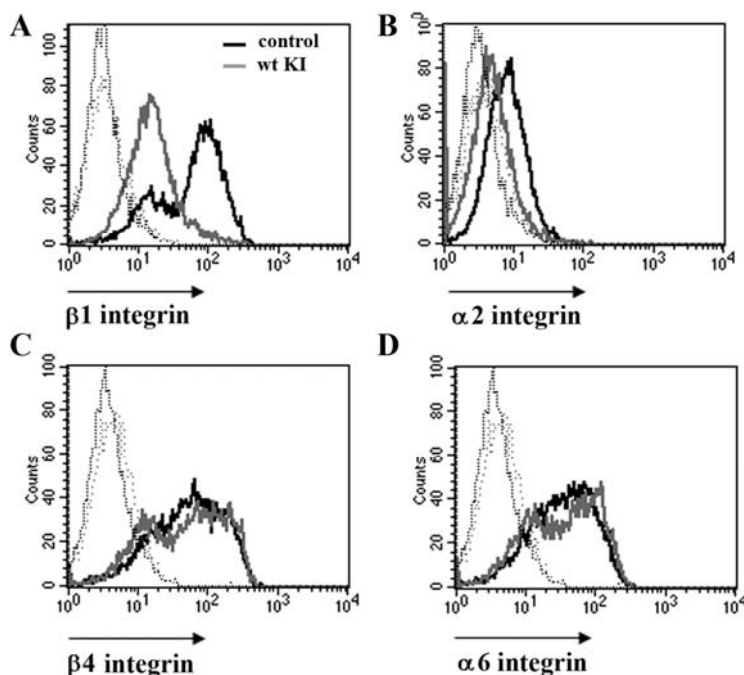


Figure 4.24 $\beta 1$ integrin expression is reduced in wtKI mouse. FACS analysis of freshly isolated keratinocytes revealed reduced expression levels of $\beta 1$ (A) and $\alpha 2$ (B) integrins and normal levels of $\beta 4$ (C) and $\alpha 6$ (D) integrins. The background staining is indicated by dotted lines and was identical for both genotypes.

These data show that the introduction of the 160 bp fragment cDNA together with a *loxP* site into exon 15 leads to reduced $\beta 1$ integrin expression and a hypomorphic phenotype. The wtKI mice was therefore renamed to hypomorph (*hpm*) mouse.

4.2.1.2.2 Reduction of the $\beta 1$ integrin expression in keratinocytes leads to hair follicle abnormalities and distortion of the basement membrane at the dermal-epidermal junction in the hypomorph mouse

To search for the reason for the reduced number of hair follicles we first assessed the morphology of skin from 14 days old *hpm* mice and compared it to skin from null mice at the same age (Brakebusch et al., 2000). The overall skin morphology revealed decreased number of hair shafts, although the number of hair follicles did not seem to be significantly altered (Figure 4.25, upper panel). The majority of hair follicles showed gross abnormalities ranging from shortened hair bulb and increased number of ORS cell layers, folding of the layers of the IRS cells and amorphous dislocated cells (Figure 4.25, lower panel). In contrast to the null mice, however, the amount of hairs with low degree of malformation was much higher in the *hpm* mouse. Reduction of the $\beta 1$ integrin expression had also influence on the morphology and organization of the interfollicular keratinocytes. However, although multiple layers of roundish or polygonal, nucleated cells were observed (Figure 4.25, middle panel), some

regions of the epidermis showed a monolayer of normal cuboidal cells. In addition, in comparison to the null-phenotype, the number of keratinocyte layers in the hyperthickened epidermis was reduced in the *hpm* mice and no blister formation was observed.

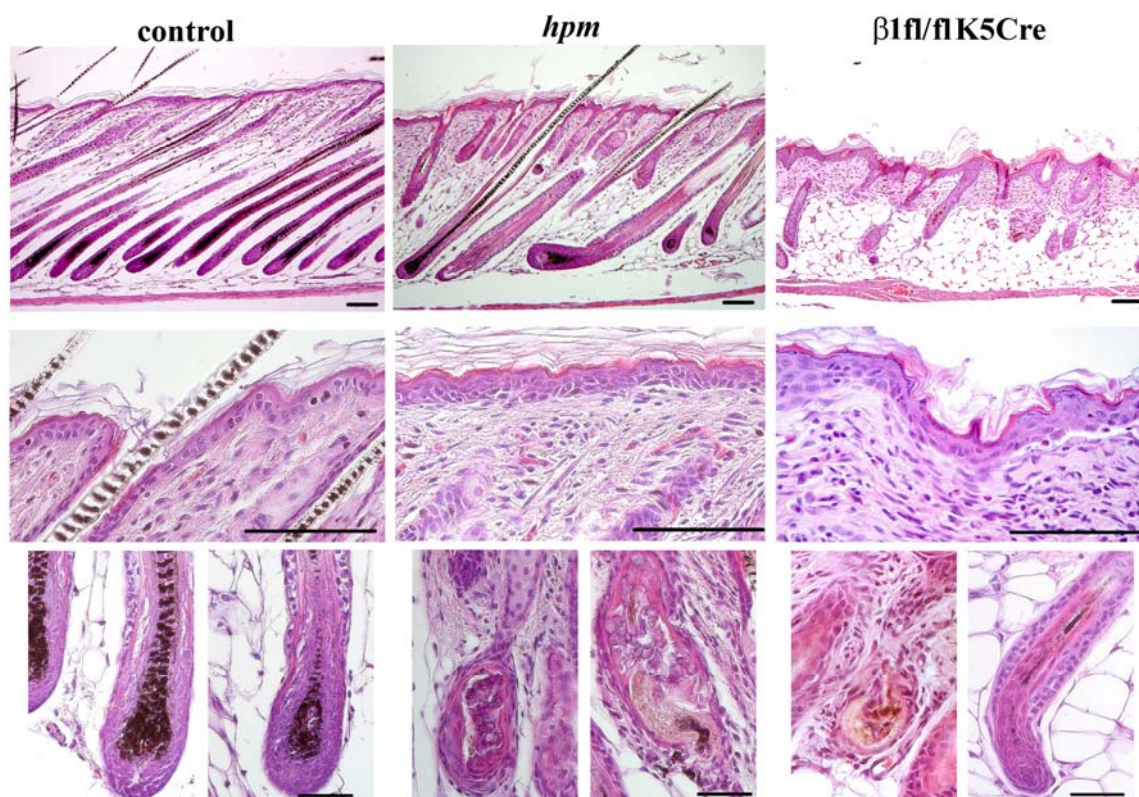


Figure 4.25 Aberrant hair follicle morphogenesis and keratinocytes morphology in the *hpm* mouse. Haematoxylin–eosin stained sections from the back skin of 14 days control, *hpm* and $\beta 1fl/fl$ K5Cre mutant mouse. Upper panel: overall skin morphology. Not all hair follicles of the *hpm* mouse grew as deeply in the subcutis as the control follicles, but are less affected than the $\beta 1$ -null hair follicles. Scale bar = 50 μ m. Middle panel: epidermis of a control mouse shows a monolayer of cuboidal cells, whereas in the mutant skin regions with multilayered, aberrant cells were observed, similar to the KO epidermis. Scale bar = 50 μ m. Lower panel: normal hair follicle morphology in comparison to the disorganized hair follicles in the mutant mice. Examples of severely malformed hair follicles in the *hpm* mouse are shown. Scale bar = 25 μ m.

Since the $\beta 1$ conditional knockout mice showed severe proliferation defects in the hair follicles and the basal keratinocytes of the interfollicular epidermis, characterized by a complete absence of proliferating cells in the hair bulbs at 16 days of age and 50% reduction of proliferating cells in the 9 days old epidermis, we wanted to test whether a similar defect could be observed in the *hpm* mouse. However, no difference in the number of BrdU positive (BrdU⁺), proliferating cells in the basal keratinocytes was found between the mutant and control mouse at the age of 14 days (Figure 4.26 A-C). Hair follicles with no major abnormalities had rather normal amounts of proliferating cells, whereas severely malformed hair follicles had no or only few positive cells, which could also be proliferating dermal

fibroblasts (Figure 4.26 D-G). These data indicate that reduced amounts of $\beta 1$ integrin found in the interfollicular epidermis of the hypomorph mice are sufficient to maintain normal proliferation. In the matrix region of the hair follicle decrease of $\beta 1$ integrin might result in a reduced proliferation. Alternatively, the reduction in proliferating cells might be due to a defective migration of hair follicle stem cells to the matrix region in case of low integrin expression.

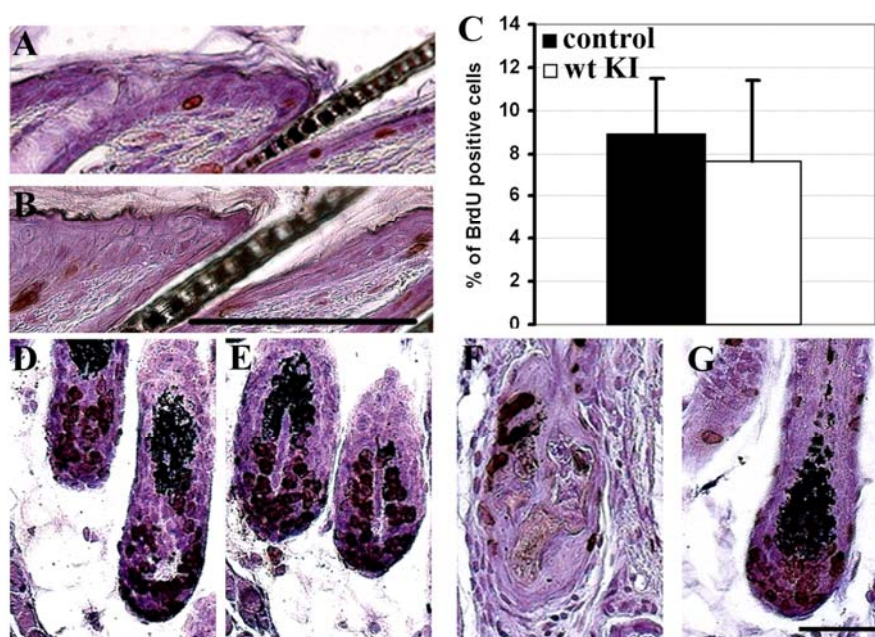


Figure 4.26 Normal proliferation in 14 day old *hpm* mice. (A) and (B) show similar proliferation in the basal keratinocytes of control and *hpm* epidermis. Scale bar = 50 μ m. (C) Quantification of BrdU⁺ cells in the interfollicular epidermis of 2 mice per genotype is shown. Examples of control (D and E) and *hpm* (F and G) hair follicles stained with BrdU (brown) are shown. Counterstaining, haematoxylin. Scale bar = 25 μ m.

Immunostaining of the hair follicles for the basement membrane protein laminin-5 (LN 5) was similar in *hpm* and control tissue, whereas the deposition of LN 5 at the dermal – epidermal junction was distorted in the *hpm* mice. However, the severity of the impairment was again much lower than in the $\beta 1$ fl/fl K5Cre mutant, probably due to the normal expression levels of the laminin 5 receptor $\alpha 6\beta 4$.

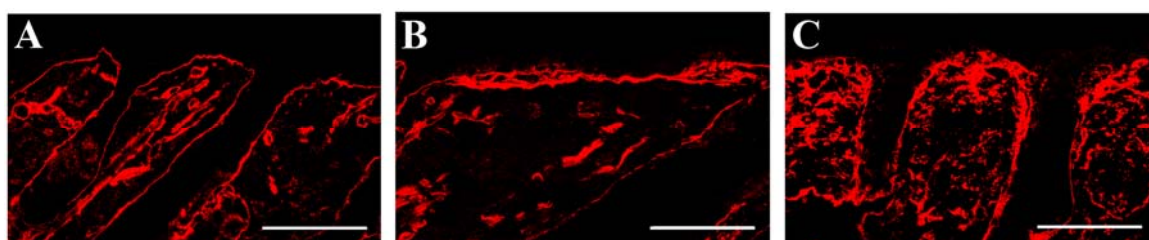


Figure 4.27 Diffuse Laminin 5 deposition at the dermal-epidermal junction of the *hpm* mouse. (B) Diffused Laminin 5 deposition in the *hpm* mouse when compared to control (A), however, not as severe as in the

age matched $\beta 1$ -null mouse (C). Scale bars = 50 μ m.

4.2.1.2.3 Reduced $\beta 1$ integrin expression levels are not sufficient to maintain normal cell spreading and survival *in vitro*.

$\beta 1$ integrin null keratinocytes failed to survive *in vitro* due to adhesion, spreading and proliferation defects (Grose et al., 2002). In order to assess whether the decreased $\beta 1$ integrin levels on *hpm* keratinocytes are sufficient for survival *in vitro*, we isolated keratinocytes from 3 months old mice. As described above, these keratinocytes had decreased levels of the collagen receptor $\alpha 2\beta 1$, whereas $\alpha 6\beta 4$ expression was not affected. When plated on collagen I and fibronectin coated culture dishes, the *hpm* keratinocytes could not adhere and spread as efficient as the control cells, remained rounded and died within 5 days of culture (Figure 4.28).

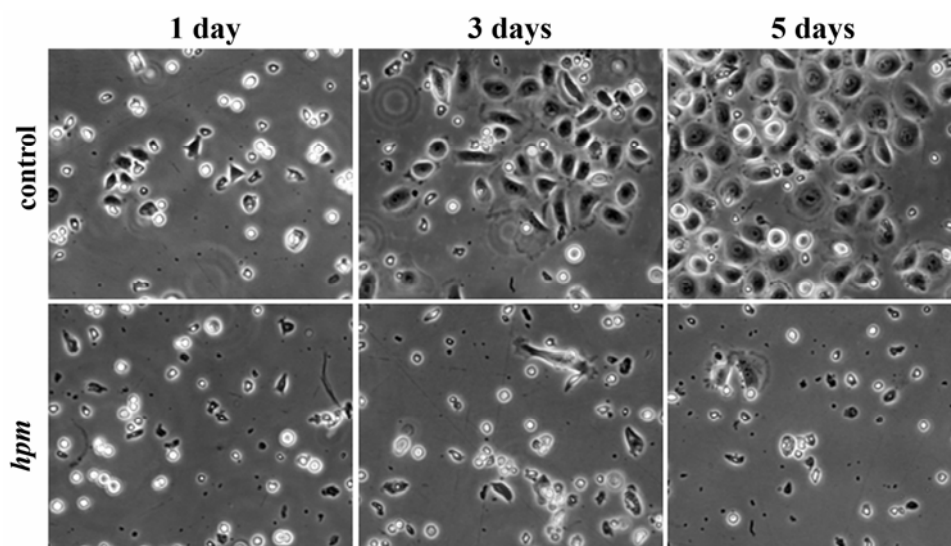


Figure 4.28 $\beta 1$ hypomorphic keratinocytes do not survive *in vitro*. Keratinocytes isolated from 3 month old control and age matched *hpm* mouse have been plated on collagen I and fibronectin coated dishes and monitored for 5 days.

Staining for filamentous actin with FITC-conjugated phalloidin and for tubulin revealed a severe defect in actin and tubulin polymerization in the hypomorphic keratinocytes. Furthermore, mutant cells were not able to form focal adhesions as assessed by immunofluorescent detection of paxillin and vinculin. Instead, these focal adhesion markers were found to be diffusely distributed in the cytoplasm. Expression levels of $\beta 1$ integrin at the cell surface of *hpm* keratinocytes were not sufficient to be detected by immunofluorescent microscopy, in contrast to control cells (Figure 4.29). These data suggest that reduced expression of the collagen receptors $\alpha 2\beta 1$ and $\alpha 3\beta 1$ does not allow keratinocytes to spread and survive *in vitro*, similarly to the $\beta 1$ integrin null cells.

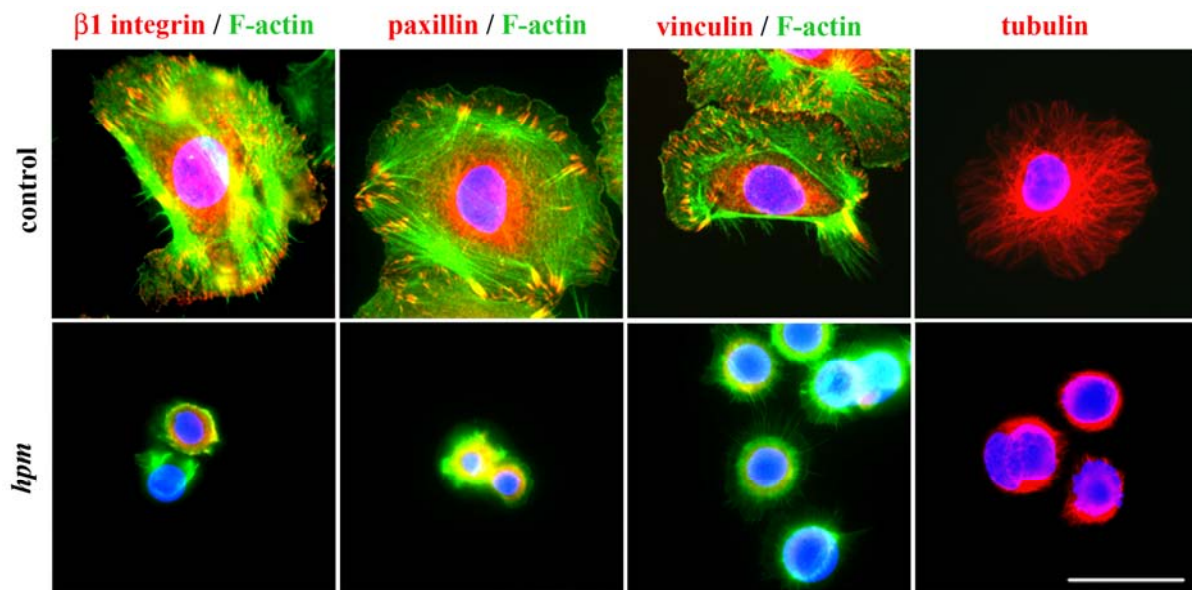


Figure 4.29 Defective spreading and cytoskeletal organization in $\beta 1$ integrin hypomorphic keratinocytes. Control and mutant keratinocytes were seeded on collagen I and fibronectin coated dishes and stained 3 days later. Filamentous actin was detected by FITC-conjugated phalloidin. Microtubules were stained by an anti-tubulin antibody. Nuclei were stained with DAPI in blue. Scale bar = 50 μ m.

4.2.1.2.4 $\beta 1$ integrin is crucial for stem cell function *in vitro*

Skin maintenance requires the continuous function of epithelial stem cells. Previous *in vitro* studies suggested an important role of $\beta 1$ integrin in epithelial stem cell function. Both in cultures of human keratinocytes and in human interfollicular epidermis, it is possible to enrich for stem cells by selecting the cells that have high levels of $\beta 1$ integrins. Similarly, the stem cell containing bulge region of the hair follicle expresses high $\beta 1$ integrin levels (Watt, 2002). *In vivo*, however, $\beta 1$ integrins seem not to be crucial for the maintenance of skin stem cells, since some of the mice with skin specific deletion of this integrin can survive up to the age of one year and maintain, albeit abnormal, skin (Brakebusch et al., 2000). In order to clarify this discrepancy, we investigated the skin of 6 months old hypomorphic mice.

Haematoxylin–eosin staining revealed that by the age of 6 months the epidermal hyperplasia was extended to the entire skin. However, similarly to the 14 days skin, the number of keratinocyte layers was reduced, when compared to the skin specific $\beta 1$ integrin knockout mice (Figure 4.30). Proliferation of the basal keratinocytes in the *hpm* interfollicular epidermis was not changed with $2.5 \pm 0.42\%$ BrdU⁺ cells, compared to $1.5 \pm 0.14\%$ in the control skin. The number and morphology of the hair follicles was difficult to compare, since at this age the mice do not have a synchronized hair cycle any more. However, the few hair follicles which could be found in 6 months old hypomorphic mice showed abnormalities

similar to those observed in 14 days old *hpm* mice (Figure 4.30). Interestingly, plenty of scattered melanin spots were found in the mutant dermis, which are most likely the remnants of distorted hair follicles. Such dermal melanin granules were absent in control mice (Figure 4.30). Concomitant with loss of hair the $\beta 1$ fl/fl K5Cre displayed increased matrix deposition in the dermis (asterisks in Figure 4.30). Also the *hpm* mice developed dermal fibrosis (asterisks in Figure 4.30), but the onset was delayed compared to the knockout mice.

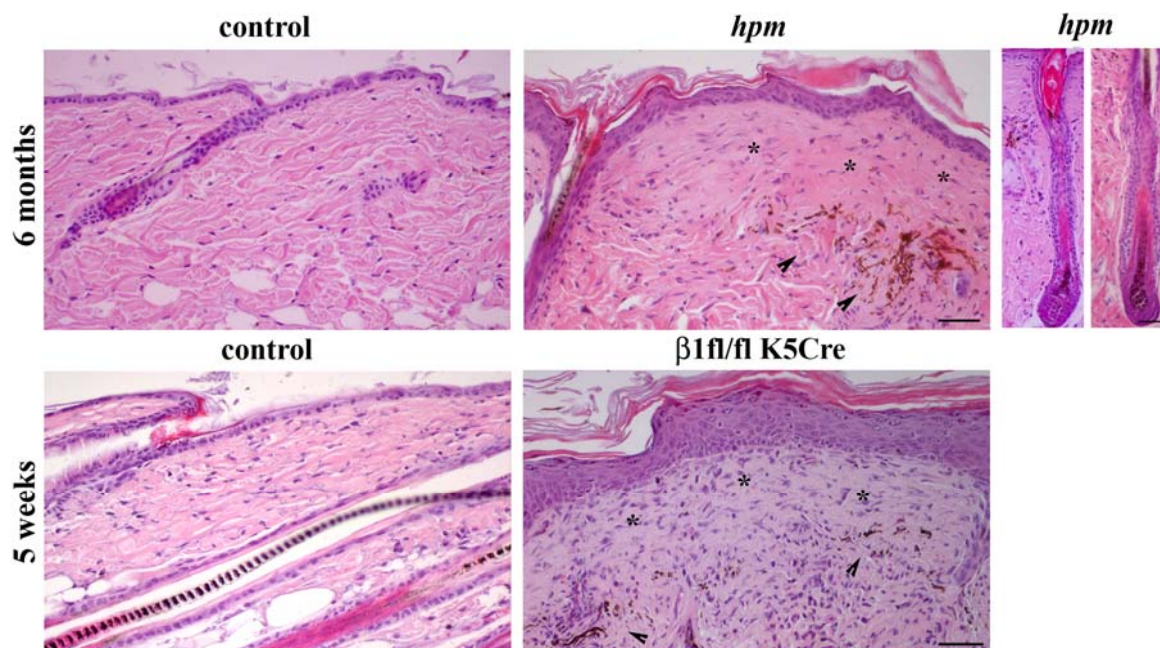


Figure 4.30 Progressive hair loss and dermal fibrosis in *hpm* mice. Haematoxylin–eosin stained sections from 6 months old *hpm* mice revealed the development of dermal fibrosis in the mutant mice (asterisks). The progressive hair loss is accompanied by scattered melanin deposition in the dermis of the mutant mouse (arrowheads) and epidermal dysplasia in the majority of the skin. In control mice no fibrosis or melanin deposition was observed. The few hair follicles found in the hypomorphic skin were malformed. In the lower panel, as comparison section from 5 weeks old $\beta 1$ integrin skin specific knockout is shown. Scale bar = 50 μ m.

In order to test whether also in 6 months old $\beta 1$ fl/wtKI K5Cre mouse the floxed allele of the $\beta 1$ integrin gene is efficiently deleted, we performed lacZ staining on control and *hpm* sections from 6 months old mice. Surprisingly, we found that approximately 40% of the basal keratinocytes in the interfollicular epidermis were lacZ negative (lacZ⁻), thus $\beta 1$ integrin positive (Figure 4.31 A). In contrast, in mice expressing one wt and one $\beta 1$ floxed allele together with the Cre recombinase ($\beta 1$ fl/wt K5Cre), the entire epidermis was LacZ positive (lacZ⁺; data not shown). Since the Cre recombination is never 100% efficient, there are always some cells in which the recombination does occur. In the $\beta 1$ fl/fl K5Cre mice the percentage of such cells is around 1 to 3% as determined by FACS analysis (Brakebusch, personal communication). The presence of 40% lacZ⁻ cells in sections from the 6 months old

hpm mouse suggests that cells, not hit by the Cre recombination, have a competitive advantage over cells expressing reduced amounts of $\beta 1$ integrin, and accumulate over time in the interfollicular epidermis of the hypomorph mice.

Interestingly, only 17% of the hair follicles within the $lacZ^-$ epidermis were also $lacZ^-$, while the majority of hairs (83%) were $lacZ^+$. In the $lacZ^+$ interfollicular epidermis, on the other hand, all hair follicles were $lacZ^+$ (Figure 4.31 B). Moreover, while 40% of cells in the interfollicular epidermis escape the Cre recombination, only 5% of all hair follicles in the hypomorphic skin do so (Figure 4.31 A and C). These findings suggest that stem cells residing in the interfollicular epidermis are rather independent from stem cells residing in the follicle.

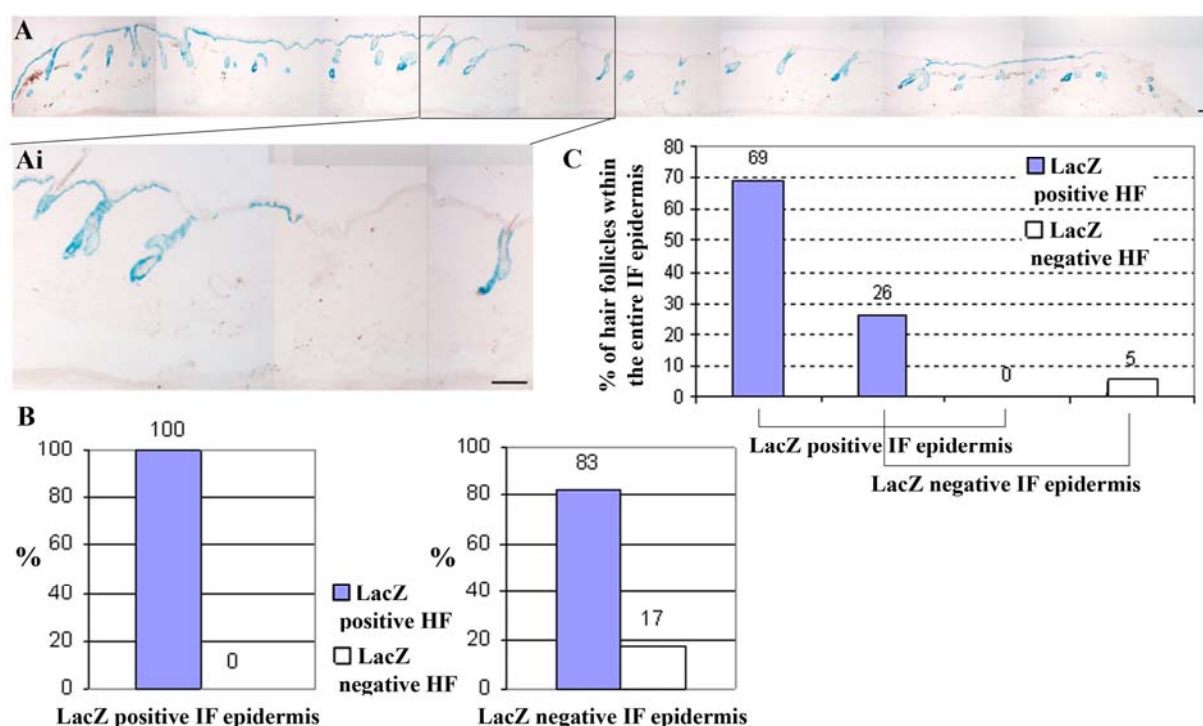


Figure 4.31 Cells expressing $\beta 1$ integrin from the $\beta 1$ integrin floxed allele repopulate the skin of the *hpm* mouse. (A) LacZ staining on sections from 6 months old *hpm* revealed the presence of $\beta 1$ integrin expressing cells in the skin of the mutant mouse strains. (Ai) Inset showing enlargement of a selected region of the skin. Scale bar = 50 μ m. (B) Quantification of the distribution of LacZ⁺ and LacZ⁻ hair follicles within LacZ positive and negative IF epidermis. (C) Quantification of the distribution of LacZ⁺ and LacZ⁻ hair follicles within the entire IF epidermis. IF, interfollicular epidermis; HF, hair follicle.

To confirm the presence of $lacZ^-$ cells expressing normal levels of $\beta 1$ integrin, we performed immunostainings on sections from 6 months old mice. Completely unexpected, however, $\beta 1$ integrin expression in the 6 months old hypomorph mice was normal in the complete epidermis (Figure 4.32), not only in those regions that are $lacZ^-$. This suggests that the expression of $\beta 1$ integrin from the *hpm* allele is increased from 3 months to 6 months old

mice by an unknown mechanism. $\alpha 6$ integrin expression was indistinguishable from control mice, similar to the results obtained with 14 days old mice.

Concomitant with the normal $\beta 1$ integrin expression, also the laminin 5 distribution at the dermal–epidermal junction was largely not distinguishable from the control littermate mice indicating normal $\beta 1$ integrin function (Figure 4.32).

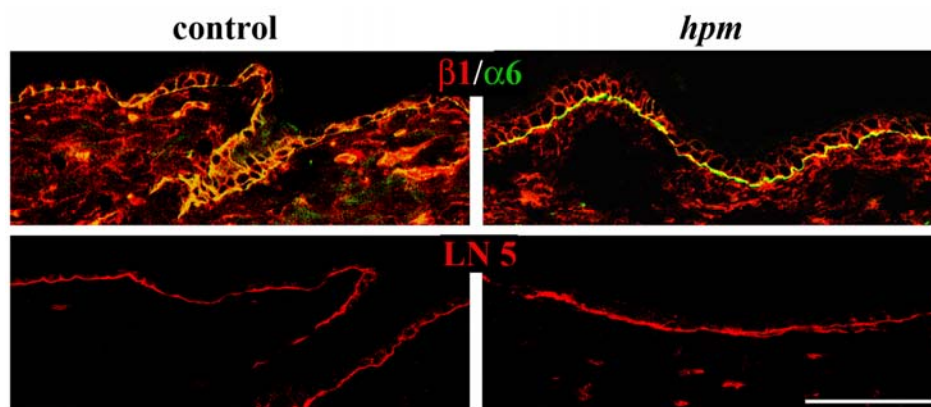


Figure 4.32 Normal $\beta 1$ integrin expression and LN5 staining in 6 months old hypomorphic mice. (A) Normal $\beta 1$ and $\alpha 6$ integrin expression in the *hpm* mouse at the age of 6 months. Laminin 5 deposition at the dermal epidermal junction is rescued in the 6 months old *hpm* mice compared to 14 days. Scale bar = 50 μ m.

To quantitatively assess the expression level of $\beta 1$ integrin in the 6 months hypomorphic mouse we isolated keratinocytes from 6 months old mice and assessed the integrin profile of these cells. When we compared surface expression levels of *hpm* keratinocytes to those of the control cells, no difference was found in $\beta 1$, $\alpha 2$, $\beta 4$ and $\alpha 6$ integrin (Figure 4.33). The FACS data, therefore, corroborated the upregulation of $\beta 1$ integrin expression from the *hpm* allele in 6 months old mice. Furthermore, adhesion and spreading of hypomorphic keratinocytes on collagen I and fibronectin coated dishes was indistinguishable from controls (data not shown).

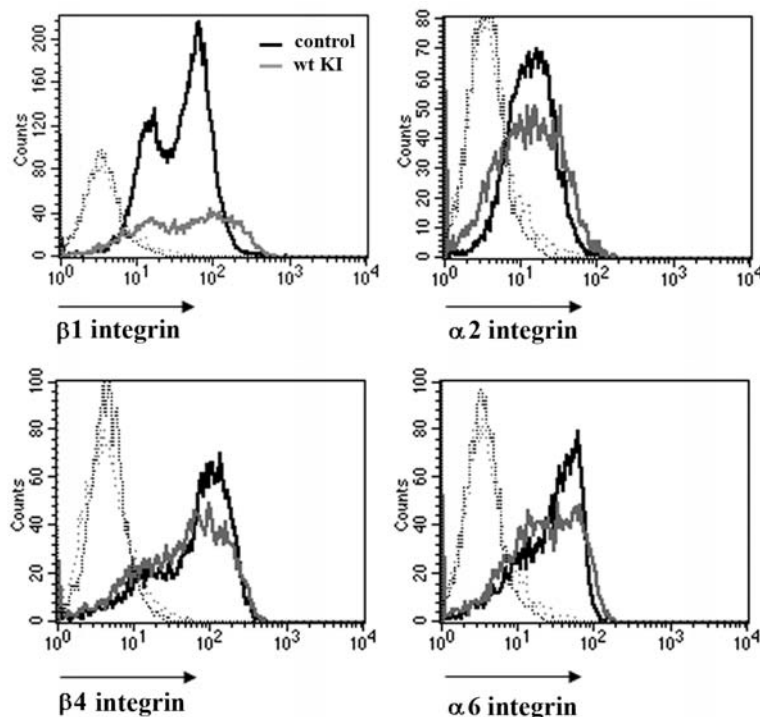


Figure 4.33 Normal $\beta 1$ integrin expression levels in the hypomorphic mice at the age of 6 months. FACS analysis on freshly isolated keratinocytes revealed expression of the most abundant integrin chains at levels comparable to control littermate. The background staining was identical for both genotypes (dotted lines).

As demonstrated above (Figure 4.31), the hypomorphic keratinocytes have a competitive disadvantage against cells expressing wt levels of $\beta 1$ integrin. Thus, $\beta 1$ -null keratinocytes should have an even stronger disadvantage. To test this hypothesis, we analyzed β -galactosidase activity and $\beta 1$ integrin expression in the $\beta 1^{fl/fl}$ K5Cre mice. Former analysis of 9 days old $\beta 1$ -null mutant mice did not reveal any competition at this stage (Brakebusch et al., 2000). However, no analysis was performed at later stages. Indeed we found that in 5 weeks old $\beta 1$ -null mutant mice approximately 16% of the epidermis is $lacZ^-$ (Figure 4.34) and 75% of basal keratinocytes express normal integrin levels when compared to control animals (Figure 4.34). In $lacZ^+$, $\beta 1$ positive regions the $\beta 1^{fl/-}$ cells have expanded, in which only one of the two conditional alleles was recombined (resulting in $lacZ^+$ phenotype), while the other floxed allele is still sufficient for normal $\beta 1$ integrin expression levels.

Although LN 5 deposition was still aberrant in 5 weeks old $\beta 1^{fl/fl}$ K5Cre mice (Figure 4.34), these defects were much less severe than in two weeks old $\beta 1^{fl/fl}$ K5Cre mice (Figure 4.27), indicating normal $\beta 1$ integrin function.

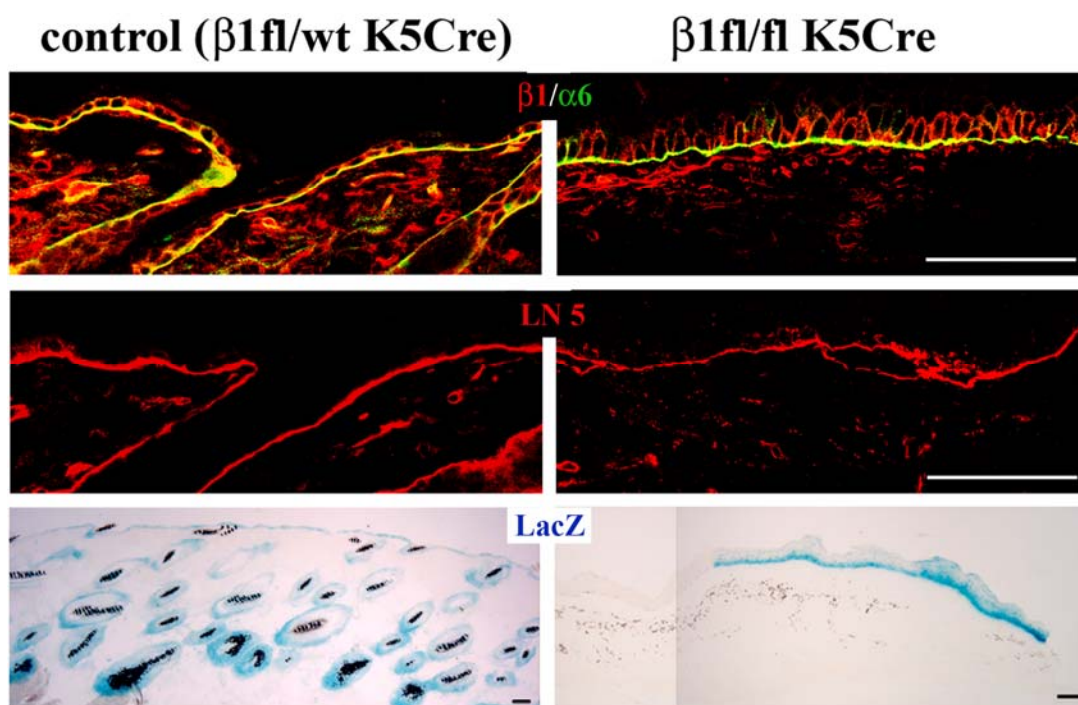


Figure 4.34 $\beta 1$ integrin floxed cells, in which the Cre mediated recombination did not work, repopulate the skin of 5 weeks old $\beta 1fl/fl$ K5Cre conditional knockout mice. Largely normal $\beta 1$ and $\alpha 6$ integrin expression in the $\beta 1$ -null mice at the age of 5 weeks is shown. Laminin 5 deposition at the dermal epidermal junction is widely rescued in the 5 weeks old mutant mice compared to 14 days. LacZ staining on sections from 5 weeks old mice revealed the presence of $\beta 1$ integrin expressing cells in the skin of the mutant mice, in which the Cre recombination did not work. On contrary, in control mice all cells were positive for LacZ staining, thus were expressing the $\beta 1$ integrin only from the wt allele. Scale bar = 50 μ m.

These data corroborate the results obtained with the hypomorphic mice showing that floxed keratinocyte stem cells, which escaped the Cre mediated recombination, have an advantage over cells expressing reduced levels or no $\beta 1$ integrin and therefore repopulate large regions of the epidermis and the ORS cells of the hair follicles. This effect was stronger and developed faster in the $\beta 1$ integrin conditional knockouts, since the advantage of the $\beta 1$ integrin expressing cells over the null-cells was bigger than the advantage over cells expressing reduced amounts of this integrin. These data provide the first direct proof that $\beta 1$ integrin is crucial for the function of stem cells of skin epithelium *in vivo*, as it was speculated before (Watt, 2002).

4.2.1.2.5 Reduced $\beta 1$ integrin levels are sufficient for normal wound healing *in vivo*

$\beta 1$ integrin was demonstrated to be crucial for wound re-epithelialisation *in vivo* (Grose et al., 2002). During the re-epithelialisation process the $\beta 1$ integrin null keratinocytes showed

impaired migration and were more densely packed in the hyperproliferative epithelium, demonstrating that $\beta 1$ integrin mediates keratinocytes adhesion and migration on the provisional wound matrix. Eventually, however, the wounds closed, most likely due to an increased expression of $\beta 5$ and $\beta 6$ integrins (Grose et al, 2002). Proliferation of mutant keratinocytes during wound closure was initially normal and increased in late wounds, maybe due to compensatory effects of the wound-related inflammatory response.

To determine whether reduced $\beta 1$ integrin levels in *hpm* mice are sufficient for efficient wound healing, full-thickness excisional wounds were introduced into 2 to 3 months old control and littermate hypomorph animals (n=6 for each genotype). At this age no visible reduction of LacZ⁺ cells in the hypomorphic skin was visible and $\beta 1$ integrin expression was reduced to 20% compared to normal levels (Figure 4.24 A). 5 days after wounding the area of the hyperproliferative epithelium was not significantly changed in the hypomorph mice and no delay in the wound re-epithelialisation was observed (Figure 4.35 A, B and E). Also the wound morphology did not show any abnormalities comparable to the $\beta 1$ skin specific knockout mice (Figure 4.35 A' and B'). There was a clearly distinguishable epithelial tongue of migrating keratinocytes and the wounds were covered with thin neoepidermis. Furthermore, the number of keratinocytes at the wound edge was comparable to control littermates. Interestingly, $\beta 1$ integrin expression at day 5 post injury was not upregulated at the wound edge of the hypomorphic skin and the percentage of proliferating cells as assessed by BrdU staining was not significantly changed in the hyperthickened wound epidermis of the *hpm* mice, when compared to control animals (Figure 4.35 C, D and F). Finally RNase protection assays revealed no increase of the pro-inflammatory cytokine interleukin 1 β in both unwounded and wounded skin (data not shown). Thus, although hypomorphic keratinocytes displayed several defects *in vitro* (Figure 4.28 and Figure 4.29) they are able to mediate normal wound closure *in vivo*. Since $\beta 1$ integrin expression was not upregulated in the wounds of *hpm* animals, maybe $\beta 5$ and $\beta 6$ integrins can compensate for the reduced $\beta 1$ integrin expression, similarly to the mechanism postulated for the phenotype observed in the $\beta 1$ -null skin specific knockout mice. Alternatively, stem cells which were not hit by the Cre recombination are induced by the wounding stimuli to quickly expand into the wound area and compensate for the reduced $\beta 1$ integrin expression levels from the *hpm* allele. This hypothesis is currently under investigation.

The *in vivo* wound healing experiments were performed in collaboration with Prof. Sabine Werner from the ETH in Zurich, Switzerland.

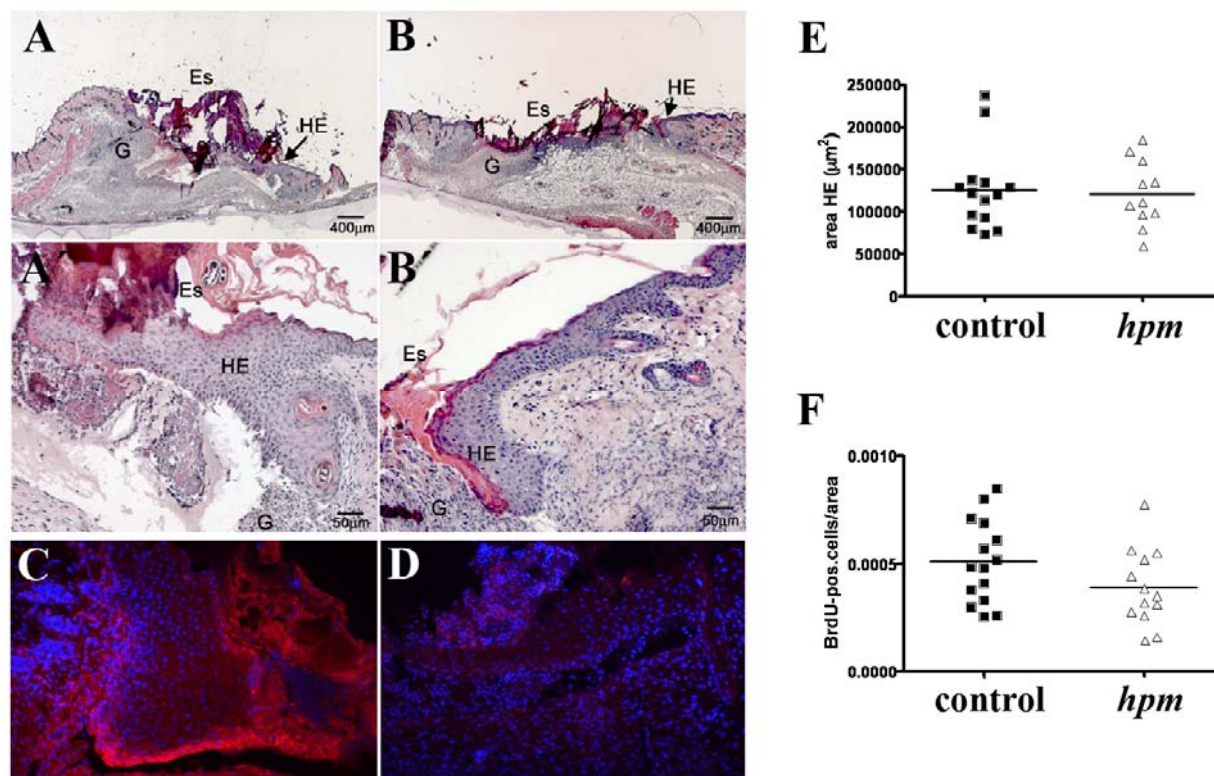


Figure 4.35 Normal wound healing in hypomorphic mice. Haematoxylin–eosin staining revealed no delay in wound re-epithelialisation 5 days after wounding in mutant mice (B) and (B') compared to control littermates (A) and (A'). The area of the hyperproliferative epithelium (E) and proliferation (F) was not significantly changed in the *hpm* mice. No upregulation of $\beta 1$ integrin (red) was observed in the mutant mice upon wounding (D) when compared to control (C). DAPI, blue; G, granulation tissue; Es, eschar; HE, hyperproliferative epithelium.

4.2.1.2.6 $\beta 1$ integrin hypomorphic mice do not develop tumours in a DMBA-TPA induced carcinogenesis model *in vivo*

Examination of human and mouse squamous cell carcinomas revealed considerable variation in integrin expression, both between tumours and in different regions of the same tumour. Normal expression, overexpression and focal or extensive loss of expression of the major keratinocytes integrins have all been observed, together with de novo expression of $\alpha \beta 6$ integrin (Jones et al., 1997; Bagutti et al., 1998). All these changes can potentially influence growth and differentiation of the primary tumour and the ability of that tumour to invade and metastasize (Watt, 2002). Yet, there is no evidence for a role of the $\beta 1$ integrin in the basal keratinocytes of the skin epithelium during carcinogenesis *in vivo*, although there are some data which point to an important role of $\beta 1$ integrin in this process in other tissues. Analysis of targeted deletion of $\beta 1$ integrin gene in mammary epithelium revealed, that $\beta 1$ integrin expression is critical for the initiation of mammary tumorigenesis *in vivo*, and for maintaining

the proliferative capacity of late stage tumour cells (White et al., 2004). More recently, it has been reported, that cells from a vulval squamous cell carcinomas cell line, in which $\beta 1$ integrin was knocked down, when injected into nude mice developed tumours, which are significantly more encapsulated and less invasive than the control cell derived ones (Brockbank et al., 2005).

Chemically induced skin cancer models would be difficult to study in the $\beta 1^{fl/fl}$ K5Cre mice due to early mortality, blistering, spontaneous wound formation and severe fibrosis. On the contrary, the *hpm* mice which have a normal life span, do not show any blistering or wounding and have a comparatively mild fibrosis, represent a nice model to study the role of $\beta 1$ in carcinogenesis *in vivo*.

The response to chemically induced skin cancer in *hpm* mice was performed using the two-stage, initiation–promotion carcinogenesis protocol, in which first 7,12-dimethylbenz[α]anthracene (DMBA) is applied on mouse skin to induce mutations in the *Hras* gene. The tumour initiation is followed by repeated introduction of the noncarcinogenic promoter, 12-*O*-tetradecanoylphorbol-13-acetate (TPA), which leads to the accumulation of additional genetic changes and clonal expansion of the initiated cells, and finally to the formation of multiple benign papillomas (Pedranzini et al., 2004).

The analysis was carried out on 11 *hpm* and 10 control littermates at the age of 3 months. While 9 of 10 mice developed an average of 2.8 ± 0.5 tumours (squamous papillomas) per mouse, the *hpm* mouse did not develop any tumour within 20 weeks (Figure 4.36). Interestingly, the TPA treatment induced severe hair loss in the hypomorph mutant mice, so that after 7 weeks of application, most of the mice were completely bald, while the control treated skin was not affected. Thus, a possible explanation for the absence of tumours observed in the hypomorph mice could be the lack of hair follicle stem cells, which are proposed to be the source of papillomas (Hansen and Tennat, 1994).

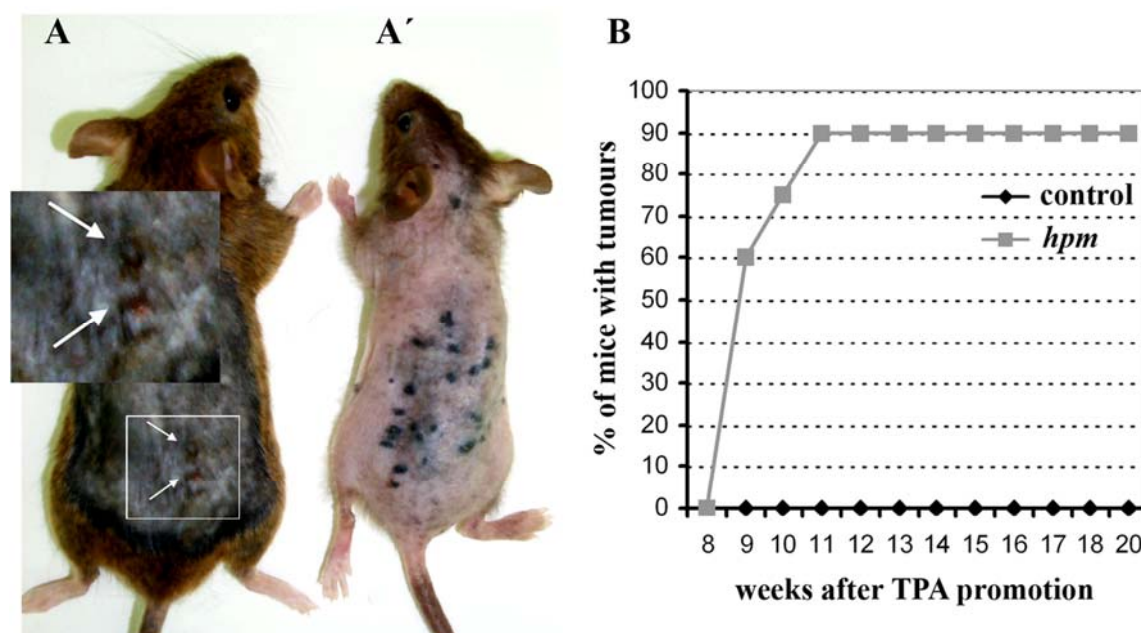


Figure 4.36 The hypomorph mice do not develop any tumours upon DMBA–TPA treatment. (A) Representative control mouse which developed 2 squamous cell carcinomas (arrows) after 20 weeks of TPA application is shown. In contrast, the hypomorph littermate mice (A') lost almost all hair, but did not develop any tumours. (B) Quantification of percentage of mice which developed tumours upon TPA treatment with time.

The DMBA–TPA carcinogenesis studies have been performed in collaboration with Jose L. Jorcano from CIEMAT in Madrid, Spain.

4.2.1.3 Generation of the $\beta 1$ knockin mouse strains. Second approach

Since the first attempt to generate knockin mouse strains carrying mutations in the cytoplasmic tail of the $\beta 1$ integrin chain resulted in a hypomorph phenotype, we had to develop a second strategy. In contrast to the previous approach, in the second approach, we introduced point mutations into the exons encoding the cytoplasmic domain of $\beta 1$ integrin, instead of introducing the entire cytoplasmic region. In addition, after Cre mediated recombination a single *loxP* site was left in an intron and not in an exon. Finally, to facilitate the study of gain of function mutations, a floxed artificial exon was introduced (Figure 4.37 Ai and Figure 4.38 Ai).

Two different types of targeting constructs have been developed, one to introduce mutations in residues encoded by exon 15 of the $\beta 1$ integrin gene and second one to mutate residues within exon 16. In both cases a cassette containing an artificial intron-exon border of the downstream exon followed by a stop codon, a polyadenylation (polyA) signal, and a neomycin (neo) resistance gene, was introduced upstream of the exon to be mutated (Figure 4.37 A and Figure 4.38 A). If this new intron-exon border is recognized by the splicing

machinery, the preceding exon will be spliced into the artificial exon resulting in a truncated $\beta 1$ receptor. In targeting constructs for mutations in exon 15, which encodes for the entire transmembrane span and the first 26 amino acids of the $\beta 1$ integrin cytoplasmic tail, the truncated protein will consist only of a soluble, not membrane-anchored $\beta 1$ integrin extracellular domain. The targeting construct for mutations in exon 16 will lead to the expression of a non functional $\beta 1$ integrin chain lacking the last 21 residues encoded by this exon. This truncation was expected not to result in dominant negative form of the $\beta 1$ integrin protein, since replacement of this coding region by random amino acids, does not lead to any phenotype in mice, when it is expressed heterozygously (Hirsch et al., 2002). If the Cre recombinase is expressed in keratinocytes the floxed cassette harbouring the intron-exon border will be deleted, leading to the skin specific expression of the mutated allele. This strategy was designed to study not only loss of function mutations, but also gain of function mutations, without the risk of a secondary phenotype due to expression of the mutants in other tissues than skin. If such an inducible knockin allele is combined with a conditional knockout allele for $\beta 1$ integrin, Cre recombination will not only switch on the expression of the knockin gene, but also delete the conditional $\beta 1$ integrin gene, so that keratinocytes express only the mutant form of $\beta 1$ integrin.

4.2.1.3.1 Generation of knockin mice strains carrying mutations in exon 15 of the $\beta 1$ integrin gene

In order to investigate mutations in the $\beta 1$ integrin chain encoded by exon 15 of the $\beta 1$ integrin gene, three different targeting constructs have been generated (for detailed description see paragraphs 3.11.20.1 and 3.11.20.2), one carrying the wild type sequence and two with mutated sequences (D759A and $\Delta 759-771$). As described above, all constructs contained a floxed artificial exon introduced 0.7 kB upstream of exon 15 (Figure 4.37 A). The artificial intron-exon border consisted of twelve 3' nucleotides of the intron upstream of exon 15 and twenty 5' nucleotides of exon 15 (Figure 4.37 Ai).

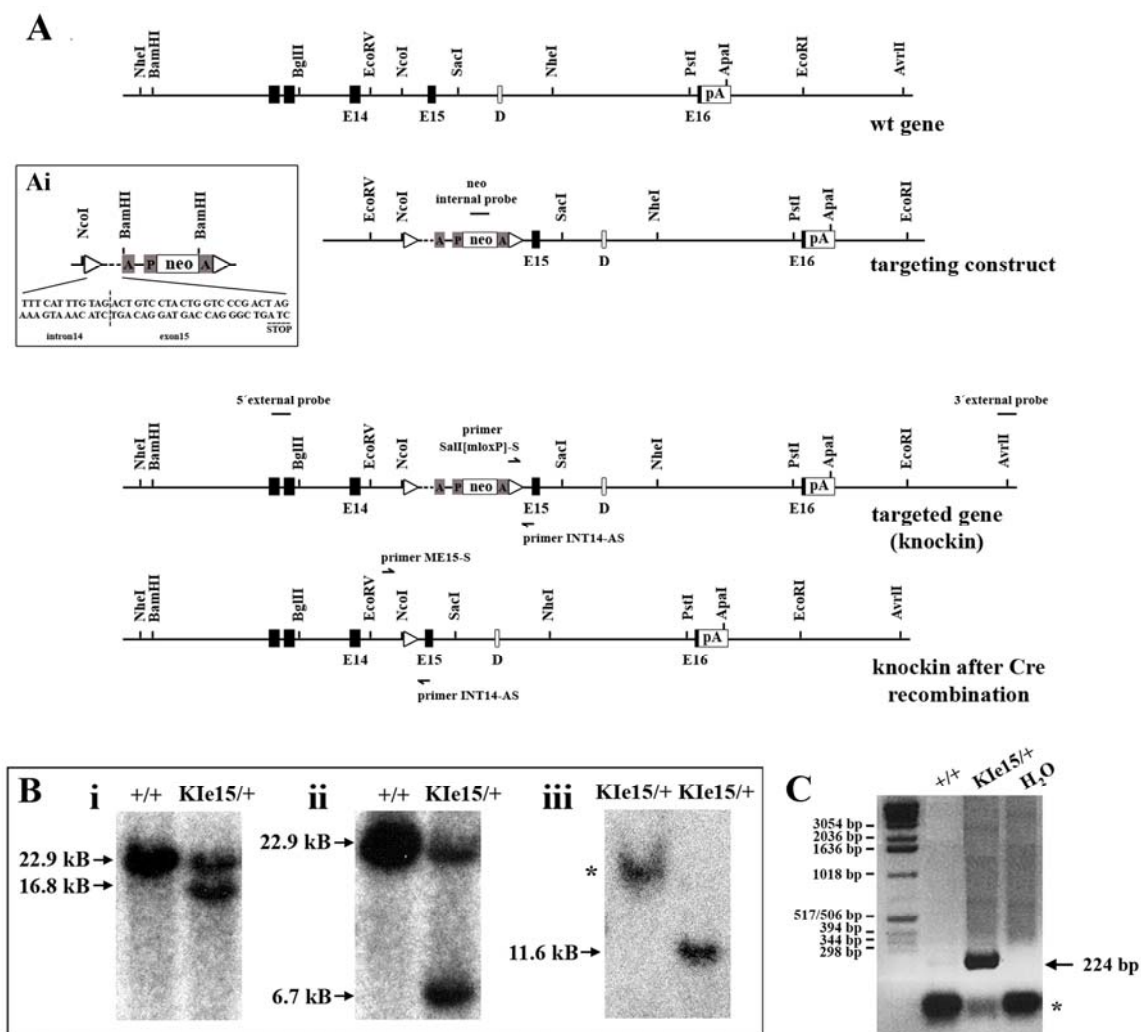


Figure 4.37 Schematic representation of the targeting strategy for the K1e15 mice. (A) K5 Cre mediated deletion of the floxed cassette leads to skin specific expression of the K1e15 allele. Southern probes and important primers are indicated. (E, exon; D, splice variant; A in the cassette and pA in the wt gene, polyadenylation signal; P, PGK promoter; neo, neo resistance gene; \triangleright , mloxP sites). (Ai) Inset showing the enlargement of the floxed cassette and the sequence of the artificial intron-exon border. Important digestion sites are indicated. (B) Southern blot analysis shows recombination of the K1e15 targeting construct in the wt β 1 integrin locus. (i) External probe 3', wt band: 22.9 kB and K1e15 band: 16.8 kB. (ii) External probe 5', wt band: 22.9 kB and K1e15 band: 6.7 kB. (iii) Internal probe (neo), K1e15 band: 11.6 kB. Asterisks indicates a clone which integrated the neo cassette, but at a wrong site. (C) Genomic PCR on DNA from the offspring of the chimeric mice. The 224 bp DNA fragment is present only in the targeted K1e15 allele and was amplified using the following primers: Sal[mloxP]-S and INT14-AS. Asterisk denotes primer dimer.

Prior to electroporation into ES cells, the KI exon 15 (K1e15) targeting constructs have been sequenced and linearized by XhoI digestion. After electroporation and selection of ES cells stably expressing the neo resistance gene, 190 ES colonies have been picked for the wild type construct and for each of the mutated constructs, 192 colonies. In order to identify ES cells which homologously recombined the targeted sequence, genomic DNA was prepared from all

colonies and analyzed by BamHI digestion and Southern blotting using two external probes: 5' external probe and 3' external probe (Figure 4.37 A). These probes bind to sequences outside of the targeting construct, upstream of exon 14 and downstream of exon 16 of the $\beta 1$ integrin gene, respectively. The predicted band sizes after hybridization with the 5' external probe were 22.9 kB for the wt allele and 6.7 kB for the KI allele, whereas hybridization with the 3' external probe should detect a wt band of 22.9 kB and a KI band of 16.8 kB. As shown in Figure 4.37 Bi and Bii, we successfully generated ES cell clones which recombined the K1e15 into the wt $\beta 1$ integrin locus. 5% of the ES cell targeted with the wt construct, and 21% or 11.4% targeted with the mutated constructs (D759A and $\Delta 759-771$, respectively) contained the correct K1e15 size. Since the external probes detect only homologous recombination, but not random integration into the genome, it is necessary to perform a Southern blot also with an internal probe, which detects all integrations of the targeting construct into the genome. After digestion of genomic DNA with NheI and Southern blot, the filters were hybridized with a sequence of the neo gene as an internal probe. In case of homologous recombination a band of 11.6 kB was expected (Figure 4.37 Biii). DNA from the ES cell containing only the expected band size was then sequenced and the correct sequences were confirmed. One positive clone from each construct was injected into blastocysts from a black C57Bl/6J mice and gave rise to high percentage chimeras. Offspring from the chimeric mice, which had an aguti fur, indicating germline transmission, were genotyped by PCR and sequenced (Figure 4.37 C). The aguti fur is indicative for germline transmission since the modified ES cells were derived from aguti 129/Sv mice and aguti fur is dominant over black. Mice carrying the wtK1e15 or mutated K1e15 were mated with mice carrying the $\beta 1$ integrin conditional allele and the K5 driven Cre recombinase transgene to obtain skin specific expression of the K1e15 allele.

4.2.1.3.2 Generation of knockin mice strains carrying mutations in exon 16 of the $\beta 1$ integrin gene

In order to investigate mutations in the $\beta 1$ integrin chain encoded by exon 16 of the $\beta 1$ integrin gene, seven different targeting constructs have been generated (for detailed description see paragraphs 3.11.20.1 and 3.11.20.3). One carrying the wild type sequence and six with mutated sequences (Y783F, Y795F, YY783/795FF, S785A, S785D and TT788/789AA). As described above, all constructs contained a floxed artificial exon 16, which was introduced 0.1 kB upstream of exon 16 (Figure 4.38 A). The artificial intron-exon

border consisted of twelve 3' nucleotides of the intron upstream of exon 16 and three nucleotides of exon 16 (Figure 4.38 Ai).

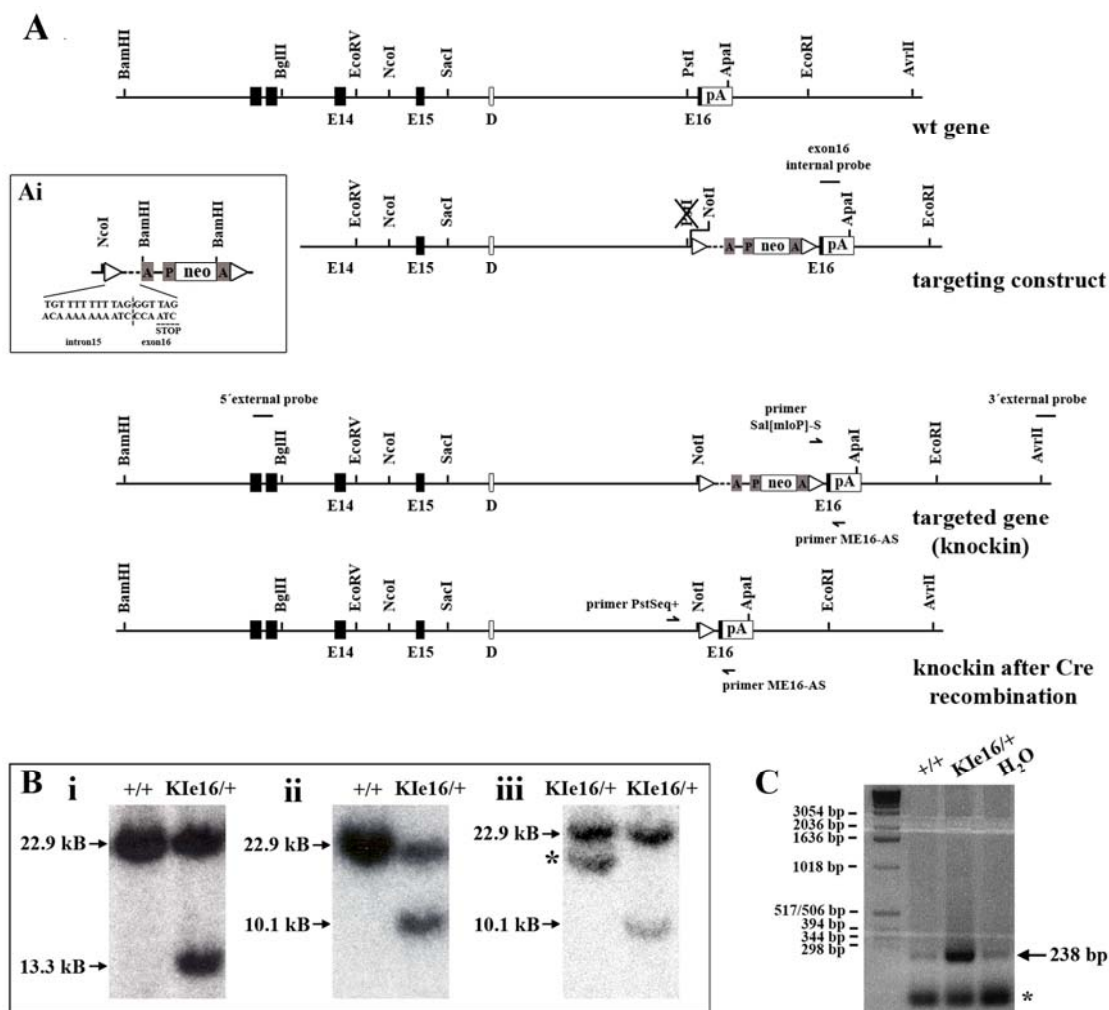


Figure 4.38 Schematic representation of the targeting strategy for the K1e16 mice. (A) K5 Cre mediated deletion of the floxed cassette leads to skin specific expression of the K1e16 allele. Southern probes and important primers are indicated. (E, exon; D, splice variant; A in the cassette and pA in the wt gene, polyadenylation signal; P, PGK promoter; neo, neo resistance gene; \triangleright , *mloxP* sites). (Ai) Inset showing the enlargement of the floxed cassette and the sequence of the artificial intron-exon border. Important digestion sites are indicated. (B) Southern blot analysis shows recombination of the K1e16 targeting construct in the wt $\beta 1$ integrin locus. (i) External probe 3', wt band: 22.9 kB and K1e16 band: 13.3 kB. (ii) External probe 5', wt band: 22.9 kB and K1e16 band: 10.1 kB. (iii) Internal probe (exon16), wt band: 22.9 kB and K1e16 band: 10.1 kB. Asterisks indicates a clone which integrated the construct, but at a wrong site. C) Genomic PCR on DNA from the offspring of the chimeric mice. The 238 bp DNA fragment is present only in the targeted K1e16 allele and was amplified using primers Sal[mloxP]-S and ME16-AS. Asterisk denotes primer dimmer.

Prior to electroporation into ES cells the KI exon 16 (K1e16) targeting constructs have been sequenced and linearized by XhoI digestion. After electroporation and selection of ES cells stably expressing the neo resistance gene, 192 ES colonies have been picked for the wild type construct and for the mutated constructs, 45 to 72 colonies. In order to identify ES cells which

homologously recombined the targeted sequence, genomic DNA was prepared from all colonies and analyzed by BamHI digestion and Southern blotting using two external probes: 5' external probe and 3' external probe (Figure 4.38 A). These probes bind to sequences outside of the targeting construct, upstream of exon 14 and downstream of exon 16 of the $\beta 1$ integrin gene, respectively. The predicted band sizes after hybridization with the 5' external probe were 22.9 kB for the wt allele and 10.1 kB for the KI allele, whereas hybridization with the 3' external probe should detect a wt band of 22.9 kB and a KI band of 13.3 kB. As shown in Figure 4.38 Bi and Bii, we successfully generated ES cell clones which recombined the KIe16 into the wt $\beta 1$ integrin locus. 49% of the ES cell targeted with the wt construct, and 4% to 17% targeted with the mutated constructs contained the correct KIe16 size. After additional digestion of genomic DNA with BamHI and Southern blot, the filters were hybridized with a sequence of exon 16 as an internal probe. In case of homologous recombination a band of 10.1 kB was expected for the KIe16 allele and of 22.9 kB for the wt allele (Figure 4.38 Biii). DNA from the ES cell containing only the expected band sizes was then sequenced for the mutation in exon 16 and the correct sequences were confirmed. One positive clone from each construct was injected into blastocysts from a black C57Bl/6J mice and gave rise to high percentage chimeras. Offspring from the chimeric mice, which had an aguti fur were genotyped by PCR and sequenced (Figure 4.38 C). Mice carrying the wtKIe16 or mutated KIe16 were mated into mice carrying the $\beta 1$ integrin conditional allele and the K5 driven Cre recombinase transgene to obtain skin specific expression of the KIe16 allele.

The generation of the knockin strains was done together with Dr. Hannelore Meyer from the MPI for Biochemistry, Martinsried, Germany. Dr. Jolanda van Hengel from the Ghent University in Belgium contributed to the ES cell work concerning the D759A and $\Delta 759-771$ mutations in exon 15.

4.2.1.3.3 The artificial exons in both targeting constructs are not recognized by the splicing machinery

To test whether the artificial exons introduced into the $\beta 1$ integrin gene are recognized by the splicing machinery, RT PCR was performed on RNA obtained from liver and keratinocytes of the KIe15/fl K5Cre and KIe16/fl K5Cre mutant mice. Since the K5 promoter is not active in liver, the artificial exon containing cassette is detected in liver, whereas in the keratinocytes Cre recombination mediates the deletion of the cassette, leading to normal splicing into the endogenous exons. However, neither for the KIe15 constructs nor for the KIe16 constructs, presence of the new exons could be demonstrated in mRNA isolated from liver. Instead,

splicing occurred in liver cells as in keratinocytes, from exon 14 to exon 15 and from exon 15 to exon 16, respectively. These results indicate that the artificial exons are not recognized by the splicing machinery (Figure 4.39).

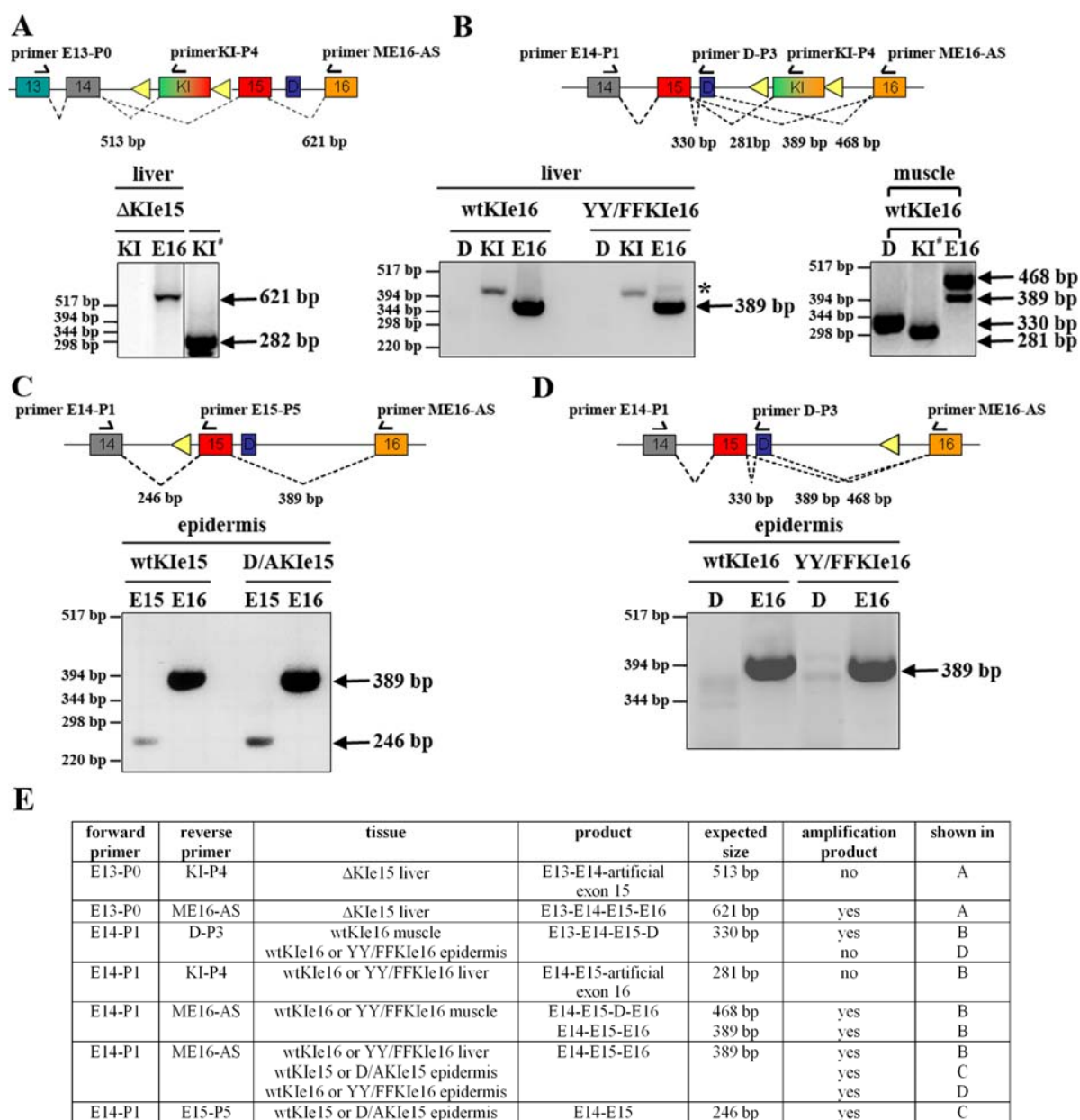


Figure 4.39 The artificial exons 15 and 16 are skipped by the splicing machinery. (A) An example of RT-PCR on RNA from liver lysates from ΔKIe15 mutant mice is shown. The obtained transcript sizes for the liver RNA do not differ from the prediction for non-modified endogenous mRNA. No amplification product is visible at 513, which is the predicted size for artificial exon derived RNA. PCR on the DNA from the KIe15 targeting construct (#) served as positive control for the KI primer (as forward primer the Pst-seq+ primer was used, see 3.11.1). (B) Left panel shows RT-PCR on RNA from liver of the wtKIe16 and YY/FFKIe16 mice, whereas in the right panel, control RT-PCR on muscle RNA from wild type mouse is shown. PCR on the DNA from the KIe16 targeting construct (#) served as positive control for the KI primer. The obtained transcript sizes for the liver RNA do not differ from the prediction for non-modified endogenous mRNA. No amplification product is visible at 281 bp, which is the predicted size for artificial exon derived RNA. Asterisks indicates an unspecific

band. (C) Shows an example of RT-PCR on RNA from epidermal lysates from wtKle5 and D/AKle15 mutant mice, whereas in (D) the RT-PCR from wtKle16 and YY/FFKle16 mutant is shown. The obtained transcript sizes do not differ from the prediction for non-modified endogenous mRNA. Exon D is not expressed in the Kle16 epidermis. For reactions shown in (A) the forward primer E13-P1 was used and for reactions shown in (B), (C) and (D), primer E14-P1 was applied. The reverse primers used in distinct reactions are indicated above the lines of the gel pictures. Primers and schematic representation of their binding sites is shown. Predicted amplification product sizes are indicated. (E) Summary of the RT-PCR results.

In muscle of normal mice, exon 15 splices preferentially in exon D, resulting in the muscle specific expression of integrin β 1D. To check whether the modification of the intron upstream of exon 16 leads to expression of this muscle specific integrin isoform, we used specific PCR primers for exon D and exon 14. However, we could not detect exon D expression in the Kle16 liver cells nor in keratinocytes, while the amplification product was readily detected in muscle RNA of mutant mice (Figure 4.39 B and D). These results were confirmed by RT-PCR using a primer pair binding to exon 14 and exon 16, which amplifies a 389 bp band for the β 1A form and a 468 bp band for the β 1D form. In both keratinocytes and liver RNA, only a 398 band was detected, while in muscle RNA the 468bp band was more prevalent (Figure 4.39 B and D). Clearly there is no expression of exon D in mutant keratinocytes.

Skipping of the artificial exon by the splicing machinery could have two reasons. First, the intron sequences introduced into the genome could have been too short (12 nucleotides; compare Figure 4.37 and Figure 4.38), since they did not include the conserved branch site represented by an adenine residue usually located 20 to 50 nucleotides upstream of the 3' end of the intron. In addition, the 3' consensus pyrimidine stretch of the introns was slightly shortened. Second, the choice of the splice sites by the splicing machinery depends on the length and nucleotide sequence of the exon, which in our case could have been of inappropriate size and sequence as well (Jeremy et al., 2002).

Therefore, the exons carrying mutations of the β 1 integrin gene are constitutively expressed in the knockin mice. This could result in phenotypes of gain-of-function mutations outside the skin. Analysis of the loss-of-function mutations, however, will be unaffected.

4.2.1.4 Analysis of the control knockin mice strains

4.2.1.4.1 The wtKle16 and wtKle15 mice have no skin phenotype

To confirm that the *loxP* site which was introduced into the introns preceding exon 15 and 16, respectively, and which is left behind in the β 1 integrin locus after Cre mediated recombination, does not cause a skin phenotype *per se*, mouse strains carrying the *loxP* site,

but no mutation in exon 15 or 16 have been generated. These mice have been further intercrossed with mice carrying the $\beta 1$ conditional allele together with the K5 driven Cre transgene. The skin phenotype of the wtKle15 (wtKle15/fl K5 Cre) and wtKle16 (wtKle16/fl K5 Cre) mice was analyzed in comparison to the control littermates which did not contain the Cre transgene (wtKle15/fl and wtKle16/fl, respectively).

Analysis of the wtKle16 mice showed that these mice are viable, have normal life expectancy and are fertile. They develop normal hair coat, and are indistinguishable from control littermates irrespective of their age (Figure 4.40 A). By LacZ staining we could show that they express the knockin allele only, since LacZ⁺ cells indicative for the deletion of the $\beta 1$ integrin floxed gene, were detected in the ORS and the interfollicular epidermis of the wtKle16 mice (Figure 4.40 B).

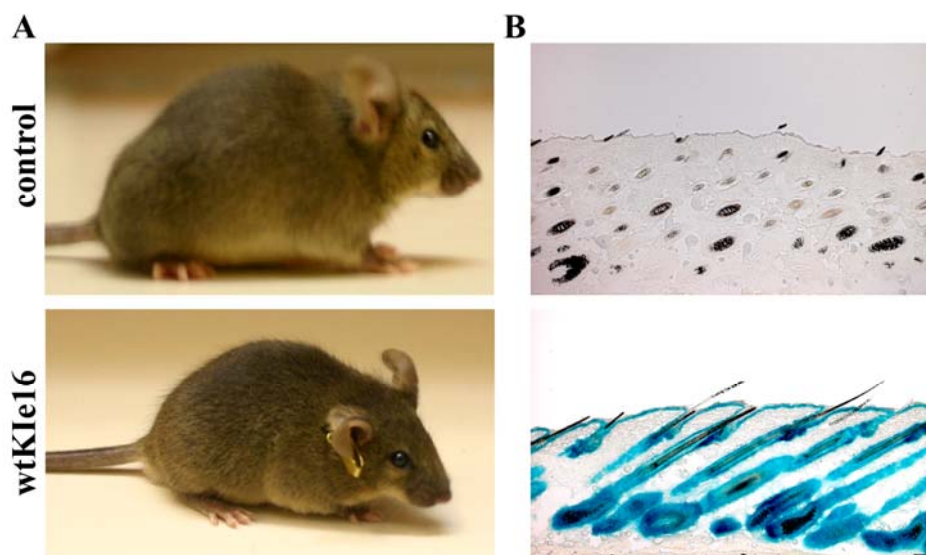


Figure 4.40 wtKle16 mice are indistinguishable from control littermates. (A) wtKle16 mice do not have any skin phenotype when compared to control littermates. Mice at the age of 2 months are shown. (B) LacZ staining on sections from 5 weeks old mice reveals efficient deletion of the $\beta 1$ integrin gene in wtKle16 mice and absence of that staining in control animal. Scale bar = 50 μ m.

Histology on sections from 14 days and 3 months old mice did not reveal any hair follicle or epidermis phenotype in the wtKle16 mice, comparable with that one described for the $\beta 1$ conditional knockout mice or the hypomorphic mice. The hair follicle frequency, length and morphology were not different from age matched control mice. No hyperthickening of the epidermis, blister formation or dermal fibrosis could be observed independently of age of the mice (Figure 4.41).

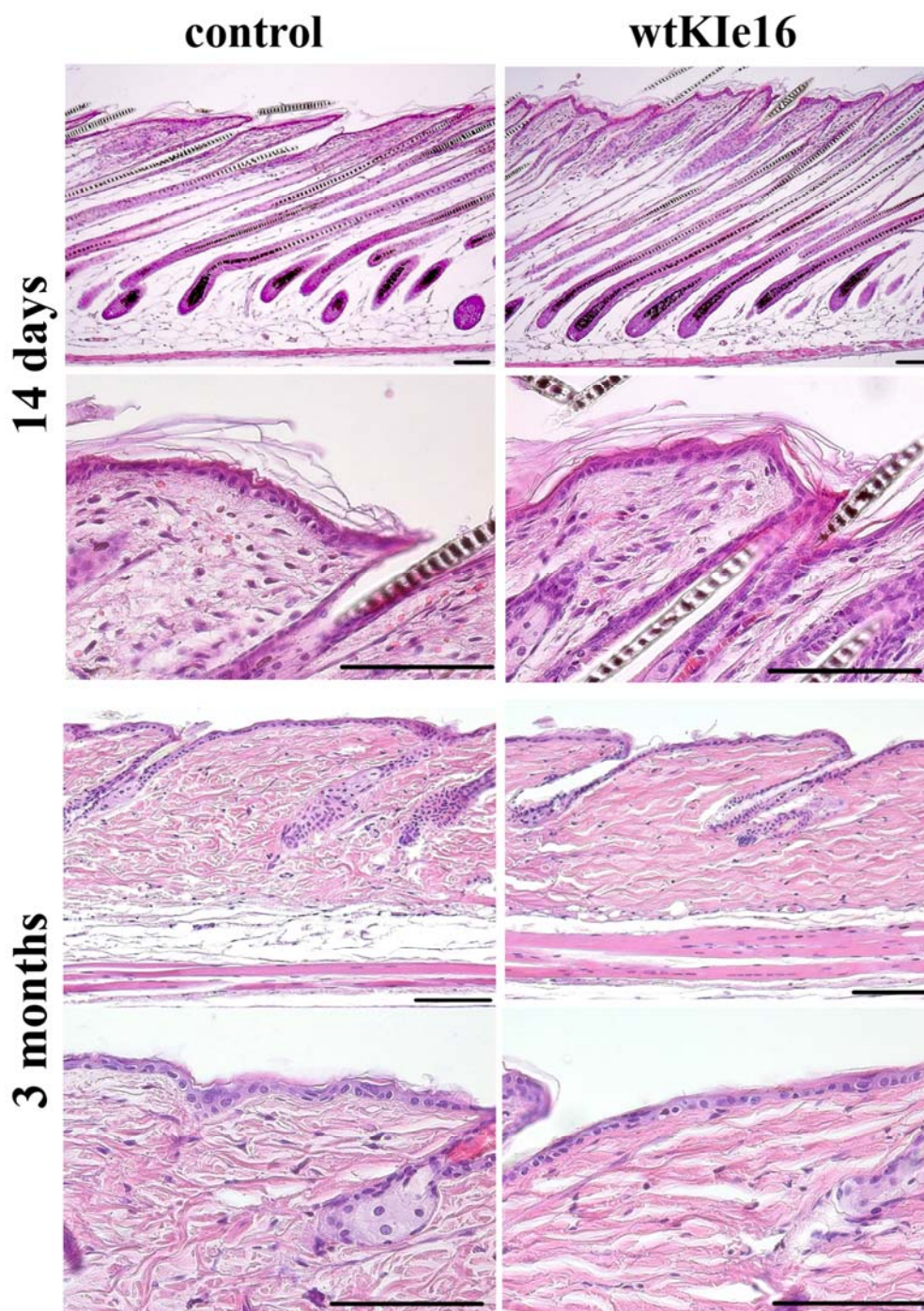


Figure 4.41 Normal skin morphology in the wtKle16 mice. Haematoxylin–eosin staining on 14 days and 3 month old sections is shown. In the upper panels normal overall morphology of the wtKle16 skin is shown. Lower panels show enlargements of the interfollicular epidermis. No blister, hyperthickening or fibrosis could be observed in the wtKle16 mice, independent of age. Scale bars = 50 μ m.

Staining for $\beta 1$ and $\alpha 6$ integrin on sections from 14 days and 3 months old Kle16 mice revealed normal expression levels of these integrins in the interfollicular epidermis and the ORS of the hair follicles (Figure 4.42, upper panel). Also the deposition of laminin 5 at the dermal-epidermal junction, which was severely affected in the $\beta 1$ integrin conditional knockout and the *hpm* mice, was not different in the wtKle16 mice when compared to control,

suggesting that the maintenance of the basement membrane is not affected in these mice (Figure 4.42, lower panel).

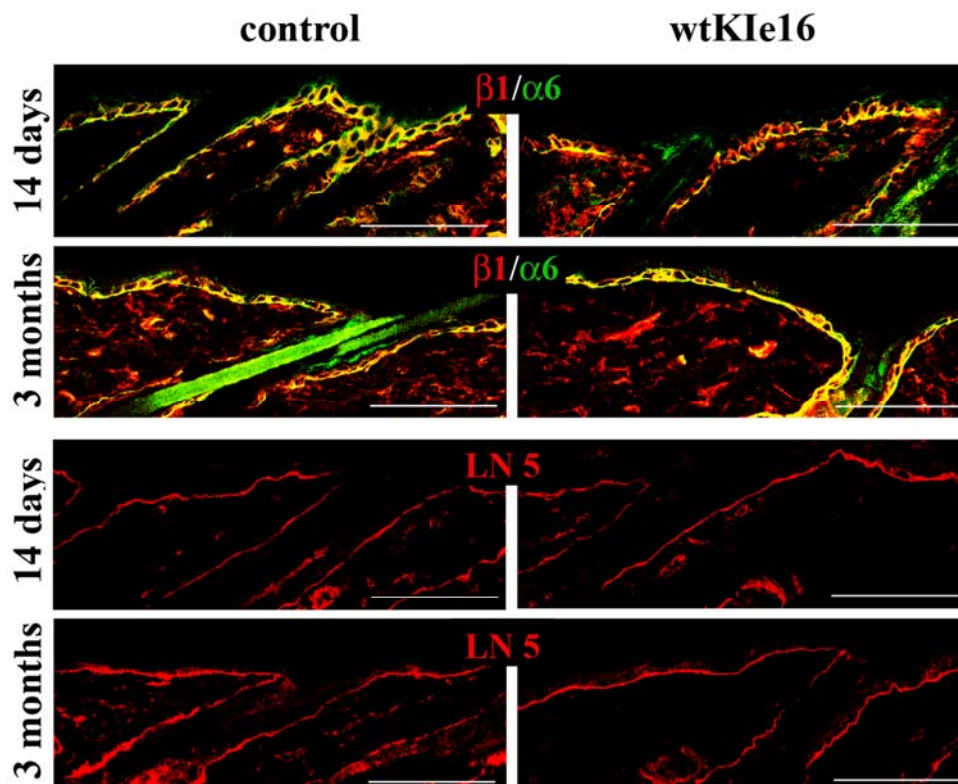


Figure 4.42 Normal $\beta 1$ and $\alpha 6$ integrin expression as well as basement membrane deposition in wtKIe16 mice. $\beta 1$ and $\alpha 6$ integrin double-staining on sections from 14 days and 3 months wtKIe16 animals did not reveal any difference, when compared to control littermates. LN 5 is normally deposited at the dermal–epidermal junction of wtKIe16 mice at 14 days and 3 month of age. Scale bars = 50 μ m.

Finally, BrdU staining of proliferating cells, did not reveal any proliferation defect in the hair follicles of wtKIe16 skin (Figure 4.43). Also in the interfollicular epidermis proliferation was normal: $12.35 \pm 0.21\%$ BrdU⁺ cells in control and $11.65 \pm 3.0\%$ in wtKIe16 mice at the age of 14 days and $3.1 \pm 0.56\%$ and $3.6 \pm 0.14\%$ in 3 months old mice, respectively. These data show that the knockin strategy *per se* does not result in any skin phenotype.

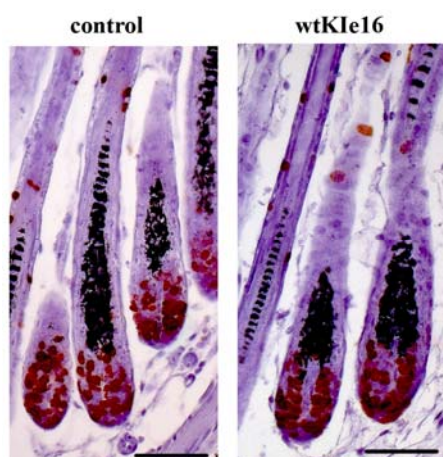


Figure 4.43 Normal proliferation in the hair matrix of wtKIe16 mice. BrdU staining (brown) of proliferating cells in the hair follicles of wtKIe16 mice did not reveal any difference when compared to control mice at the age of 14 days. Haematoxylin, counterstaining. Scale bar = 25 μ m.

The wtKle15 mice have so far not been analyzed in detail, but are also viable, fertile, and show normal hair coat development.

4.2.1.5 Analysis of the mutant knockin mice strains

All mutations introduced in the cytoplasmic domain of $\beta 1$ integrin were previously analyzed *in vitro* and were described to change the cellular phenotype. The analysis focused on mutations of highly conserved potential phosphorylation sites in the $\beta 1$ integrin cytoplasmic chain (Y783, Y795, S785, T778 and T789), ascribed to regulate integrin activity and the cross-talk with the cytoskeleton through actin regulating and binding proteins (Sakai et al., 1998a, 1998b and 2001; Moolroney et al., 2001; Wennerberg et al., 1998 and 2000). The mutations either abolished the phosphorylation of these residues (replacement by alanine or phenylalanine residues) or mimicked constitutively phosphorylated states (replacement by aspartic acid). We also introduced a point mutation in a conserved D759 residue, which was proposed to regulate integrin activity through the formation of a salt bridge with a R995 residue on the integrin α chains. Introduction of an alanine at this position disrupts this interaction and should result in integrin activation (Calderwood, 2004). Finally a deletion of 13 membrane proximal amino acids was introduced, which was proposed to support MAPK signalling, but inhibit FAK mediated cellular events (Lin et al., 1997). This mutation was designed to distinguish between MAPK and FAK mediated integrin signalling.

$\beta 1$ A wt	KLLMIIHDRREFAKFEKEKMNAKWDAT	GENPIYKSAVTTVVNPKYEGK
$\beta 1$ D759A	KLLMIIHARREFAKFEKEKMNAKWDAT	GENPIYKSAVTTVVNPKYEGK
$\beta 1$ Δ 759-771	KLLMIIH-----NAKWDAT	GENPIYKSAVTTVVNPKYEGK
$\beta 1$ Y783F	KLLMIIHDRREFAKFEKEKMNAKWDAT	GENPIFKSAVTTVVNPKYEGK
$\beta 1$ Y795F	KLLMIIHDRREFAKFEKEKMNAKWDAT	GENPIYKSAVTTVVNPKFEGK
$\beta 1$ YY783/795FF	KLLMIIHDRREFAKFEKEKMNAKWDAT	GENPIFKSAVTTVVNPKFEGK
$\beta 1$ S785A	KLLMIIHDRREFAKFEKEKMNAKWDAT	GENPIYKAAVTTVVNPKYEGK
$\beta 1$ S785D	KLLMIIHDRREFAKFEKEKMNAKWDAT	GENPIYKDAVTTVVNPKYEGK
$\beta 1$ TT788/789AA	KLLMIIHDRREFAKFEKEKMNAKWDAT	GENPIYKSAVAAVVNPKYEGK

Figure 4.44 Schematic representation of wild type and mutated $\beta 1$ A integrin cytoplasmic chains. All mutants analyzed in this studied are listed. In black residues encoding by exon 15 of the $\beta 1$ integrin gene are shown; in blue residues encoded by exon 16. In red mutated residues are indicated. Dotted line highlights the deleted amino acids.

4.2.1.5.1 Potential activating mutations in the $\beta 1$ integrin gene do not result in a skin phenotype in vivo or a cellular phenotype in keratinocytes in vitro

The two tyrosine residues in the NPXY motifs of the $\beta 1$ integrin cytoplasmic domains and the D759 residue in the membrane proximal region of the tail have been both implicated to play an important role in integrin activation, by regulating talin binding and the formation of a salt bridge with a corresponding R995 residue from the α chain, respectively (Hynes, 2002; Calderwood, 2004). Phosphorylation of the Y783 and Y795 residues was proposed to be important for talin release from the $\beta 1$ integrin tail and shifting integrin conformation towards the inactive state. Mutations of the tyrosine residues to phenylalanine have been reported to result in an activated integrin, since these sites cannot be phosphorylated thus preventing integrin inactivation by phosphorylation (Calderwood, 2004). Expression of the mutated $\beta 1$ integrin chain in $\beta 1$ deficient fibroblastoid cells resulted in enhanced fibronectin assembly, impaired migration and an increase in the number of focal adhesions (Table 5; Sakai et al., 1998a and 1998b). Expression of the same mutation in ESb T lymphoma knockout cells had no effect on invasion, but resulted in an impaired adhesion (Table 5; Stroeken et al., 2000).

The cytoplasmic domains of α and β integrin subunits are connected via a juxtamembrane salt bridge between an aspartic residue in the β subunit and an arginine in the α subunit. This salt bridge is considered to keep the integrin heterodimers in inactive state, since mutational deletion of the salt bridge resulted in activation of the $\alpha \text{IIb}\beta 3$ integrin characterized by increased fibronectin assembly and enhanced binding to the PAC1 antibody, specific for the active conformation of $\alpha \text{IIb}\beta 3$ integrin (Hughes et al., 1996). In case of $\alpha 5\beta 1$ loss of the salt bridge caused increased fibronectin assembly and increased binding to soluble fibronectin (Sakai et al., 1998b).

Table 5 Comparison of the phenotypes described for the $\beta 1$ D579A and $\beta 1$ YY783/795FF mutations *in vitro*. Results indicating active conformation of the integrin are in italics.

D759A mutation <i>in vitro</i>	YY783/795FF mutation <i>in vitro</i>
normal expression levels of $\beta 1$ integrin ^{1b,#}	normal expression levels of $\beta 1$ integrin ^{1b,#}
normal subcellular localization of $\beta 1$ integrin ^{1b,#}	normal subcellular localization of $\beta 1$ integrin ^{1b,#}
<i>enhanced fibronectin (FN) assembly & increased binding of the 70 kD N-terminal fragment of FN (1.5 – 2.5 fold)</i> ^{1b,#}	<i>enhanced fibronectin (FN) assembly & increased binding of the 70 kD N-terminal fragment of FN (1.5 – 2.5 fold)</i> ^{1b,#}
<i>larger, coarser and more numerous focal contact</i> ^{1b,#}	<i>finer and more numerous focal contact</i> ^{1b,#}
normal, thick F-actin cables ^{1b,#}	more peripheral, thinner F-actin ^{1b,#}
normal migration in response to LPA on gelatine coated filters, reduced through filters coated with adhesive proteins ^{1a,#}	strongly impaired directed migration towards EGF and PDGF ^{1b,#} ; reduced migration in response to LPA ^{1a,#} , normal invasion and metastasis ^{3,*}
normal motility ^{1b,#}	normal motility ^{1b,#}
normal adhesion to fibronectin and vitronectin, decreased to LN 1 ^{1b,#}	normal adhesion to fibronectin, vitronectin and LN 1 ^{1b,#} ; reduced adhesion to FN ^{3,*}
supports FAK autophosphorylation ^{4,Δ}	defective FAK autophosphorylation ^{2,#}
normal spreading on vitronectin and fibronectin ^{1b,#}	normal spreading on vitronectin and fibronectin ^{1b,#} , delayed spreading kinetics on LN 1 and FN ^{2,#}
not studied	less affected by v-src mediated transformation ^{5,#}

Sakai et al., 1998b^{1b,#}; Sakai et al., 1998a^{1a,#}; Wennerberg et al., 2000^{2,#}; Stroeken et al., 2000^{3,*}; David et al., 1999^{4, Δ} ; Sakai et al., 2001^{5,#}

GD25 $\beta 1$ fibroblastoid knockout cells expressing mutant $\beta 1$ integrin chains

*ESb T lymphoma $\beta 1$ knockout cells expressing either mutant $\beta 1$ chains or $\beta 1\beta 2$ chimeras

^{Δ} NIHT3T cells overexpressing mutated chicken $\beta 1$ integrin fused to a Tac antigen

In order to investigate the possible role of these mutations in keratinocyte migration and skin maintenance *in vivo* we generated mice carrying single Y783F and Y795F mutations, which *in vitro* represented an intermediate phenotype between control experiments and experiments with the YY783/795FF double mutant (Wennerberg et al., 1998; Sakai et al., 1998a and 1998b), the double mutant itself and the D759A mutation. All mutant knockin alleles have been expressed together with the $\beta 1$ integrin floxed gene and the K5 Cre transgene (KI/fl K5Cre), and were compared to their control littermates which did not express the Cre transgene (KI/fl).

The Y783FKIe16, Y795FKIe16 and the YY/FFKIe16 double mutant mice displayed normal hair coat phenotype, were viable and fertile (as an example, the YY/FFKIe16 mutant mice is shown, Figure 4.45). Since the double tyrosine mutation was expected to result in a stronger phenotype, than either of the single point mutations, mice with single tyrosine mutations were not further analysed and the detailed analysis was restricted to the double tyrosine mutant.



Figure 4.45 No obvious hair coat phenotype in the YY/FFKIe16 mutant. Control and mutant mice at the age of 2 months are shown.

To confirm that the YY/FFKIe16 mice express only the mutated allele in the skin LacZ staining was performed, which indicates loss of the $\beta 1$ integrin conditional allele. Staining of sections from 14 days and 6 months old mice showed that the $\beta 1$ integrin gene from the $\beta 1$ integrin floxed allele is efficiently deleted since LacZ⁺ cells in the interfollicular epidermis and ORS of the hair follicles were clearly visible in the mutant mice. Presence of LacZ⁺ cells also at the age of 6 months, suggested that there is no competition between stem cells not hit by the Cre recombination and cells expressing the mutated integrin (Figure 4.46).

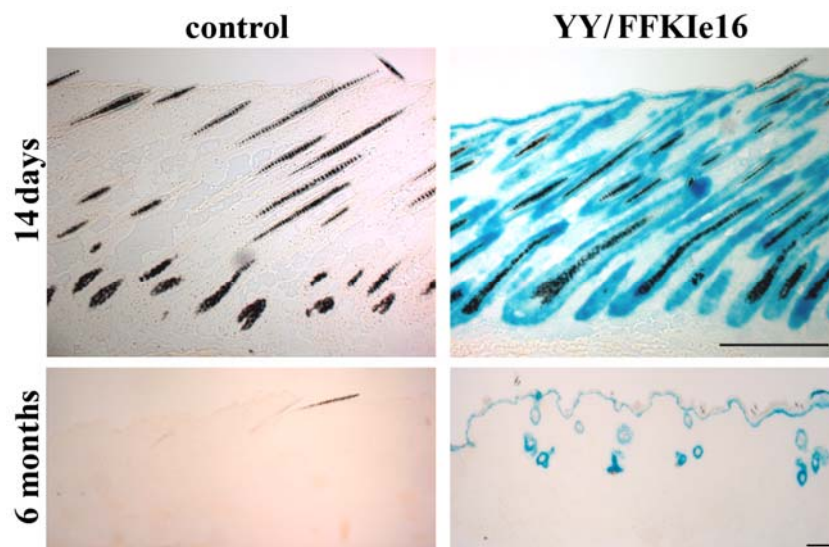


Figure 4.46 YY783/795FF mutant mice express only the mutated allele in the skin. At the age of 14 days and at 6 months clear LacZ positive epidermis and hair follicles are visible in the YY/FFKIe16 mice. There is no LacZ staining in the 14 days and 6 months old control mice. Scale bars = 50 μ m.

Next we wanted to check whether the introduced mutation does not change the expression level of $\beta 1$ integrin and other known keratinocyte specific integrins. Immunostainings on sections from 14 days and 6 months old mice revealed no difference in the staining pattern for $\beta 1$ and $\alpha 6$ integrins between age matched control and mutant animals (Figure 4.47).

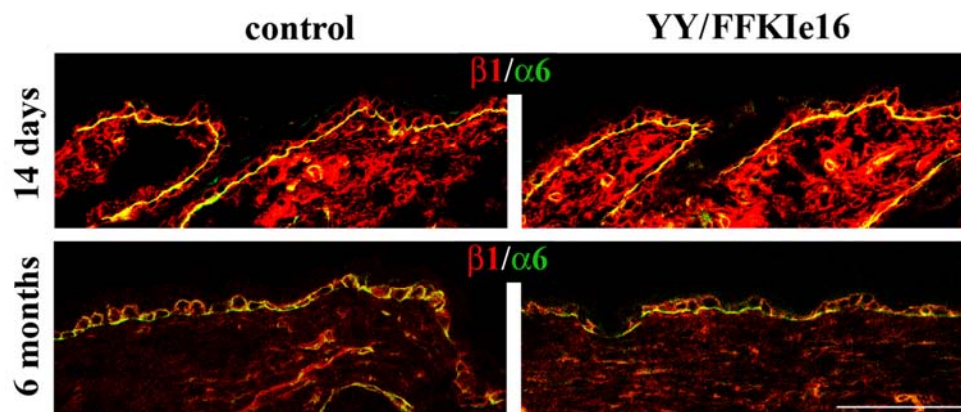


Figure 4.47 Normal $\beta 1$ integrin expression in the skin of YY/FFK1e16 mice. Mutant mice express normal $\beta 1$ and $\alpha 6$ integrin levels at 14 days and 6 months of age. Scale bar = 50 μ m.

To quantitatively assess the expression level of these integrins we performed FACS analysis on keratinocytes from 4 month old mice and could confirm that the expression levels of $\beta 1$, $\alpha 6$, $\beta 4$ and $\alpha 2$ are not changed (Figure 4.48). These data quantitatively demonstrated that the YY783/FF795 mutation does not influence $\beta 1$ integrin expression and in addition showed that also the expression of $\alpha 6\beta 4$ integrin is not affected by the mutation of $\beta 1$ integrin.

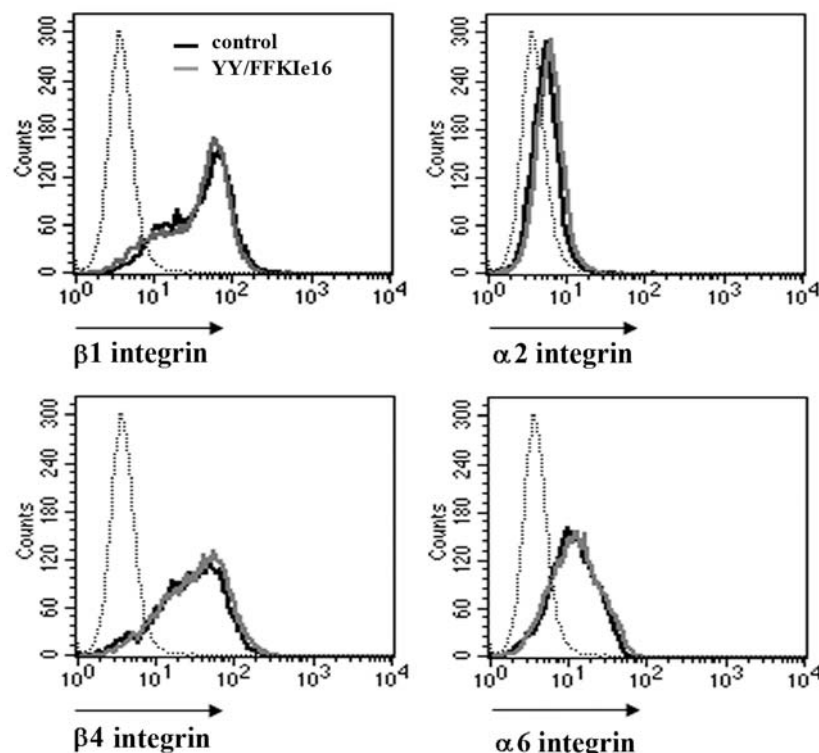


Figure 4.48 YY/FFK1e16 mutant mice express normal levels of $\alpha 2\beta 1$ and $\alpha 6\beta 4$ integrin in skin. FACS analysis of keratinocytes isolated from 4 months old control and mutant mice is shown. There was no difference in the expression levels of $\beta 1$, $\beta 4$, $\alpha 2$ and $\alpha 6$ integrin. The background staining (light grey, dotted line) was identical for both genotypes.

Analysis of the skin morphology of the mutant mice did not reveal any abnormalities regarding the organization of interfollicular epidermis and hair follicle morphogenesis, neither at 14 days, nor at 6 months of age (Figure 4.49).

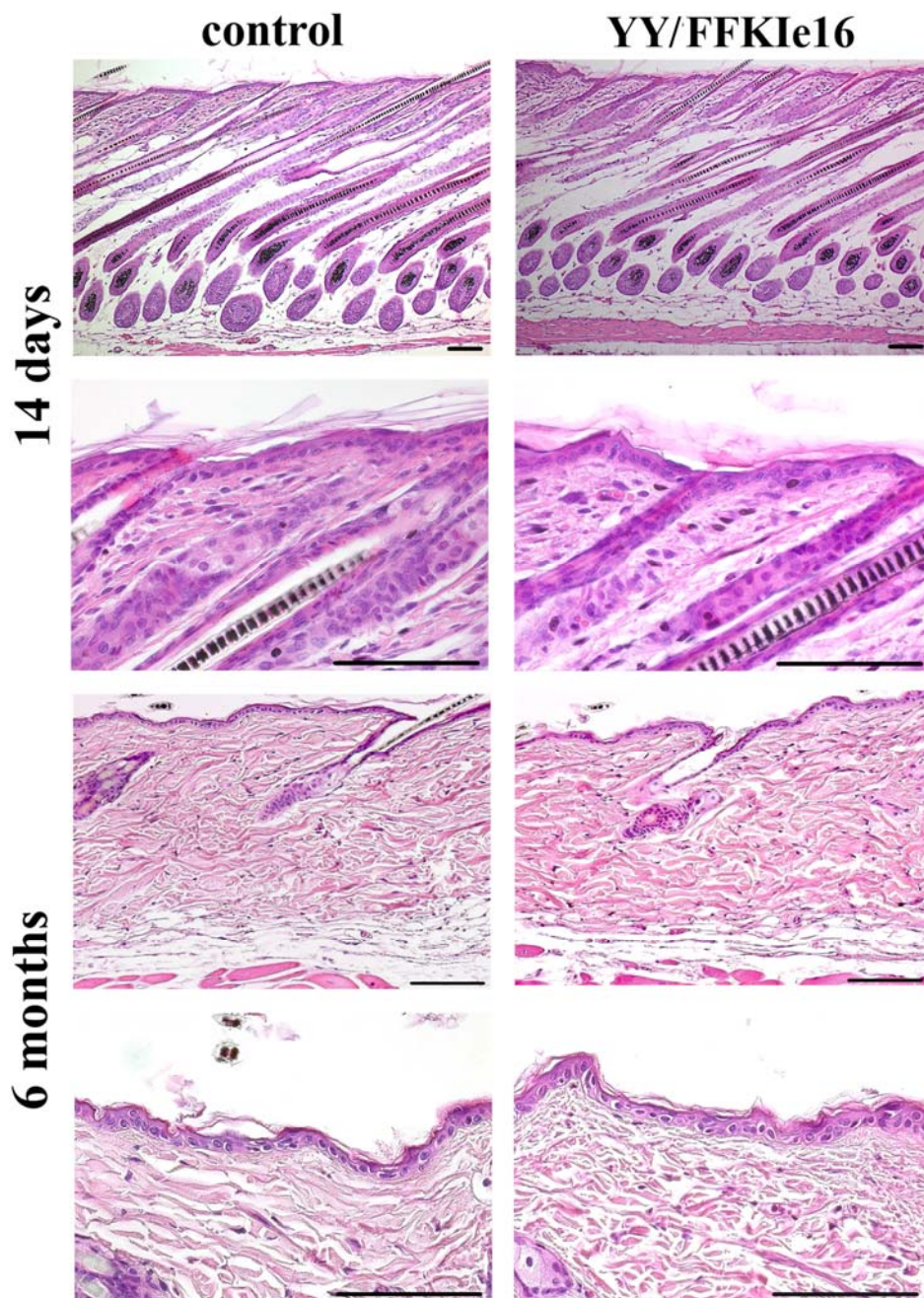


Figure 4.49 Normal skin morphology in the YY/FFK1e16 mutant mice. Haematoxylin–eosin staining on 14 days and 6 month old sections is shown. Upper panels show normal overall morphology of the mutant skin, compared to the control animal. Lower panels show enlargements of the interfollicular epidermis. No blister, hyperthickening or fibrosis could be observed in the mutant mice. Scale bars = 50 μ m.

Since one of the most prominent defects in the β 1 conditional knockout mice was defective deposition of LN 5 at the dermal–epidermal junction, we checked whether we can observe an alteration in LN 5 deposition in the YY/FFK1e16 mutant mice. Yet, no difference in laminin

deposition was found at the age of 14 days, and also at 6 months LN 5 organization was still indistinguishable from control animals (Figure 4.50).

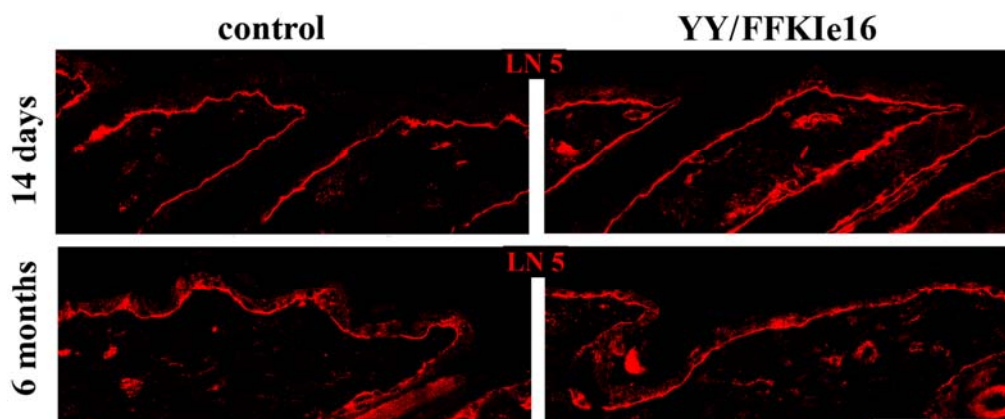


Figure 4.50 Normal LN5 deposition at the epidermal-dermal junction of YY/FFK1e16 mice. Basement membrane maintenance is not affected in 14 days and 6 month old mutant mice. Scale bar = 50 μ m.

The tyrosines of β 1 integrin tail have been reported to be critical mediators of focal adhesion kinase (FAK) activation at the level of the initial autophosphorylation step (Wennerberg et al, 2000). To test whether we have any evidence *in vivo*, for impaired FAK phosphorylation, we stained sections from 14 days and 6 months mutant and control mice with an antibody recognizing the autophosphorylation site (Y397) on the activated FAK molecule. No difference in the staining pattern was observed, which in both control and mutant mice was restricted to suprabasal cells (Figure 4.51). This is surprising, since the suprabasal cells express only limited amounts of β 1 integrin. However, FAK can also be activated by growth factors independently of integrins. Alternatively, we cannot exclude that this suprabasal staining is unspecific, since we do not have an appropriate negative control. Thus, it is difficult to conclude, whether the mutated integrin can support FAK autophosphorylation *in vivo*.

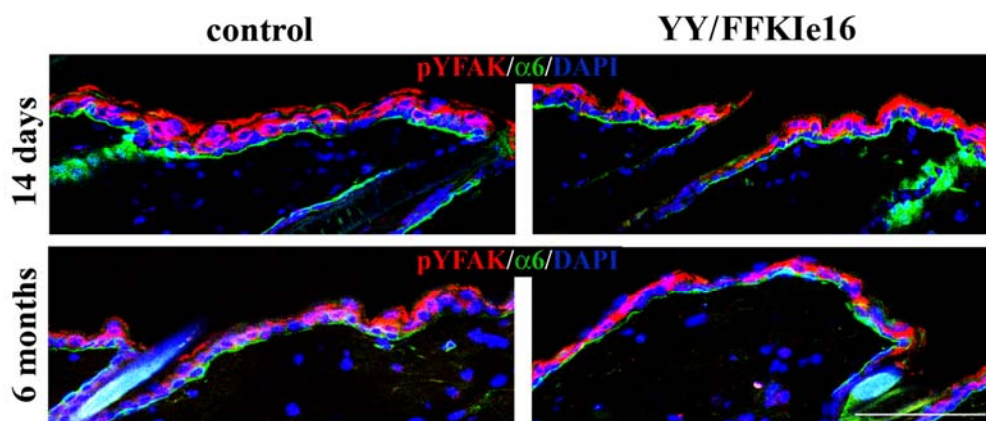


Figure 4.51 Normal FAK pY397 phosphorylation in YY783/FFK1e16 mutant mouse. There is no reduction of the staining with the FAKpY397 antibody in mutant mice at 14 days and 6 months, when compared to

control. Note, that the staining is restricted to the suprabasal layer of keratinocytes. Scale bar = 50 μ m.

As already described in the paragraphs above, the β 1 conditional knockout mice had a strong proliferation defect in the hair follicles and the interfollicular epidermis. We assessed the number of proliferating, BrdU⁺ cells in the interfollicular epidermis of 14 days and 6 months old mice and did not find a major difference between the control and mutant mice (Figure 4.52 A). Also in the matrix region of the hair follicles, no obvious difference in the number of BrdU⁺ cells was detected (Figure 4.52 B).

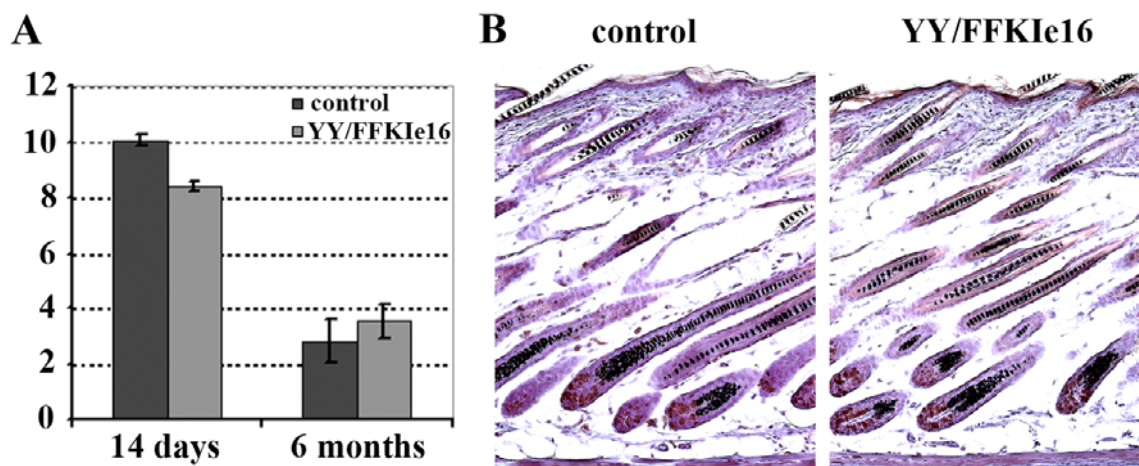


Figure 4.52 Normal proliferation in the YY/FFK1e16 mice. (A) Quantification of the BrdU⁺ cells in the interfollicular epidermis of mutant and control mice is shown. (B) The BrdU staining (brown) pattern in the mutant mice is similar to the control littermate at the age of 14 days. Counterstaining, haematoxylin. Scale bar = 50 μ m.

These experiments showed that the phosphorylation of Y783 and Y795 of β 1 integrin cytoplasmic domain is not important for skin development and maintenance.

In vitro fibroblastoid cells expressing the YY783/795FF mutation were found to have a significantly reduced migration (Sakai et al. 1998a and 1998b). We therefore analyzed function of mutant keratinocyte *in vitro*. Keratinocytes were isolated from 4 months old mutant mice and tested in adhesion and migration assays, similar to assays in which fibroblastoid cells expressing mutant YY783/795FF β 1 integrin chains have been analyzed previously (compare Table 5). The fibroblastoid cells carrying the YY783/795FF mutation were shown to exhibit delayed spreading (Wennerberg et al., 2000). Yet, the mutant keratinocytes were spreading on fibronectin and collagen I coated dishes with the same kinetics as the control cells (Figure 4.53).

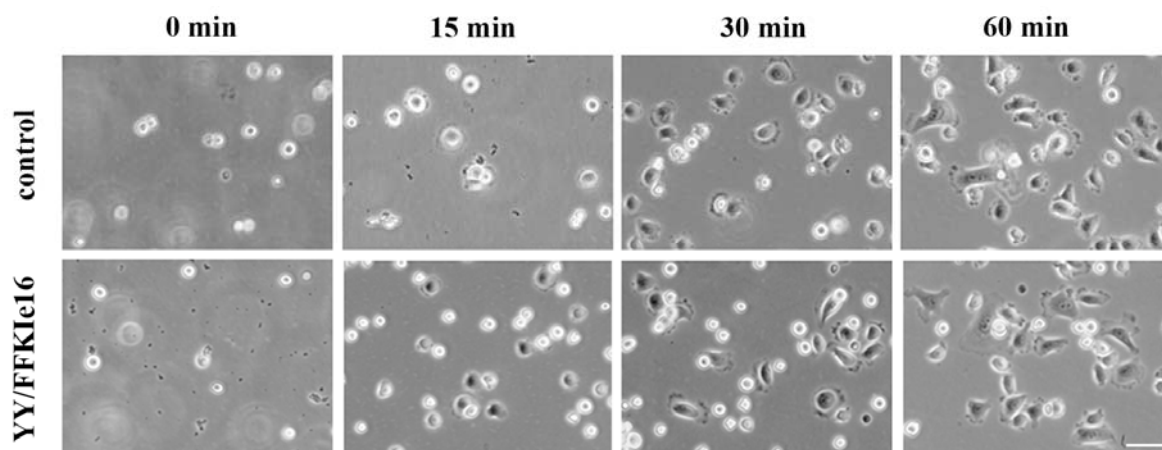


Figure 4.53 Normal spreading kinetics of the mutant keratinocytes. Cells were plated on collagen I and fibronectin coated dishes and the spreading was monitored. Scale bar = 50 μ m.

When plated on fibronectin and collagen I coated culture dishes, the mutant cells nicely attached to the surface, spread and grew in a manner not distinguishable from control cells (data not shown), thus, giving no indication for an impaired affinity or avidity of the mutated integrins in keratinocytes. These data are in agreement with the unchanged cell surface expression of integrins (Figure 4.47 and Figure 4.48).

In order to investigate the F-actin distribution and focal contact organization we stained the cells with phalloidin-FITC, and the focal contact marker paxillin. No difference could be found in the F-actin organization, and in size and number of the focal adhesions (Figure 4.54). To qualitatively assess FAK phosphorylation in the mutant keratinocytes, which was altered in β 1 mutant fibroblastoid cells *in vitro*, we performed immunofluorescent staining using the pY397 FAK antibody. Double staining with paxillin revealed that pY397FAK is found in focal adhesions. There was no obvious reduction of the phosphorylation at these sites (Figure 4.54). Finally we looked at talin localization in the focal adhesions. Talin was described to bind to the mutated tyrosine residues, whereas tyrosine phosphorylation of the β 1 tail at the NPXY motif inhibited talin binding (Tapley et al., 1989). This suggested that phosphorylation of the tyrosines in the β 1 integrin is negatively regulating the talin-integrin interaction. We did not find any difference in the staining pattern for talin between control and mutant keratinocytes, suggesting that β 1 integrins are not tyrosine-phosphorylated or that other mechanisms regulate integrin-talin interaction in fibroblastoid cells *versus* keratinocytes (Figure 4.54).

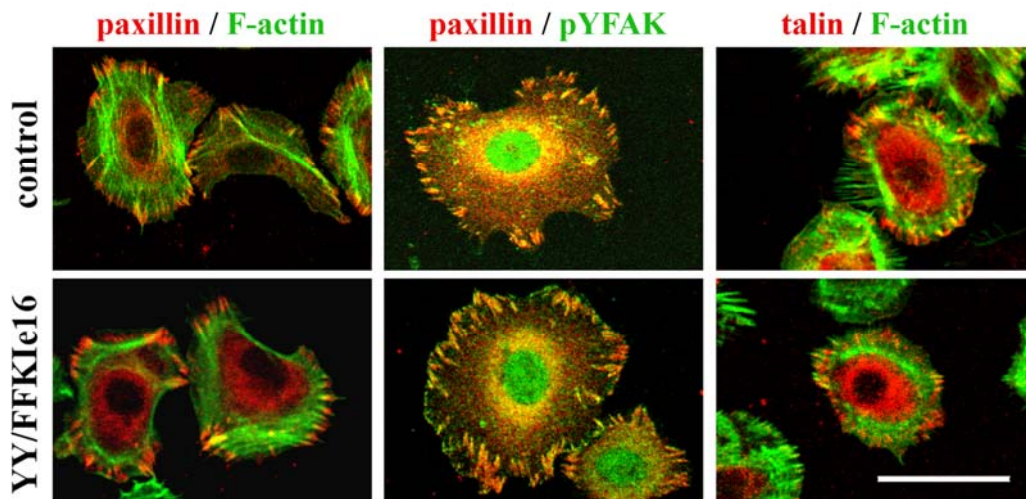


Figure 4.54 Normal F-actin and focal contacts organization in mutant keratinocytes. Paxillin localizes to the tips of actin filaments of the mutant cells similarly to the control cells and pY397FAK co-localizes with paxillin in the focal contacts of mutant keratinocytes. Talin staining in the mutant keratinocytes resembles the control distribution. Scale bar = 50 μ m.

YY783/7795FF fibroblastoid cells have an impaired ability to transverse filters in chemotaxis assays indicating defective migration (Sakai et al., 1998b). In order to investigate migration of our mutated keratinocytes *in vitro* we performed scratch assays as described for the analysis of Cdc42 fibroblastoid cell lines (see paragraph 4.1.10). In two independent assays we could not find a clear indication for a migratory defect of the mutant keratinocytes, since the wound closure speed was indistinguishable from control keratinocytes (Figure 4.55 A and B).

If β 1 integrin is constantly activated, this might lead to an increased activation of downstream signalling pathways such as Erk, FAK and paxillin. To assess the activation status of these integrin effectors, we checked for wounding induced phosphorylation of Erk, FAK and paxillin. No difference was found between control and mutant cells (Figure 4.55 C). Taken together we could not find any evidence for constitutive activation of YY/FF β 1 integrin receptors in keratinocytes.

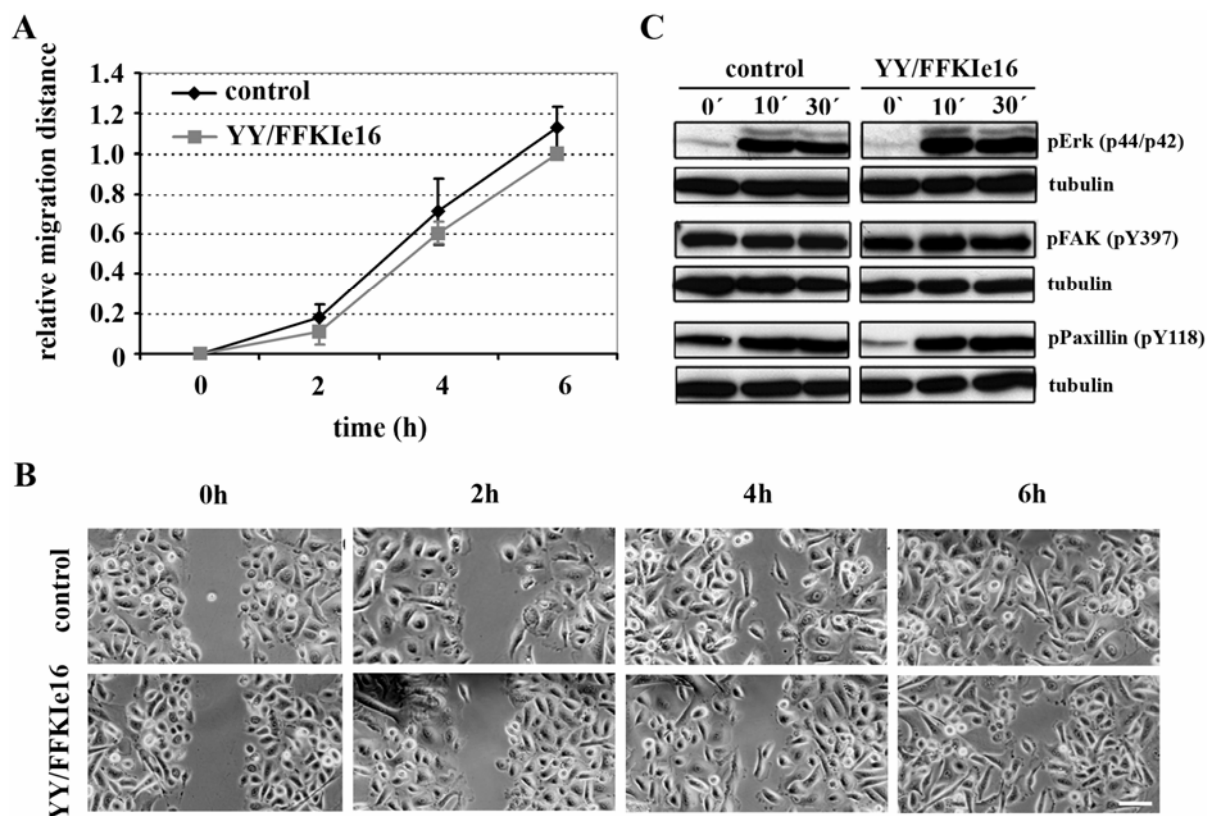


Figure 4.55 Comparable migration capacity of the mutant keratinocytes and wounding induced activation of effector molecules. (A) Similar relative migration of mutant and control cells in a wounding assay (n=2). (B) Phase contrast pictures of migrating keratinocytes (scale bar = 50 μ m). (C) Wounding induced activation of pErk, pFAK and pPaxillin is not different in the keratinocytes carrying the YY783/795FF mutation, compared to control cells. Tubulin served as loading control.

Also mice of the second mouse strain carrying a supposedly activating mutation in the cytoplasmic domain of the β 1 integrin, the D759AKIe15 mutant mice, had normal hair coat phenotype, were viable and fertile. To investigate the skin of these mutant animals in more detail, we performed the same series of experiments as for the YY/FFK1e16 mice, including LacZ staining, integrin expression level evaluation, staining for laminin 5 deposition at the dermal-epidermal junction, proliferation analysis and general interfollicular epidermis and hair follicle morphology assessment. The study was performed with 14 days and 3 months old animals. As the YY/FFK1e16 mutant mice, also the D/AKIe15 mice did not show any phenotype different from normal mice (data not shown).

Normal skin development and maintenance in the D/AKIe15 mice suggests that in keratinocytes *in vivo*, the formation of the salt bridge between the D759 residue on the β 1 integrin chain and the R995 residue in the α subunit does not regulate integrin activity, in contrast to the results obtained with the fibroblastoid cells *in vitro* (Sakai et al., 1998a and 1998b).

4.2.1.5.2 Analysis of the mice carrying mutations mimicking constitutive phosphorylation state of the $\beta 1$ integrin cytoplasmic tail

In vitro studies with fibroblastoid cells expressing $\beta 1$ integrin mutations at the S785 residue indicated that changes in phosphorylation state at this position regulate cell spreading and directed migration. The S785D mutation, which is proposed to mimic a phosphorylated serine, was shown to promote cell attachment and to inhibit cell spreading and migration (Mulrooney et al., 2001). The S785A mutation, which cannot be phosphorylated, behaved similar to wild type $\beta 1$ expressing cells, with respect to cell adhesion, focal contact formation and FAK activation (Wennerberg et al. 1998). We developed knockin mouse strains carrying either of these mutations to study the function of this serine residue in skin development and wound healing *in vivo*. So far only the S/AKIe16 mice at 14 days and 6 months of age were analyzed as described above for the D759A mice. The S/AKIe16 mice had normal hair coat, were viable and fertile. The LacZ and $\beta 1$ integrin staining confirmed normal expression of only the mutated allele in the skin. Analysis of the interfollicular epidermis and hair follicles did not reveal any morphological abnormalities, and the basement membrane was properly organized. Finally, the number of proliferating cells was not affected, both in the interfollicular epidermis and in the hair matrix cells (data not shown).

For the S785D mutation, we generated mice, which homozygously express the mutated integrin receptor by intercrossing the S/DKIe16 knockin mice into nestin Cre transgenic mice (Betz et al., 1996). These mice have no obvious phenotype and are fertile. A more detailed analysis will be carried out in the future.

Although preliminary, our data show that phosphorylation of S785 is not required for normal $\beta 1$ integrin function in keratinocytes.

4.2.1.5.3 Deletion of the membrane proximal region ($\Delta 759-771$) of the $\beta 1$ integrin cytoplasmic domain leads to $\beta 1$ integrin-null like phenotype

Integrin engagement and clustering has been shown to be involved in FAK and mitogen activated protein kinase (MAPK) activation. Studies with a $\beta 1$ integrin mutant, in which the membrane proximal amino acids D759 to M771, overlapping with the putative binding site for FAK, have been deleted, provided evidence, that integrin mediated activation of these molecules can represent distinct sets of events. Thus, adhesion dependent MAPK activation does not necessarily require FAK activation (Lin et al., 1997). In addition, cells expressing the mutated integrin were able to attach, but not to spread on anti- $\beta 1$ antibody coated surface

suggesting that also attachment and spreading requires distinct integrin functions (Reszka et al., 1992). To investigate the *in vivo* consequences of a specific impairment of integrin mediated activation of FAK and cell spreading we developed a mouse strain expressing the deletion mutant of $\beta 1$ integrin in a skin specific manner ($\Delta K1e15$).

The $\Delta K1e15$ mice were born without any obvious phenotype, but soon after birth a reduced pigmentation of the skin became visible, and at 14 days of age the animals showed clearly reduced number of hairs (Figure 4.56). At 5 weeks of age almost all hair was lost and the skin became reddish and tight (Figure 4.56). In addition, wounds appeared in mechanically stressed regions of the body. This phenotype closely resembled the phenotype described for the $\beta 1$ integrin knockout mice (Brakebusch et al., 2000).

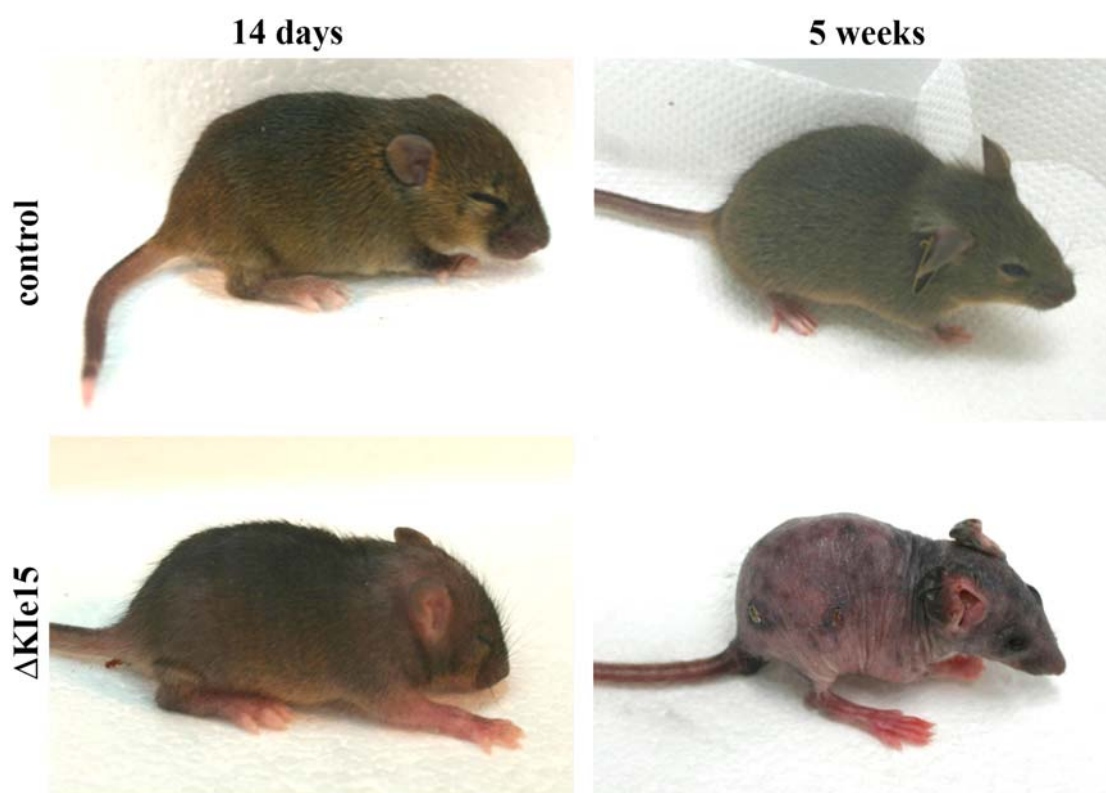


Figure 4.56 The $\Delta K1e15$ mice have a severe, $\beta 1$ -null like hair coat phenotype. Mutant mice at the age of 14 days and 5 weeks of age are shown.

To confirm that only the truncated $\beta 1$ integrin is expressed in the mutant skin, we performed lacZ staining showing the deletion of the $\beta 1$ integrin gene from the $\beta 1$ integrin floxed allele. Sections from 14 days old mutant animals showed strong lacZ staining in the interfollicular epidermis and the hair follicles (Figure 4.57 A and B), whereas similar to the results obtained with the $\beta 1^{fl/fl}$ K5Cre mice, the lacZ staining in 5 weeks old mice was not ubiquitous and covered approximately 40% of the epidermis (Figure 4.57 C and D).

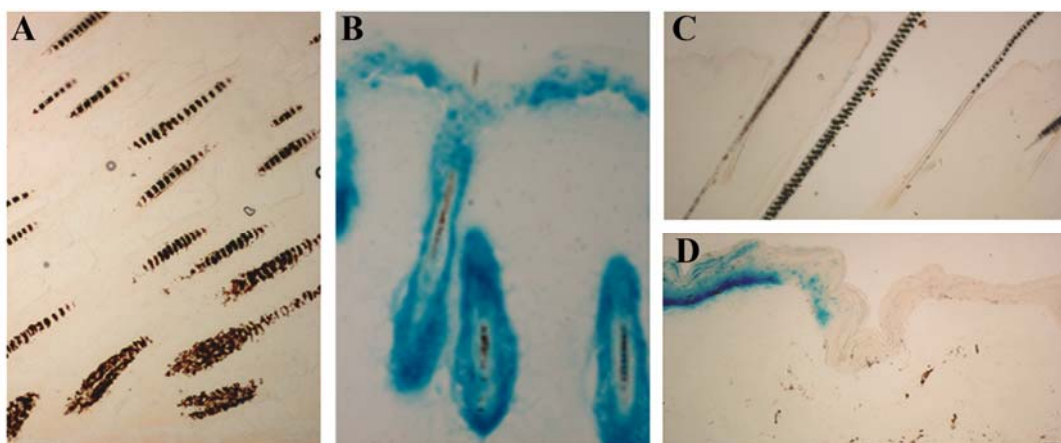


Figure 4.57 Competition between cells expressing only the Δ KIE15 allele and cells not hit by the Cre recombination in the skin of the Δ KIE15 mice. Staining on 14 days sections from Δ KIE15 mice revealed that both the interfollicular epidermis and ORS of the hair follicles are lacZ positive (B), whereas by 5 weeks LacZ negative regions overweigh (D). (A) and (C) show the corresponding control littermate mice. Scale bar = 50 μ m.

Staining for the β 1 integrin expression on sections from 14 day old mice revealed no difference when compared to the control animal (Figure 4.58), suggesting normal expression of the truncated β 1 receptor. In contrast, α 6 integrin staining at the basal side of basal keratinocytes was reduced and often discontinuous (Figure 4.58).

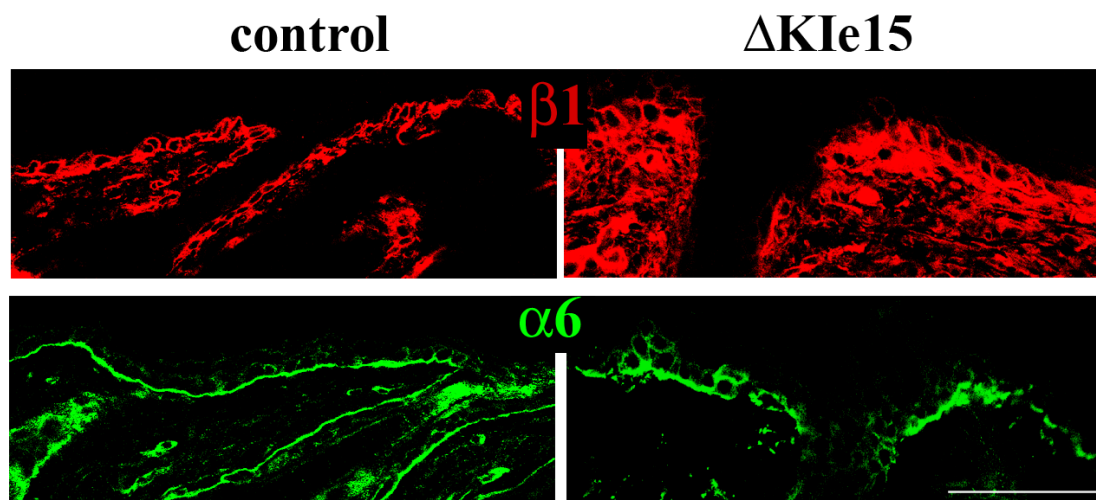


Figure 4.58 Δ KIE15 mice express β 1 integrin on the cell surface. β 1 integrin staining on 14 day old mutant mice is comparable to the staining on control sections. α 6 integrin staining revealed regions with normal and regions with decreased expression levels of this integrin chain. Scale bar = 50 μ m.

Histological analysis of the Δ KIE15 mice further corroborated the similarity of these mice to the β 1 skin specific conditional knockout mice. Analysis of sections from 14 day old mutant mice showed hyperthickened epidermis, blister formation and severe hair follicle abnormalities similar to the β 1 integrin conditional knockout mice (Figure 4.59). Also after 5 weeks the phenotype of the Δ KIE15 mice was consistent with the null phenotype. At this age,

the mutant mice had lost the majority of hair follicles, had less subcutaneous fat layer and developed dermal fibrosis (Figure 4.59).

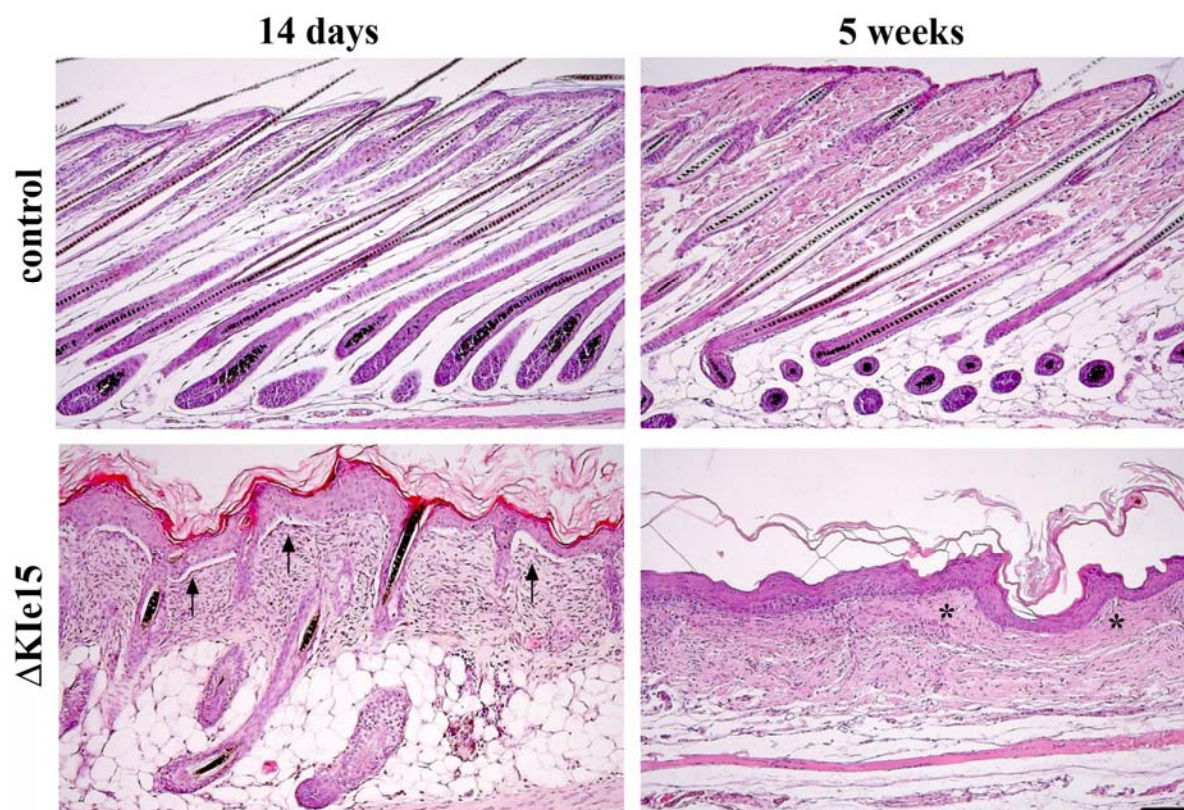


Figure 4.59 Severe interfollicular epidermis and hair follicle phenotype in $\Delta K1e15$ mice. Haematoxylin – eosin stain on 14 days sections from the deletion mutant shows blister formation (arrows), hyperthickened epidermis and aberrant hair follicles, not found in the control mice. By 5 weeks of age, the mutant mice has lost all hairs and dermal fibrosis developed (asterisks). By that time the control mice progressed to the second hair cycle. Scale bar = 50 μ m.

14 day old mutant mice had laminin 5 diffusely deposited at the dermal–epidermal junction, in a manner similar to the $\beta 1$ -knockout mice in skin (Figure 4.60).

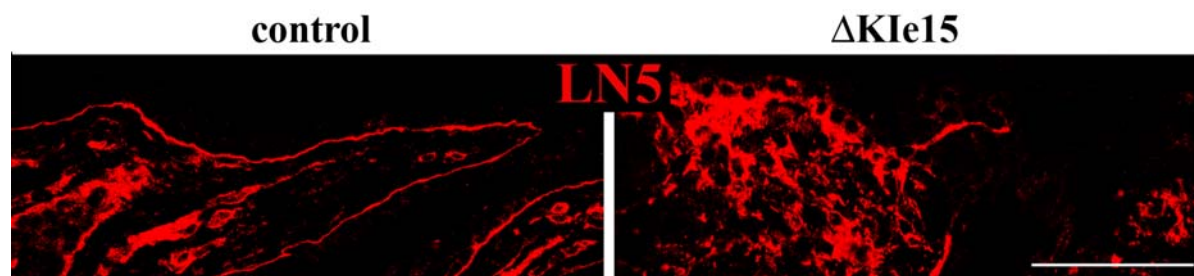


Figure 4.60 Impaired basement membrane maintenance in the $\Delta K1e15$ mice. Laminin 5 is diffusely deposited at the dermal-epidermal junction in the skin of 14 days old deletion mice. Scale bar = 50 μ m.

Mice lacking the $\beta 1$ integrin in skin had reduced proliferation of basal keratinocytes at birth and at 9 days of age (Brakebusch et al., 2000; Raghavan et al., 2000). In 14 days $\Delta K1e15$ mice however, we found that there was no difference in the number of proliferating cells in the

interfollicular epidermis (Figure 4.61 C). At 5 weeks of age even a hyperproliferation was observed (Figure 4.61 B and C).

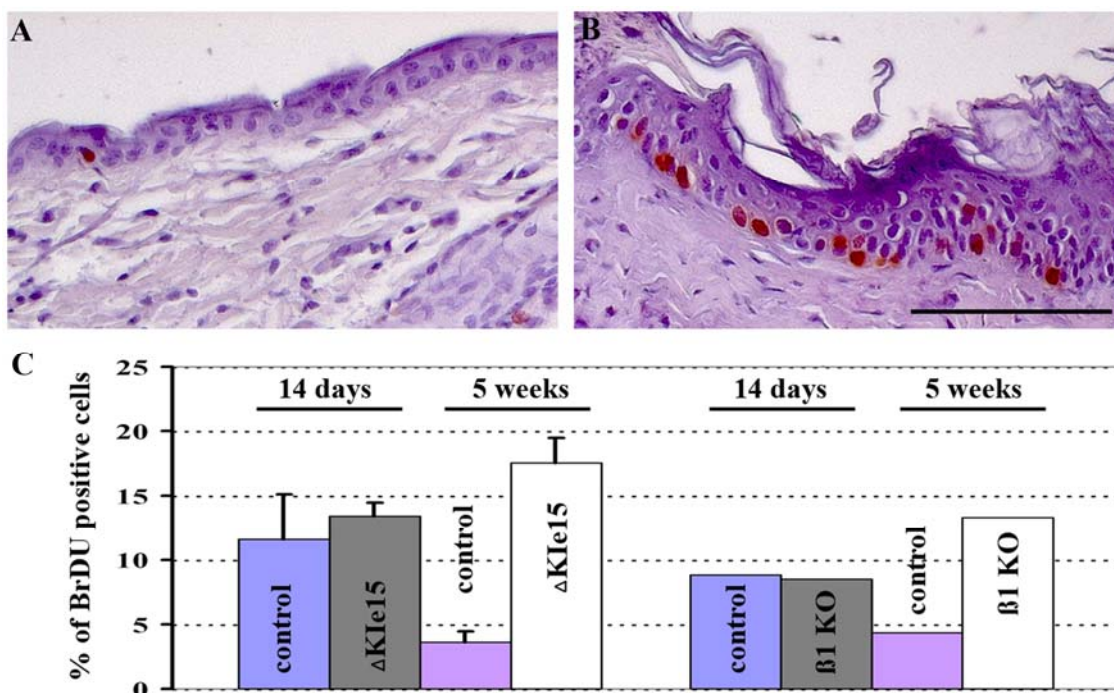


Figure 4.61 Increase in number of BrdU positive, proliferating cells in the interfollicular epidermis of Δ K1e15 and β 1-null mice at five weeks of age. Hyperproliferative epidermis of 5 weeks mutant mice is shown (B), whereas in the control (A) only few cells proliferate. BrdU, brown; counterstaining, haematoxylin. In (C) quantification of BrdU positive cells in the interfollicular epidermis of Δ K1e15 (n=2) and β 1KO (n=1), together with the matched controls is shown. Scale bar = 50 μ m.

We then checked keratinocytes proliferation also in 14 days and 5 weeks β 1 integrin conditional knockout mice and obtained similar results to the deletion mutant (Figure 4.61 C). This increased proliferation from birth to 5 weeks of age could be due to proliferation promoting cytokines or growth factors released during the inflammation that occurs in response to the decaying hair follicles (Brakebusch et al., 2000). Alternatively, it could be due to the expansion and proliferation of wild type stem cells (see Figure 4.34 and Figure 4.57).

Since the Δ 759-771 deletion in the β 1 integrin cytoplasmic domain was associated with defective FAK signalling *in vitro* (Lin et al., 1997), we checked for the phosphorylation of FAK in our mutant mice *in vivo*. No difference between 14 days control and mutant Δ K1e15 mice could be found (Figure 4.62). However, similarly to the data reported for the YY/FFK1e16 mice, the pY397 was only detected in suprabasal cells, both in control and mutant mice.

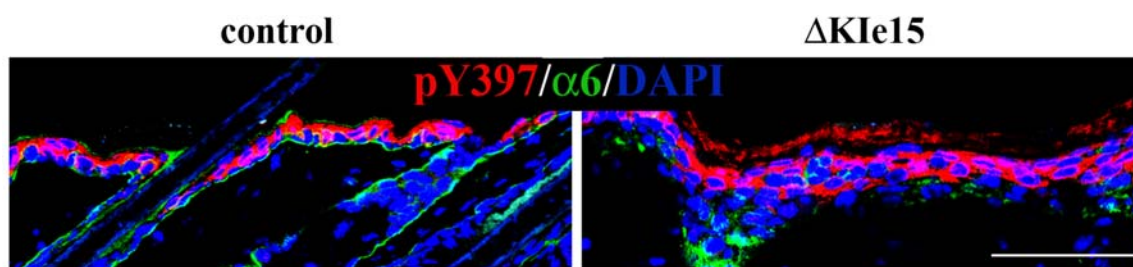


Figure 4.62 No difference in the staining pattern for FAK autophosphorylation in the Δ Kle15 mutant mice. FAK autophosphorylation is similar in the mutant and control mice at the age of 14 days. Notably only the suprabasal cells are stained. Scale bar = 50 μ m.

Finally, to assess whether the truncated β 1 integrin has the ability to bind to certain cytoplasmic molecules, known to be associated with β 1 integrin (Liu et al., 2000), we stained sections from 14 days old mice for ILK, talin and ICAP-1. Staining for ICAP-1 and talin revealed strong variations between different regions of the Δ Kle15, β 1fl/fl K5Cre and control skin. While in some areas the staining was found in the cytoplasm in others it was concentrated at the cell membrane. The subcellular distribution of ILK, however, was impaired in the β 1-null skin. ILK was clearly found in the cytoplasm of these mice, while in the Δ Kle15 and control mice the majority of the basal keratinocytes displayed a rather a membrane-associated pattern (Figure 4.63).

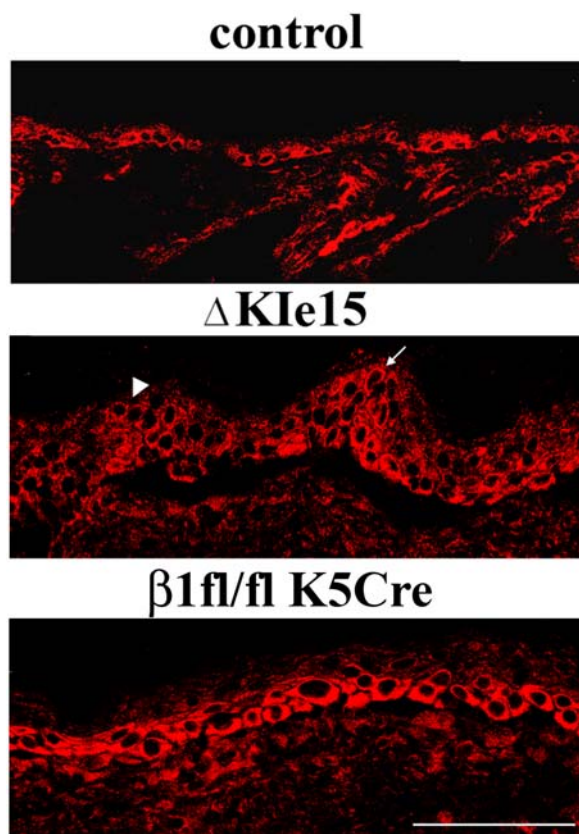


Figure 4.63 The truncated integrin in the Δ Kle15 mouse is not functional. ILK staining on sections from 14

days old mutant mice is shown. Arrowhead indicates membrane staining, whereas arrow shows cytoplasmic localization of ILK. Scale bar = 50 μ m.

Since ILK is known to be an important regulator of integrin avidity and may also be involved in outside-in signalling (Sakai et al., 2003), these results suggest that the truncated β 1 integrin is able to bind ILK, but not able to provide ILK dependent inside-out and outside-in signalling, leading to a β 1-null like phenotype. To dissect the contribution of defective inside-out and inside-in signalling, we will in the future analyze primary keratinocytes from these mice *in vitro*. Cross-linking of truncated integrin receptors by β 1 integrin antibodies will overcome any outside-in signalling defect and exclude its contribution to the phenotype.

5 Discussion

Cell migration is a highly integrated, multistep process, which requires constant generation and disassembly of adhesion sites, cell polarization, protrusion and extension formation as well as cell contraction. All these processes, have been shown to be regulated by an extensive cross-talk between integrins and Rho GTPases, among them Cdc42.

The aim of this study was to investigate the role of integrins and Cdc42 in regulating cell migration and in particular the cross-talk between these two molecules required for the cells to move. In addition the integrin structure–function relationship in migration associated events was studied.

5.1 Cdc42 contributes to actin cytoskeleton organization but is not essential for integrin mediated adhesion, cell spreading and filopodia formation

5.1.1 Cdc42 does not regulate integrin avidity

During migration cells have to generate new adhesion sites, which stabilize newly formed protrusions and generate forces required for cell contraction. On the other hand a migrating cell has to disassembly adhesion sites at the cell rear in order to move forward (Ridley et al., 2003). The integrin receptor family represents the major group of cell surface receptors mediating adhesion to the extracellular matrix. Rho GTPases have been proposed to control clustering of integrin receptors and thus integrin mediated cell adhesion (Schwartz and Shattil, 2000). Whereas clustering of ligated integrins within focal complexes was shown to require Cdc42 or Rac1 activation, integrin clustering within focal adhesions was proposed to depend on Rho activity (Nobes and Hall, 1995; Hall, 1998; Rottner et al., 1999). In line with these findings, preliminary data reported by Chen et al. (2000), suggested severely defective adhesion of these Cdc42 deficient fibroblastoid cells (Chen et al., 2000). We tested adhesion of our fibroblastoid Cdc42-deficient cells on several extracellular matrix proteins and found no indication for an impaired adhesion to laminin, fibronectin or vitronectin (see Figure 4.5 A). Furthermore, expression of $\beta 1$, $\beta 3$, $\alpha 5$, αv and $\alpha 2$ integrins were not changed in Cdc42-deficient cells (see Figure 4.5 B) and focal contact formation as assessed by paxillin staining was normal as well (see Figure 4.4). These data indicate that Cdc42 does not regulate integrin expression on the cell surface of fibroblastoid cells, and moreover, since Cdc42 is not

required for integrin mediated adhesion to the extracellular matrix, it does not control integrin avidity.

5.1.2 Filopodia can form independently of Cdc42

Upon integrin mediated adhesion, Cdc42 was shown to be activated at the cell membrane and to promote actin filament polymerization. Actin polymerization results in the formation of protrusive structures and thereby promotes cell spreading and cell migration (Price et al., 1998; Itoh et al., 2002).

Filopodia are finger-like, active protrusions that emerge from the cell periphery in an actin polymerization-dependent manner (Small et al., 2002). These structures have been proposed to function in sensing environmental cues to guide cell migration or axon extension (Passey et al., 2004). Only by time-lapse microscopy can filopodia be distinguished from retraction fibres, which result from incomplete membrane retraction. Expression of constitutively active Cdc42 induces the formation of actively protruding filopodia with or without concomitant lamellipodium formation, depending on the cell type. Dominant negative inhibition of Cdc42 in fibroblastoid cell lines and deletion of the Cdc42 gene in ES cells was concluded to prevent the formation of filopodia and suggested an essential role for Cdc42 in this process (Kozma et al., 1995; Nobes and Hall, 1999; Chen et al., 2000). We have analyzed Cdc42-deficient fibroblastoid and ES cells by time lapse video microscopy and found that both cell types are capable of constitutive filopodium and lamellipodium formation (see Figure 4.10 and Figure 4.11), demonstrating that Cdc42 is not required for the formation of these protrusions. Interestingly, in contrast to previous reports, also the dnCdc42 expressing cells were capable of filopodia formation. It is however quite possible that the expression level of the mutant Cdc42 was not high enough to completely suppress filopodia formation and that at higher levels of expression filopodia formation would be completely abolished.

Besides Cdc42, other Rho GTPases such as Rif (Ellis and Mellor, 2000), TC10 (Neudauer et al., 1998; Murphy et al., 1999; Vignal et al., 2000), TCL (Abe et al., 2003) and Wrch-1 (Tao et al., 2001) were suggested to induce filopodium formation, although only few studies used time lapse microscopy to distinguish actively protruding filopodia from retraction fibres. Furthermore, the appearance of the filopodia induced by activated mutant forms of these Rho GTPases was often rather different from Cdc42-induced protrusions and cell type dependent (Saras et al., 2004). Only for Rif it was shown that dnCdc42 did not block filopodium formation (Ellis and Mellor, 2000). Our data prove that there are Cdc42-independent

pathways of formation of filopodia and that filopodium formation by other Rho GTPases is not generally due to cross-activation of Cdc42.

Protrusion formation and thus filopodia and lamellipodia formation represents a crucial step in integrin induced cell spreading, since dominant negative mutant of Cdc42 and Rac1 were shown to inhibit cell spreading in NIH 3T3 cells (Price et al., 1998). Cdc42 null cells showed normal spreading kinetics (see Figure 4.6), but the final cell area was significantly smaller than that of control cells (see Figure 4.3) indicating that Cdc42 does contribute to a spread cell morphology.

5.1.3 Reduced Rac1 activity in the absence of Cdc42

The Rho GTPases are regulated by a variety of regulatory proteins like GEFs, GDIs and GAPs, which are controlled by different signalling pathways, for example by integrins, growth factors receptors and cytokine receptors. In addition, there is more and more evidence for a complex crosstalk between the distinct Rho GTPases, by which the amount of activated proteins is influenced (Evers et al., 2000). Cdc42 was previously shown to cross-activate Rac1 in mammalian cells, since constitutive activation of Cdc42 resulted in lamellipodium formation which could be blocked by dnRac1 (Nobes and Hall, 1995; Kozma et al., 1995). More recently also a possible mechanism of this activation has been described (DerMardirossian et al., 2004; Nishimura et al., 2005). It was, however, not clear to which extent Cdc42 contributes to active Rac1 levels. We showed now that in fibroblastoid cells about 50% of Rac1 activity derives from the presence of Cdc42, while 50% are independent of Cdc42. This decrease in Rac1 activity was not related to a decrease in the level of Rac1 protein which was not changed in the absence of Cdc42 (see Figure 4.8).

Since dominant negative forms of Rho GTPases sequester GEFs, which are not always specific for a single Rho GTPase, it was speculated that the inhibitory effects of dnRho GTPases are not specific for a single Rho GTPase (Feig, 1999). Indeed, we could show a further reduction of active Rac1 levels in Cdc42-null cells by dnCdc42 expression, demonstrating that dnCdc42 reduces Rac1 activity also by non-specific inhibition, conceivably by blocking GEFs shared by Cdc42 and Rac1 (see Figure 4.8). This finding raises the possibility that also cellular effects observed using dominant negative mutants are not entirely specific. As discussed in the next paragraphs we could also experimentally prove this hypothesis.

5.1.4 Cdc42 regulates cell morphology

Integrins have been shown to regulate cell morphology not only by influencing protrusion formation but also by regulating Rho activity and thereby stress fibre and tension formation (Price et al., 1998). In addition, there is evidence for Cdc42 to regulate RhoA activity, both directly and indirectly (Evers et al., 2000). Investigation of the cell morphology of our fibroblastoid Cdc42 deficient cells revealed that lack of Cdc42 results in elongated cell shape, reflected by an increase in cell elongation ratio and decreased cell area (see Figure 4.3). This effect was even more pronounced when dominant negative Cdc42 was expressed in these cells. Both, Cdc42 null and control cells formed stress fibres, but while in control cells differentially oriented groups of stress fibres could be identified, in the mutant cells nearly all stress fibres appeared to be parallel to each other and to the long axis of the cell (see Figure 4.4) indicating an important role of Cdc42 in stress fibres organization. To test possible cross-talk between Cdc42 and RhoA, which is known to regulate stress fibre formation, we investigated the RhoA activity in the Cdc42-null cells. The pull down analysis for active RhoA revealed no difference between these cells and cells expressing normal levels of Cdc42 (see Figure 4.9), suggesting that Cdc42 is not regulating RhoA activity in our cells, at least not at levels detectable in total lysates. Furthermore, it indicates no or very low cross-regulation of RhoA activity by Cdc42 and activation of RhoA by GEFs shared between Cdc42 and RhoA. Finally, these data suggest that Cdc42 can influence stress fibre formation independently of RhoA activity.

We show that loss of Cdc42 results in a decrease of Rac1 activity (see Figure 4.8). Similar to our cells Rac1-deficient macrophages are more elongated than control cells (Wells et al., 2004). This similar phenotype suggested that the morphological alterations observed in our Cdc42-null cells could result from the reduced Rac1 activity. To test this hypothesis, the constitutively active mutant form of Rac1 was overexpressed in cells lacking the functional Cdc42 gene. Upon infection these cells showed increased cell area and displayed a highly migratory phenotype with strong lamellipodium formation, suggesting that the reduced cell area in Cdc42 null cells is dependent on the reduction of Rac1 activity. The increased migration in comparison to control cells is conceivably due to an increased activity of Rac1 in cells expressing constitutively Rac1 compared to control cells.

Interestingly, Rac-1 null macrophages showed reduced adhesion to cell culture plastic and fibronectin (Wells et al., 2004), different from Cdc42-null fibroblasts. Whether this is due to cell type specific differences or to the only partial reduction of Rac1 activity in the absence of Cdc42 remains to be tested.

5.1.5 Cdc42 and Cdc42 related proteins regulate tail retraction in migrating cells

In order to move, cells not only have to generate new adhesion sites, but also to disassemble existing ones at the rear of the cell. RhoA activation was suggested to be crucial for the decrease in integrin mediated adhesion at the trailing edge (Price et al., 1998; Ridley et al., 2003). Here we show that Cdc42 null cells and even more prominently cells reconstituted with dominant negative Cdc42 have defective rear detachment resulting in increase of the tail length in the mutant cells (see Figure 4.12). However, both cell lines expressed normal levels of active RhoA (see Figure 4.9), suggesting that in fibroblastoid cells not RhoA, but rather Cdc42 and other members of the Rho GTPases family inhibitable by dnCdc42 regulate rear detachment, or that local changes in RhoA activity are too small to be detected in total lysates of our fibroblastoid cells.

5.2 Cdc42 is not important for the speed of migration, but regulates together with other Rho GTPases directionality of migration

5.2.1 Cdc42 has no major impact on wound closure speed

In previous studies, primary fibroblasts expressing dnCdc42 or WASp(201-321), which binds and inhibits Cdc42, showed a 50% reduction of wound closure in an *in vitro* wound closure assay suggesting an important function of Cdc42 in directed migration (Nobes and Hall, 1999). Our data revealed that Cdc42 has no major impact on migration speed in wound closure assays (see Figure 4.13 and Figure 4.19), reflected by a rather normal capacity of these cells to close the wounds, both in mutant fibroblastoid cells and endodermal cells. To the contrary, introduction of the dominant negative Cdc42 into Cdc42-null fibroblastoid cells resulted in severely impaired wound closure similarly to previous reports (Nobes and Hall, 1999; see Figure 4.13). This suggests that other Rho GTPases than Cdc42, which are non specifically inhibited by dnCdc42, contribute to the migration speed. One possible candidate is Rac1, since inhibition of Rac1 in primary rat fibroblasts with dnRac1 resulted in complete block of migration upon wound-induced cues (Nobes and Hall, 1999). However, reduction of Rac1 activity to 50% in Cdc42-null cells had no major effect, and only further inhibition to 36% by dnCdc42 correlated with decreased migration speed. Since in control cells we could not detect any change in Rac1 activity upon migration, the reduction of Rac1 activity observed in non-migrating mutant cells conceivably reflects reduced Rac1 activity in migrating Cdc42-null cells and cells expressing dnCdc42.

5.2.2 Polarized protrusion formation in Cdc42-null cells

For a cell to migrate, it must be polarized, meaning that processes at the front and the back of a moving cell must be different. Thus, polarized protrusion formation is a key event in directed cell migration in response to wound-induced cues. In primary rat fibroblasts, expression of dnCdc42 was found to result in a complete loss of cell polarization with lamellipodial activity seen all around the cell periphery (Nobes and Hall, 1999; Cau and Hall, 2005). We investigated protrusion formation of our Cdc42-null fibroblastoid cells by time-lapse video microscopy and could show that, the polarized formation of lamellipodia towards the wound is not significantly affected by the loss of Cdc42. In contrast, when dnCdc42 was expressed, cells initially polarized, but could not maintain protrusion formation stably oriented towards the wound (see Figure 4.14). This indicates that polarized protrusion formation can occur independently of Cdc42. Furthermore, other Rho GTPases, which are inhibited by dominant negative Cdc42 also regulate this process.

Recently, Stramer et al. reported that in *Drosophila* Cdc42-deficient hemocytes show a two-fold increased migration speed and an inability to maintain persistent polarity in response to wound-induced cues (Stramer et al., 2005). In our study we analyzed single cell migration in a wounding assay and found that in contrast to insects, mammalian fibroblastoid Cdc42-null cells demonstrate rather stable directionality and no increase in migration speed (see Figure 4.14). However, a certain reduction in directionality was measurable by a decrease of the value of the mean angle vector, a highly sensitive indicator of directed migration (see Figure 4.14). Expression of dominant-negative Cdc42 in Cdc42-deficient cells resulted in a significantly decreased single cell velocity during wound closure, opposite to the increased speed of Cdc42-null hemocytes in *Drosophila* (Stramer et al., 2005), and a further reduction of the mean angle vector (see Figure 4.14).

Interestingly, dominant negative inhibition of Cdc42 in hemocytes resulted in the same migratory phenotype as inactivation of the Cdc42 gene giving no evidence of other Rho GTPases with overlapping functions in *Drosophila* (Stramer et al., 2005). Indeed, the Cdc42 subfamily in *Drosophila* consists only of the Cdc42 protein, whereas in mammals besides Cdc42, Cdc42-like Rho GTPases, such as TC10, TCL and Wrch-1 and -2 can be found (Ridley, 2001; Wennerberg and Der, 2004). These structurally highly related GTPases of the Cdc42 subfamily are possible candidates for Rho GTPases with redundant functions (Wennerberg and Der, 2004). Expression analysis in the fibroblastoid cells indicated that TC10 and Wrch-2 are expressed in fibroblastoid cells at medium levels, while TCL and Wrch-1 were low or non-detectable. Therefore, TC10 and Wrch-2 are good candidates for

proteins to share similar functions with Cdc42, compensating for the loss of Cdc42 in our fibroblastoid cells. Since no guanine exchange factors for TC10 or Wrch-2 have been identified so far, it is very likely that these GTPases share the regulatory proteins, with other Rho GTPases. Therefore, it is well conceivable that TC10 and Wrch-2 are inhibited by dnCdc42.

5.2.3 Cdc42 contributes to Golgi apparatus re-orientation during wounding induced migration

In migrating fibroblasts polarised protrusion formation is accompanied by the reorientation of the microtubule-organising centre (MTOC) and the Golgi apparatus towards the migrating direction as well as temporal capture and stabilization of specific microtubule (MT) plus ends near the leading edge (Fukata et al., 2003). Expression of dnCdc42 in rat fibroblasts not only interfered with polarized protrusion formation, but completely blocked the re-orientation of the Golgi apparatus into the direction of migration (Nobes and Hall, 1999). Since the Golgi apparatus is always positioned around the MTOC, these data suggest an essential role of Cdc42 in the polarization of the microtubule system (Rios and Bornens, 2003). Our results, however, revealed that in the absence of Cdc42 the re-orientation of the Golgi was reduced in fibroblastoid cells, but not completely blocked (see Figure 4.15), contrary to previous suggestions (Nobes and Hall, 1999). In endodermal cells, which are fast migrating cells with a lower directionality than fibroblastoid cells, the Golgi polarization was similar in control and Cdc42 mutant cells (see Figure 4.20). When dnCdc42 was expressed in Cdc42-null fibroblastoid cells, Golgi re-orientation was abrogated similar to the results previously obtained with astrocytes and primary fibroblasts (Nobes and Hall, 1999; Etienne-Manneville and Hall, 2001; see Figure 4.15). Again, Cdc42-like Rho GTPases seem to be involved in this aspect of cell polarity.

Interestingly, at expression levels of the dominant negative Cdc42 mutant, which completely abrogated Golgi re-orientation during directed migration, filopodium and lamellipodium formation was not completely suppressed. This suggests that filopodium formation is regulated by GEFs different from the ones controlling cell polarization in migrating fibroblasts. Thus, in our system, the molecular mechanism of protrusion formation seems to be independent of the mechanism defining the subcellular site where the protrusions are formed, similarly to previous observations (Nobes and Hall, 1999). Very recent data from the Hall laboratory suggested a mechanism for polarized protrusion formation. While the Cdc42-Gsk3 β related pathway is suggested to control Golgi polarization (this issue is also discussed

in the next paragraph), a PAK and β -PIX related pathway is ascribed to control protrusion formation. These data, however, are in contrast to some other reports showing that in migrating Vero cells Cdc42 and Rac1 together control both lamellipodium formation at the leading edge and re-orientation of the Golgi-associated microtubule organizing center by binding to IQGAP-1 (Watanabe et al., 2004).

5.2.4 Golgi reorientation in fibroblastoid cells does not correlate with changes in Gsk3 β phosphorylation

In astrocytes and in primary rat fibroblasts, the polarization of the Golgi was suggested to be controlled via Cdc42-mediated phosphorylation of Gsk3 β (Etienne-Manneville and Hall, 2003; Cau and Hall, 2005). It was shown that β 1 integrins mediate transient Cdc42 activation at the leading edge of migrating astrocytes, thereby leading to a Cdc42-dependent translocation of the Par6-PKC ζ complex to the cell membrane and subsequent activation of PKC ζ . Activation of PKC ζ in turn results in Gsk3 β phosphorylation, which inactivates Gsk3 β kinase activity. Inactivation of Gsk3 β at the leading edge was proposed to allow APC to stabilize the growing ends of microtubules, and thus provide a mechanism for MTOC polarization (Etienne-Manneville and Hall, 2001). In our system, however, no indication was found for an involvement of migration-induced phosphorylation of Gsk3 β in the establishment of cell polarity in migrating fibroblastoid cells (see Figure 4.17), suggesting different effector pathways in fibroblastoid cells *versus* primary rat fibroblasts and astrocytes.

In astrocytes phosphorylation of Gsk3 β was also required for the stabilization of β -catenin at the leading edge (Etienne-Manneville and Hall, 2001). In none of the fibroblastoid cells investigated in this study obvious stabilization of β -catenin could have been observed. In fact, β -catenin was always present at the leading edge of migrating cells independent from Golgi re-orientation or maintenance of directionality during migration (see Figure 4.16 and Figure 4.17), indicating that subcellular positioning of this protein neither requires stabilization of β -catenin nor Gsk3 β phosphorylation. However, an involvement of Gsk3 β phosphorylation in the regulation of Golgi re-orientation in fibroblastoid cells cannot be excluded, because local changes might be non-detectable in analysis of total cell lysates as carried out by us.

Integrin mediated activation of Cdc42 was also shown to contribute to other pathways than the Par6-PKC ζ -Gsk3 β cascade. Cdc42 has been shown to participate in integrin mediated activation of the lipid kinase PI 3-kinase, and of the protein kinases Akt and Cdc42 associated tyrosine kinase-2 (ACK-2) and Erk, although cell type specific differences were reported

(Frost et al., 1997; Chen et al., 2000; Zugasti et al., 2001). Rac1, which as we showed, is activated to a great deal by Cdc42, has been implicated in Erk and JNK activation (Clark et al., 1998; Dolfi et al., 1998; Yang et al., 1999). These signalling events could be important for fibroblast migration, since there is increasing evidence that particularly Erk and JNK can regulate cell migration by phosphorylating cytoskeletal components as well as by modifying gene expression. To check whether differences in basal activity of these proteins or in activation of these molecules during migration could contribute to the migratory phenotypes, we tested activation of these molecules after wounding. In control cells we were unable to detect significant activation of p38 or Akt upon wounding, whereas activation of Erk and JNK was observed as expected. However, this activation was not significantly changed in Cdc42 deficient cells or cells expressing dnCdc42 (see Figure 4.17). Although in case of JNK a trend for reduced activation and faster decay of the signal was observed in mutant cell lines, it is not clear whether this is sufficient to cause the observed migratory defects. We would speculate, that other Cdc42 dependent pathways such as activation of PAK kinases are involved in polarization and migration of fibroblastoid cells (Bokoch, 2003). However, we cannot exclude that Erk, JNK, p38 or Akt phosphorylation are changed only locally, to an extent not detectable in total cell lysates.

5.3 Reduced β 1 integrin expression in relation to keratinocyte migration in skin development and maintenance in vivo and in keratinocytes in vitro

5.3.1 Reduction of β 1 integrin expression results in abnormal skin development

β 1 integrins are crucial for skin development and maintenance *in vivo*, since mice deprived of the β 1 integrin receptors in a skin restricted manner were reported to develop a severe hair coat phenotype (Brakebusch et al., 2000; Raghavan et al., 2000). This phenotype was characterized by progressive hair loss, malformation of the hair follicles, hyperthickened epidermis, blister formation, defective laminin 5 deposition at the dermal-epidermal junction and dermal fibrosis. In addition these mice had reduced proliferation in the interfollicular epidermis and the hair matrix cells (Brakebusch et al., 2000; Raghavan et al., 2000).

Here we generated a hypomorph mouse, which due to the insertion of a wild type cDNA encoding for the entire cytoplasmic domain of β 1 integrin and a *loxP* site into exon 15 of the

$\beta 1$ integrin gene, expresses only 20% of normal $\beta 1$ integrin levels (see Figure 4.24). Analysis of these mice revealed that reduced expression levels of $\beta 1$ integrin are not sufficient to support normal hair follicle development and interfollicular epidermis organization (see Figure 4.22 and Figure 4.25). In addition, reduced $\beta 1$ integrin expression cannot prevent development of fibrosis due to an inflammatory reaction in the mutant skin (see Figure 4.30). However, all these phenotypes of hypomorphic mice are less severe and much more delayed in time, when compared to mice lacking the $\beta 1$ integrin gene in skin. Nevertheless, these data corroborates the essential role of $\beta 1$ integrins in the maintenance of skin integrity and the hair follicle development.

Integrin mediated adhesion to the extracellular matrix and signals provided by growth factors are jointly required to stimulate cyclin-dependent kinases resulting in cell cycle progression through the G1 phase. Many of these effects are mediated by the members of the small Rho GTPases family (Danen and Yamada, 2001; Mettouchi et al., 2001; Welsh et al., 2001). Interestingly, reduction in $\beta 1$ integrin expression did not interfere with proliferation of the interfollicular hypomorphic keratinocytes, but resulted in reduced proliferation of the hair matrix cells (see Figure 4.43). In normal skin, $\beta 1$ integrin is strongly expressed in the ORS and the matrix cells of the hair follicle. During hair follicle morphogenesis, the proliferation of matrix cells halts at the beginning of catagen and is re-initiated at the beginning of anagen. The rapid proliferation of the matrix cells leads to the extension of the hair follicle into the subcutis of the skin. It is quite likely that, similarly as proposed for the cells expressing no $\beta 1$ integrin (Brakebusch et al., 2000), hair follicle stem cells with reduced levels of this cell surface receptor are not efficiently activated at the beginning of anagen. Alternatively, stem cells can be activated, but have a migration defect. It is also possible that $\beta 1$ integrin is essential to maintain the follicular stem cell population.

Besides hemidesmosomes the basement membrane is composed of anchoring filaments and anchoring fibrils. Blister formation observed in the $\beta 1$ skin specific knockout mice was ascribed to reduced adhesion of the basal keratinocytes to the underlying basement membrane, due to the loss or decreased expression of laminin receptors $\alpha 3\beta 1$ integrin, dystroglycan and the hemidesmosomal integrin $\alpha 6\beta 4$. These might cause the incomplete processing and irregular deposition of the basement membrane component laminin 5 (Brakebusch et al., 2000). Since laminin 5 is crucial for basement membrane integrity, it might secondarily lead to defective basement membrane maintenance and aberrant deposition of other basement membrane molecules such as nidogen and collagen IV.

In contrast to the $\beta 1$ -null mouse, however, the $\beta 1$ hypomorphic mouse does not develop blisters (see Figure 4.25). Both FACS analysis on hypomorphic keratinocytes and immunostainings on skin sections for the $\alpha 6$ and $\beta 4$ integrins revealed that while $\beta 1$ integrin expression is severely reduced, expression levels of the $\alpha 6\beta 4$ cell surface receptor are normal (see Figure 4.23 and Figure 4.24). Mutations in the genes for $\alpha 6$ or $\beta 4$ integrin result in severe skin detachment both in human and mice (Georges-Labouesse et al., 1996; van der Neut et al., 1996), much more severe than those observed in the $\beta 1$ -null skin or the $\alpha 3$ knockout skin (DiPersio et al., 1997; Brakebusch et al., 2000). Thus, although the hypomorphic mice express reduced levels of $\beta 1$ integrin and presumably also $\alpha 3$ integrin, normal $\alpha 6\beta 4$ integrin expression might preserve the dermal-epidermal integrity of the skin. Alternatively, the low levels of $\alpha 3\beta 1$ are still sufficient to maintain tight adhesion of basal keratinocytes to the underlying basement membrane. Although LN5 was irregularly deposited in some regions of the dermal-epidermal junction (see Figure 4.27), this did not cause blister formation, suggesting that in the presence of normal hemidesmosomes possible disruption of anchoring fibrils does not influence the dermal-epidermal connection.

5.3.2 $\beta 1$ integrin is essential for the function of stem cells of the skin epithelium

It has been shown previously that high expression of $\beta 1$ integrin is a marker for stem cell-like properties of keratinocyte *in vitro* and that keratinocyte differentiation is associated with a complete downregulation of $\beta 1$ integrin (reviewed by Watt, 2002). FACS analysis of epidermal keratinocytes from normal mice revealed the co-existence of two populations of cells differentially expressing the $\beta 1$ integrins (see Figure 4.24). Since around 25% percent of keratinocytes in a preparation of primary keratinocytes express markers of suprabasal keratinocytes, it is reasonable to assume that the 20% of cells expressing reduced $\beta 1$ integrin levels are the suprabasal keratinocytes. This implicates that cells downregulate $\beta 1$ integrin expression when they differentiate into suprabasal cells, but that the expression is not completely lost as speculated before (Watt, 2002).

Data reported from knockout studies, did not confirm an essential role of $\beta 1$ integrin for epithelial stem cells *in vivo*, since ablation of the $\beta 1$ integrin gene in skin did not result in a complete block of keratinocyte proliferation and did not cause immediate terminal differentiation of all basal keratinocytes (Brakebusch et al., 2000; Raghavan et al., 2000). The analysis of the $\beta 1$ hypomorph mice changed this picture a bit. Although $\beta 1$ integrin seems not

to be essential for keratinocyte proliferation *in vivo*, it promotes expansion of keratinocyte stem cells. With age, β 1-hypomorphic and even more pronounced β 1-null keratinocytes are overgrown by wild type keratinocytes, which at birth are hardly detectable in the epidermis (see Figure 4.23 B and D, and Figure 4.31 A). The Cre mediated recombination of a floxed locus is never 100% efficient, so that there are always some few cells (1 - 3% in the β 1 conditional K5 Cre knockout mice), which escape recombination. In 6 months old hypomorphic mice and 5 weeks old mice with a skin specific knockout of β 1 integrin, cells in which the β 1 gene was not recombined widely repopulate the interfollicular epidermis (see Figure 4.31 and Figure 4.34), demonstrating, that cells expressing normal β 1 integrin levels have a huge competitive advantage against cells expressing low, or no β 1 integrin on the cell surface. This finding indicates a crucial role for β 1 integrin in the maintenance of the epithelial stem cell compartment.

Analysis of the skin of 6 months old hypomorph mice gave also interesting insights into the possible hierarchy of stem cell organization within the skin epithelium. The bulge region of the hair follicle is believed to be the major epidermal stem cell niche of the skin. Stem cells from this region were shown to either stay in the niche, to migrate upwards to the epidermis and the sebaceous glands, or to move down to regenerate the hair follicle (So and Epstein, 2004). Stem cell-like cells are also thought to reside within the basal layer of the epidermis and in sebaceous glands. However, whether bulge cells maintain their multipotency and molecular properties when they exit their niche is still largely a matter of speculation and controversy in the epithelial stem cell field. It is furthermore not clear whether under physiological conditions bulge cells contribute to interfollicular epidermis (Alonso and Fuchs, 2003b; So and Epstein, 2004).

Our findings suggest that stem cells residing in the interfollicular epidermis are rather independent from stem cells residing in the hair follicle, since hypomorphic hair follicles were found in the region of wild type interfollicular epidermis (see Figure 4.31 A). Thus at least in this region the hair follicle stem cells do not contribute to interfollicular epidermis. Although it was suggested that the hair follicle is the major source of stem cells for the adult hair follicle and epidermal homeostasis (Morris et al., 2004; Tumber et al., 2004), there are regions of the human body that have non-follicular skin (e.g. palms, foreskin) and thus cannot possess follicular stem cells. In a recent review So and Epstein Jr (2004) speculated that non-follicular epidermis must have its own reservoir of stem cells because it is unlikely that follicular stem cells migrate relatively large distances to repopulate non-follicular skin. In 6 months old hypomorph mice 40% of cells of the interfollicular epidermis escape the Cre

recombination and only 5% of all hair follicles in the skin do so (see Figure 4.31 A and C). Similarly to the situation described for follicular and non-follicular skin, one could speculate, that it is rather unlikely that stem cells from these limited number of $\beta 1$ integrin expressing hair follicles could repopulate relatively large areas of the epidermis. These observations would support the findings that maintenance of interfollicular epidermis is independent of follicle derived cells (Ghazizadeh and Taichman, 2001).

Conversely, it may even be that epidermal stem cells can repopulate hair follicles, opposite to the previous suggestions. This speculation is based on the observation that wild type hair follicles were only found in wild type epidermis, but not in hypomorph or knockout epidermis. However, more experiments are necessary to substantiate and prove this speculation.

5.3.3 Reduced $\beta 1$ integrin expression is sufficient to mediate keratinocyte migration in vivo

In vivo wound healing studies performed with mice lacking the $\beta 1$ integrin gene in a skin specific manner, revealed a crucial role for this integrin in keratinocyte migration *in vivo* (Grose et al., 2002). Also *in vitro*, $\beta 1$ -null keratinocytes failed to migrate. In addition $\beta 1$ integrins are crucial for cell migration *in vitro* in various other cells types (Gimond et al., 1999; Sakai et al., 1999; Danen et al.; 2005). We now addressed the question, whether reduced $\beta 1$ integrin levels are sufficient to promote keratinocyte migration both *in vivo* and *in vitro*. To assess the migratory response of hypomorphic keratinocytes *in vivo*, we performed wound healing studies with hypomorphic mice at the age of 2 months, where $\beta 1$ integrin expression was reduced to 20% on more than 95% of all basal keratinocytes. Surprisingly, the analysis of 5 days old wounds did not reveal any difference in wound size, morphology, and proliferation of the wound keratinocytes, implicating that reduced $\beta 1$ integrin expression is sufficient to mediate normal wounding-response *in vivo* (see Figure 4.35). Alternatively, an increased expression of $\beta 5$ and $\beta 6$ integrins could compensate for the reduced $\beta 1$ integrin expression, similarly to the speculations proposed by Grose et al. for the skin specific $\beta 1$ conditional knockout mice (Grose et al., 2002). $\beta 5$ and $\beta 6$ integrins themselves are not essential for wound healing, since wound healing in $\beta 5$ and $\beta 6$ skin specific knockout mice was reported to be normal (Huang et al., 1996; Huang et al., 2000a). A third explanation for the normal wound closure in the hypomorph mice and also for the fact that even the wounds in the $\beta 1$ -null skin finally closed, could be the expansion of stem cells not hit by Cre

recombination. As already discussed in the above paragraph these keratinocytes have a competitive advantage over cells expressing no or reduced levels of $\beta 1$ integrin and with time repopulate the mutant skin. Wounding could accelerate this process, since proliferation of hair follicle and epidermal keratinocytes is greatly increased during re-epithelialisation. This could result in a quick expansion of cells expressing normal $\beta 1$ integrin levels, which then are responsible for normal (hypomorph) or incompletely impaired (knockout) migratory response. This hypothesis is currently under investigation.

Finally, we wanted to confirm the *in vivo* migration data by performing wound healing assays *in vitro*. However, keratinocytes expressing reduced amounts of $\beta 1$ integrin fail to spread and survive *in vitro*, thus making it impossible to study directed migration of these cells. The difference between the rather mild defect in the interfollicular epidermis *in vivo* and the severe defects observed *in vitro* can be explained by the absence of the normal three dimensional extracellular matrix environment in a cell culture dish. In our *in vitro* system keratinocytes are cultured on collagen I and fibronectin coated dishes and adhesion to this substratum is only possible via the collagen receptor $\alpha 2\beta 1$ and through the fibronectin receptor $\alpha 5\beta 1$ which is reported to be upregulated upon keratinocyte culture *in vitro* (Watt, 2002). Since the hypomorph keratinocytes have reduced expression levels of the $\beta 1$ integrin heterodimers (see Figure 4.24) they cannot properly adhere and spread on the matrix composed of collagen I and fibronectin. However, the mutant cells express normal levels of the Laminin 5 receptor, $\alpha 6\beta 4$ integrin (see Figure 4.24), thus adhesion mediated events through this integrin receptor might partially rescue lack of $\beta 1$ integrin *in vivo* but not *in vitro*.

5.4 Structure-function analysis of the $\beta 1$ cytoplasmic domain in the regulation of keratinocyte migration

5.4.1 $\beta 1$ integrin activation and integrin mediated migration does not depend on integrin phosphorylation in keratinocytes

The tyrosine residues in the two NPXY motifs of the $\beta 1$ integrin cytoplasmic domains as well as a serine residue and a threonine cluster between these two motifs have been all shown to be phosphorylated upon v-src transformation in fibroblasts. Furthermore, phosphorylation-dephosphorylation cycles for the tyrosine and the serine motifs have both been ascribed to be required for movement of the $\beta 1$ integrins in and out of focal adhesions (Sakai et al., 1998b; Mulrooney et al., 2000) and thus for the regulation of $\beta 1$ integrin activity. The biological

consequence of integrin phosphorylation at the tyrosine motifs has been mainly associated with the impaired talin binding to the NPXY motifs. Talin knockdown by RNAi resulted in inactive $\beta 1$ and $\beta 3$ integrins in a variety of cell types (Tadokoro et al., 2003). Conversely, binding of talin to the NPXY motif disrupts the interaction between the cytoplasmic tails of αIIb and $\beta 3$ integrin resulting in integrin activation, as revealed by NMR and X-ray analysis (Vinogradova et al., 2002; Garcia-Alvares et al., 2003). Phosphorylation of the β tail NPXY motif inhibits talin binding (Tapley et al., 1989). Preventing tyrosine phosphorylation by mutation of the tyrosines to phenylalanine does not interfere with talin binding or with integrin activation by physiological stimuli (Calderwood, 2004). Mutations of the tyrosine to alanine have been shown to interfere with talin binding and strongly inhibited integrin activation of $\alpha \text{IIb}\beta 3$ integrin (Ulmer et al., 2001). The two NPXY motifs of $\beta 3$ integrin are conserved in $\beta 1$ integrin. However, in contrast to $\alpha \text{IIb}\beta 3$, mutation of the two cytoplasmic tyrosines of $\beta 1$ integrin to phenylalanine resulted in impaired migration, enhanced fibronectin assembly, increased number of focal adhesions and defective adhesion (Sakai et al., 1998a and 1998b, Stroeken et al., 2000). Based on these results the tyrosine to phenylalanine mutation was postulated to increase $\beta 1$ integrin activity by preventing talin removal by tyrosine phosphorylation.

As mentioned above, loss of $\beta 1$ integrin in skin results in a severe developmental phenotype and defective wound healing due to impaired keratinocyte migration (Brakebusch et al., 2000; Raghavan et al., 2000). However, not much is known about the downstream signalling events missing in the absence of $\beta 1$ integrin, which might contribute to these phenotypes. In order to investigate the role of $\beta 1$ integrin phosphorylation for keratinocyte function and migration *in vivo*, we generated knockin mice, in which the endogenous $\beta 1$ integrin was replaced by an YY783/795FF mutant which cannot be tyrosine-phosphorylated. Surprisingly, epidermis and hair follicles of knockin mice which in keratinocytes express only the mutated $\beta 1$ integrin, did not reveal any abnormalities when compared to the development of normal mice (see paragraph 4.2.1.5.1). Based on these data we do not have any evidence for increased activity of YY783/795FF $\beta 1$ integrin and for involvement of integrin phosphorylation at tyrosines in the regulation of this process *in vivo*. Wound healing studies in these mice will reveal whether in such a disease model keratinocytes expressing the mutated integrin show a phenotype.

Since all data reported up to now for the $\beta 1$ YY783/795FF mutation were obtained by *in vitro* experiments, it could well be that the lack of any phenotype *in vivo* could be explained by the difference between the *in vitro* and *in vivo* system. Compensatory mechanisms present *in*

vivo, but absent *in vitro* could rescue the mutant phenotype. Therefore, we tested whether the mutated keratinocytes, when placed in a two dimensional environment display some of the phenotypes described in the literature. However, also these investigations of the cellular phenotype of keratinocytes isolated from the mutant mice did not reveal any differences to normal keratinocytes. In contrast to the data reported for the fibroblastoid cells, $\beta 1^{YY783/795FF}$ keratinocytes had normal spreading kinetics on collagen I and fibronectin coated matrix and normal migration in *in vitro* wound healing assays. Furthermore, integrin dependent autophosphorylation of FAK, spreading and focal adhesion formation was fully preserved. All these cellular processes were described to be defective in the fibroblastoid cells (Sakai et al., 1998a and 1998b; Wennerberg et al., 2000). In addition, we could show that the integrin effectors Erk and paxillin are normally activated in keratinocytes upon wounding induced stimuli. No evidence was found for a constitutive activation of $YY783/795FF$ $\beta 1$ integrin in the keratinocytes, suggesting that phosphorylation of the $\beta 1$ integrin NPXY motifs is not crucial for $\beta 1$ integrin function in keratinocytes *in vitro*.

Apart from the integrin phosphorylation, other mechanisms have been described to displace talin from the $\beta 1$ integrin cytoplasmic tails. ICAP-1 was shown to bind to the same region of the $\beta 1$ integrin tail as talin and was proposed to shift integrin activity into the inactive state and thus antagonize talin action (Bouvard et al., 2003). PIPKI γ -90 was found to compete with integrin β tails for overlapping binding sites in the talin head domain. Thus, under some conditions PIPKI γ -90 might also inhibit integrin activation by displacing talin from β tails (Barsukov et al., 2003). Since the $\beta 1$ integrin cytoplasmic tails were never shown to be phosphorylated in keratinocytes, it could well be that the tyrosine residues in the NPXY motifs are not phosphorylated in this cell type and thus, one of the above described mechanisms rather than phosphorylation regulates integrin-talin interaction and integrin activation in keratinocytes. This would explain why mutations of the tyrosine residues to non-phosphorylatable phenylalanines do not interfere with normal keratinocyte function both *in vivo* and *in vitro*. Since in the sequence of the leukocyte integrin $\beta 2$ both tyrosine residues in the $\beta 1$ integrin NPXY motifs are exchanged to phenylalanines, also $\beta 2$ activation must be regulated independent from tyrosine phosphorylation. Independent of whether $\beta 1$ is tyrosine phosphorylated in keratinocytes or not, our data demonstrate that for $\beta 1$ integrin inside-out signalling regulation in keratinocytes other activation mechanisms than phosphorylation are important.

To clarify whether the discrepancy between the crucial role of integrin phosphorylation in fibroblastoid cells *in vitro* and the absence of any major function in keratinocytes, is related to cell type specificity, mice ubiquitously expressing the YY783/795FF mutant $\beta 1$ integrin will be generated. In addition, primary mouse embryonic fibroblasts (MEF's) from the mutant mice will be established. Furthermore, it will be important to check with antibodies recognizing the active conformation of $\beta 1$ integrin (e.g. 9EG7 antibody), whether the YY783/795FF mutation induces conformational changes indicative for activated integrins. Finally, effects of v-src transformation in the mutated MEF's and / or keratinocytes will be analyzed. V-src transformation of wild type fibroblastoid cells was described to result in a severe cellular phenotype, characterized by loss of adhesion, defective spreading and complete block of migration. Only in v-src transfected fibroblasts, phosphorylation of the tyrosine residues of $\beta 1$ integrin was detected (Sakai et al., 2001). Therefore, perhaps only in the presence of v-src YY783/795FF keratinocytes will display a defect.

Analysis of mice carrying mutations at an other potential phosphorylation site in the $\beta 1$ integrin cytoplasmic domain, the serine residue S785, located in-between the two NPXY motif, could not confirm that phosphorylation of S785 regulates $\beta 1$ integrin function. Mice carrying the S785D mutation, mimicking a phosphorylated serine, or the S785A mutation, which cannot be phosphorylated, both have fully developed hair coats, are viable and fertile. This indicates that also phosphorylation of this serine residue does not play a crucial role in integrin function in keratinocytes. Since the S785D mutation was homozygously expressed in all cells of the mutant mice, this implicates that also in non-keratinocyte cells phosphorylation of the serine residue is not important for integrin regulation. Future analysis of these mice on cellular level and in wound healing experiments might reveal subtle or stress model related phenotypes.

Fibroblasts expressing v-src showed phosphorylation of threonine 778 and 789 (Sakai et al., 2001). To test the importance of these phosphorylation sites, fibroblastoid cells expressing only the TT788/789AA mutant forms of $\beta 1$ integrin were generated. Analysis of these cells showed that TT778/789AA $\beta 1$ integrin does not support integrin mediated adhesion, spreading and fibronectin fibril formation, as well as invasion *in vivo*. Furthermore, the conformation of the extracellular domain was reported to be shifted towards the inactive state as measured by the 9EG7 antibody (Wennerberg et al., 1998; Stroeken et al., 2000; Gustavsson et al., 2002). We generated mice heterozygous for the TT788/789AA $\beta 1$ integrin mutant. Inter-crossing of these mice with skin specific knockout mice will elucidate the

importance of these residues in keratinocytes. With these mice, all possible phosphorylation sites of $\beta 1$ integrin have been mutated *in vivo*.

5.4.2 Loss of salt bridge formation between $\beta 1$ integrin and the α subunits does not cause $\beta 1$ integrin activation in keratinocytes *in vivo*

The cytoplasmic domains of α and β integrin subunits are connected via a juxtamembrane salt bridge between an aspartic residue in the β subunit and an arginine in the α subunit. Mutation of a corresponding aspartic acid to an alanine was shown to disrupt the formation of the salt bridge between the α IIb and $\beta 3$ integrin subunit and to result in an activated integrin. Enhanced activation of the mutated α IIb $\beta 3$ integrin was characterized by increased fibronectin assembly and enhanced binding to the PAC1 antibody, specific for the active conformation of α IIb $\beta 3$ integrin (Hughes et al., 1996). Therefore, the salt bridge is believed to keep integrins in an inactive state (Calderwood, 2004). Analysis of $\beta 1$ D759A mutants in fibroblastoid cells suggested that also $\beta 1$ integrins are activated by disruption of this salt bridge, since fibronectin assembly and binding to soluble fibronectin was increased (Sakai et al., 1998b). As for the YY783/795FF mutants we expected aberrant adhesion and migration of mutant keratinocytes resulting in impaired skin development and maintenance. However, detailed analysis of the skin morphology and hair follicle development of mice expressing in keratinocyte only the D759A mutant of $\beta 1$ integrin, revealed normal skin and hair follicle maintenance. These data suggest that either disruption of the salt bridge between the D759 residue on the $\beta 1$ integrin chain and the R995 residue in the α subunit does not activate integrin in keratinocytes *in vivo*, or, less likely, that the consequences of such activation are more subtle than expected. Interestingly, the arginine to aspartic acid mutation in the $\alpha 6A$ tail, which also disrupts a corresponding salt bridge, fails to activate $\alpha 6A\beta 1$ integrin (De Melker et al., 1997). Furthermore, mutation of the aspartic acid residue in the $\beta 2$ chain does not activate ligand binding in $\alpha L\beta 2$ or $\alpha M\beta 2$ integrins (Lu et al., 2001). This suggests, that the salt bridge is differentially important for different integrin heterodimers. Alternatively or in addition, cell type specific roles of the salt bridge might play a role. To distinguish between these options analysis of mice ubiquitously expressing the D759A integrin as well as analysis of mutated MEF's will be performed in the future. Furthermore, analysis of mutant keratinocytes will address the question whether the observed difference between the data presented in this thesis and the published phenotypes can be explained by the difference between *in vivo* and *in vitro* conditions.

5.4.3 Deletion of the putative binding site for FAK on the $\beta 1$ integrin cytoplasmic domain results in a $\beta 1$ -null like phenotype

FAK is suggested to be important for integrin mediated signalling and was shown to bind to peptides of the $\beta 1$ integrin cytoplasmic domain. Furthermore, mutational analysis of the $\beta 1$ integrin tail revealed that the deletion of the membrane proximal amino acids D759 to M771 of the $\beta 1$ cytoplasmic domain abolishes FAK binding (Reszka et al., 1992; Schaller et al., 1995). However, since integrin binding region of FAK is not required for FAK localization to focal adhesions, it could be that *in vivo* integrin FAK interaction is indirect (Tahiliani et al., 1999; Shen and Schaller, 1999). FAK activation is characterised by autophosphorylation on position Y397 and was proposed to be regulated by integrins, both directly and indirectly via Src (Schaller, 2001). Activated FAK can activate by several means Rho GTPases to regulate the cytoskeleton and cell migration. FAK was also shown activate Erk and thereby mediate integrin signalling to promote cell migration. However, there is evidence that integrin mediated Erk activation can also take place in a FAK independent manner. First evidence for this came from studies by Lin et al., who showed that adhesion dependent Erk activation can occur independently of FAK activation (Lin et al., 1997). To distinguish the role of FAK and Erk dependent pathways downstream of $\beta 1$ integrin we now developed a mouse strain, which in keratinocytes expresses only the deletion mutant (Δ D759-M771) of $\beta 1$ integrin. Detailed analysis of the hair coat phenotype of these mice (see paragraph 4.2.1.5.3) revealed that it almost entirely resembles the $\beta 1$ integrin knockout phenotype. In contrast to $\beta 1$ null keratinocytes which lack $\beta 1$ integrin, Δ D759-M771 $\beta 1$ integrin mutants express normal amounts of the integrin receptor with an internal deletion of the cytoplasmic domain. Testing whether known integrin binding proteins are still able to associate with the truncated $\beta 1$ integrin receptor, we found that Δ D759-M771 $\beta 1$ integrin is apparently still able to bind to ILK (see Figure 4.63). ILK was initially described as a Ser/Thr kinase that interacts with the cytoplasmic tails of $\beta 1$, $\beta 2$ and $\beta 3$ -integrin (Hannigan et al., 1996). However, both *in vivo* and *in vitro* studies with cells lacking the functional ILK gene did not support that ILK is functioning as a kinase in cells (Zervas and Brown, 2002; Sakai et al., 2003, Grashoff et al., 2003). Instead, ILK seems to be a binding platform for several adaptor proteins linking integrins to the actin cytoskeleton. Furthermore, ILK was shown to be an important regulator of integrin avidity, since ILK-null cells had impaired integrin mediated adhesion (Sakai et al., 2003). Our results suggest that the truncated $\beta 1$ integrin is able to bind ILK, but not able to provide ILK dependent inside-out and outside-in signalling, leading to a $\beta 1$ -null like

phenotype. The dissection of the contribution of defective inside-out and inside-in signalling will be the task for the future. This analysis can give interesting insights into the contributions of ILK signalling into integrin mediated events.

With the data presented in this thesis we could not convincingly show whether FAK activation is impaired in mice expressing the deletion mutation. Staining of skin sections from these mice with an antibody recognizing the autophosphorylation site (Y397) on the activated FAK molecule revealed a pattern, which in both control and mutant mice was similar and restricted to suprabasal cells (see Figure 4.62). This is surprising, since the suprabasal cells express only limited amounts of $\beta 1$ integrin. However, FAK can also be activated by growth factors independently of integrins. Since there is no appropriate negative control, we cannot exclude that this suprabasal staining is unspecific. Therefore, it is difficult to conclude, whether the mutated integrin can support FAK autophosphorylation *in vivo* or not. In the future, studies with primary keratinocytes from these mice will be performed to clarify this issue and to test whether in the mutated cells Erk activation can occur independently of FAK similarly to the previously reported data (Lin et al., 1997).

6 Conclusions

Using Cdc42-deficient cells and dominant negative inhibition of Cdc42, we could demonstrate in this study that the establishment and maintenance of polarity during cell migration is mediated not only by integrin mediated activation of Cdc42, but also by other Rho GTPases. Moreover dnCdc42 may effectively inhibit several members of the Rho-GTPase family and might be considered, therefore, a subfamily inhibitor rather than an inhibitor specific for Cdc42. Multiple knockouts or knockdowns of Rho GTPases will certainly be helpful in identifying those GTPases involved in the regulation of cell polarity in migrating fibroblastoid cells.

The analysis of several knockin mice strains presented in this thesis, which express in keratinocytes only mutated forms of $\beta 1$ integrin, revealed that integrin phosphorylation and disruption of the salt bridge between the α and β subunits in an integrin heterodimer cannot be considered as general regulators of integrin activity. Together with published investigations our data indicate that the mechanisms controlling integrin activation might be specific for a certain cell type or integrin heterodimers, rather than to be important for the whole integrin family in all cells. Future studies with $\beta 1$ integrin mutants expressed in non-keratinocyte cells, both *in vivo* and *in vitro* will help to experimentally verify this hypothesis. Moreover, diseases models will be used to uncover subtle, stress induced phenotypes.

7 References

- Abe, T., Kato, M., Miki, H., Takenawa T. and Endo, T.** (2003). Small GTPase Tc10 and its homologue RhoT induce N-WASP-mediated long process formation and neurite outgrowth. *J Cell Sci* 116, 155-68.
- Allen, W.E., Zicha, D., Ridley, A.J., and Jones, G.E.** (1998). A role for Cdc42 in macrophage chemotaxis. *J Cell Biol* 141, 1147-1157.
- Alonso, L., and Fuchs, E.** (2003a). Stem cells in the skin: waste not, Wnt not. *Genes Dev* 17, 1189-1200.
- Alonso, L., and Fuchs, E.** (2003b). Stem cells of the skin epithelium. *Proc Natl Acad Sci U S A* 100 Suppl 1, 11830-11835.
- Aronheim, A., Broder, Y.C., Cohen, A., Fritsch, A., Belisle, B., and Abo, A.** (1998). Chp, a homologue of the GTPase Cdc42Hs, activates the JNK pathway and is implicated in reorganizing the actin cytoskeleton. *Curr Biol* 8, 1125-1128.
- Aspenström, P., Fransson, A., and Saras, J.** (2004). Rho GTPases have diverse effects on the organization of the actin filament system. *Biochem J* 377, 327-337.
- Bagrodia, S., and Cerione, R.A.** (1999). Pak to the future. *Trends Cell Biol* 9, 350-355.
- Bagutti, C., Speight, P.M., and Watt, F.M.** (1998). Comparison of integrin, cadherin, and catenin expression in squamous cell carcinomas of the oral cavity. *J Pathol* 186, 8-16.
- Barsukov, I.L., Prescott, A., Bate, N., Patel, B., Floyd, D.N., Bhanji, N., Bagshaw, C.R., Letinic, K., Di Paolo, G., De Camilli, P., Roberts, G.C., and Critchley, D.R.** (2003). Phosphatidylinositol phosphate kinase type 1gamma and beta1-integrin cytoplasmic domain bind to the same region in the talin FERM domain. *J Biol Chem* 278, 31202-31209.
- Berg, J. M.; Tymoczko, J. L.; and Stryer, L.** (2002). *Biochemistry*. W. H. Freeman and Co. New York.
- Betz, U.A., Vosshenrich, C.A., Rajewsky, K., and Muller, W.** (1996). Bypass of lethality with mosaic mice generated by Cre-loxP-mediated recombination. *Curr Biol* 6, 1307-1316.
- Bishop, A. L., and Hall, A.** (2000). Rho GTPases and their effector proteins. *Biochem J* 348, 241-255.
- Bokoch, G. M.** (2003). Biology of the p21-activated kinases. *Annu Rev Biochem* 72, 743-781.
- Bouvard, D., Vignoud, L., Dupe-Manet, S., Abed, N., Fournier, H.N., Vincent-Monegat, C., Retta, S.F., Fässler, R., and Block, M.R.** (2003). Disruption of focal adhesions by integrin cytoplasmic domain-associated protein-1 alpha. *J Biol Chem* 278, 6567-6574.

- Braga, V. M., Betson, M., Li, X., and Lamarche-Vane, N.** (2000) Activation of the small GTPase Rac is sufficient to disrupt cadherin-dependent cell-cell adhesion in normal human keratinocytes. *Mol Biol Cell* 11, 3703-3721.
- Brakebusch, C., and Fässler, R.** (2003). The integrin-actin connection, an eternal love affair. *Embo J* 22, 2324-2333.
- Brakebusch, C., Grose, R., Quondamatteo, F., Ramirez, A., Jorcano, J.L., Pirro, A., Svensson, M., Herken, R., Sasaki, T., Timpl, R., Werner, S., and Fässler, R.** (2000). Skin and hair follicle integrity is crucially dependent on beta 1 integrin expression on keratinocytes. *Embo J* 19, 3990-4003.
- Brockbank, E.C., Bridges, J., Marshall, C.J., and Sahai, E.** (2005). Integrin beta1 is required for the invasive behaviour but not proliferation of squamous cell carcinoma cells in vivo. *Br J Cancer* 92, 102-112.
- Calderwood, D.A.** (2004). Integrin activation. *J Cell Sci* 117, 657-666.
- Carl, U.D., Pollmann, M., Orr, E., Gertler, F.B., Chakraborty, T., and Wehland, J.** (1999). Aromatic and basic residues within the EVH1 domain of VASP specify its interaction with proline-rich ligands. *Curr Biol* 9, 715-8.
- Cary, L.A., Han, D.C., Polte, T.R., Hanks, S.K., and Guan, J.L.** (1998). Identification of p130Cas as a mediator of focal adhesion kinase-promoted cell migration. *J Cell Biol* 140, 211-221.
- Cau, J., and Hall, A.** (2005). Cdc42 controls the polarity of the actin and microtubule cytoskeletons through two distinct signal transduction pathways. *J Cell Sci* 118, 2579-2587.
- Chen, F., Ma, L., Parrini, M. C., Mao, X., Lopez, M., Wu, C., Marks, P. W., Davidson, L., Kwiatkowski, D. J., Kirchhausen, T., Orkin, S. H., Rosen, F. S., Mayer, B. J., Kirschner, M. W., and Alt, F. W.** (2000). Cdc42 is required for PIP2 induced actin polymerization and early development but not for cell viability. *Curr Biol* 10, 758-765.
- Chen, J., Diacovo, T.G., Grenache, D.G., Santoro, S.A., and Zutter, M.M.** (2002). The alpha(2) integrin subunit-deficient mouse: a multifaceted phenotype including defects of branching morphogenesis and hemostasis. *Am J Pathol* 161, 337-344.
- Chiang, S.H., Baumann, C.A., Kanzaki, M., Thurmond, D.C., Watson, R.T., Neudauer, C.L., Macara, I.G., Pessin, J.E., and Saltiel, A.R.** (2001). Insulin-stimulated GLUT4 translocation requires the CAP-dependent activation of TC10. *Nature* 410, 944-948.
- Clark, E.A., King, W.G., Brugge, J.S., Symons, M., and Hynes, R.O.** (1998). Integrin-mediated signals regulated by members of the rho family of GTPases. *J Cell Biol* 142, 573-586.

- Cote, J.F., and Vuori, K.** (2002). Identification of an evolutionarily conserved superfamily of DOCK180-related proteins with guanine nucleotide exchange activity. *J Cell Sci* 115, 4901-4913.
- Cunningham, C.C.** (1995). Actin polymerization and intracellular solvent flow in cell surface blebbing. *J Cell Biol* 129, 1589-1599.
- Danen, E.H., and Sonnenberg, A.** (2003). Integrins in regulation of tissue development and function. *J Pathol* 201, 632-641.
- Danen, E.H., and Yamada, K.M.** (2001). Fibronectin, integrins, and growth control. *J Cell Physiol* 189, 1-13.
- Danen, E.H., van Rheenen, J., Franken, W., Huveneers, S., Sonneveld, P., Jalink, K., and Sonnenberg, A.** (2005). Integrins control motile strategy through a Rho-cofilin pathway. *J Cell Biol* 169, 515-526.
- Daniels, R.H., and Bokoch, G.M.** (1999). p21-activated protein kinase: a crucial component of morphological signalling? *Trends Biochem Sci* 24, 350-355.
- De Melker, A.A., Kramer, D., Kuikman, I., and Sonnenberg, A.** (1997). The two phenylalanines in the GFFKR motif of the integrin alpha6A subunit are essential for heterodimerization. *Biochem J* 328 (Pt 2), 529-537.
- Degani, S., Balzac, F., Brancaccio, M., Guazzone, S., Retta, S.F., Silengo, L., Eva, A., and Tarone, G.** (2002). The integrin cytoplasmic domain-associated protein ICAP-1 binds and regulates Rho family GTPases during cell spreading. *J Cell Biol* 156, 377-387.
- DelPozo, M.A., Alderson, N.B., Kiosses, W.B., Chiang, H.H., Anderson, R.G., and Schwartz, M.A.** (2004). Integrins regulate Rac targeting by internalization of membrane domains. *Science* 303, 839-842.
- DelPozo, M.A., Price, L.S., Alderson, N.B., Ren, X.D., and Schwartz, M.A.** (2000). Adhesion to the extracellular matrix regulates the coupling of the small GTPase Rac to its effector PAK. *Embo J* 19, 2008-2014.
- DeMali, K.A., Wennerberg, K., and Burridge, K.** (2003). Integrin signalling to the actin cytoskeleton. *Curr Opin Cell Biol* 15, 572-582.
- DerMardirossian, C., and Bokoch, G.M.** (2005). GDIs: central regulatory molecules in Rho GTPase activation. *Trends Cell Biol* 15, 356-363.
- DerMardirossian, C., Schnelzer, A., and Bokoch, G.M.** (2004). Phosphorylation of RhoGDI by Pak1 mediates dissociation of Rac GTPase. *Mol Cell* 15, 117-127.

- DiPersio, C.M., Hodivala-Dilke, K.M., Jaenisch, R., Kreidberg, J.A., and Hynes, R.O.** (1997). alpha3beta1 Integrin is required for normal development of the epidermal basement membrane. *J Cell Biol* 137, 729-742.
- DiPersio, C.M., van der Neut, R., Georges-Labouesse, E., Kreidberg, J.A., Sonnenberg, A., and Hynes, R.O.** (2000). alpha3beta1 and alpha6beta4 integrin receptors for laminin-5 are not essential for epidermal morphogenesis and homeostasis during skin development. *J Cell Sci* 113 (Pt 17), 3051-3062.
- Dolfi, F., Garcia-Guzman, M., Ojaniemi, M., Nakamura, H., Matsuda, M., and Vuori, K.** (1998). The adaptor protein Crk connects multiple cellular stimuli to the JNK signalling pathway. *Proc Natl Acad Sci U S A* 95, 15394-15399.
- Dowling, J., Yu, Q.C., and Fuchs, E.** (1996). Beta4 integrin is required for hemidesmosome formation, cell adhesion and cell survival. *J Cell Biol* 134, 559-572.
- Eggert, U.S., Kiger, A.A., Richter, C., Perlman, Z.E., Perrimon, N., Mitchison, T.J. and Field, C.M.** (2004). Parallel Chemical Genetic and Genome-Wide RNAi Screens Identify Cytokinesis Inhibitors and Targets. *PLoS Biol* 2, e379.
- Ellis, S. and Mellor, H.** (2000). The novel Rho-family GTPase Rif regulates coordinated actin-based membrane rearrangements. *Curr Biol* 10, 1387-90.
- Etienne-Manneville, S., and Hall, A.** (2001). Integrin-mediated activation of Cdc42 controls cell polarity in migrating astrocytes through PKC ζ . *Cell* 106, 489-498.
- Etienne-Manneville, S., and Hall, A.** (2002). Rho GTPases in cell biology. *Nature* 420, 629-635.
- Etienne-Manneville, S., and Hall, A.** (2003). Cdc42 regulates GSK-3 β and adenomatous polyposis coli to control cell polarity. *Nature* 421, 753-756.
- Evers, E.E., Zondag, G.C., Malliri, A., Price, L.S., ten Klooster, J.P., van der Kammen, R.A., and Collard, J.G.** (2000). Rho family proteins in cell adhesion and cell migration. *Eur J Cancer* 36, 1269-1274.
- Fässler, R., and Meyer, M.** (1995). Consequences of lack of beta 1 integrin gene expression in mice. *Genes Dev* 9, 1896-1908.
- Feig, L. A.** (1999). Tools of the trade: use of dominant-inhibitory mutants of Ras-family GTPases. *Nat Cell Biol* 1, E25-E27.
- Frost, J. A., Steen, H., Shapiro, P., Lewis, T., Ahn, N., Shaw, P. E., and Cobb, M. H.** (1997). Cross-cascade activation of ERKs and ternary complex factors by Rho family proteins. *EMBO J* 16, 6426-6438.

- Fujikura, J., Yamato E., Yonemura S., Hosoda K., Masui S., Nakao K., Miyazaki J. and Niwa H.** (2002). Differentiation of embryonic stem cells is induced by GATA factors. *Genes Dev* 16, 784-789.
- Fukata, M., Nakagawa, M., Kaibuchi, K.** (2003) Roles of Rho-family GTPases in cell polarisation and directional migration. *Curr Opin Cell Biol* 15, 590-597.
- Gandarillas, A.** (2000). Epidermal differentiation, apoptosis, and senescence: common pathways? *Exp Gerontol* 35, 53-62.
- Garcia-Alvarez, B., de Pereda, J.M., Calderwood, D.A., Ulmer, T.S., Critchley, D., Campbell, I.D., Ginsberg, M.H., and Liddington, R.C.** (2003). Structural determinants of integrin recognition by talin. *Mol Cell* 11, 49-58.
- Gauthier-Rouvière, C., Vignal, E., Mériane, M., Roux, P., Montcourier, P., and Fort, P.** (1998). RhoG GTPase controls a pathway that independently activates Rac1 and Cdc42Hs. *Mol Biol Cell* 9, 1379-94.
- Georges-Labouesse, E., Messaddeq, N., Yehia, G., Cadalbert, L., Dierich, A., and Le Meur, M.** (1996). Absence of integrin alpha 6 leads to epidermolysis bullosa and neonatal death in mice. *Nat Genet* 13, 370-373.
- Ghazizadeh, S., and Taichman, L.B.** (2001). Multiple classes of stem cells in cutaneous epithelium: a lineage analysis of adult mouse skin. *Embo J* 20, 1215-1222.
- Giancotti, F.G., and Ruoslahti, E.** (1999). Integrin signalling. *Science* 285, 1028-1032.
- Gimond, C., van Der Flier, A., van Delft, S., Brakebusch, C., Kuikman, I., Collard, J.G., Fässler, R., and Sonnenberg, A.** (1999). Induction of cell scattering by expression of beta1 integrins in beta1-deficient epithelial cells requires activation of members of the rho family of GTPases and downregulation of cadherin and catenin function. *J Cell Biol* 147, 1325-1340.
- Ginsberg, M.H., Yaspan, B., Forsyth, J., Ulmer, T.S., Campbell, I.D., and Slepak, M.** (2001). A membrane-distal segment of the integrin alpha IIb cytoplasmic domain regulates integrin activation. *J Biol Chem* 276, 22514-22521.
- Gomes, E.R., Jani, S., and Gundersen, G.G.** (2005). Nuclear movement regulated by Cdc42, MRCK, myosin, and actin flow establishes MTOC polarization in migrating cells. *Cell* 121, 451-463.
- Gottschalk, K.E.** (2005). A coiled-coil structure of the alphaIIbbeta3 integrin transmembrane and cytoplasmic domains in its resting state. *Structure (Camb)* 13, 703-712.
- Govind, S., Kozma, R., Monfries, C., Lim, L., and Ahmed, S.** (2001). Cdc42Hs facilitates cytoskeletal reorganization and neurite outgrowth by localizing the 58-kD insulin receptor substrate to filamentous actin. *J Cell Biol* 152, 579-594.

- Grashoff, C., Aszodi, A., Sakai, T., Hunziker, E.B., and Fässler, R.** (2003). Integrin-linked kinase regulates chondrocyte shape and proliferation. *EMBO Rep* 4, 432-438.
- Grashoff, C., Thievensen, I., Lorenz, K., Ussar, S., and Fässler, R.** (2004). Integrin-linked kinase: integrin's mysterious partner. *Curr Opin Cell Biol* 16, 565-571.
- Grose, R., Hutter, C., Bloch, W., Thorey, I., Watt, F.M., Fässler, R., Brakebusch, C., and Werner, S.** (2002). A crucial role of beta 1 integrins for keratinocyte migration in vitro and during cutaneous wound repair. *Development* 129, 2303-2315.
- Guan, J.L.** (2004). Cell biology. Integrins, rafts, Rac, and Rho. *Science* 303, 773-774.
- Guo, W., and Giancotti, F.G.** (2004). Integrin signalling during tumour progression. *Nat Rev Mol Cell Biol* 5, 816-826.
- Gustavsson, A., Armulik, A., Brakebusch, C., Fässler, R., Johansson, S., and Fallman, M.** (2002). Role of the beta1-integrin cytoplasmic tail in mediating invasion-promoted internalization of Yersinia. *J Cell Sci* 115, 2669-2678.
- Hagmann, J., Burger, M.M., and Dagan, D.** (1999). Regulation of plasma membrane blebbing by the cytoskeleton. *J Cell Biochem* 73, 488-499.
- Hall, A.** (1998). Rho GTPases and the actin cytoskeleton. *Science* 279, 509-514.
- Hannigan, G.E., Leung-Hagesteijn, C., Fitz-Gibbon, L., Coppolino, M.G., Radeva, G., Filmus, J., Bell, J.C., and Dedhar, S.** (1996). Regulation of cell adhesion and anchorage-dependent growth by a new beta 1-integrin-linked protein kinase. *Nature* 379, 91-96.
- Hansen, L.A., and Tennant, R.W.** (1994). Follicular origin of epidermal papillomas in v-Ha-ras transgenic TG.AC mouse skin. *Proc Natl Acad Sci U S A* 91, 7822-7826.
- Haraguchi, T., Ding, D-Q., Yamamoto, A., Kaneda, T., Koujin, T. and Hiraoka, Y.** (1999). Multiple-color fluorescence imaging of chromosomes and microtubules in living cells. *Cell Structure and Function* 24, 291-298.
- Hirsch, E., Barberis, L., Brancaccio, M., Azzolino, O., Xu, D., Kyriakis, J.M., Silengo, L., Giancotti, F.G., Tarone, G., Fässler, R., and Altruda, F.** (2002). Defective Rac-mediated proliferation and survival after targeted mutation of the beta1 integrin cytodomain. *J Cell Biol* 157, 481-492.
- Holtkotter, O., Nieswandt, B., Smyth, N., Muller, W., Hafner, M., Schulte, V., Krieg, T., and Eckes, B.** (2002). Integrin alpha 2-deficient mice develop normally, are fertile, but display partially defective platelet interaction with collagen. *J Biol Chem* 277, 10789-10794.
- Huang, C., Rajfur, Z., Borchers, C., Schaller, M.D., and Jacobson, K.** (2003). JNK phosphorylates paxillin and regulates cell migration. *Nature* 424, 219-223.

- Huang, X., Griffiths, M., Wu, J., Farese, R.V., Jr., and Sheppard, D.** (2000a). Normal development, wound healing, and adenovirus susceptibility in beta5-deficient mice. *Mol Cell Biol* 20, 755-759.
- Huang, X.Z., Wu, J.F., Cass, D., Erle, D.J., Corry, D., Young, S.G., Farese, R.V., Jr., and Sheppard, D.** (1996). Inactivation of the integrin beta 6 subunit gene reveals a role of epithelial integrins in regulating inflammation in the lung and skin. *J Cell Biol* 133, 921-928.
- Huang, X.Z., Wu, J.F., Ferrando, R., Lee, J.H., Wang, Y.L., Farese, R.V., Jr., and Sheppard, D.** (2000b). Fatal bilateral chylothorax in mice lacking the integrin alpha9beta1. *Mol Cell Biol* 20, 5208-5215.
- Hübner, G., Brauchle, M., Smola, H., Madlener, M., Fässler, R. And Werner, S.** (1996). Differential regulation of pro-inflammatory cytokines during normal and impaired wound healing. *Cytokine* 8, 548-556.
- Hughes, P.E., Diaz-Gonzalez, F., Leong, L., Wu, C., McDonald, J.A., Shattil, S.J., and Ginsberg, M.H.** (1996). Breaking the integrin hinge. A defined structural constraint regulates integrin signalling. *J Biol Chem* 271, 6571-6574.
- Humphries, M.J., Symonds, E.J., and Mould, A.P.** (2003). Mapping functional residues onto integrin crystal structures. *Curr Opin Struct Biol* 13, 236-243.
- Hynes, R.O.** (2002). Integrins: bidirectional, allosteric signalling machines. *Cell* 110, 673-687.
- Itoh, R.E., Kurokawa, K., Ohba, Y., Yoshizaki, H., Mochizuki, N., and Matsuda, M.** (2002). Activation of rac and cdc42 video imaged by fluorescent resonance energy transfer-based single-molecule probes in the membrane of living cells. *Mol Cell Biol* 22, 6582-6591.
- Jones, J., Watt, F.M., and Speight, P.M.** (1997). Changes in the expression of alpha v integrins in oral squamous cell carcinomas. *J Oral Pathol Med* 26, 63-68.
- Juliano, R.L., Reddig, P., Alahari, S., Edin, M., Howe, A., and Aplin, A.** (2004). Integrin regulation of cell signalling and motility. *Biochem Soc Trans* 32, 443-446.
- Kawasaki, Y., Sato, R., and Akiyama, T.** (2003). Mutated APC and Asef are involved in the migration of colorectal tumour cells. *Nat Cell Biol* 5, 211-215.
- Klemke, R.L., Cai, S., Giannini, A.L., Gallagher, P.J., de Lanerolle, P., and Cheresch, D.A.** (1997). Regulation of cell motility by mitogen-activated protein kinase. *J Cell Biol* 137, 481-492.
- Klemke, R.L., Leng, J., Molander, R., Brooks, P.C., Vuori, K., and Cheresch, D.A.** (1998). CAS/Crk coupling serves as a "molecular switch" for induction of cell migration. *J Cell Biol* 140, 961-972.

- Kozma, R., Ahmed, S., Best, A., and Lim, L.** (1995). The Ras-related protein Cdc42Hs and bradykinin promote formation of peripheral actin microspikes and filopodia in Swiss 3T3 fibroblasts. *Mol Cell Biol* 15, 1942-1952.
- Krugmann, S., Jordens, I., Gevaert, K., Driessens, M., Vandekerckhove, J., and Hall, A.** (2001). Cdc42 induces filopodia by promoting the formation of an IRSp53:Mena complex. *Curr Biol* 11, 1645-1655.
- Laster, S.M., and Mackenzie, J.M., Jr.** (1996). Bleb formation and F-actin distribution during mitosis and tumor necrosis factor-induced apoptosis. *Microsc Res Tech* 34, 272-280.
- Lee, J.W., and Juliano, R.** (2004). Mitogenic signal transduction by integrin- and growth factor receptor-mediated pathways. *Mol Cells* 17, 188-202.
- Li, G., Gustafson-Brown, C., Hanks, S.K., Nason, K., Arbeit, J.M., Pogliano, K., Wisdom, R.M., and Johnson, R.S.** (2003). c-Jun is essential for organization of the epidermal leading edge. *Dev Cell* 4, 865-877.
- Li, Z., Hannigan, M., Mo, Z., Liu, B., Lu, W., Wu, Y., Smrcka, A.V., Wu, G., Li, L., Liu, M., Huang, C.K., and Wu, D.** (2003). Directional sensing requires G beta gamma-mediated PAK1 and PIX alpha-dependent activation of Cdc42. *Cell* 114, 215-227.
- Lin, T.H., Aplin, A.E., Shen, Y., Chen, Q., Schaller, M., Romer, L., Aukhil, I., and Juliano, R.L.** (1997). Integrin-mediated activation of MAP kinase is independent of FAK: evidence for dual integrin signalling pathways in fibroblasts. *J Cell Biol* 136, 1385-1395.
- Liu, S., Calderwood, D.A., and Ginsberg, M.H.** (2000). Integrin cytoplasmic domain-binding proteins. *J Cell Sci* 113 (Pt 20), 3563-3571.
- Lommel, S., Benesch, S., Rottner, K., Franz, T., Wehland, J., and Kuhn, R.** (2001). Actin pedestal formation by enteropathogenic Escherichia coli and intracellular motility of Shigella flexneri are abolished in N-WASP-defective cells. *EMBO Rep* 2, 850-857.
- Lu, C., Takagi, J., and Springer, T.A.** (2001). Association of the membrane proximal regions of the alpha and beta subunit cytoplasmic domains constrains an integrin in the inactive state. *J Biol Chem* 276, 14642-14648.
- Mettouchi, A., Klein, S., Guo, W., Lopez-Lago, M., Lemichez, E., Westwick, J.K., and Giancotti, F.G.** (2001). Integrin-specific activation of Rac controls progression through the G(1) phase of the cell cycle. *Mol Cell* 8, 115-127.
- Michaelson, D., Silletti, J., Murphy, G., D'Eustachio, P., Rush, M., and Philips, M.R.** (2001). Differential localization of Rho GTPases in live cells: regulation by hypervariable regions and RhoGDI binding. *J Cell Biol* 152, 111-126.

- Miki, H., Yamaguchi, H., Suetsugu, S., and Takenawa, T.** (2000). IRSp53 is an essential intermediate between Rac and WAVE in the regulation of membrane ruffling. *Nature* 408, 732-735.
- Miranti, C.K., and Brugge, J.S.** (2002). Sensing the environment: a historical perspective on integrin signal transduction. *Nat Cell Biol* 4, E83-90.
- Moon, S.Y., and Zheng, Y.** (2003). Rho GTPase-activating proteins in cell regulation. *Trends Cell Biol* 13, 13-22.
- Morris, R.J., Liu, Y., Marles, L., Yang, Z., Trempus, C., Li, S., Lin, J.S., Sawicki, J.A., and Cotsarelis, G.** (2004). Capturing and profiling adult hair follicle stem cells. *Nat Biotechnol* 22, 411-417.
- Mulrooney, J., Foley, K., Vineberg, S., Barreuther, M., and Grabel, L.** (2000). Phosphorylation of the beta1 integrin cytoplasmic domain: toward an understanding of function and mechanism. *Exp Cell Res* 258, 332-341.
- Murphy, G.A., Solski, P.A., Jillian, S.A., Perez de la Ossa, P., D'Eustachio, P., Der, C.J., and Rush, M.G.** (1999). Cellular functions of TC10, a Rho family GTPase: regulation of morphology, signal transduction and cell growth. *Oncogene* 18, 3831-3845.
- Neudauer, C.L., Joberty, G., Tatsis, N. and Macara I.G.** (1998). Distinct cellular effects and interactions of the Rho-family GTPase TC10. *Curr Biol* 8, 1151-60.
- Nishimura, T., Yamaguchi, T., Kato, K., Yoshizawa, M., Nabeshima, Y., Ohno, S., Hoshino, M., and Kaibuchi, K.** (2005). PAR-6-PAR-3 mediates Cdc42-induced Rac activation through the Rac GEFs STEF/Tiam1. *Nat Cell Biol* 7, 270-277.
- Nobes, C. D., and Hall, A.** (1995). Rho, rac, and cdc42 GTPases regulate the assembly of multimolecular focal complexes associated with actin stress fibers, lamellipodia, and filopodia. *Cell* 81, 53-62.
- Nobes, C. D., and Hall, A.** (1999). Rho GTPases control polarity, protrusion, and adhesion during cell movement. *J Cell Biol* 144, 1235-1244.
- Noritake, J., Watanabe, T., Sato, K., Wang, S., and Kaibuchi, K.** (2005). IQGAP1: a key regulator of adhesion and migration. *J Cell Sci* 118, 2085-2092.
- Paladi, M., and Tepass, U.** (2004). Function of Rho GTPases in embryonic blood cell migration in *Drosophila*. *J Cell Sci* 117, 6313-6326.
- Palazzo, A.F., Eng, C.H., Schlaepfer, D.D., Marcantonio, E.E., and Gundersen, G.G.** (2004). Localized stabilization of microtubules by integrin- and FAK-facilitated Rho signalling. *Science* 303, 836-839.

- Passey, S., Pellegrin, S., and Mellor, H.** (2004). What is in a filopodium? Starfish versus hedgehogs. *Biochem Soc Trans* 32, 1115-1117.
- Paulsson, M., Aumalley, M., Deutzmann, R., Timpl, R., Beck, K. and Engel, J.** (1987). Laminin - nidogen complex. Extraction with chelating agents and structural characterization. *Eur J Biochem.* 166:,11-19.
- Pedranzini, L., Leitch, A., and Bromberg, J.** (2004). Stat3 is required for the development of skin cancer. *J Clin Invest* 114, 619-622.
- Pollard, T.D., Blanchoin, L., and Mullins, R.D.** (2000). Molecular mechanisms controlling actin filament dynamics in nonmuscle cells. *Annu Rev Biophys Biomol Struct* 29, 545-576.
- Price, L.S., Leng, J., Schwartz, M.A., and Bokoch, G.M.** (1998). Activation of Rac and Cdc42 by integrins mediates cell spreading. *Mol Biol Cell* 9, 1863-1871.
- Raftopoulou, M., and Hall, A.** (2004). Cell migration: Rho GTPases lead the way. *Dev Biol* 265, 23-32.
- Raghavan, S., Bauer, C., Mundscha, G., Li, Q., and Fuchs, E.** (2000). Conditional ablation of beta1 integrin in skin. Severe defects in epidermal proliferation, basement membrane formation, and hair follicle invagination. *J Cell Biol* 150, 1149-1160.
- Ramirez, A., Page, A., Gandarillas, A., Zanet, J., Pibre, S., Vidal, M., Tusell, L., Genesca, A., Whitaker, D.A., Melton, D.W., and Jorcano, J.L.** (2004). A keratin K5Cre transgenic line appropriate for tissue-specific or generalized Cre-mediated recombination. *Genesis* 39, 52-57.
- Reid T, Furuyashiki T, Ishizaki T, Watanabe G, Watanabe N, Fujisawa K, Morii N, Madaule P, Narumiya S.** (1996) Rhotekin, a new putative target for Rho bearing homology to a serine/threonine kinase, PKN, and rhotekin in the rho-binding domain. *J Biol Chem* 271, 13556-60.
- Ren, X.D., Kiosses, W.B., and Schwartz, M.A.** (1999). Regulation of the small GTP-binding protein Rho by cell adhesion and the cytoskeleton. *Embo J* 18, 578-585.
- Reszka, A.A., Hayashi, Y., and Horwitz, A.F.** (1992). Identification of amino acid sequences in the integrin beta 1 cytoplasmic domain implicated in cytoskeletal association. *J Cell Biol* 117, 1321-1330.
- Ridley, A.J.** (2000). Rho GTPases. Integrating integrin signalling. *J Cell Biol* 150, F107-109.
- Ridley, A.J.** (2001). Rho GTPases and cell migration. *J Cell Sci* 114, 2713-2722.
- Ridley, A.J., and Hall, A.** (1992). Distinct patterns of actin organization regulated by the small GTP-binding proteins Rac and Rho. *Cold Spring Harb Symp Quant Biol* 57, 661-671.

- Ridley, A.J., Paterson, H.F., Johnston, C.L., Diekmann, D., and Hall, A.** (1992). The small GTP-binding protein rac regulates growth factor-induced membrane ruffling. *Cell* 70, 401-410.
- Ridley, A.J., Schwartz, M.A., Burridge, K., Firtel, R.A., Ginsberg, M.H., Borisy, G., Parsons, J.T., and Horwitz, A.R.** (2003). Cell migration: integrating signals from front to back. *Science* 302, 1704-1709.
- Rios, R. M., and Bornens, M.** (2003) The Golgi apparatus at the cell centre. *Curr Opin Cell Biol* 15, 60-66.
- Rodriguez, O.C., Schaefer, A.W., Mandato, C.A., Forscher, P., Bement, W.M., and Waterman-Storer, C.M.** (2003). Conserved microtubule-actin interactions in cell movement and morphogenesis. *Nat Cell Biol* 5, 599-609.
- Rogers, G.E.** (2004). Hair follicle differentiation and regulation. *Int J Dev Biol* 48, 163-170.
- Rosenberger, G., Jantke, I., Gal, A., and Kutsche, K.** (2003). Interaction of alphaPIX (ARHGEF6) with beta-parvin (PARVB) suggests an involvement of alphaPIX in integrin-mediated signalling. *Hum Mol Genet* 12, 155-167.
- Rossman, K.L., Der, C.J., and Sondek, J.** (2005). GEF means go: turning on RHO GTPases with guanine nucleotide-exchange factors. *Nat Rev Mol Cell Biol* 6, 167-180.
- Rottner, K., Behrendt, B., Small, J. V., and Wehland, J.** (1999). VASP dynamics during lamellipodia protrusion. *Nat Cell Biol* 1, 321-322.
- Rottner, K., Hall, A., and Small, J.V.** (1999). Interplay between Rac and Rho in the control of substrate contact dynamics. *Curr Biol* 9, 640-648.
- Russell, D., Andrews, P.D., James, J., and Lane, E.B.** (2004). Mechanical stress induces profound remodelling of keratin filaments and cell junctions in epidermolysis bullosa simplex keratinocytes. *J Cell Sci* 117, 5233-5243.
- Sakai, T., de la Pena, J.M., and Mosher, D.F.** (1999). Synergism among lysophosphatidic acid, beta1A integrins, and epidermal growth factor or platelet-derived growth factor in mediation of cell migration. *J Biol Chem* 274, 15480-15486.
- Sakai, T., Jove, R., Fässler, R., and Mosher, D.F.** (2001). Role of the cytoplasmic tyrosines of beta 1A integrins in transformation by v-src. *Proc Natl Acad Sci U S A* 98, 3808-3813.
- Sakai, T., Li, S., Docheva, D., Grashoff, C., Sakai, K., Kostka, G., Braun, A., Pfeifer, A., Yurchenco, P.D., and Fässler, R.** (2003). Integrin-linked kinase (ILK) is required for polarizing the epiblast, cell adhesion, and controlling actin accumulation. *Genes Dev* 17, 926-940.

- Sakai, T., Peyruchaud, O., Fässler, R., and Mosher, D.F.** (1998a). Restoration of beta1A integrins is required for lysophosphatidic acid-induced migration of beta1-null mouse fibroblastic cells. *J Biol Chem* 273, 19378-19382.
- Sakai, T., Zhang, Q., Fässler, R., and Mosher, D.F.** (1998b). Modulation of beta1A integrin functions by tyrosine residues in the beta1 cytoplasmic domain. *J Cell Biol* 141, 527-538.
- Saras, J., Wollberg, P. and Aspenström, P.** (2004). Wrch1 is a GTPase-deficient Cdc42-like protein with unusual binding characteristics and cellular effects. *Exp Cell Res* 299, 356-69.
- Schaller, M.D.** (2001). Biochemical signals and biological responses elicited by the focal adhesion kinase. *Biochim Biophys Acta* 1540, 1-21.
- Schaller, M.D., Otey, C.A., Hildebrand, J.D., and Parsons, J.T.** (1995). Focal adhesion kinase and paxillin bind to peptides mimicking beta integrin cytoplasmic domains. *J Cell Biol* 130, 1181-1187.
- Schmidt, A., and Hall, A.** (2002). Guanine nucleotide exchange factors for Rho GTPases: turning on the switch. *Genes Dev* 16, 1587-1609.
- Schwartz, M.A., and Shattil, S.J.** (2000). Signalling networks linking integrins and rho family GTPases. *Trends Biochem Sci* 25, 388-391.
- Schwartz, M.** (2004). Rho signalling at a glance. *J Cell Sci* 117, 5457-5458
- Serrador, J.M., Nieto, M., and Sanchez-Madrid, F.** (1999). Cytoskeletal rearrangement during migration and activation of T lymphocytes. *Trends Cell Biol* 9, 228-233.
- Sieg, D.J., Hauck, C.R., Ilic, D., Klingbeil, C.K., Schaefer, E., Damsky, C.H., and Schlaepfer, D.D.** (2000). FAK integrates growth-factor and integrin signals to promote cell migration. *Nat Cell Biol* 2, 249-256.
- Small, J. V., Stradal, T., Vignall, E., and Rottner, K.** (2002) The lamellipodium: where motility begins. *Trend Cell Biol* 12, 112-120.
- Snapper, S.B., Takeshima, F., Anton, I., Liu, C.H., Thomas, S.M., Nguyen, D., Dudley, D., Fraser, H., Purich, D., Lopez-Illasaca, M., Klein, C., Davidson, L., Bronson, R., Mulligan, R.C., Southwick, F., Geha, R., Goldberg, M.B., Rosen, F.S., Hartwig, J.H., and Alt, F.W.** (2001). N-WASP deficiency reveals distinct pathways for cell surface projections and microbial actin-based motility. *Nat Cell Biol* 3, 897-904.
- So, P.L., and Epstein, E.H., Jr.** (2004). Adult stem cells: capturing youth from a bulge? *Trends Biotechnol* 22, 493-496.
- Stenn, K.S., and Paus, R.** (2001). Controls of hair follicle cycling. *Physiol Rev* 81, 449-494.

- Stramer, B., Wood, W., Galko, M. J., Redd, M. J., Jacinto, A., Parkhurst, S. M., and Martin, P.** (2005) Live imaging of wound inflammation in *Drosophila* embryos reveals key roles for small GTPases during in vivo cell migration. *J Cell Biol* 168, 567-573.
- Stroeken, P.J., van Rijthoven, E.A., Boer, E., Geerts, D., and Roos, E.** (2000). Cytoplasmic domain mutants of beta1 integrin, expressed in beta 1-knockout lymphoma cells, have distinct effects on adhesion, invasion and metastasis. *Oncogene* 19, 1232-1238.
- Tadokoro, S., Shattil, S.J., Eto, K., Tai, V., Liddington, R.C., de Pereda, J.M., Ginsberg, M.H., and Calderwood, D.A.** (2003). Talin binding to integrin beta tails: a final common step in integrin activation. *Science* 302, 103-106.
- Tahiliani, P.D., Singh, L., Auer, K.L., and LaFlamme, S.E.** (1997). The role of conserved amino acid motifs within the integrin beta3 cytoplasmic domain in triggering focal adhesion kinase phosphorylation. *J Biol Chem* 272, 7892-7898.
- Tao, W., Pennica, D., Xu, L., Kalejta, R.F., and Levine, A.J.** (2001) Wrch-1, a novel member of the Rho gene family that is regulated by Wnt-1. *Genes Dev* 15, 1796-807.
- Tapley, P., Horwitz, A., Buck, C., Duggan, K., and Rohrschneider, L.** (1989). Integrins isolated from Rous sarcoma virus-transformed chicken embryo fibroblasts. *Oncogene* 4, 325-333.
- Travis, M.A., Humphries, J.D., and Humphries, M.J.** (2003). An unraveling tale of how integrins are activated from within. *Trends Pharmacol Sci* 24, 192-197.
- Tu, Y., Li, F., and Wu, C.** (1998). Nck-2, a novel Src homology2/3-containing adaptor protein that interacts with the LIM-only protein PINCH and components of growth factor receptor kinase-signalling pathways. *Mol Biol Cell* 9, 3367-3382.
- Tumbar, T., Guasch, G., Greco, V., Blanpain, C., Lowry, W.E., Rendl, M., and Fuchs, E.** (2004). Defining the epithelial stem cell niche in skin. *Science* 303, 359-363.
- Ulmer, T.S., Yaspan, B., Ginsberg, M.H., and Campbell, I.D.** (2001). NMR analysis of structure and dynamics of the cytosolic tails of integrin alpha IIb beta 3 in aqueous solution. *Biochemistry* 40, 7498-7508.
- Vallar, L., Melchior, C., Plancon, S., Drobecq, H., Lippens, G., Regnault, V., and Kieffer, N.** (1999). Divalent cations differentially regulate integrin alphaIIb cytoplasmic tail binding to beta3 and to calcium- and integrin-binding protein. *J Biol Chem* 274, 17257-17266.
- van der Neut, R., Krimpenfort, P., Calafat, J., Niessen, C.M., and Sonnenberg, A.** (1996). Epithelial detachment due to absence of hemidesmosomes in integrin beta 4 null mice. *Nat Genet* 13, 366-369.

- Velyvis, A., Vaynberg, J., Yang, Y., Vinogradova, O., Zhang, Y., Wu, C., and Qin, J.** (2003). Structural and functional insights into PINCH LIM4 domain-mediated integrin signalling. *Nat Struct Biol* 10, 558-564.
- Vignal, E., De Toledo, M., Comunale, F., Ladopoulou, A., Gauthier-Rouvière, C., Blangy, A., and Fort, P.** (2000). Characterization of TCL, a new GTPase of the rho family related to TC10 and Cdc42. *J Biol Chem* 275, 36457-64.
- Vinogradova, O., Velyvis, A., Velyviene, A., Hu, B., Haas, T., Plow, E., and Qin, J.** (2002). A structural mechanism of integrin alpha(IIb)beta(3) "inside-out" activation as regulated by its cytoplasmic face. *Cell* 110, 587-597.
- Watanabe, T., Wang, S., Noritake, J., Sato, K., Fukata, M., Takefuji, M., Nakagawa, M., Izumi, N., Akiyama, T., and Kaibuchi, K.** (2004) Interaction with IQGAP1 links APC to Rac1, Cdc42, and actin filaments during cell polarization and migration *Dev Cell* 7, 871-883.
- Watt, F.M.** (2002). Role of integrins in regulating epidermal adhesion, growth and differentiation. *Embo J* 21, 3919-3926.
- Wells, C.M., Walmsley, M., Ooi, S., Tybulewicz, V., and Ridley, A.J.** (2004). Rac1-deficient macrophages exhibit defects in cell spreading and membrane ruffling but not migration. *J Cell Sci* 117, 1259-1268.
- Welsh, C.F., Roovers, K., Villanueva, J., Liu, Y., Schwartz, M.A., and Assoian, R.K.** (2001). Timing of cyclin D1 expression within G1 phase is controlled by Rho. *Nat Cell Biol* 3, 950-957.
- Wennerberg, K., and Der, C. J.** (2004). Rho-family GTPases: it's not only Rac and Rho (and I like it). *J Cell Sci* 117, 1301-1312.
- Wennerberg, K., Armulik, A., Sakai, T., Karlsson, M., Fässler, R., Schaefer, E.M., Mosher, D.F., and Johansson, S.** (2000). The cytoplasmic tyrosines of integrin subunit beta1 are involved in focal adhesion kinase activation. *Mol Cell Biol* 20, 5758-5765.
- Wennerberg, K., Fässler, R., Warmegard, B., and Johansson, S.** (1998). Mutational analysis of the potential phosphorylation sites in the cytoplasmic domain of integrin beta1A. Requirement for threonines 788-789 in receptor activation. *J Cell Sci* 111 (Pt 8), 1117-1126.
- White, D.E., Kurpios, N.A., Zuo, D., Hassell, J.A., Blaess, S., Mueller, U., and Muller, W.J.** (2004). Targeted disruption of beta1-integrin in a transgenic mouse model of human breast cancer reveals an essential role in mammary tumor induction. *Cancer Cell* 6, 159-170.
- Wood, W., and Martin, P.** (2002). Structures in focus--filopodia. *Int J Biochem Cell Biol* 34, 726-730.

-
- Yang, W., Lin, Q., Guan, J.L., and Cerione, R.A.** (1999). Activation of the Cdc42-associated tyrosine kinase-2 (ACK-2) by cell adhesion via integrin beta1. *J Biol Chem* 274, 8524-8530.
- Yasuda, S., Oceguera-Yanez, F., Kato, T., Okamoto, M., Yonemura, S., Terada, Y., Ishizaki, T., and Narumiya, S.** (2004). Cdc42 and mDia3 regulate microtubule attachment to kinetochores. *Nature* 428, 767-771.
- Yatohgo, T., Izumi I., Kashiwagi, H. and Hayashi, M.** (1988). Novel purification of vitronectin from human plasma by heparin affinity chromatography. *Cell Structure Function* 13, 281-292.
- Zervas, C.G., and Brown, N.H.** (2002). Integrin adhesion: when is a kinase a kinase? *Curr Biol* 12, R350-351.
- Zondag, G. C., Evers, E. E., ten Klooster, J. P., Janssen, L., van der Kammen, R. A., and Collard, J. G.** (2000). Oncogenic Ras downregulates Rac activity, which leads to increased Rho activity and epithelial-mesenchymal transition. *J Cell Biol* 149, 775-778
- Zugasti, O., Rul, W., Roux, P., Peyssonnaud, C., Eychene, A., Franke, T. F., Fort, P., and Hibner, U.** (2001). Raf-MEK-Erk cascade in anoikis is controlled by Rac1 and Cdc42 via Akt. *Mol Cell Biol* 21, 6706-6717.

8 Supplements

8.1 Supplementary material on the attached CD

Supplementary Movie 1 Cdc42-null fibroblasts form normal filopodia and lamellipodia. Cdc42(-/-) cells were transfected with an expression vector encoding EGFP- β -actin fusion protein resulting in fluorescent labelling of the actin cytoskeleton. Immunofluorescence time lapse microscopy revealed normal formation of filopodia and lamellipodia in these cells. (27 s/frame collection rate; 12 frames/s display rate). Scale bar = 5 μ m.

Supplementary Movie 2 Expression of dnCdc42 in Cdc42-null cells results in increased membrane blebbing and loss of trailing edge. Phase contrast time lapse microscopy of Cdc42(-/- + N17) cells indicated membrane blebbing and loss of trailing edge of cells. Quantification of 4 different movies of Cdc42(fl/-), Cdc42(-/-) and Cdc42(-/- + N17) revealed the differences in membrane blebbing described in the result section. (18 s/frame collection rate; 12 frame/s display rate). Scale bar = 50 μ m.

Supplementary Movies 3, 4 and 5 Unstable direction of cell migration in Cdc42(-/- + N17) cells in a wound closure assay, but not in Cdc42-null cells. A wound closure migration assay of Cdc42(fl/-) (movie 3), Cdc42(-/-) (movie 4) and Cdc42(-/- + N17) cells (movie 5) was monitored by phase contrast time lapse microscopy during 6h. The leading edge is stably oriented towards the scratch in Cdc42(fl/-), but also in Cdc42(-/-) cells. In Cdc42(-/- + N17) cells the leading edge was not stably oriented towards the scratch, but pointed in all possible directions. (4 min/frame collection rate; 12 frames/s display rate). Scale bar = 100 μ m.

Supplementary Movies 6 and 7 Filopodium formation in Cdc42(fl/-) and Cdc42(-/-) ES cells. Phase contrast time lapse microscopy showing filpodium formation in Cdc42(fl/-) (movie 6) and Cdc42(-/-) (movie 7) embryonic stem cells. (10 s/frame collection rate; 12 frames/s display rate). Scale bar = 10 μ m.

This work would have never been possible without the help of many people to whom I am grateful. I wish to express my sincere gratitude to:

My supervisor, Dr. Cord Brakebusch for giving me the opportunity to be a PhD student in his group, for his help and continues support throughout my PhD study, and for stimulating discussions and critical reading this thesis.

Prof. Dr. Reinhard Fässler, for giving me the possibility to work in his department and for sharing his knowledge and ideas about integrins.

Prof. Dr. Charles N. David, for accepting to be my supervisor at the university and for reviewing this work.

I am also grateful to Prof. Dr. Michael Schleicher, Prof. Dr. Heinrich Leonhardt, Prof. Dr. Kirsten Jung, Prof. Dr. Manfred Schliwa and Prof. Dr. Hans-Ulrich Koop for accepting to be a member of the thesis committee and for critically reading this work.

All the members of the “Brakebusch lab”, for the nice, motivating atmosphere, helpfulness and lots of discussions not only about science, but also about all the other important things in life. Especially, Anna and Gerd, for being friends from the very first day in the lab.

Drs. Hanni Meyer and Jolanda van Hengel, for being my co-workers in the integrin project and their contribution to the generation of the $\beta 1$ integrin knockin mice. Furthermore, for lots of stimulating discussions.

Drs. Günter Kostka and Sebastian Wiesner, for helping me to establish the time-lapse analysis and advice in other microscopy techniques.

Dr. Klemens Rottner, Profs. Sabine Werner and Jose L. Jorcano, for very fruitful collaborations.

Finally, my special thanks go to my parents for their continuous support and to Wojtek for his patience, support, discussions and most importantly for not letting me forget that there are also other things besides science.

Aleksandra Maria Czuchra

ADDRESS

Mariahilfstr. 20

D-81541 München

Phone: + 89 62 42 11 22

DATE AND PLACE OF BIRTH

26.10.1978 Gdansk, Poland

EDUCATION & SCIENTIFIC EXPERIENCE

- | | | |
|-------------------|---|-------------------------|
| 08/2002 – now | Max-Planck-Institute of Biochemistry | München, Germany |
| | Ph.D. student in the junior research group of Dr. Cord Brakebusch, in the Department of Molecular Medicine headed by Prof. Dr. Reinhard Fässler | |
| 02/2002 – 03/2002 | Max-Planck-Institute of Biochemistry | München, Germany |
| | 2 months research training in the group of Prof. Dr. Reinhard Fässler, in the Department of Molecular Medicine
Field of research: Integrins in skin disease | |
| 10/2001 – 12/2001 | Lund University | Lund, Sweden |
| | 3 months research training in the group of Prof. Dr. Reinhard Fässler, in the Department of Experimental Pathology
Field of research: Integrins in skin disease | |
| 02/1999 – 09/1999 | University of Bremen | Bremen, Germany |
| | SOCRATES-Erasmus Scholarship Program
7 months research training in the group of Prof. Dr. Bernd Jastorff, in the Department of Bioorganic Chemistry
Field of research: cAMP and cGMP as tools in pharmacological and cell biological research | |
| 10/1997 – 06/2002 | University of Gdansk,
Intercollegiate Faculty of Biotechnology | Gdansk, Poland |
| | Master thesis: Analysis of the TNF α (-308) and LT α (+252, NcoI) gene polymorphisms in pancreatic cancer
Degree: Master of Science in Biotechnology | |
| 09/1993 - 05/1997 | Dr. Wladyslaw Pniewski High School | Gdansk, Poland |
| | General qualification for university entrance | |

08/1990 – 09/1993	Wilhelm-Raabe-Schule Secondary school	Bremerhaven, Germany
09/1985- 06/1990	Primary school no. 45	Gdansk, Poland
